# NEW GENERATION OF DISPERSANTS BY GRAFTING LIGNIN OR XYLAN

**A Thesis Presented to the**

**Faculty of Graduate Studies of**

**Lakehead University**

**by**

**Mohan Konduri**

**Submitted in partial fulfillment of requirements**

**for the degree of Doctor of Philosophy in Biotechnology**

**April 19, 2017**

# DEDICATION

To my parents for their valuable support and endless encouragement

To my wife, who has supported in all my endeavors

To my lovely daughter

## ABSTRACT

Synthetic dispersants are commonly used in the stabilization of various colloidal suspensions. However, their non-biodegradable and toxic natures hamper their industrial use. The use of natural polymers as dispersants for various colloidal suspensions has been reported in the past, but the incentive for producing highly efficient natural polymeric dispersants is high. Lignin and xylan are the most abundant and sustainable natural polymers on earth, which are produced as by-products of pulping and cellulosic ethanol industries. These chemicals can be considered as the raw materials for producing value added products such as dispersants. In this dissertation, the anionic modification of kraft lignin and xylan via carboxymethylation, sulfomethylation and oxidation were comprehensively investigated and the applications of the products as dispersants in kaolin and coal suspensions were systematically assessed. The influence of reaction conditions on charge density and solubility of kraft lignin or xylan were systematically investigated. The anionic products obtained were characterized using NMR, FTIR, TGA, molecular weight and elemental analyses. The adsorption of anionic lignin or xylan on kaolin and coal particles and their effect on zeta potential of the suspensions was comprehensively assessed. The relative turbidity and viscosity analyses of colloidal suspensions confirmed the better dispersion performance of the products compared with commercial ones. The impact of dispersant dosage, pH of the suspension and time of mixing on dispersant performance of anionic lignin or xylan in kaolin and coal suspensions was also studied. The dispersion efficiency of suspensions found to increase with anionic lignin or xylan dosage and time of mixing. The dispersion efficiency of anionic lignin or xylan was at maximum under neutral conditions. The influences of molecular weight and charge density on the dispersant performance of anionic lignin in kaolin suspensions were also studied. The results showed that a highly charged anionic lignin adsorbed more compared with the low charged ones, and an increase in the molecular weight of anionic lignin showed no significant effect on its adsorption performance. Both charge density and molecular weight had an influence on dispersant activity of anionic lignin in kaolin suspensions. The dispersion studies of anionic kraft lignin or xylan in kaolin and coal suspensions showed that the increase in the dispersibility of these colloidal suspensions depends on adsorbed amount of anionic lignin or xylan on kaolin and coal particles, but not on the unadsorbed amount present in the suspensions. In the presence of anionic lignin or xylan dispersants, the zeta potential of kaolin or coal particles cannot determine directly the stability of colloidal suspensions. The

adsorbed anionic lignin or xylan on kaolin and coal particles induced electrostatic repulsion between the particles and thereby improved the dispersibility of suspensions.

The results obtained in this work confirms the possibilities for use of kraft lignin or xylan as dispersants in kaolin and coal suspensions and provides more insights on how the dispersability of these suspensions will be impacted by the properties of the produced dispersants. The results of this thesis contributed to knowledge on the chemical modification of lignin and xylan, characterization of modified products and to the fundamentals associated with the performance analysis of dispersion systems.

## ACKNOWLEDGEMENTS

I would like to express my sincere gratitude to my Supervisor Dr. Pedram Fatehi for all his hope, efforts and precious time he has put on me. His guidance and immense support helped me in all the time of research and writing of this thesis.

I would like to extend my sincere thanks to my committee members, Dr. Baoqiang Liao, Dr. Sudip Rakshit, Dr. Ying Zheng and Dr. Mathew Lietch for their valuable suggestions in preparing this thesis

I also wish to extent my sincere thanks to Mr. Michael Sorokopud, Dr. GuosehengWu, Mr. Martin Griffith and Mr. Greg Krepka, LUIL department, Lakehead University.

I would also like to thank all the previous and current lab members for encouraging me and providing me an ideal workplace environment. Specially, I thank Dr. Mehdi Dhastban, Dr. Fangong Kong and Mr. Agha Hasan for their continuous encouragement and great support. I thank both faculty and the staff members of Department of Biology for their assistance.

I would also like to thank my beloved parents, Rama Krishna Reddy Konduri and Adilakshmi Konduri for their overwhelming support and sacrifice they made for me. Special thanks to my wife Sudhalakshmi Mareddy and my daughter Lakshmi Sahasra Konduri. There are no words that can truly express the level of gratitude and appreciation I have for you.

I thank all my friends, especially Suresh Kumar Konda, Vinay Kumar Reddy Chejerla, who generously devoted their time and supported me.

The financial assistance from FPInnovations, OGS and NSERC, Canada are also much appreciated.

Table of Contents

## List of Figures:

## List of Tables:

# INTRODUCTION

Dispersants are generally used in clay and coal suspensions in order to improve their dispersibility and generate stable homogenous colloidal systems [1]. These stable clay colloidal systems are critical in various mining, chemical and mineral processing industries for the production of cosmetics, ceramics paints and coating formulas [1]. On the other hand, stable and highly concentrated coal water slurry can serve as promising alternative fuels [2].

Inorganic and synthetic polymeric dispersants are commonly used in the stabilization of clay and coal suspensions [3, 4]. Although synthetic dispersants are effective, there are concerns about their non-biodegradable nature and health impacts. As a result, there is a strong incentive for producing green dispersants [5, 6]. The natural polymers could be tailored to act as dispersants. However, there are very few reports on modified natural polymers as dispersants for colloidal suspensions, and the need for cost effective natural polymeric dispersants is augmenting [5, 6, 7].

Polymers such as cellulose, starch, guar gum are modified and used as dispersants for clay or coal suspensions. However, the heavy use of these polymers in papermaking, agriculture, medicine, food and other related areas limited their availability as dispersants [5, 7, 8]. On the other hand, lignin and xylan are the most abundant sustainable natural polymers on earth, next to cellulose with limited industrial applications. Due to their large production worldwide, kraft lignin and xylan were recognised as a potential raw materials in preparing dispersants for clay and coal dispersions [9, 10]. However, the application of kraft lignin and xylan as dispersants for clay and coal suspensions is limited due to lack of required functional groups on kraft lignin or xylan, which results in poor interaction between them and clay or coal particles. To improve the interaction between them, anionic groups were introduced on the backbone of kraft lignin or xylan using carboxymethylation, sulfomethylation and oxidation routes, causing them to interact with clay or coal particles via electrostatic interaction [11, 12, 13].

Although numerous studies on dispersion of colloidal suspensions using polymeric dispersants were reported, the choice of polymer is still a debate [14, 15]. The dispersion of colloidal suspensions is a complex process. Some key characteristics of polymers such as charge density, molecular weight were known to affect the dispersion process [15, 16, 17].

Evaluating the adsorption performance of polymeric dispersants is crucial, because the adsorbed polymers can change the properties and chemistry of clay or coal particle surface. It is widely known that the polymer concentration, time of interaction and pH of the suspension affects the adsorption of polymers on colloidal particles [16, 18]. If the polymer concentration and time of interaction are small, the polymers cannot adsorb to a significant degree and contribute to dispersion of colloidal particles. The pH of the suspension dictates the ionization potential of the polymer's functional groups and thereby influences the adsorption of polymer on particle surface [16, 18]. Therefore, it is important to study the adsorption of polymeric dispersants on clay or coal particles under varied process conditions.

The behaviour of clay or coal particles is also affected by the chemistry of the suspensions and the properties of particles in the suspensions. These factors significantly influence the repulsive and attractive inter-particle forces between the particles, and significantly affect the dispersibility of clay or coal suspensions [19, 20]. To optimize the polymer properties to be used as dispersants for clay or coal suspensions, it is crucial to investigate the influence of surface chemistry and properties of clay or coal samples on dispersant performance of polymeric dispersants.

**Rationale behind the study**

- Limitations in use of synthetic dispersants because of their nonbiodegradable and toxic nature
- Limitation in use of lignin or xylan as dispersants due to lack of sufficient reactive groups and solubility
- Limitation in dispersion of kaolin or coal suspensions due to complexity of dispersion process
- Lack of fundamental studies on the correlation of properties and performance for modified lignin or xylan properties as dispersants

**Novelty of current research**

- Preparation of dispersants via modification of hardwood kraft lignin with carboxymethylation and sulfomethylation for clay suspension.
- Production of carboxymethylated xylan in an aqueous medium and investigation on the dispersion performance of the product in clay suspensions under varied conditions.

- Investigation on the influence of charge density and molecular weight of oxidised kraft lignin as a dispersant for kaolin suspensions.
- Investigation on the influence of oxidized sulfomethylated kraft lignin (OSL) as a dispersant for coal particles of different particle sizes.

Thus, the overall objectives of this study were to:

- solubilize kraft lignin with carboxymethylation and sulfomethylation methods for enhancing their application as dispersants;
- synthesize and characterize carboxymethylataed xylan as a dispersant for kaolin suspensions;
- synthesize oxidized and sulfiomethylated lignin as a dispersant for kaolin suspensions;
- study the influence of charge density and molecular weight of oxidized lignin on dispersion of kaolin suspensions;
- study the influence of oxidised sulfomethylated lignin as a dispersant for coal slurries

Chapter one provides a synopsis of the literature pertaining to the current studies. It includes two main sections. The first section reviews the general background information on the literature, about the present work and also the importance of the current research. The second section includes various methods employed in literature and in current research for analyzing the results.

Chapter two centered on the synthesis of the carboxymethylated lignin (CML) using sodium chloroacetate and characterization. The application of CML as a dispersant in kaolin clay suspensions is also investigated. The results obtained in the chapter can be used to optimize the reaction conditions to attain CML with targeted properties. Also, the techniques that can be employed to characterize CML is comprehensively described in this chapter. The results depicted that the molar ratio of sodium chloroacetae to lignin as well as time were crucial to produce CML with targeted properties. Also, the produced CML was greatly soluble under aqueous conditions. Effective dispersion performance of CML in clay suspensions could be obtained by increasing the charge density of lignin.

Chapter three discusses the synthesis and characterization sulfomethylated lignin (SML). Also the application of SML as a dispersant in cement admixtures was investigated. The influence of reaction conditions to produce SML with targeted properties was significantly studied and optimized using Taguchi orthogonal method. ANOVA is also employed to signify the effect of

reaction conditions. The results obtained depicted that the solubility of lignin could be greatly improved in aqueous conditions via sulfomethylation of lignin. Dispersion studies using SML in cement admixtures suggested that the anionic polymers with high charge density and low molecular weight properties were effective in improving the fluidity of cement suspensions.

Chapter four focuses on the synthesis and characterization of carboxymethylated xylan (CMX). It also discusses the application of CMX as a dispersant for kaolin suspensions. The reaction conditions for synthesis of CMX with targeted properties were optimized using Taguchi orthogonal method, and ANOVA analysis also applied to indicate the impact of process conditions on the generated results. The results obtained illustrated that the carboxyl groups could be effectively grafted on the xylan using carboxymethylation procedure under aqueous conditions, which further also increased the molecular weight and improved the thermal stability of xylan. Dispersion studies using CMX in clay suspensions showed that CMX could be an effective dispersant for highly concentrated clay suspensions compared to commercial polymeric dispersants (Polyacrylic acid, sodium carbonate and polyacrylic acid systems).

Chapter five demonstrates the impact of reaction parameters, such as CMX dosage, pH of the medium on the dispersion of kaolin suspensions. Also, the effect of these parameters on the properties of clay suspensions was systematically investigated. The results obtained depicted that the dispersion performance of CMX in clay suspensions was quick and increased with dosage and pH. Also, the CMX was effective under both static and dynamic conditions. Adsorption and dispersion studies implied that the dispersion performance of CMX depended on its adsorbed amount on kaolin particles, which affected the zeta potential and relative turbidity of kaolin suspensions. CMX dosage and pH of the medium also influenced the stability and size of kaolin particles in the suspensions. The addition of CMX was found to be more effective in stabilizing clay suspensions than a shear rate increase.

Chapter six substantiates the effect of charge density and molecular weight (MW) of oxidised lignin (anionic lignin) on its dispersion performance in kaolin suspensions. The results obtained suggested that the charge density substantially influenced the adsorption of oxidised lignin (OL) on kaolin particles. However, the MW had a little effect. The zeta potential of kaolin suspensions was also greatly influenced by the charge density (compared to MW of OL) and also strongly depended on the adsorbed amount of OL on kaolin particles. The relative turbidity studies

revealed that the changes in charge density and molecular weight of OL had significant effects on kaolin dispersion. The most effective OL was found to be the one with charge density of 3.6 meq/g and molecular weight of 30,000 g/mol. The stability analysis of kaolin particles, also indicated that both charge density and molecular weight of OL had strong influence on its dispersion performance. Kinetic studies also confirm that both charge density and molecular weight of OL were influential in the dispersant performance of kaolin suspensions.

Chapter seven demonstrates the application of oxidized sulfomethylated lignin (OSL) with a charge density of 4.4 meq/g and molecular weight of 21,000 g/mol as a dispersant for coal water suspensions (CWS). Also, the effect of coal's particle size on the rheological properties of CWS was investigated in the presence of OSL. The results showed that the OSL improved the dispersibility of CWS by decreasing the apparent viscosity of suspensions. Increase in particle size of coal improved the adsorption of OSL on surface, which in turn improved the wettability of coal. The zeta potential of coal was reduced with the increase in the adsorbed amount of OSL. The apparent viscosity and rheological properties of coal particles were greatly influenced by the adsorbed amount of OSL on coal surface and coal particle size. The pseudoplatic behaviour of CWS was increased with OSL adsorbed amount on coal surface irrespective of the particle size. The stability of coal particles was greatly enhanced by the addition of OSL. OSL improved the flow properties of CWS by improving the wettability of coal, as well as by generating electrostatic repulsion between the particles.

Chapter eight draws conclusions from all the results obtained and provide some recommendation for further study.

## References


1. Sofra F, Boger DV. Environmental rheology for waste minimisation in the minerals industry. Chemical Engineering Journal, 2002, 319-330.
2. Manganaro J, Lawal A. Economics of Thermochemical Conversion of Crop Residue to Liquid Transportation Fuel. Energy Fuels. 2012, 26, 2442-2453.
3. Amoros JL, Beltron V, Sanaz V, Jarque JC. Electrokinetic and rheological properties of highly concentrated kaolin dispersions: Influence of particle volume fraction and dispersant concentration. Applied Clay Science, 2010, 49, 33-43.

4. Ma M. The dispersive effect of sodium silicate on kaolinite particles in process water: Implications for iron ore processing. Clay and Clay Minerals, 2011, 59, 233-239.
5. Conceicao SI, Velho JL, Ferreira JMF. Influence of deagglomeration and carboxymethylcellulose binders on rheological behaviour of kaolin suspensions. Applied Clay Science, 2003, 23, 257-264.
6. Laskowski JT, Liu Q, O'Connor CT. Current understanding of the mechanism of polysaccharide adsorption at the mineral/aqueous solution interface. International Journal of Mineral Processing, 2007, 84, 59-68.
7. Pawlik M, Laskowski JS, Ansari A. Effect of carboxymethyl cellulose and ionic strength on stability of mineral suspensions in potash ore flotation systems. Journal of Colloid Interface Science, 2003, 260, 251-258.
8. Umaran MVA, Menchavez RL. Aqueous dispersion of red clay based ceramic powder with the addition of starch. Materials Research, 2013, 16, 375-384.
9. Li Z, Pang Y, Lou H, Qiu X. Influence of lignosulfonates on the properties of dimethomorph water-dispersible granules. Bioresources, 2009, 4, 589-601.
10. Qin Y, Yang D, Guo W, Qiu X. Investigation of grafted sulfonated alkali lignin polymer as dispersant in coal water slurry. Journal of Industrial Engineering Chemistry, 2015, 27, 192-200.
11. Wu H, Chen F, Feng Q, Yue X. Oxidation and sulfomethylation of alkali extracted lignin from corn stalk. Bioresources. 2012, 7, 2742-2751.
12. Konduri MKR, Kong F, Fatehi P, Production of carboxymethylated lignin and its application as a dispersant. European Polymer Journal, 2015, 70, 371-383.
13. Lin X, Zhou M, Wang S, Lou H, Yang D, Qiu X. Synthesis, Structure, and dispersion property of a novel lignin based polyoxyethylene ether from kraft lignin and poly(ethylene glycol). ACS Sustianable Chemistry and Engineering, 2014, 2, 1902-1909.
14. Pawlik M. Polymeric dispersants for coal water slurries. Colloids and Surfaces A: Physicochemical and Engineering Aspects, 2006, 266, 82-90.
15. Nasser, M. S.; James, A. E.; The effect of polyacrylamide charge density and molecular weight on the flocculation and sedimentation behaviour of kaolinite suspensions. Separation and Purification Technology, 2006, 52, 241-252.

16. Zhou Y, Gan Y, Wanless EJ, Jameson GJ, Franks GV. Interaction forces between silica surfaces in aqueous solutions of cationic polymeric flocculants: effect of polymer charge. Langmuir. 2008, 24, 10920-10928.
17. Chung YL, Ansari S, Estevez L, Hayrapetyan S, Gainnelis EP, Lai HM. Preparation and properties of biodegradable starch-clay nanocomposites. Carbohydrate Polymers. 2010, 79, 391-396.
18. Qin Y, Yang D, Gu F, Li X, Xiong W, Zhu JY. Biorefinery lignosulfonates as a dispersant for coal water slurry. Sustainable Chemical Processes, 4, 2016, 1-8.
19. Das D, Panigrahi S, Mishra PK, Nayak A. Effect of organized assemblies, Part-4. Formulation of highly concentrated coal-water slurry using a natural surfactant. Energy Fuels, 2008, 22, 1865-1872.
20. Li P, Yang D, Lou H, Qiu X. Study on stability of coal water slurry using dispersant-stability analyzer. Journal of Fuel Chemistry and Technology, 2008, 36, 524-529.

# Chapter 1. Literature review

## 1.1 Introduction

This chapter presents an overview of the literature pertinent to the current research of the topic studied in this PhD study. Firstly, general significance about the stabilization of kaolin and coal water slurries will be discussed, and the effect of several dispersing agents applied in the stabilization of clay and coal water slurries will be reviewed. Then, a typical description about kraft lignin and xylan, and their potential application as dispersants will be described. The need for modification of kraft lignin and xylan and different methods employed in the literature for these modifications will be elucidated.

The physiochemical properties of clay and coal particles, as well as the polymers will be discussed. The adsorption of polymers on clay or coal surfaces and significance of adsorption under various conditions will be described. The parameters used in literature to represent the behaviour of clay or coal suspensions will be elucidated.

Secondly, the description and significance of various methods including nuclear magnetic resonance (NMR) spectroscopy, gel permeation chromatography (GPC), dynamic shear rheometer (DSR), Brunauer-Emmett-Teller (BET), zeta potential analyzer, scanning electron microscopy (SEM), thermo gravimetric analyzer, particle charge detector, photometric dispersion analyzer, X-ray diffractometer (XRD), particle size analyzer, and static light scattering analyzer (TURBISCAN), which were extensively used in this work to meet the objectives, will be discussed.

## 1.2 Background

### 1.2.1 Colloidal systems

Colloids are diverse materials with the size range from few nanometers to about 1 micron, uniformly distributed in a dispersion medium. Such diverse materials (colloidal particles) could include solid, liquid or gas. Gels, aerosols, emulsions and foams includes colloidal dispersions [1]. Most of the cases, these colloidal systems are thermodynamically unstable due to their lyophobic nature, and tend to aggregate [2]. In order to prevent aggregation, colloidal particles are typically stabilized by electrostatic repulsions. In the energy outlook, the developed electrostatic repulsion overcomes van der Waals attraction and generates an energy barrier that

depreciates the aggregation. This phenomenon of colloidal systems is interpreted by the DLVO (Derjaguin-Landau-Vervey-Overbeek) theory [3].

### 1.2.2 Use of colloidal systems

Colloid systems are present in many industrial processes, such as the mining, mineral, painting, ceramics, pharmaceutical and ceramics [4]. In many practical applications, , such as drug formulations and delivery systems [5], paintings or film forming dispersions [6], formulation of printing inks, dispersion of mud during drilling of oil sands [7] and clay dispersions in mining, mineral and cosmetic industries [8], the controlled dispersion of the colloidal particles is necessary. Kaolin is the major clay mineral present in various processing and production stages of paper, mining, mineral and ceramic industries [9]. Colloidal dispersions of coal in water seems to be a promising alternative fuel for fossil fuels [10]. In all of these cases, a fundamental understanding of interactions between the colloidal particles will lead to have a better dispersion outcome.

### 1.2.3 Morphology and surface chemistry of kaolin

Kaolin is a white, soil mineral that is composed of fine grained hexagonal plate-like particles. It is most commonly found in the form of kaolin clay, a fine clay which was originally produced in China, and thus sometimes referred as “China clay.” In addition, kaolin clay is composed of numerous minerals such as quartz, kaolinite, hematite, magnetite, gibbsite and halloysite [11, 12]. The chemical and mineralogical compositions of kaolin clay are shown in Table 1.1.

Table 1-1.Chemical and mineralogical compositions of typical kaolin clay [17]

| Chemical compositions | | | | Mineral compositions | |
|---|---|---|---|---|---|
| Element | wt.% | Calculated oxides | wt.% | Mineral | wt.% |
| O | 49.88 | | | kaolinite | 34 |
| Al | 21.54 | $Al_2O_3$ | 40.71 | Dickite | 29 |
| Si | 25.94 | $SiO_2$ | 55.49 | Narcite | 28 |
| Ti | 0.65 | $TiO_2$ | 1.09 | Tridymite | 4 |
| Fe | 0.51 | $FeO_2$ | 0.66 | Hematite | 2 |
| Cu | 0.60 | CuO | 0.75 | Magnetite | 2 |
| Mn | 0.33 | MnO | 0.61 | | |
| P | 0.18 | $P_2O_5$ | 0.42 | | |
| Na | 0.21 | $Na_2O_8$ | 0.28 | | |

Chemically, kaolin is a hydrated aluminosilicate structure with empirical formula of $Al_2Si_2O_5(OH)_4$ (39,8 % alumina, 46,3 % silica, 13,9 % water) [11]. Structurally, kaolin is a 1:1 sheet structure consisting of $SiO_4$ tetrahedral sheet and $Al(O,OH)_6$ octahedral sheet. Both the sheets are arranged alternately with silicon oxygen tetrahedral layer joined to alumina octahedral layer by hydrogen bonding [$O_6 – Si_4 – O_4 – (OH)_2 – Al_4 – (OH)_6$] [11, 13]. The model structure of kaolin designed by Brindley and Nakahira was shown in Figure 1.1. Kaolin crystal has a molecular weight of 258,071 g/mol. The diameter of kaolin crystals was reported in the range of 0.2–10 μm, with thickness, 0.7 nm and density, 2.6 g/cm$^3$ [12, 13].

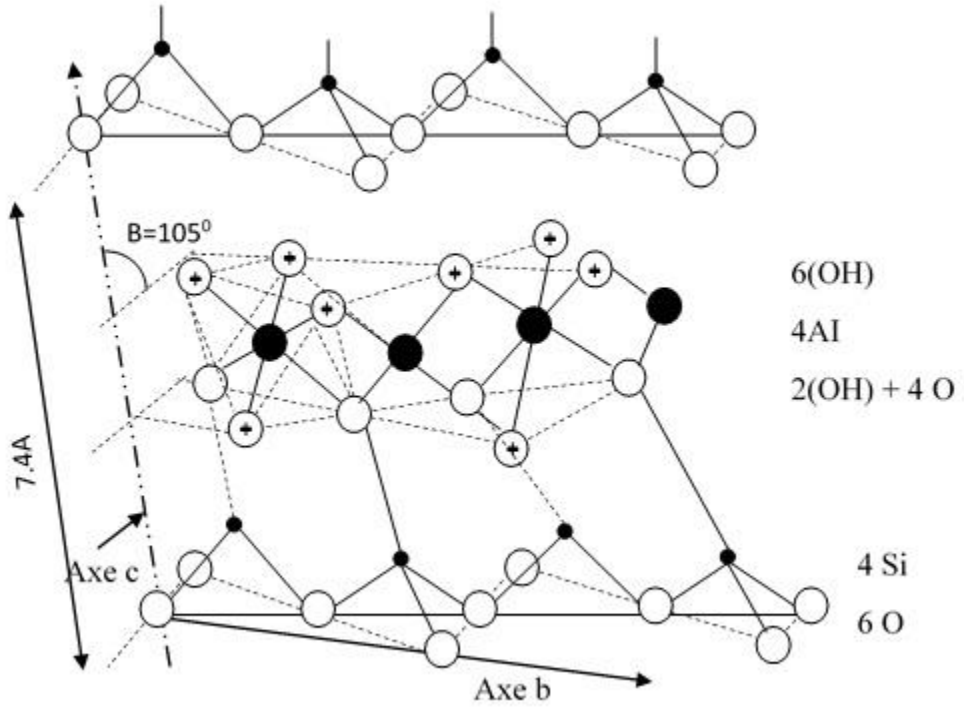


Figure 1-1. Model structure of kaolin by Brindley and Nakahira [13]

It was reported that the silica basal plane of kaolin carry a permanent negative charge due to isomorphous substitution of $Al^{3+}$ for $Si^{4+}$ in the silica tetrahedral sheet [11]. The octahedral sheet carries hydroxyl groups on surface, being less reactive compared OH groups on edges, which render pH dependent charges [13]. Also, $Al^{3+}$ renders positive charge and/or negative charge due to isomorphic substitution with $Mg^{2+}$. The edges of silica and alumina sheets possess highly reactive $H^+$ and $OH^-$ ions and therefore changing pH greatly affects the edge charges of kaolin

[11, 12, 13]. This indicates kaolin particles carry both positive and negative charges over a wide pH range (3.5-8.5).

### 1.2.4 Morphology and surface chemistry of coal

Coals are heterogeneous solids that vary widely in their chemical and physical properties. Typically, coal is a complex material consisting of organic and inorganic compounds. Organic compounds that includes carbon, hydrogen, oxygen, nitrogen and sulfur dominates and constitutes about 85-95 wt% of coal [14]. As reported previously, coal possess very low sulfur content (< 1 %) making it a suitable material for power generation and synthesis of clean conversion products [14]. Inorganic components, particularly alumino silicates and pyrites constitutes of 5-15% of coal. The carbon content of coals ranges between 65 and 95 %, while oxygen and hydrogen contents typically range between 2 and 30% as well as 2 and 7%, respectively. The nitrogen and sulfur contents of coal is only 1-4%. This hydrogen deficient, and atomic hydrogen to carbon ratio (~ 0.9) suggests a complex aromatic structure of coal (Figure 1.2) [15].

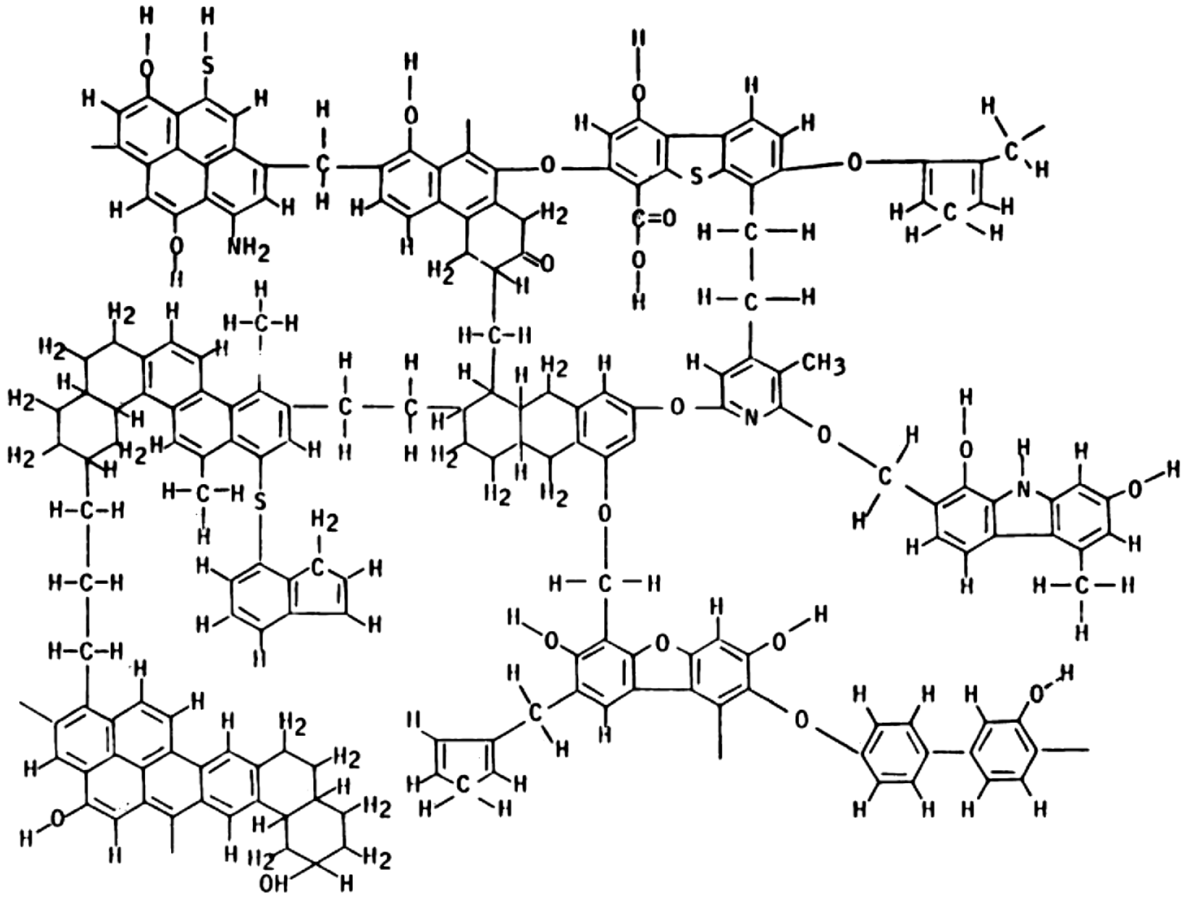

Figure 1-2. Model structure of bituminous coal with chemical groups as proposed by W. H.Wiser [15]

Another important feature associated with coal is extensive network of pores, which gives a high surface area (> 100 $m^2/g$) to the coals. Depending on carbon content, the percentage of volatile matter and heating value, coals are classified in to four types of anthracite, bituminous, subbituminous and lignite, and are shown in Table 1.2 [14].

Table 1-2. Classification of coals [14]

| Type | Carbon content, % | Calorific value, BTU/lb | Volatile matter, % |
|---|---|---|---|
| Anthracite | 90-95 | ~15000 | 2-8 |
| Bituminous | 75-90 | 12000-15000 | 14-22 |
| Subbituminous | 70-75 | ~10000 | 22-31 |
| Lignite | 65-70 | ~7000 | >32 |

The significant amounts of aromatic and naphthalene structures of coal (as shown in Figure 1.2) represent the hydrophobic nature of coal, which causes the coal particles to aggregate via hydrophobic interactions [20, 21]. In addition to nonpolar groups, the significant number of polar groups such as hydroxyls (-OH), carboxyls (COO-) also contribute to chemistry of coal. These types of oxygen functional groups strongly influence the reactivity of coal and gives coal negative charge under natural conditions. The inorganic content, which constitutes polyvalent metal ions ($Si^{+4}$, $Al^{+3}$ and $Fe^{+2}$) acts as the source of positive sites on coal [13, 14, 15].

### 1.2.5 Dispersion of kaolin suspensions

The flow behavior of kaolin suspensions is important in paper, mining, ceramic and paint industries, which is crucial to produce final products with best properties and to optimize the economics of process and energy requirements [9, 10]. However, as described previously (section 1.2.3), the surface of kaolin particles is usually heterogeneous consisting of positive charges at the edges and negative charges on the basal face, and the interaction of these charges with surrounding environment promotes the aggregation of particles and hinders suspension fluidity. Practically, the dispersion of kaolin particles can be improved by increasing the shear rate [10]. However, considering their energy need, it was an expensive method. Numerous studies on stability of kaolin suspensions reported that chemicals, such as dispersants, were effective in improving the fluidity of suspensions [16, 17, 18].

### 1.2.6 Dispersion of coal suspensions

The indiscriminate use of oil and their derived products has led to energy depletion. Numerous studies have reported alternative energy sources, such as biodiesel, hydrogen fuel, biofuel and coal water slurry (CWS) [10, 16, 19]. Coal water suspensions (CWS) seems to be a promising fuel due to its low production cost and ease of handling, and thus may be considered as an efficient alternative. For CWS to be an effective fuel, it should have a high coal content for heat demand [10, 19]. However, at such high coal solid concentrations, coal particles may not remain stable in slurry due to increased interactions between the coal particles due to hydrophobic interactions between the particles as described in section 1.2.4. The addition of chemicals, such as dispersants, can minimize the interaction of particles and improve the fluid properties of the slurries, thus improving the performance of CWS as fuel.

### 1.2.7 Dispersants for mineral suspensions

Dispersants are chemicals that reduce the interactions between mineral particles by binding on their surface and increasing their surface charges. Various types of dispersants and their applications in various areas was shown in Table 1.3.

Table 1-3. Represents various current market available dispersants and their applications

| Dispersant | Application | Reference |
|---|---|---|
| Sodium hexametaphosphate | Iron ore-ultrafine/recovery | [20] |
| Sodium dodecyl benzene | Bentonite dispersion/$Fe_3O_4$ in suspension/recovery | [20] |
| Sodium humate | Dispersion of Iron ore fines | [21] |
| Sodium silicate | Minerals/fine grinding | [21] |
| Sodium hydroxide and nitric acid | Quartz dispersion | |
| Polyacrylic acid | Dispersion of paint emulsions or latex/ceramic systems, thinning agents for clay based drilling muds | [22] |
| Polymethacrylic acid | Dolomite dispersion | [22] |
| Polyurethanes | Dispersants for mill base pigment loadings | [23] |
| Polyphosphates | Dispersion of clay, hydroxyapatite and silica based suspensions | [22] |
| Polyaspartic acid | Stabilization of kaolin suspensions | [24] |
| Acrylic acid and maleic acid based polymers | Dispersion of iron oxide suspensions | [25] |
| Napthalene fomaldehyde sodium salt | Static coal dispersion stability | [26] |
| Polycarboxylic acids and polyoxyesters | Stability of high coal loadings, superplasticizers in concrete industry | [25, 26] |
| Lignosulfonates | Super plasticizer in concrete mixtures, thinning agents for clay based drilling muds | [25] |
| Carboxymethyl cellulose | Improves evenness of paper due to high affinity with pulp fibers and filler particles | [25] |

Although synthetic dispersants are effective, there are concerns about their non-biodegradable nature and health impacts, and as such, there is a strong incentive for producing green dispersants [25, 26].

In the past, the utilization of natural polymers as dispersants in clay and coal dispersions was reported [26, 27, 28, 29]. Penkavova and coauthors added carboxymethylated cellulose (0.8 wt.%) to a kaolin dispersion, which increased its stability by 20% at pH 6 [8]. Pawlik and coauthors used carboxymethylated cellulose (CMC) for the stabilization of dolomite dispersions, which improved the turbidity of dispersions from 20 to 90% [30]. The starch, as a dispersant, for red kaolin based ceramic dispersions (at pH 7) was studied previously [31], which successfully improved the fluidity of dispersions. However, starch is mainly used as a food product and cellulose is widely used in the paper production, thus they may have limited availability to be used for other purposes including dispersant productions. On the other hand, lignin and xylan, most abundant sustainable polymers in nature, has limited industrial applications. Kraft lignin and xylan, which are produced in plentiful during kraft pulping process, have enormous potential for the production of value added products such as phenols, carbon fibers, dispersants, flocculants, films, and adhesives [32, 33, 34].

### 1.2.8 Lignin

Lignin is the second most abundant natural polymer on earth, which constitutes ~30% of the dry weight of softwood and ~20% of hardwood [32]. It binds other wood components that are mainly cellulose and hemicelluloses. In trees, lignin provides structural integrity and also minimizes the effects of mechanical stress. The presence of lignin in woody plants improves water impermeability and also enhances the resistance against microorganisms [32, 33].

#### 1.2.8.1 Structure of lignin

Lignin is comprised of three basic phenylpropanoid monomers, also known as 'monolignols' which includes coniferyl alcohol, *p*-coumaryl alcohol, and sinapyl alcohol, as shown in Figure 1.3. [33]. These monomers differs only by the presence of substituted methoxy group at the phenyl ring. Furthermore, the composition of each lignin monomer differs significantly with the type of plant material (Table 1.4). Softwood lignin, found in coniferous trees such as pine tree, composed mainly of coniferyl alcohol and a trace amount of sinapyl alcohol, while, hardwood lignin, found in tropical and subtropical trees such as oak and teak, contains both coniferyl and

sinapyl alcohols in considerable amounts. On the other hand, lignin present in grasses contains significant amounts of *p*-coumaryl alcohol [34, 35].

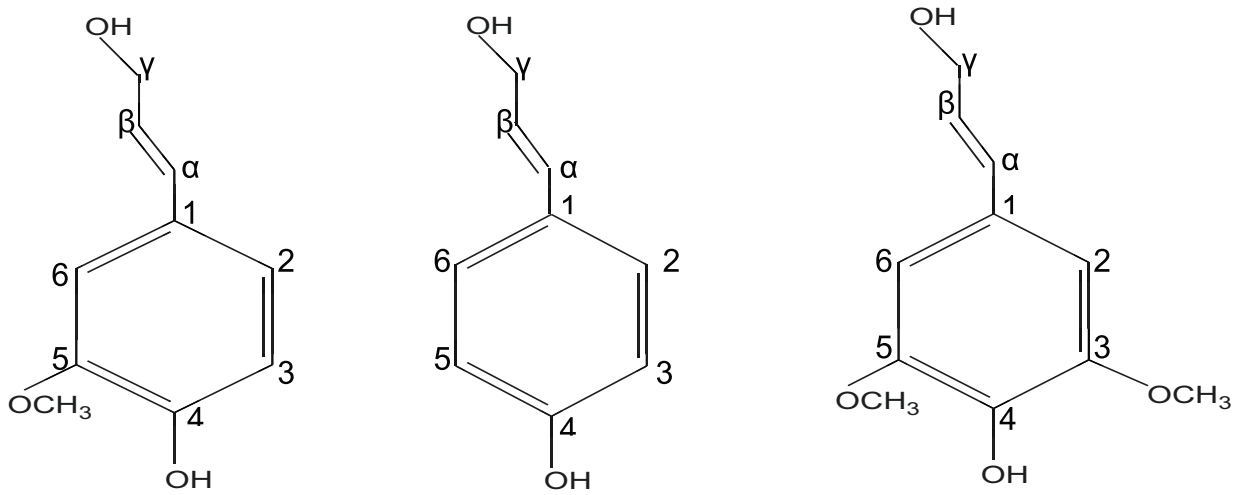


Figure 1-3. Lignin monomers: a) coniferyl b) *P*-coumaryl and c) sinapyl alcohols

Table 1-4.Compositions of lignin monomers in wood and non-wood plants [34, 35]

| Type of material | Coniferyl alcohol | P-Coumaryl alcohol | Sinapyl alcohol |
|---|---|---|---|
| Hardwood | 1-9 | 23-49 | 45-77 |
| Softwood | 1-5 | 90-95 | Neglisable amounts |
| Grasses | 3-36 | 35-79 | 22-82 |

The random coupling reactions between these lignin monomers result in a complex three-dimensional network with a high heterogeneity in composition, linkages and functional groups. Therefore, there is no definitive structure model for lignin in native form. The most common model is described by Alder [35, 36] and is shown in Figure 1.4.

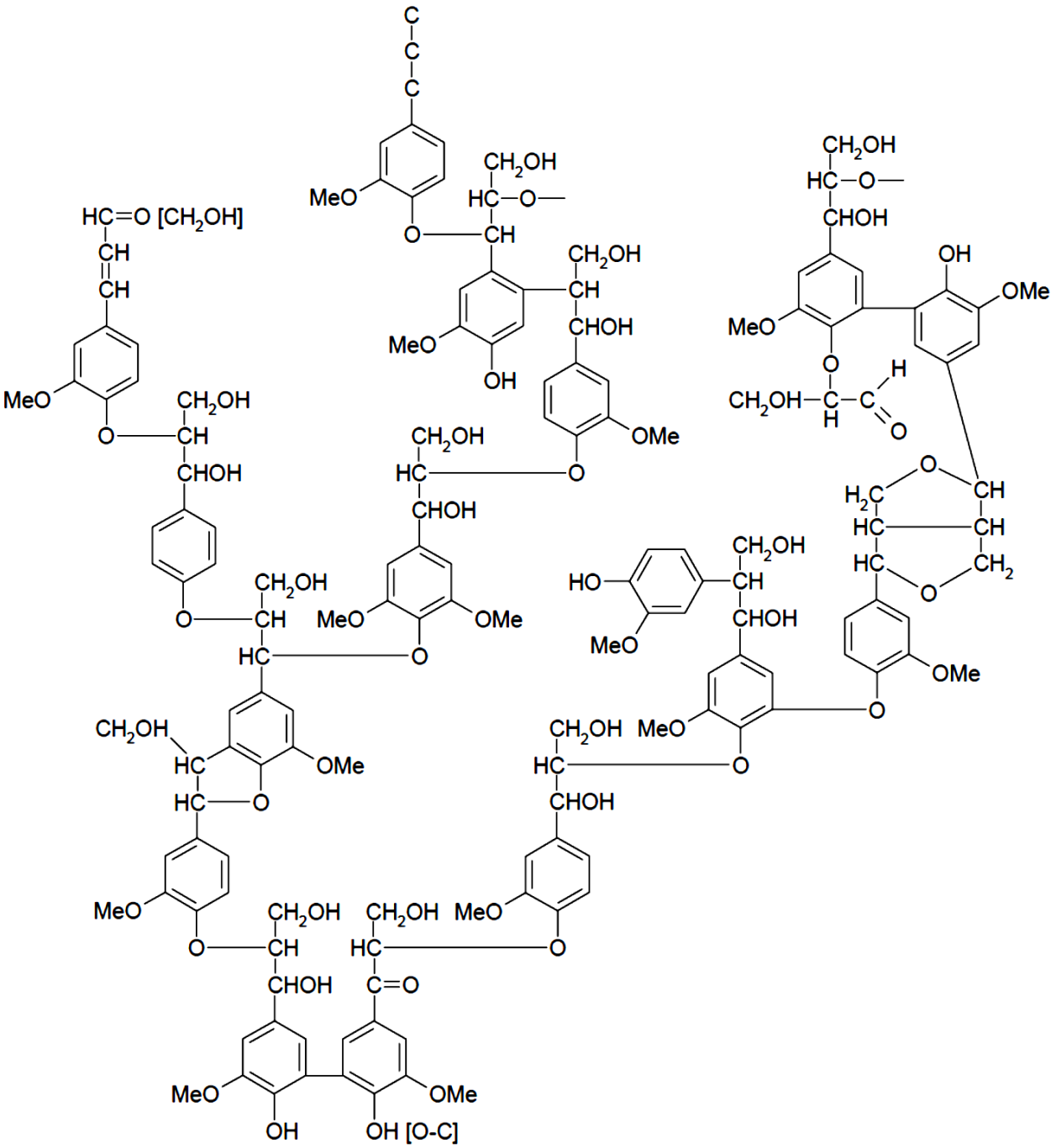


Figure 1-4. Structural model of hardwood kraft lignin [36]

The structural model shown in figure 1.4 indicates that lignin monomers are joined together by several types of ether and carbon-carbon linkages. Although, there are 20 different types of linkages, the most common types of linkages found in lignin macromolecule are β-O-4, α-O-4, 5-5, β-5, 4-O-5, β-β and β-1, and as represented in Figure 1.5. The ether type of linkages were dominant and accounts for two thirds of lignin linkages. Furthermore, the respective amounts of

these linkages vary between softwood and hardwood species, adding to the complexity of lignin [35, 36] The types of linkages and their respective amounts in softwood and hardwood species were shown in Table 1.5.

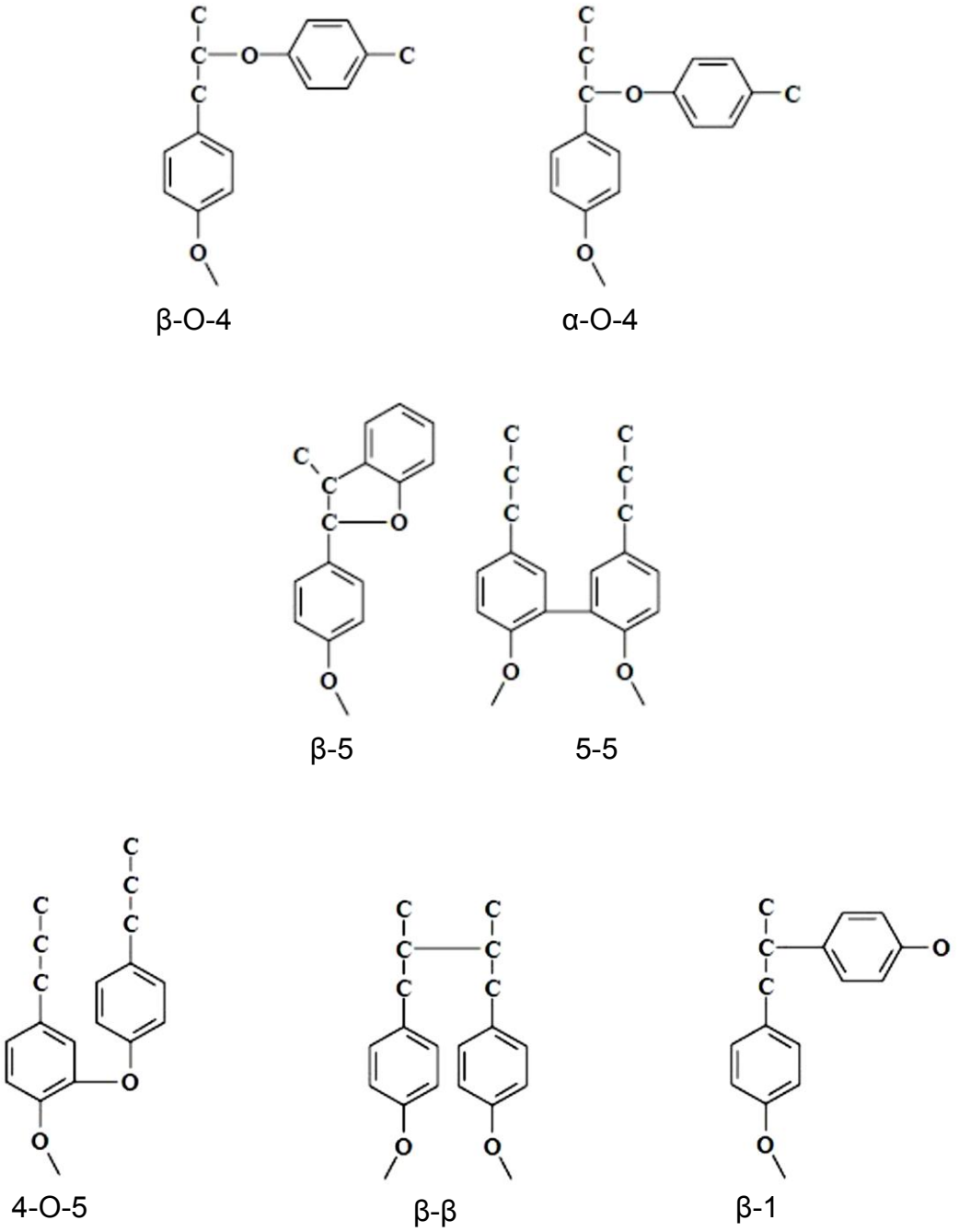


Figure 1-5.Phenylpropane linkages in lignin [36]

Table 1-5: Proportion of linkages types in hardwood and softwood in terms of percentage [35]

| Linkage types | Hardwood | Softwood |
|---|---|---|
| β-O-4 | 60 | 46 |
| α-O-4 | 6-8 | 6-8 |
| 4-O-5 | 6.5 | 4 |
| β-5 | 6 | 9-12 |
| 5-5 | 6 | 9-11 |
| β-β | 3 | 2 |
| β-1 | 7 | 7 |

#### 1.2.8.2 Production of lignin

Lignin present in the plant biomass is currently isolated in large amounts via sulfite and kraft pulping chemical processes. Around 8-9 million tonnes of lignin are produced annually in chemical pulp mills. The sulfite pulping process produces wood pulp, which is almost pure cellulose fibers by using various salts of sulfurous acid to extract the lignin from wood chips. However, the production of lignosulfonates is limited due to limited sulfite mills worldwide [37, 38, 39].

Kraft pulping process involves conversion of wood into wood pulp by treating wood chips with sodium hydroxide and sodium sulfide, which are used in breaking of bonds between lignin and cellulose. The lignin fragments dissolve in strongly basic medium, and the mixture is termed as black liquor [40, 41]. Due to its surplus production, and their potential to produce various valuable products, kraft lignin can be a suitable biopolymer to be studied as dispersants for clay or coal suspensions.

### 1.2.9 Xylan

Xylan is the second most abundant hemicellulosic polysaacharide, found commonly in hardwood and annual plants [42]. Xylan is closely associated with cellulose in the cell walls and accounts for about 30-35 % dry weight of wood [42]. Lignin carbohydrate complexes are also assumed to be formed between lignins and xylans. Mostly, xylans are heteropolysaccharides with β-1,4 linked D-xylopyranosyl linear backbone and a variety of side chains based on D-glucuronopyranosyl, L-arabinofuranosyl, D-xylopyranosyl, D-galactopyranosyl, 4-O-methyl-D-

glucuronopyranosyl, acetyl and feruloyl groups [42, 43]. The structure of xylans varies significantly between different plant species.

### 1.2.9.1 Common types of xylan and their structure

Arabinoxylans are commonly found in annual plants *viz*., corn, rice, rye, barley and wheat, composed of linear xylose backbone with arabinofuranosyl substitutes attached as the side chains as shown in Figure 1.6. These side chains are substituted either at C2 or C3 positions or at both carbon positions. The presence of arabinose substituent decreases the flexibility of polymer. However, the type of substituent varies with the source. The degree of polymerization (DP) of xylan would be generally in the range of 50-110 [42, 43].

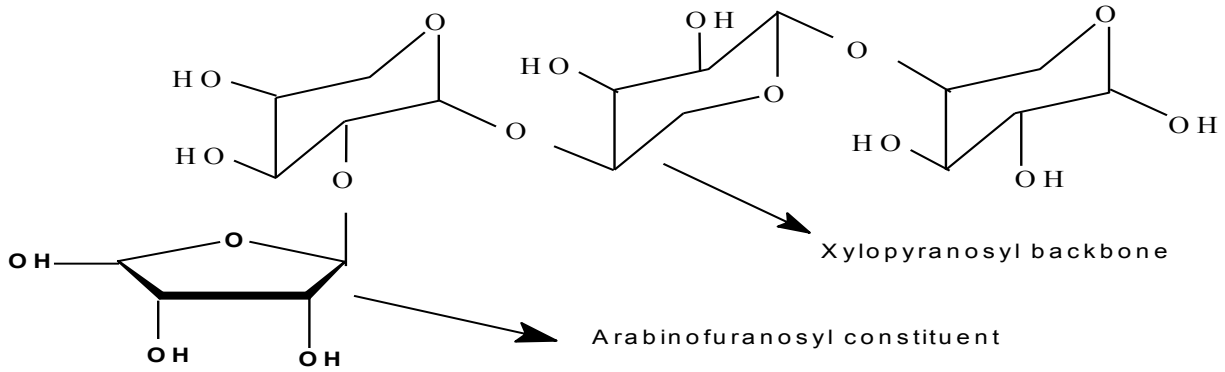


Figure 1-6. Structure of arabinoxylan

Glucuronoxylans and arabinoglucuronoxylans are the typical xylans found in hardwood (aspen, beech, birch) and softwood species (pine, spruce, cedar). The degree of polymerization (DP) of both hardwood and softwood xylans was between 100- 200. Both xylans composed of linear xylopyranosyl backbone with substituted methyl glucuronic acids in the side chains. However, in addition to side groups, glucronoxylan have O-acetyl substituents at C2 or C3 positions of xylose units (Figure 1.7) [42, 43]. The presence of these acetyl groups makes xylan partially soluble in water.

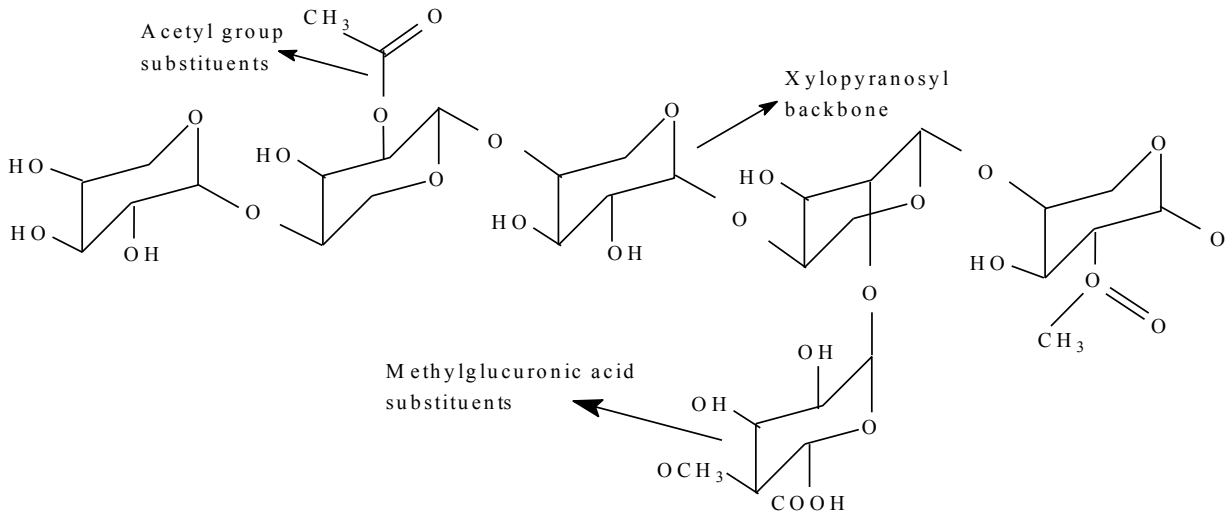


Figure 1-7. Structure of glucuronoxylan present in hardwood species

It has been reported that, unsubstituted xylan able to form crystals in water. However, the diverse substituent groups on the xylan back bone prevent the xylan macromolecule to form crystal structures as cellulose does, thus significantly influencing the properties of xylans [43, 44]. This leads to the amorphous structure and water solubility of the xylans. Previously, it has been reported that an increase or decrease of arabinose substitution directly influenced the solubility of arabinoxylans in water [44]. Substituent groups determine not only the xylan morphology and solubility in water but also the interactions with other surrounding systems. For example, parts of the xylan backbone with low substitution are more rigid in nature. These chemical and physical properties of hardwood or softwood xylan make it a suitable natural polymer for the dispersion of clay or coal suspensions [45, 46].

#### 1.2.9.2 Production of xylan

The prehydrolysis step of kraft pulping method is crucial in the production of dissolving pulp. Furthermore, kraft processes provide the option to extract hemicelluloses before or after pulping in a separate process step, which makes the isolation of the different wood components easier. Much effort has been undertaken to investigate the possibility of hemicellulose removal before alkaline cooking [47]. Van Heiningen and co-workers suggest the integration of water prehydrolysis into alkaline pulping concepts to develop a biorefinery. 70% of the hemicelluloses of southern mixed hardwood could be dissolved as xylo-oligosaccahrides in the autohydroylsis step before the cooking process [48]. The extracted xylan can be used as a dispersant for clay or coal dispersion.

### 1.2.10 Modification of kraft lignin or xylan

In comparison with other wood based materials, such as cellulose, which can be easily modified, the modification of kraft lignin is challenging due to its structural complexity [41, 49]. In the absence of any modification, the α position and phenolic OH groups of these phenyl propene subunits of kraft lignin present the most reactive sites for any reaction. However, the β-O-4 aryl ether linkages and others interconnecting bonds create significant steric hindrance or occupy these reactive sites, which leads to limited reactivity of kraft lignin for modification [33, 34, 35]. Similarly, xylan in the dissolving pulp production process is partially soluble in water and with limited reactivity due to lack of sufficient number of functional groups. Furthermore, the structural complexity of xylan makes its challenging for modification. The OH groups at C2 or C3 positions of xylan backbone are the most reactive sites. However, the substituent groups linked to xylan backbone via glycosidic linkages prevent accessibility to these reactive sites [41, 42]. Thus, the modification of xylan is essential to improve its functional properties as well as its solubility in water. Various processes have been proposed to modify lignin and xylan, which includes carboxymethylation, sulfomethylation, oxidation, phenolation, demethylation and hydroxymethylation [50, 51, 52, 53, 54].

#### 1.2.10.1 Modification processes

The carboxymethylation is an important etherification process performed to improve the reactivity of lignin or xylan using sodium chloroacetate as a carboxylate group donor (Figure 1.8). Under alkali conditions, NaOH reacts with the hydroxyl group of the xylan backbone or lignin's aromatic ring, generating a strong nucleophile. In case of lignin, both phenolic OH and aliphatic OH serve as reactive sites, however, the former one is more reactive, as mostly the aliphatic OH are involved in strong aryl ether linkages. The alkoxide ion from the alkali lignin or xylan attacks the chloroacetate via a $S_N2$ reacting resulting in the ether methyl carboxylation of lignin or xylan. The degree of carboxymethylation depends on the number of hydroxyl group substitution with carboxymethyl groups [50].

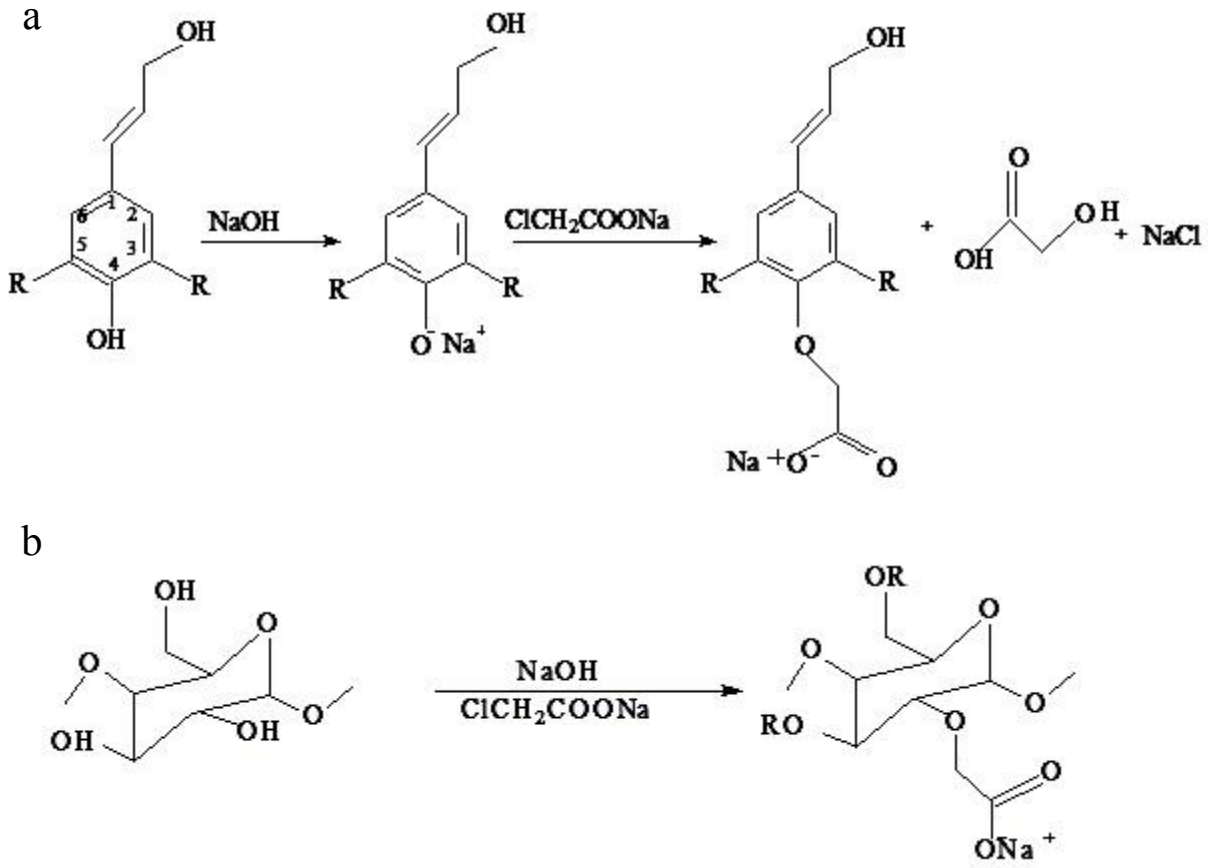


Figure 1-8.Carboxymethylation of a) lignin and b) xylan under alkali conditions with sodium chloroacetate

Sulfomethylation process is the addition of methylene sulfonate, $–CH_2SO_3$, group to lignin or xylan. The addition of methylene sulfonate groups to lignin has been proposed as a means of improving the tanning capacity of lignin. The reaction is performed in the presence of formaldehyde, alkali metal sulfite salt, and reactable phenolic OH groups in water under neutral to basic pH and 100 °C temperature [52].These methyl sulfonate groups are grafted onto the OH groups of lignin or xylan during the sulfomethylation reaction via the nucleophilic substitution mechanism as shown in Figure 1.9. This sulfomethylation improves the reactivity of lignin or xylan by grafting functional sulfomethyl groups at the ortho sites of lignin or at the backbone of xylan [51]. Previously, it was applied to kraft lignins by the Westvaco Corporation to form dye dispersants that are marketed under the Reaxtrade name [55].

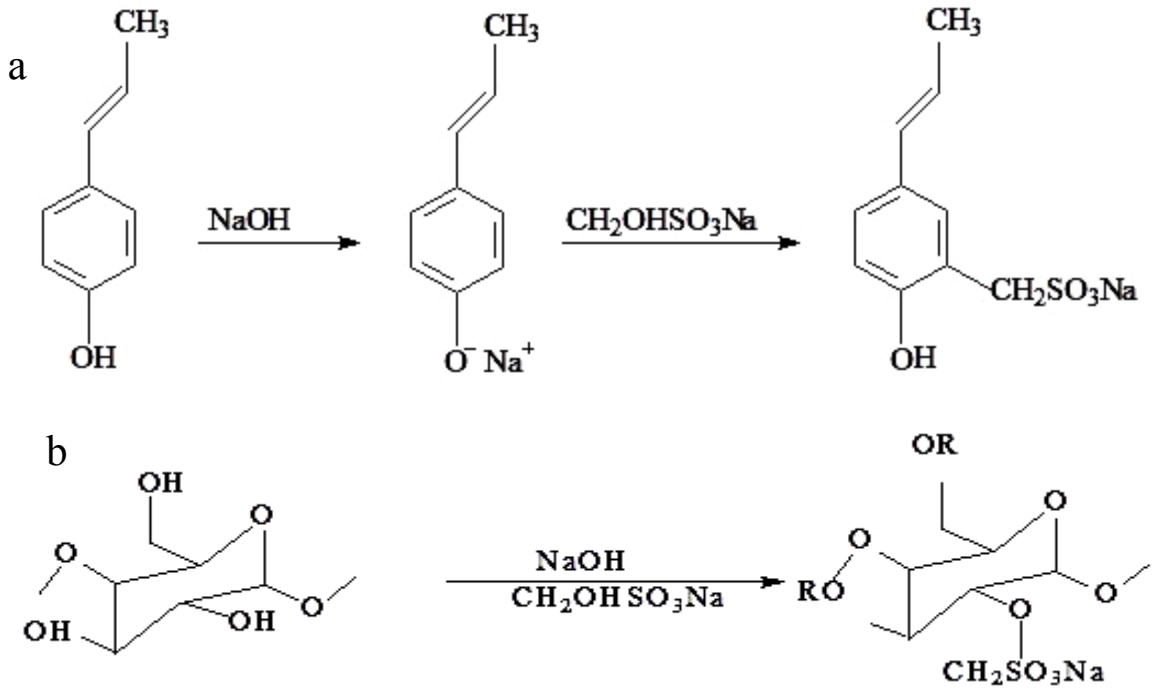


Figure 1-9. Sulfomethylation of a) lignin or b) xylan under alkali conditions with formaldehyde and sodium sulfite

The chemical oxidation of lignin with hydrogen peroxide or nitric acid found to improve the reactivity of lignin via generating 4-hydroxy 3-methoxybenzaldehyde and variety of low molecular weight compounds with carboxyl groups in the aliphatic side chains (Figure 1.10). The investigations led by Kadla and coauthors showed that the oxidation of etherified lignin model compounds using hydrogen peroxide at 90 °C generated carboxyl groups in the side chains keeping the phenolic ring intact [52]. The tendency of oxidation of xylan depends on the nature of oxidation and the conditions of the reactions. As described in the literature, the oxidation of xylan under selective conditions produced intermediates with carboxyl and carbonyl groups and also resulted in depolymerisation of xylan macromolecule. In principle, the oxidation of xylan with sodium periodate results in 2 keto, 3 keto, 2,3 diketoxylan, 2, 3 dialdehyde and 2,3 dicarboxyl intermediates as shown in Figure 1.10b [53]. This oxidation of kraft lignin or xylan is a simple method to improve the reactivity of lignin by generating functional groups.

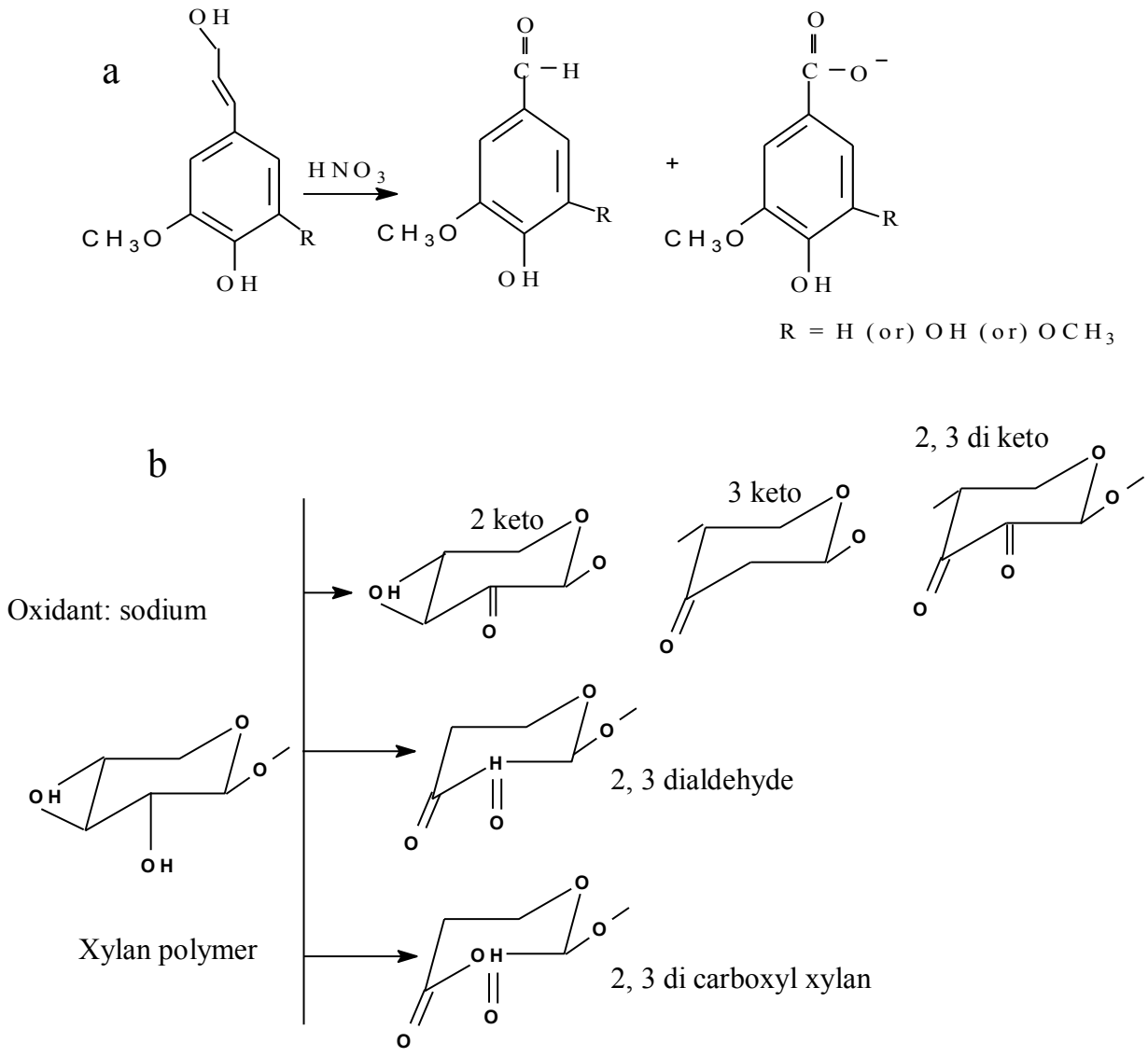


Figure 1-10. a) Oxidation of lignin with nitric acid and b) oxidation of xylan with sodium periodate

The demethylation of lignin selectively removes methoxy group, which blocks the reactive hydroxide group attached to the aromatic unit of lignin. However, this reaction involves enzymes for oxidative cleavage of methoxy groups. Although enzymatic processes are selective, the longer reaction times and cost of these processes complicate their industrial applicability [54].

The reactivity of lignin can also be improved through the hydroxymethylation, which involves the introduction of reactive hydroxymethyl groups in the ortho position of the lignin's aromatic unit via Lederer-Manasse reaction (Figure 1.11) and also at the β carbon of aliphatic chain via Tollens reaction [54]. The reaction includes alkali conditions with formaldehyde as a

hydroxymethylation agent. The activation energy of hydroxymethylation is very low (15 kcal/mol), which implies that accessibility is the significant factor for hydroxymethylation of lignin [54].

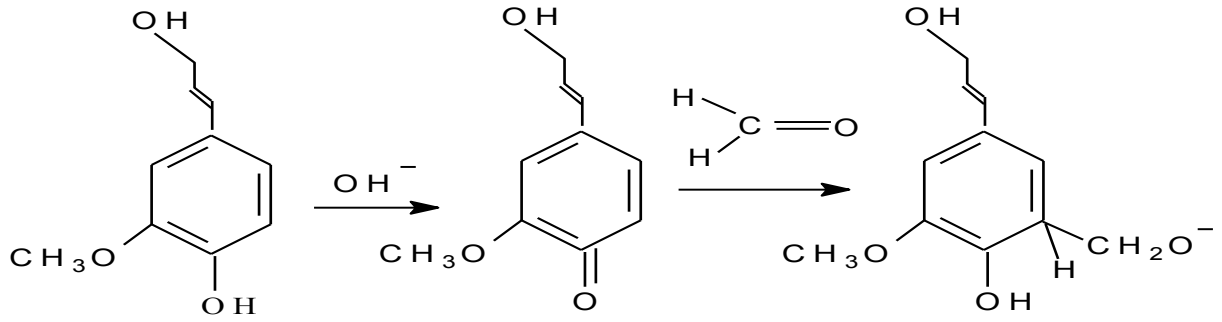

Figure 1-11.Hydromethylation of lignin with formaldehyde under aqueous conditions

Acetylation is a modification typically employed to improve the functional reactivity of xylan in film and thickening agent productions. The ester groups are attached to hydroxyl groups of xylan in the presence of catalyst under alkali conditions as shown in the Figure (Figure 1.12). The basic reaction mechanism in this case starts with a nucleophilic attack of the lone electron pair of the alcoholic sugar OH group on the carbonyl carbon atom of the acetic acid anhydride molecule. Due to the consequent splitting of acetic acid, acetylated carbohydrates are formed [53]. This reaction is often performed with acid or base catalysis.

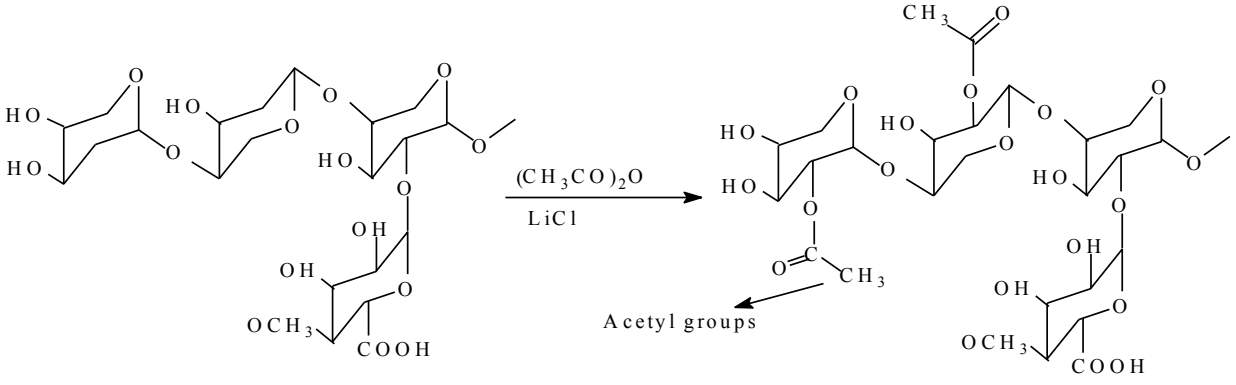


Figure 1-12.Acetylation of xylan using acetic anhydride with LiCl as a catalyst

Among all the methods discussed, carboxymethylation, sulfomethylation and oxidation were found to be simple (includes less time consuming) and more productive modification processes (i.e. more efficient grafting ratio) than others. Thus, in our work carboxymethylation, sulfomethylation and oxidation mechanisms are employed to modify kraft lignin or xylan.

#### 1.2.10.2 Lignin applications

Lignosulfonates with sulfonate groups are used as superplasticizers in cement admixture due to their sulfonated group [25, 26]. Previously, wheat straw lignin, which was hydroxymethylated and sulfonated by $Na_2SO_3$ in a formaldehyde solution, exhibited better fluidity compared to commercially available lignosulfonates [56]. He and Fatehi produced oxidised sulfomethylated lignin using hydrogen peroxide and sodium sulfite, which exhibited better plasticizer performance in cement suspensions than commercial lignosulfonate [57]. Alternatively, an anionic lignin-based product (0.2 wt.%) obtained via chemical modification of hardwood kraft lignin with sodium chloroacetate improved the dispersion efficiency of clay suspensions (20 g/L) by 50 % [58]. In a study on the dispersion of dimethomorph pesticide granules in an aqueous medium, kraft lignin-polyethylene glycol copolymer at 2.5 wt.% dosage decreased the viscosity of suspension from 1000 to 100 mPa.s [59]

### 1.2.11 Applications of xylan

Due to a variety of functional group attachment to xylans, different applications were produced for modified xylans [42, 50, 51]. Xylooligosaccharides are of interest due to their health benefits as prebiotics on the intestinal, their food flavour modifying characteristics and acidic oligosaccharides that possess antimicrobial properties [42, 43]. Studies on the modification of xylan to improve their functional properties suggest that the modified anionic xylans could be used as dispersants for kaolin suspensions [52, 53, 54].

### 1.2.12 Adsorption of polymers on colloidal particles

#### 1.2.12.1 Significance of polymer adsorption

For a polymer to improve the dispersion properties of colloidal suspensions, it has to adsorb on the surface of colloidal particles. By adsorbing polymers on the surface of clay or coal particles, the surface morphology and chemistry of coal or clay particles are changed [58]. However, the adsorption of polymers may be affected by the concentration of polymer, suspension pH and also presence of salts in the suspensions. The low concentration of polymers may result in poor dispersion of clay or coal suspensions due to low adsorption. The presence of salts may compete and interfere with the adsorption of polymers on colloidal particles [60]. Thus, it is important to understand the interactions between the polymers and the particles in the suspensions and to investigate the impact of adsorption conditions on the stabilization of colloidal suspensions.

The adsorption characteristics of polymers on clay or coal particles have been extensively studied [58, 59, 60]. As described previously, polymer is adsorbed through different interaction

mechanisms, e.g., van der Waals attraction, hydrogen bonding and electrostatic ion exchange interaction [25, 26]. Since lignosulfonates and polyacrylic acid are generally used in the stabilization of clay, coal and cement dispersions, there are several studies about the adsorption characteristics of these polymers under various conditions on clay and coal particles [25, 26]. However, the adsorption characteristics of the anionic kraft lignin or xylan on clay and coal particles have not been systematically investigated yet.

#### 1.2.12.2 Adsorption isotherms and kinetics

Adsorption isotherms indicate the equilibrium between the adsorbed and remaining amounts in the suspension and exhibit the adsorption affinity of polymers on surfaces. [61]. The maximum change in surface morphology and chemistry of coal or clay, which affects the dispersion properties of suspensions, can be determined by adsorption isotherm analysis. The time required for adsorbing anionic polymers on clay or coal particles in the suspensions is also critical. The adsorption configuration of anionic polymer on clay or coal particles depends on rate of adsorption. If a polymer adsorbed quickly, it could act as a dispersant quickly, which would impact its end-use applications [61, 62].

#### 1.2.12.3 Effect of pH

The pH of reaction processes in various mineral industries usually varies from acidic to alkaline with pH as low as 2-3 due to the oxidation of sulfide minerals and 10-11 due to dissolution of basic minerals such as carbonates [9, 10]. Therefore, dispersants used in mineral industry should be resistant to pH changes and able to disperse suspensions under varied pH conditions. As described previously, the surface of clay and coal particles possess both negative and positive charges and the amount of respective charges varies with pH. These changes will impact the adsorption of polymers on the surfaces, and thus the efficiencies of polymers as dispersants. Thus, it is crucial to investigate the adsorption behavior of polymers on clay and coal particles at different pHs.

#### 1.2.12.4 Effect of charge density and molecular weight

The dispersion of colloidal suspensions is a complex process, and is influenced by the adsorption of polymers and the characteristics of adsorbed polymers as described in section 1.2.15.3. The characteristics of polymers, such as charge density and molecular weight, are known to affect their adsorption [63, 64, 65]. As described in the literature, anionic polymers with different charge densities tend to adsorb and configure differently on the clay or coal surfaces [64, 65].

Nasser and James reported that high charge density anionic polymers adsorbed more than low charge density polymers on clay surface [66]. As reported, highly charged polymers tend to adsorb more on the positive regions of clay surface due to strong electrostatic interactions [63, 64]. Lowly charged anionic polymers tend to develop tail and loop configuration, while highly charged ones tend to exhibit a flat configuration on clay or coal surface [65, 66]. This indicates that various anionic polymers cover the cationic sites of clay or coal surface differently, which affects their adsorption amounts.

Zhu and co-authors reported that low molecular weight anionic polymers incline to adsorb more quickly on the clay surface compared to high molecular weight polymers [64]. As is well known, low molecular weight polymers are able to adsorb and reconfigure completely and quickly on the clay surface which would facilitate the adsorption of other approaching polymers on the surface. On the other hand, the high molecular weight anionic polymers adsorb and configure at a slower pace, which would hamper the adsorption of other approaching polymers from the adsorption medium on surfaces. [66]. Therefore, it is worth investigating how the charge density and molecular weight of anionic polymers affect their adsorption on clay or coal surfaces.

### 1.2.13 Zeta potential of colloidal suspensions

Colloidal particles attain charge due to dissolution of surface functional groups in suspensions. The net surface charges, that are developed at the surface affects the distribution of ions in the surrounding interfacial region, resulting in an increased concentration of counter ions close to the surface of particles. Thus, an electrical double layer exists around each particle as shown in Figure 1.13 [67, 68]. This liquid layer surrounding the particles consist of two regions, inner region called stern layer, where ions are firmly attached to particle surface and an outer region called diffused layer, where ions are less firmly attached. Moreover, with in the diffuse layer, there exists a boundary where ions and particles forms a stable entity. When the particle moves either due to gravity or due to any applied force, the ions with in the boundary also travels with it, while the ions beyond the boundary do not travel. This boundary is called slipping plane or surface of hydrodynamic shear and the potential that exists at this boundary is referred to as zeta potential [67, 68]. The magnitude of zeta potential indicates the stability of colloidal particles. The particles with high negative or positive zeta potential tend to repel each other and exhibit no tendency to aggregate. On the other hand, particles with low negative or positive zeta potential tend to aggregate due to weak repulsion forces between them. As reported in the literature,

particles with zeta potential greater than +30 or -30 mV are considered to be normally stable [68, 69]. This indicates that when a charged polymer is added to the suspensions, the zeta potential of the particles in the suspensions varies, which in turn affect the stability of suspensions. However, the effect of charge density and molecular weight of lignin and xylan based polymers on zeta potential of colloidal suspensions, specially clay and coal, was not investigated in detail. Thu, it is important to investigate the effect of these polymers on the zeta potential of clay or coal colloidal suspensions.

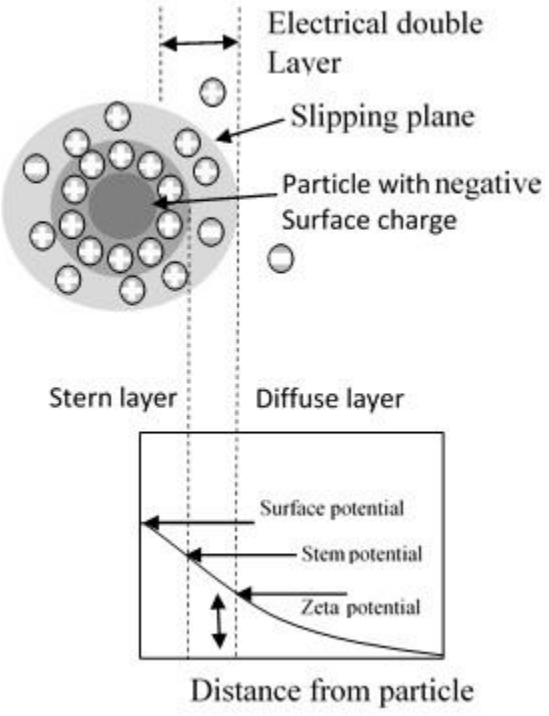


Figure 1-13.Showing electrical double layer surrounding the particle

### 1.2.14 Effect of polymer characteristics on relative turbidity and apparent viscosity of clay or coal suspensions

As describe in the literature [70, 71, 72], the anionic polymers introduce more negative charge on the clay particles causing them to repel each other upon adsorption. This results in more dispersion of particles in the suspensions, and thereby improving the turbidity of clay suspensions [70, 71]. Furthermore, the increase in the dispersion of particles makes the suspension less viscous due to uniform distribution of particles [73, 74]. Hong and co-authors reported that a rise in the polycarboxylic acid concentration to 0.5 wt.% reduced the viscosity of a coal suspension from 1200 to 580 mPa.s via generating electrostatic repulsion between the coal particles [73]. As described in section 1.2.15.4, the adsorption of the polymers on the surface of

coal or clay samples depends on the charge density and molecular weight of polymers. To design an effective dispersant, it is important to study the effect of charge density and molecular weight of polymers on the relative turbidity of clay suspensions. In the literature, it was reported that lignosulfonates with high charges (sulfonate) were effective in reducing the apparent viscosity of highly concentrated coal water suspensions [75]. However, there is little information on the effect of molecular weight and charge density of anionic polymers in improving the relative turbidity of coal or clay suspensions. Thus, it is worth investigating the effect of polymer characteristics on the relative turbidity of coal or clay suspensions.

### 1.2.15 Effect of polymer characteristics on particle size of clay or coal samples.

As described previously in the literature, the size of particles in the suspensions had a great impact on dispersion of colloidal suspensions. Accordingly, particles with large size tend to settle down at a faster rate compared to smaller size ones, which further reduces the dispersion performance of colloidal suspensions [76, 77, 78]. In suspensions, size of particles depend on their aggregation behavior. As described in sections 1.2.15.2 and 1.2.15.3, the concentration, charge density and molecular weight of anionic polymers would impact the size of clay or coal particles, which in turn affects the dispersibility of coal or clay suspensions. Previously, the rise in the dosage of carboxymethylated xylan to 15 mg/L improved the relative turbidity of a clay suspension up to 1.27 and the volume of suspended partciles from 0 to 8 %. [76]. However, there are no reports on effect of charge density and molecular weight of lignin and xylan based polymers on size of clay particles, and this will be investigated in this thesis work.

### 1.2.16 Effect of polymer characteristics on stability of clay or coal suspensions.

As described in sections 1.2.5 and 1.2.6, the stability of clay or coal suspensions is critical in the mining and mineral industries to achieve products with desired performance. However, the settling of clay or coal particles present is a major challenge due to their high concentrations [9, 10]. It is important to study the settling or stability characteristics of coal or clay suspensions in the presence of anionic kraft lignin or xylan in order to design effective dispersants. Previously, it was reported that an increase in the dosage of anionic polyacrylamide (APAM) to 10 mg/L improved the stability of kaolin suspension by 60 % [79]. There are no reports on the effect of charge density and molecular weight of lignin and xylan based polymers on the settling behavior of clay or coal suspensions, which is one objective of this thesis work.

## 1.3 Methodology

### 1.3.1 Charge density analysis of polymers, clay or coal

Particle charge detectors, PCDs, have been extensively used in the literature to measure the charge density of anionic polymers [26, 58, 63]. In this measurement, the polymer samples are neutralized by a standard polymer solution of opposite charge, i.e. poly diallyldimethylammonium chloride, PDADMAC. Considering the amount of oven dried polymer added to the cell of PCD, the charge density, and the concentration of standard polymer, the charge density of lignin and xylan based polymers can be determined. This analysis is valid if the standard polymer and polymer sample interact with each other stoichiometrically [63].

A back titration method was applied to measure the surface charge density of clay or coal particles in the past [58, 79]. In this analysis, PVSK and PDADMAC solutions are employed as standard solutions since their interactions with the charges of clay or coal particles are stoichiometrically controlled [80]. In this method, the PDADMAC standard solution, which has an opposite charge density compared with the charge of clay or coal particles, is added to colloidal suspensions to adsorb on the coal or clay surface. After mixing and filtering, the concentration of PVSK or PDADMAC solution is determined by the PCD, and compared with the concentration of PVSK or PDADMAC in the control solutions (i.e. the solutions with no clay or coal in them). The difference between the concentration of polymers in the filtrate and in its control solutions provides the surface charge density of coal or clay particles [79], as the difference is because of the adsorption of PVSK or PDADMAC polymers on the surface of the particles for charge neutralization.

Solubility is generally characterized as the maximum amount of a substance that can be dissolved in a solution (g/L) at equilibrium. To reduce the amount of lignin and xylan use in experiments, the solublity of unmoidifed and modified lignin and xylan at 10 g/L was analyzed, and the solublity was reported as percentage of this 10 g/L concentration throughout this thesis. By modifying lignin and xylan, not all of xylan and lignin segements could be solubllize as these segments may be different in chemical strutre and molecular weight, and this behavior can be observed as the percentage of modified/unmodified lignin and xylan dissolved in solution.

The sulfonate and carboxylate groups generated during modification of lignin or xylan was determined by using potentiometric titration method as described in the literature [80, 81]. Peng

and coauthors reported that potentiometric titration is a reliable method to determine the concentrations of charged groups present in the native and modified polymers [81].

### 1.3.2 Methods to characterize modified polymers

Nuclear magnetic resonance spectroscopy (NMR) is a powerful tool in elucidating the chemical structure of polymers [60, 73, 82]. This phenomenon is used to interpret the chemical structure of the polymers. In this thesis work, NMR was used to characterize the structure of modified and unmodified lignin or xylans. It is relied on the phenomenon that the atomic nuclei of various functional groups resonate differently under a magnetic field and when irradiated with radio waves they are excited. These excited nuclei absorb some energy and subsequently release energy as the nuclei relax back to their original states. The released energy can be scanned and expressed as chemical shifts, and considered as fingerprints of chemical structures. This relaxation time of the nuclei depends on the surrounding chemical groups and occurs differently depending on the type of chemical groups [83].

As described in the literature, Fourier transform infrared spectrophotometer (FTIR) can be employed in characterizing polymers to determine the functional groups associated with them [58, 76, 84]. Infrared spectroscopy is the study of interactions between molecules and electromagnetic (EM) light in the IR region. In this spectral region, the EM waves mainly couple with the molecular vibrations. In other words, a molecule can be excited to a higher vibrational state by absorbing IR radiation. The probability of a particular IR frequency being absorbed depends on the actual interaction between this frequency and the molecule. In general, a frequency will be strongly absorbed if its photon energy coincides with the vibrational energy levels of the molecule. IR spectroscopy is therefore a very powerful technique that provides fingerprint information on the chemical compositions of materials [84].

The FTIR spectrophotometer operates on a principle called Fourier transform [85]. The mathematical expression of Fourier transform was stated in Equation 1.1.

$$F(\omega) = \int_{\infty}^{\infty} f(x) e^{ix\omega} \qquad (1.1)$$

And the reverse Fourier transform is

$$F(x) = \frac{1}{2\pi} \int_{-\infty}^{+\infty} f(\omega) e^{i\omega x} dx \qquad (1.2)$$

where ω is angular frequency (1/s) and x is the optical path difference. F(ω) is the spectrum and f(x) is called the interferogram. In this study, lignin or xylan based polymers were studied by FTIR to elucidate the difference in functional groups between unmodified and modified lignin or xylan.

Thermo gravimetric analyzer (TGA) is a powerful method in analyzing the thermal characteristics of polymers [27, 58, 86]. It is a technique in which the mass of a substance is monitored as a function of temperature and/or time as the sample is subjected to a controlled temperature change in a controlled atmosphere. The schematic principle of TGA is shown in Figure 1.14 [87].

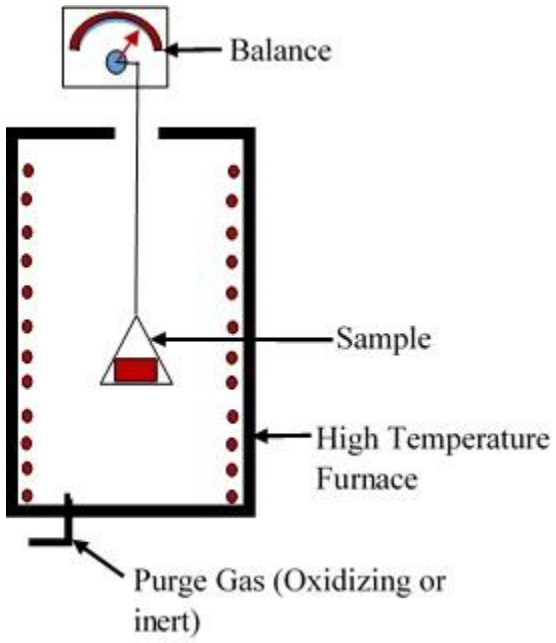


Figure 1-14. Schematic principle of TGA measurement

In this study, the TGA analyses of dried polymeric samples (lignin or xylan) were conducted. The difference of the mass of the polymers during this process is measured using micro-thermal balance. A mass loss indicates that the degradation of polymers at a specific temperature [87].

Elemental analyzer is a technique employed in determining the elemental compositions of polymers [24, 58, 88]. It involves rapid determination of carbon, hydrogen, sulphur and nitogen elements of different samples in the field of pharmaceuticals, polymers and chemicals. CHNS analysis requires high temperature combustion in an oxygen-rich environment and is based on

the classical Pregl-Dumas method. The principle includes a combustion process in a furnace at 1000 °C, where, carbon is converted to carbon dioxide; hydrogen to water; nitrogen to nitrogen gas and sulphur to sulphur dioxide. Afterwards, the combustion gases are reduced and analyzed for carbon, hydrogen, nitrogen and oxygen contents [88]. In this study, the elemental compositions of lignin or xylan polymers were determined. The combustion was carried out at high temperatures under a constant flow of oxygen for a set period of time. Then, the liberated gases were analyzed for carbon, hydrogen, nitrogen and oxygen content of the polymers.

According to literature, hydrodynamic size of polymers can be measured using a dynamic light scattering technique (DLS) [89, 90, 91]. This method is based on the principle that particles suspended in a liquid have Brownian movement and the speed at which the particles diffuse due to Brownian motion is measured by recording the rate at which the intensity of the scattered light fluctuates. Smaller particles cause the intensity to fluctuate more rapidly than large particles. The DLS technique measures time dependent scattering intensity fluctuations to determine the translational diffusion coefficient (D), and subsequently the hydrodynamic size of polymers using Stokes-Einstein equation (1.3) [90]

$$R_H = \frac{KT}{6\pi nD} \qquad (1.3)$$

where D is the diffusion coefficient, $R_H$ is radius (nm), k is Boltzmann constant, T is temperature (°C), and η is solvent viscosity (Pa.s).

In this thesis work, dried polymers (lignin or xylan) were dissolved in water. After mixing, potassium nitrate salt was added to the polymer solutions and allowed to stabilize. The addition of salt prevents the aggregation of polymers by neutralizing their functional groups. After mixing, the polymer solutions are filtered and the filtrates containing polymer are subjected to the hydrodynamic size analysis using DLS.

Gel permeation chromatography (GPC) is one of the most powerful and versatile analytical techniques available for the characterization of size of polymers [26, 92]. It is the most convenient technique for characterizing the complete molecular weight distribution of a polymer. GPC separates molecules in solution based on their effective size. This technique includes a column comprising of porous gel particles. Thus, a sample containing different polymeric molecules, when flow through a column, larger molecules elute first, as they cannot flow through

the pores, while the smaller molecules diffuse into pores and elute later. The elution behavior of sample is displayed in chromatogram, which represents the time taken for molecules of particular size (a fraction) to elute from column (retention time). Furthermore, a correlation can be made between size and molecular weight by plotting a graph between log molecular weight (M) and retention time for standard samples, and this correlation can be used for determining the molecular weight distribution of polymers. For a more precise determination of molecular weight of polymers, the chromatogram is divided into several equidistant slices and the molecular weight averages are calculated following equations 1.4, 1.5 and 1.6 [93].

$$M_w = \frac{\sum_i N_i M_i^2}{\sum_i N_i M_i} = \frac{\sum_i w_i M_i}{\sum_i w_i} \quad (1.4)$$

$$M_n = \frac{\sum_i N_i M_i}{\sum_i N_i} \quad (1.5)$$

$$PDI = \frac{M_w}{M_n} \quad (1.6)$$

In these equations, N refers to the number of polymer chains having molecular weight of M, $w_i$, corresponds to weight fraction distribution, while Mn represents the number average molecular weight, and Mw represents the weight average molecular weight. The ratio of Mw over Mn provides information about the distribution of the chain lengths, which is denoted as polydispersity index (PDI). The number or weight fraction distribution ($N_i$ or $M_i$) can be obtained from the concentration of molecules measured by the viscometer and refractive index detectors associated with GPC. In this work, polymer samples (lignin or xylan) were dissolved in sodium nitrate salt solution, which was the mobile phase of the GPC system used in this work. After dissolving, the polymer solutions were filtered and the filtrates were subjected to molecular weight analysis. The molecular weight and polydispersity of the polymers were assessed using GPC equipped with viscometer and refractive index detectors.

As described previously, the wettability of polymers can be determined by measuring the contact angle of water on their surfaces using an optical tensiometer [94, 95, 96]. When a liquid droplet

comes in contact with the solid surface, the droplet adheres to the solid surface at an angle (contact angle) formed by the intersection of solid-liquid interface and liquid vapour interface. This can be supposed geometrically by drawing a tangent line from the droplet contact point along the liquid-vapor interface as shown in Figure 1.15. When a contact angle is less than 90°, it indicates that wetting of the surface is favorable, and the solid surface is hydrophilic in nature; if contact angle is greater than 90°, it shows that wetting of the surface is unfavorable and solid surface is more hydrophobic in nature [95].

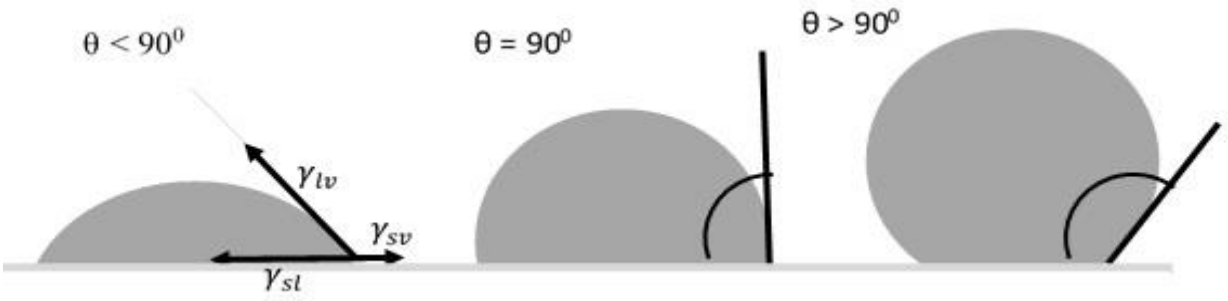


Figure 1-15.Representation of contact angles formed by sessile liquid drops on a smooth homogeneous solid surface.

Theoretically, the contact angle is a distinctive property of a given solid-liquid system under specific conditions [14]. As described by Young [96] in 1805, the contact angle of a liquid droplet on an ideal solid surface is defined as, mechanical equilibrium of the droplet balanced by the action of three interfacial tensions as represented in Equation 1.7.

$$\gamma_{lv}\, cos\theta_Y = \gamma_{sv} - \gamma_{sl} \qquad (1.7)$$

where, $\gamma_{lv}$, $\gamma_{sv}$, and $\gamma_{sl}$ represent the liquid-vapor, solid-vapor, and solid-liquid interfacial tensions, respectively, and $\theta_Y$ is the contact angle in degrees (°).

In this thesis, polymers (lignin or xylan) or coal samples were coated on microscopic glass slides using a spin coater under controlled conditions in nitrogen atmosphere. After coating, the slides were wetted with required volume of water droplets by the sessile drop technique, and the wettability of the polymers or coal samples were determined by contact angle and interfacial measurements using an optical tensiometer.

### 1.3.3 Coal or clay properties

Brunauer-Emmett-Teller (BET) model of adsorption, is a well-known method to study the surface area of materials [13, 14, 97]. The specific surface area is determined by physical adsorption of a gas on the surface of a solid and by calculating adsorption amount of adsorbate gas corresponding to a monomolecular layer on the surface. Physical adsorption results from relatively weak forces (e.g. van der Waals forces) between the gas molecules and the surface area of the solid material. As nitrogen is usually used for this purpose, the experiment is carried out at the boiling temperature of liquid nitrogen to ensure accuracy in adsorption and desorption of nitrogen on solid surface. In this method, a monolayer adsorption of the gas is determined on the surface, from which the surface area is measured by the BET presented in Equation 1.8 [13, 98, 99].

$$\frac{p}{V_a(p_0 - p)} = \frac{1}{V_m c} + \frac{c-1}{V_m c}\left(\frac{p}{p_0}\right) \qquad (1.8)$$

where P (Pa) and $P_0$ (Pa) are the equilibrium and the saturation pressure of the gas at the temperature of adsorption, v (ml) is the gas adsorption amount (for example, in volume units), and $v_m$ (ml) is the amount of gas adsorbed in a monolayer form on the surface and c is the BET constant. This equation can be rearranged to

By plotting $\frac{p}{V_a(p_0 - p)}$ against $\frac{p}{p_0}$, the BET plot can be obtained. The intercept and slope of the BET plot can be identified, from which $V_m$ and c can be calculated.

The total surface area (BET) of the solid can be calculated from Equation 1.9.

$$a_s = \frac{V_m}{22414} L \sigma_g \qquad (1.9)$$

where L is the Avogadro constant and $\sigma_g$ is the cross section area of the adsorbed gas molecules ($\sigma_g$ for Nitrogen is 0.162 $nm^2$).

As described in literature, the particle size distribution of clay or coal suspensions can be assessed using a particle size analyzer that is a laser diffraction instrument [14, 23, 66, 100]. In this thesis, clay or coal suspensions prepared in aqueous conditions were characterized using laser diffraction instrument. This technique predicts the scattering of light caused by the coal or

clay particles, when a laser beam is passed through the particle suspension. The information related to size of the clay or coal particles was predicted based on performance of the particles to scatter light according to Mie theory as shown in Equation 1.10 [101, 102]. Each particle will have its own characteristic scattering pattern that is unlike any other particles.

$$I = \frac{2\pi r N_m}{\lambda} \qquad (1.10)$$

In this equation, I is denoted the intensity of incident light, r is the radius of the particles (nm), $N_m$ is the refractive index of the medium and $\lambda$ is the wavelength of incident light (nm).

Senoussi and coauthors reported the chemical compositions of various types of clay particles using scanning electron microscopy (SEM) in tandem with energy dispersive X-ray spectroscopy (EDX) [13, 78, 103]. In this thesis, the clay samples are initially mixed in acetone under ultrasonic vibrations to disperse the particles and allowed to dry. After drying, the samples were coated with carbon under vacuum using carbon coating technique and analyzed using SEM-EDX technique. In EDX Analysis, the particles (specimen) are bombarded with an electron beam inside the scanning electron microscope. The bombarded electron beam collide with the electrons of specimen's atoms and knock out the electrons present in the inner shell of atoms to outer shell. In this process, the void generated in the lower shell is occupied by a higher-energy electron from an outer shell of specimen atom by releasing energy in the form of X-rays. Furthermore, the atom of every element in the particles releases X-rays with unique amounts of energy in the transferring process. Thus, by measuring the amounts of energy present in the X-rays released by the sample during electron beam bombardment, the identity of the atom can be established [104, 105].

According to the literature, X-ray diffractometer (XRD) is described as a powerful tool in assessing the mineral compositions of substances [18, 52, 106]. In this analysis, the samples were dried to remove any moisture and loaded on the spinner of the XRD and scanned for mineral compositions. The three-dimensional structure of crystalline materials, such as clay minerals, is defined by regular, repeating planes of atoms that form a crystal lattice. When a X-ray beam interacts with these planes of atoms, one part of the beam is transmitted, one part is absorbed by the sample, one part is refracted and scattered, and another part is diffracted. Diffraction of an X-ray beam by a crystalline solid produces a spectra, and furthermore each mineral diffracts the X-ray beam differently, depending on what atoms present in the crystal lattice and how they are

arranged. When an X-ray beam hits the clay sample and is diffracted, the distances (d-spacings) between the planes of the atoms that constitute the sample can be measured by applying Bragg's Law using Equation 1.11 [107, 108],

$$n\lambda = 2d \sin\theta \quad (1.11)$$

where the integer n is the order of the diffracted beam, $\lambda$ is the wavelength of the incident X-ray beam in nm, d is the distance between adjacent planes of atoms (the d-spacings) in nm, and θ is the angle of incidence of the X-ray beam in degrees (°).

The configuration of an XRD unit is aimed to perform this measurement. The distinctive set of d-spacings generated in a typical X-ray scan provides a unique feature of the mineral or minerals present in the clay sample. When properly interpreted, by comparison with standard reference patterns and measurements, minerals present in the clay sample can be identified.

### 1.3.4 Properties of clay or coal suspensions

As described in literature, zeta potential, which is also referred to as electrokinetic potential of particles in the suspension, can be measured by zeta potential analyzer. This technique includes an electrophoresis principle. When an electric field is applied across an electrolyte solution, charged particles suspended in the electrolyte are attracted towards the electrode of opposite charges, while viscous forces acting on the particles tend to oppose this movement. However, when an equilibrium is reached between these two opposing forces, the particles move with constant velocity. This velocity of the particle is also referred to as electrophoretic mobility. Based on this principle, the zeta potential of particles can be measured by the Smoluchowski equation (Equation 1.12) [67, 68]

$$U_E = \frac{2\varepsilon z f(ka)}{3\eta} \quad (1.12)$$

where z is zeta potential (mV), $U_E$ is electrophoretic mobility (m/s), Ɛ is dielectric constant, η is viscosity of suspension (mPa.s) and f (ka) is Smoluchowski constant (either 1 or 1.5).

In this study, clay or coal suspensions in the presence or absence of lignin and xylan based polymers of required concentrations was prepared under neutral conditions and subjected to a zeta potential analysis at a constant electric filed and the obtained electrophetic mobility of the particles is used to identify their zeta potential using the Smoluchoski equation as described above.

Relative turbidity is one of the important criteria used for studying the dispersibility of colloidal suspensions [28, 56, 78]. Colloidal particles in the suspensions possess charges on their surfaces, which may result in dispersion (due to more repulsion forces) or aggregation (due to more aggregation forces) of the particles. If the repulsion forces between the particles dominate, the particles tend to repel each other and be more distributed within the system, which is accompanied by an increase in the relative turbidity. On the other hand, if the repulsion forces diminish, the particles tend to aggregate and settle, which results in decreased relative turbidity of colloidal suspensions. As described elsewhere, a dynamic drainage jar (DDJ) equipped with photometric dispersion analyzer (PDA) is widely employed to analyze the dispersibiliity of colloidal suspensions via measuring the relative turbidity of colloidal suspensions. PDA is a fibre-optical monitor that measures the fluctuation in the intensity of light transmitted through a flowing suspension. The fluctuations in the intensity of light were quantified in terms of direct current (DC) voltage signals [32]. In this analysis, distilled water was transferred to DDJ and circulated from DDJ to PDA for a required period of time and the corresponding DC voltage values were recorded. Later, clay or coal suspension in the presence or absence of polymers (lignin or xylan) was added to DDJ and allowed for passing through PDA. The change in DC voltage signals were recorded and used further to calculate the relative turbidity of clay suspensions by the Equation 1.13 [58]

$$\text{Relative turbidity, } \tau_r = \frac{\tau_f}{\tau_i} = \frac{ln(\frac{V_0}{V_f})}{ln(\frac{V_0}{V_i})} \qquad (1.13)$$

where $\tau_f$ is denoted as the final suspension turbidity, and $\tau_i$ is denoted as initial suspension turbidity, $V_0$ is initial base DC voltage, $V_i$ stands for unflocculated suspension DC voltage, and $V_f$ is final suspension DC voltage.

In addtion, the stability of kaolin and coal suspensions in the presence and absence of lignin or xylan polymers were determined using a vertical scan analyzer, Formulaction, France as described in the literature [109, 110]. In this analysis, kaolin or clay suspensions of required concentration were prepared under aqueous conditions in the presence or absence of polymers (lignin or xylan). The suspensions were transferred to vial and the analysis is performed by allowing light beams pass through a clay or coal dispersion. The light passes through a transmission zone of the samples, while it cannot pass through the sediment zone of the samples.

Two synchronous optical sensors receive light transmitted through the sample (180° from the incident light, transmission sensor) and light backscattered by the sample (45° from the incident radiation, backscattering detector). The higher transmission zone implies less stable kaolin or coal dispersions due to the sedimentation of particles. These transmittance and backscattering signals were recorded as a percentage of transmittance signals in regard to that of the reference chemical, silicon oil.

The transmission and backscattering data was used for determining the destabilization index (DSI) and average particle diameter using the turbisoft software by equations 1.14 and 1.15 [110].

$$\mathrm{DSI} = \Sigma_i \frac{\Sigma_h |scan_i(h) - scan_{i-1}(h)|}{H} \quad (1.14)$$

where $scan_i$ (h) and $scan_{i-1}$ (h) are the transmission signals for two consecutive time intervals at a given height and H is the total height of sample.

Correlation between the particle migration velocity and the properties of the suspensions can be determined using Equation 1.17.

$$V(\Phi, \mathrm{d}) = \frac{|p_p - p_c| g d^2}{18 v p_c} \times \frac{[1-\Phi]}{\left[1 + \frac{4.6\,\Phi}{(1-\Phi)^2}\right]} \quad (1.15)$$

where $V$ is the particle migration velocity (μm/min), $p_c$ is the continuous phase density (g/ml), $p_p$ is the particle density (g/ml), d is the particle mean diameter (μm), $v$ is the continuous phase dynamic viscosity (mPa.s) and $\Phi$ is the volume fraction of dispersed particles (i.e. kaolin particles) in %.

The size of kaolin or coal particles in the dispersed state (i.e. not settled) and their volume fractions can be obtained based on the backscattering data collected. Based on the Mie theory, the back scattering data measured by the instrument can be expressed as a function of photo transport mean free path, I* in Equation 1.16.

$$\mathrm{BS} = \frac{1}{\sqrt{I^*}} \quad (1.16)$$

In addition, the photo transport mean free path, I* (μm), could be obtained via following Equation 1.17

$$I^*(d, \theta) = \frac{2d}{3\theta\,(1-g)Q_s} \quad (1.17)$$

where, d is the particle mean diameter (μm), θ is the particle volume fraction (%), g and Qs are the dimensionless scattering efficiency factors, which depend on the particle diameter (d), wave length of light (λ) in nm, refractive index of dispersed kaolin particles ($n_p$) and the refractive index of continuous phase ($n_f$). In this work, the refractive indices of kaolin particles and water were considered to be 1.54 and 1.33.

According to Eqs. 1.16 and 1.17, back scattering data is directly dependent on the particle mean diameter, d, and their volume fraction, θ [39]. By providing refractive indices of kaolin, coal and water, the turbisoft 2.1 software associated with the instrument would generate a correlation between the size of kaolin or coal particles and their volume fraction in the dispersion from the backscattering data.

Furthermore, a rheometer is employed as a powerful tool for analyzing the apparent viscosity and viscoelasticity of various fluids, semi solids and solids [66, 111, 112]. The viscosity of a material is generally referred to as a material's resistance to deformation with time and temperature as a function of shear stress or shear rate, which is described by the following Equation 1.18 [112]

$$\eta = \frac{\sigma}{\lambda} \quad (1.18)$$

where η is the viscosity of material (mPa.s), σ is the shear strain (1/s) that a material has undergone due to applied shear stress, $\lambda$ (Pa)

In this method required concentrations of coal suspensions were prepared by mixing required amount of grounded coal in deionized water. After mixing, coal suspensions were transferred to sample holder associated with the rheometer instrument and the viscosity of suspensions with or without anionic lignin polymers were determined by applying the shear stress using rotar equipped with the instrument over a required period of time.

References

1. Brady PV, Cygan RT, Nagy KL. Molecular controls on kaolinite surface charge. Journal of Colloid Interface Science, 1996, 183, 356-364.
2. Zaman AA, Tsuchiya R., Moudgil BM. Adsorption of a low-molecular weight polyacrylic acid on silica, alumina and kaolin. Journal of Colloid Interface Science. 2002, 256, 73-78.

3. Eygi MS, Atesok G. An investigation on utilization of poly-electrolytes as dispersant for kaolin slurry and its slip casting properties. Ceramics International. 2008, 34, 1903-1908.
4. Loginov M, Larue O, Lebvoka N, Vorobeiv E. Fluidity of highly concentrated kaolin suspensions: Influence of particle concentration and presence of dispersant. Colloids and Surfaces A: Physiochemical Engineering Aspects. 2008, 325, 64-71.
5. Garcia OA, Vazquez SB, Medina JZ. Mixture design to optimize the amount of deflocculants in aqueous porcelain suspensions. Journal of Ceramic Processing Research. 2009, 10, 125-128.
6. Nuntiya A, Prasanphan S. The rheological behaviour of kaolin suspensions. Chaing Mai Journal of Science. 2006, 33, 271-281.
7. Boisvert JP, Persello J, Castaing JC, Cabane B. Dispersion of alumina coated $TiO_2$ particles by adsorption of sodium polyacrylate. Colloids and Surfaces A: Physiochemical Engineering Aspects. 2001, 178, 187-198.
8. Penkavova V, Guerreiro M, Tihan J, Teixeira JAC. Deflocculation of kaolin suspensions – The effect of various electrolytes. Applied Rheology, 2015, 25, 24151-24165.
9. Hong N, Zhang S, Yi C, Xueqing Q. Effect of Polycarboxylic Acid Used as High-Performance Dispersant on Low Rank Coal-Water Slurry. Journal of Dispersion Science and Technology, 37, 2015, 415-422.
10. Li R, Yong D, Lou H, Zhou M, Qiu X. Influence of sulfonated acetone-formaldehyde used as dispersant on low rank coal slurry. Energy Conservation and Management, 2012, 64, 139-144.
11. Atesok G, Somasundaram P, Morgan LJ. Charge effects in the adsorption of polyacrylamide on sodium kaolinite and its flocculation. Powder Technology, 1998, 54, 77-83.
12. Chen Y, Liu S, Wang G. A kinetic investigation of cationic starch adsorption and flocculation in kaolin suspension. Chemical Engineering Journal. 2007, 33, 325-333.
13. Tombac E, Szekeres M, Surface charge heterogeneity of kaolinite in aqueous suspension in comparison with montmorillonite. Applied Clay Science, 2006, 34, 105-124.
14. Loginov M, Larue O, Lebovka N, Vorobeiv E. Fludity of highly concentrated kaolin suspensions: Influence of particle concentration and presence of dispersant. Colloids and Surfaces A: Physiochemical Engineering Aspects, 2008, 325, 64-71.

15. Tombacz E. Szekeres M. Colloidal behaviour of aqueous montomorillonite suspensions: the specific role of pH in the presence of indifferent electrolytes. Appl Clay Science, 2004, 27, 75–94.
16. Manganaro J, Lawal A. Economics of Thermochemical Conversion of Crop Residue to Liquid Transportation Fuel. Energy Fuels. 2012, 26, 2442-2453.
17. Demirbas A. Bioethanol from Cellulosic Materials: A Renewable Motor Fuel from Biomass. Energy Sources. 2005, 27, 327-337.
18. Das D, Dash U, Nayak A, Misra PK. Surface Engineering of Low Rank Indian Coals by Starch-Based Additives for the Formulation of Concentrated Coal-Water Slurry. Energy and Fuels, 2010, 24, 1260-1268.
19. Boisvert JP, Persello J, Castaing JC, Cabane B. Dispersion of alumina coated $TiO_2$ particles by adsorption of sodium polyacrylate. Colloids and Surfaces A: Physiochemical Engineering Aspects, 2001, 178, 187-198.
20. Ma M. The dispersive effect of sodium silicate on kaolinite particles in process water: Implications for iron ore processing. Clay and Clay Minerals, 2011, 59, 233-239.
21. Qin W, Wei Q, Jiao F, Li N, Wang P, Ke L. Effect of sodium pyrophosphate on the flotation separation of chalcopyrite from galena. International Journal of Mining Science and Technology, .2012, 22, 345-349.
22. Ece OI, Alemdar A, Gungor N, Hayashi S. Influence of non-ionic poly (ethylene glycol) polymer PEG on electrokinetic and rheological properties of bentonite suspensions. Journal of Applied Polymer Science, 2002, 86, 341-346.
23. Zhang G, Li J, Zhu J, Wu Q, Xiong W. Synthesis and evaluations of three sulfonated polycondensate dispersants for coal-water slurries. Powder Technology, 2014, 24, 572-578.
24. Das D, Dash U, Meher J, Misra PK. Improving stability of concentrated coal-water slurry using mixture of a natural and synthetic surfactants. Fuel Processing and Technology, 2013, 113, 41-51.
25. Zhou M, Huang K, Yang D, Qiu X. Development and evaluation of polycarboxylic acid hyper-dispersant used to prepare high-concentrated coal–water slurry. Powder Technology. 2012, 229, 185-190.

26. Huang J, Xu J, Wang D, Li L, Guo X. Effects of amphiphilic copolymer dispersants on rheology and stability of coal water slurry. Industrial Engineering and Chemistry Research, 2013, 52, 8427-8435.
27. Heinze T, Koschella A. Carboxymethylesters of cellulose and starch-A review. Macromolecular Symposium, 2005, 223, 13-40.
28. Hebeish A, Khalil MI, Hasheem A. Carboxymethylation of starch and oxidised starches. Starch, 1990, 42, 185-191.
29. Pawlik M, Laskowski JS, Ansari, A. Effect of carboxymethyl cellulose and ionic strength on stability of mineral suspensions in potash ore flotation systems. Journal of Colloid Interface Science. Carbohydrate Polymers, 2003, 260, 251-258.
30. Heinze T, Liebert T, Heinze U, Schwikal K. Starch derivatives of high degree of functionalization; Carboxymethyl starches. Cellulose, 2004, 11, 239-245.
31. Schmorak J, Adams GA. The preparation and properties carboxymethylated xylan. Tappi Journal, 1957, 40, 378-383.
32. Petzold K, Schwikal K, Gunther W, Heinze T. Carboxymethyl xylan-control of properties by synthesis. Macromolecular Symposium, 2006, 232, 27-36.
33. Voitl T, Von Roh PR. Demonstration of process for the conversion of kraft lignin into vanillin and methyl vanillate by acidic oxidation in aqueous methanol. Industrial Engineering and Chemistry Research, 2010, 49, 520-525.
34. Wu H, Chen F, Feng Q, Yue X. Oxidation and sulfomethylation of alkali extracted lignin from corn stalk. Bioresources, 2012, 7, 2742-2751.
35. Ouyang X, Ke L, Qiu X, Guo Y, Pang Y. Sulfonation of alkali lignin and its potential use in dispersant for cement. Journal of Dispersion Science and Technology, 2009, 30, 1-6.
36. Sarkanen KV, Ludwig CH. Lignins; Occurrence, Formation, Structure and Reactions. John Wiley & Sons, Inc: New York, 1971, pp. 250-255.
37. Windt M, Meier D, Marsman JH, Heeres HJ, De Koning S. Micropyrolysis of technical lignins in a new modular rig and product analysis by GC-MS/FID and GCXGC-TOFMS/FID. Journal of Analytical and Applied Pyrolysis, 2009, 85, 38-46.
38. Wenbo Y, Huanzhen MU, Yanchu H. Treatment of black liquor from the paper making industry by acidification and reuse. Journal of Environmental Science, 2003, 15, 697-700.

39. Sarwar Jahan M, Liu Z, Wang H, Saeed A, Ni Y. Isolation and characterization of lignin from prehydrolysis liquor of kraft based dissolving pulp production. Cellulose Chemistry and Technology, 2012, 46, 261-267.
40. Hansen NML, Plackett, D. Sustainable films and coatings from hemicelluloses: A Review. Biomacromolecules, 2008, 9, 1493-1505.
41. Sjostrom E. Wood chemistry: Fundamentals and applications (2nd ed.). Academic press: San Diego, CA, 1993, (Chapter 1).
42. Mueller-Harvey I, Hartley RD. Linkages of p-coumaroyl and feruloyl groups to cell wall polysaccharides of barley straw. Carbohydrate Research, 1986, 148, 71-85.
43. Saghir S, Iqbal MS, Hussain MA, Koschella A, Heinze T. Structure characterization and carboxymethylation of arabinoxylan isolated from Isphagula (*Plantago ovata*) seed husk. Carbohydrate Polymers, 2008, 74, 309-317.
44. Kouisni L, Holt-Hindle P, Maki K, Paleologou M. The LignoForce system: a new process for the production of high-quality lignin from black liquor**.** Journal of Science and Technology for Forest Products and Processes**,** 2012; 2, 6-10.
45. Hon, DNS. Chemical modification of lignocellulosic materials, New York, USA, Marcel Dekker Inc, 1996, (p.64).
46. Mendes CVT, Carvalho MGVS, Baptista CMSG, Rocha JMS, Soares BIG, Sousa GDA. Valorisation of hardwood hemicelluloses in kraft pulping process by using an integrated biorefinery concept. Food Bioproducts and Processes, 2009, 87, 197-207.
47. Helmerius J, Von Walter JV, Rova U, Berglund KA, Hodge DB. Impact of hemicellulose pre-extraction for bioconversion on birch Kraft pulp properties. Bioresource Technology, 2010, 101, 5996-6005.
48. Van Heiningen A. Converting a kraft mill into an integrated forest biorefinery. Pulp and Paper Canada, 2000, 107, 38-43.
49. Kosikova B, Duris M, Demianova V. Conversion of lignin biopolymer into surface active derivatives. European Polymer Journal*,* 2000, 36, 1209-1212.
50. Petzold WK, Schwikal K, Daus S, Heinze T. Xylan derivatives and their application potential – Mini review of our results. Carbohydrate Polymers, 2014, 100, 80-88.

51. Söderqvist Lindblad M, Albertsson AC. "Chemical modification of hemicelluloses and gums," in Polysaccharides: Structural Diversity and Function, S. Dumitriu, Ed., p. 491, CRC Press, New York, NY, USA.
52. Kadla J.F, Chang H.M. The recations of peroxides with lignin and lignin model compounds. Oxidative deligninfication chemistry. ACS Symposium series, 2001, Vol 785, Chapter 6, 108-109.
53. Chien SN, Amidon TE, Lai YZ. Fractionation of wood polymers by carboxymethylation: Exploring the strategy. Tappi Journal, 2012, 11, 29-37
54. Heize T. Polysaccharides structure, characterization and use; Springer publications: Germany, 2013.
55. Gan L, Zhou M, Qiu X. Preparation of water soluble carboxymethylated lignin from wheat straw alkali lignin. Advances in Material Research, 2012, 550-555, 1293-1298.
56. He W, Fatehi P. Preparation of sulfomethylated softwood kraft lignin as a dispersant for cement admixture. RSC Advances, 2015, 5, 47031-47039.
57. Konduri M.K.R, Kong F, Fatehi P. Production of water soluble kraft lignin via carboxymethylation using sodium chloroacetate. European Polymer Journal, 2015, 70, 371-383.
58. Li Z, Ge Y. Extraction of lignin from sugarcane bagasse and its modification into a high performance dispersant for pesticide formulations. Journal of Brazilian Chemical Society, 2011, 22, 1866-1871.
59. Lu JH, Wu L, Letey J. Effects of Soil and Water Properties on Anionic Polyacrylamide Sorption. Soil Science Society of American Journal, 2002, 66 578–584.
60. Deng Y, Dixon JB, White GN. Adsorption of Polyacrylamide on Smectite, Illite, and Kaolinite. Soil Science Society of American Journal, 2006, 70, 297-304.
61. Nasser MS, James AE. The effect of polyacrylamide charge density and molecular weight on the flocculation and sedimentation behaviour of kaolinite suspensions. Separation and Purification Technology, 2006, 52, 241-252.
62. Yong-jie, D, Feng G, Yong-jin L. Effect of the molecular weight of sodium polystyrene sulfonate on the properties of coal water slurry. Journal of Fuel Chemistry and Technology, 2006, 34, 3

63. Ma X. Effect of a low-molecular-weight polyacrylic acid on the coagulation of kaolinite particles. International Journal of Mineral Processing, 2011, 99 17-120.
64. Li Y, Zhang Y, Zheng J, Guo H, Yang C, Li Z, Lu, M. Dispersion and rheological properties of concentrated kaolin suspensions with polycarboxylate copolymers bearing comb like side chains. Journal of European Ceramic Society, 2014, 34 137-146.
65. Hunter RJ. Zeta potential in colloid science-principles and applications. Academic press, London: 1988.
66. Lyklema J, Fundamentals of Interface and Colloid Science. Elsevier Publishing Company, Amsterdam, Netherlands: 1991.
67. Riddick MT. Control of colloid stability through Zeta-potential, Inc., New York, 1961.
68. Araki J, Wada M, Kuga S, Okano, T. Flow properties of microcrystalline cellulose suspension prepared by acid treatment of native cellulose. Colloids and Surfaces A: Physiochemical Engineering Aspects, 142, 1992, 75.82.
69. Mike S. Turbidity Measurement: A Simple, Effective Indicator of Water Quality Change. http://www.ott.com/download/turbidity-white-paper/.
70. Wang S, Konduri M.K.R, Hou Q, Fatehi, P. Cationic xylan-METAC copolymer as a flocculant for clay suspensions. RSC Advances, 2016, 6, 40258-40269.
71. Marco P, Llorens J. Surface charge and rheological properties of raw porcelain gres suspension with acrylic copolymers bearing carboxylic groups. Journal of European Ceramic Society, 2009, 29, 559-564.
72. Ramphal SR, Sibiya MS. Optimization of coagulation-flocculation parameters using a photometric dispersion analyzer. Drinking Water Engineering and Science, 2014, 7, 73-82.
73. Hong N, Zhang S, Yi C, Xueqing Q. Effect of Polycarboxylic Acid Used as High-Performance Dispersant on Low Rank Coal-Water Slurry. Journal of Dispersion Science and Technology, 37, 2015, 415-422.
74. Vie R, Azema N, Quantin JC, Touraud E, Fouletier M. Study of suspension settling: A approach to determine suspension classification and particle interactions. Colloids and Surfaces A: Physiochemical Engineering Aspects, 2007, 298, 192-200.
75. Yang D, Qiu X, Zhou M, Lou, H Properties of sodium lignosulfonate as dispersant of coal water slurry. Energy Conversion and Management, 2007, 48, 2433-2438.

76. Konduri MKR, Fatehi, P. Dispersion of kaolin partciles with carboxymethylated xylan. Applied Clay Science, 2017, 137, 183-191.
77. Wisniewska M, Chibowski S, Urban T, Sternik D, Terpilowski K. Impact of anionic polyacrylamide on stability and surface properties of the $Al_2O_3$–polymer solution system at different temperatures. Colloid Polymer Science, 2016, 294, 1511-1517.
78. Wu H, Chen F, Feng Q, Yue X. Oxidation and sulfomethylation of alkali extracted lignin from corn stalk. Bioresources, 2012, 7, 2742-2751.
79. Lou H, Lai H, Wang M, Pang Y, Yang D, Qiu X, Wang B, Zhang H. Preparation of lignin-based superplasticizer by graft sulfonation and investigation of the dispersive performance and mechanism in a cementitious system. Industrial and Engineering Chemistry and Research, 2013, 52, 16101-16109.
80. Peng XW, Ren JL, Zhong LX, Cao XF, Sun, RC. Microwave-induced synthesis of carboxymethyl hemicelluloses and their rheological properties. Journal of Agriculture and Food Chemistry, 2011, 59, 570-576.
81. Lutzenkirchen J, Preocanin T, Kovacevic D, Tomisic V, Lovgren L, Kallay N. Potentiometric titrations as a tool for surface charge determination. Croatica Chemica Acta, 2012, 85, 391-417.
82. Gunther H. NMR Spectroscopy: Basic Principles, Concepts and Applications in Chemistry. Wiley & Sons, USA, 2014.
83. Gerothanosis, IP, Troganis A, Exarchou V, Barbarossou K. Nuclear magnetic spectroscopy: Basic principles and phenomena, and their applications to chemistry, biology and medicine. Chemsitry Education: Research and Practice In Europe, 2002, 3, 229-252.
84. Griffiths PR, De Haseth JA. Fourier Transform Infrared Spectrometry. Wiley, New York, 1986.
85. Folland GB, Sitaram A. The uncertainity principle: a mathematical survey. Journal of Fourier Analysis and Application, 1997, 3, 207-238.
86. Stodghill SP. Thermal Analysis – A Review of Techniques and Applications in the Pharmaceutical Sciences. American Pharamaceutical Review, 2010, 13, 29-36.
87. Gabbott P. Prinicples and applications thermal analysis. Blackwell Publishing Ltd, 2008, Oxford, UK.

88. Thompson M. AMC technical briefs. CHNS elemtal analyzers. AMCTB No 29 , April 2008, http://www.rsc.org/images/CHNS-elemental-analysers-technical-brief-29_tcm18-214833.pdf.
89. Forster S, Schmidt M. Static and dynamic light scattering by aqueous polyelectrolyte solutions: effect of molecular weight, charge density and added salt. Polymer, 1990, 31, 781-792.
90. Murphy RM. Static and dynamic light scattering of biological macromolecules: what can we learn. Current opinion in Biotechnology, 1997, 8, 25-30.
91. Rodd AB, Dunstan DE, Boger DV. Characterisation of xanthan gum solutions using dynamic light scattering and rheology. Carbohydrate Polymers, 2000, 42, 159-174.
92. Kostanski LK, Keller DM, Hamielec AE. Size-exclusion chromatography-a review of calibration methodologies. Journal of Biochemical and Biophysical Methods, 2004, 58, 159-186.
93. Striegel AM, Kirkland JJ, Yau WW, Bly D.D. Modern Size Exclusion Chromatography, Practice of Gel Permeation and Gel Filtration Chromatography, 2009, 2nd ed, Wiley: NY.
94. Kwok DY, Neumann AW. Contact angle interpretation in terms of solid surface tension. Colloids and Surfaces, A: Physicochemical and Engineering Aspects, 161, 2000, 31–38.
95. Grundke K, Bogumil T, Gietzelt T, Jacobasch H-J, Kwok DY, Neumann AW. Wetting measurements on smooth, rough and porous solid surfaces. Progress in Colloid and Polymer Science, 101, 1996, 58–67.
96. Rogers K, Takacs E, Thompson MR. Contact angle measurement of select compatibilizers for polymersilicate layer nanocomposites. Polymer Testing, 24, 2005, 423–427.
97. Howang M, Barron AR. BET Surface Area Analysis of Nanoparticles. OpenStax-CNX module: m3827. p.1-11.
98. Lowell S, Joan E, Martin A, Matthias T. Characterization of porous solids and powders: Surface area, pore size and density. Vol series 16, Chapter: Surface area analysis from the langmuir and BET theories. Springer, Netherlands, 2004, pp 58-81.
99. Walton KS, Snurr RQ. Applicability of the BET Method for Determining Surface Areas of Microporous Metal−Organic Frameworks. Journal of the American Chemical Society, 2007, 129, 8552-8556.

100. Ryzak M, Bieganowski A, Walczak RT. Application of laser diffraction method for determination of particle size distribution of grey-brown podzolic soil. Research and Aricultural Engineering, 2007, 53, 34-38.
101. Fu Q, Sun W. Mie theory for light scattering by a spherical particle in an absorbing medium. Applied Optics, 2001, 40, 1354-1361.
102. Andrews S, Nover D, Schladow SG. Using laser diffraction data to obtain accurate particle size distributions: the role of particle composition. Limology and Oceanography: Methods, 2010, 8, 507-526.
103. Theiss FL, Lopez A, Scholz R, Frost RL. A SEM, EDS and vibrational spectroscopic study of the clay mineral fraipontite. Spectrochimica Acta Part A: Molecular and Biomolecular Spectroscopy, 2015, 147, 230-234.
104. Kanematsu H, Barry DM. Biofilm and Materials, 2015, Chapter 23, pp. 188-189, Springer Publications, Switzerland.
105. Huang J, Cavanaugh T, Nur B. An Introduction to SEM Operational Principles and Geologic Applications for Shale Hydrocarbon Reservoirs. The American Association of Petroleum Geologists, 2013, 102, 1-6.
106. Nonrorv FH. Critical study of the differential thermal method for the identification of the clay minerals. Journal of American Ceramic Society, 22, 1979, 54-63.
107. SanAnot I. Recent developments in identification and analysis of crystalline material in powder form. Royal Society of Western Australia, 35, 1983, 9-25.
108. Senrr S. Application of thermal analysis to clays and aluminous minerals: U. S. Bureau of Mines, 1994.
109. Vie R, Azema N, Quantin JC, Touraud E, Fouletier M. Study of suspension settling: A approach to determine suspension classification and particle interactions. Colloids and Surfaces A: Physiochemical Engineering Aspects, 2007, 298, 192-200.
110. Mengual O, Meunier G, Cayre I, Puech K, Snabre P. Characterization of instability of concentrated dispersions by a new optical analyzer: the TURBISCAN MA 1000. Colloids and Surfaces A: Physiochemical Engineering Aspects, 1999, 152, 111-123.
111. Weipert D. The benefits of basic rheometry in studying dough rheology. American Association of cereal chemists, 1990, 67, 311-317.

112. Likavcan L, Kosik M, Bilik J, Martinkovic M. Determination of apparent viscosity as function of shear rate and fiber fractions in propoylene. International Journal of Engineering and Innovative Technology, 2014, 4, 23-26.

# **Chapter 2.** Production of carboxymethylated lignin and its application as a dispersant

Adapted from: Mohan K. Konduri[a], Fangong Kong[a, b], Pedram Fatehi*[a, ,]

European Polymer Journal, 70, 2015, 371-383.

[a] Department of Chemical Engineering,
Lakehead University,
955 Oliver Road,
Thunder Bay, ON P7B 5E1, Canada

[b] Key Laboratory of Pulp and Paper Science and Technology of Education Ministry of China,
Qilu University of Technology,
Jinan 250353, China.

*Corresponding author

## 2.1 Abstract

Kraft lignin is currently combusted in the pulping process to produce heat. It can be extracted from the process and converted to value-added products, but its limited water solubility hampers its end use applications. The main objective of this study was to investigate the carboxymethylation of hardwood kraft lignin to produce an anionic water soluble product. The results showed that the optimal conditions for carboxymethylation were 1.5 M NaOH concentration, 3 mol/mol sodium chloroacetate (SCA)/lignin ratio, 40 °C, 4 h and 16.7 g/L lignin concentration. The produced lignin had a charge density and carboxylate group of 1.8 meq/g and 1.68 mmol/g, respectively. The carboxymethylated lignin was further characterized using thermogravimetric analyzer (TGA), Fourier Transform Infrared (FTIR) spectrophotometer, Nuclear magnetic resonance spectroscopy (HNMR) and elemental analyses. Moreover; the application of carboxymethylated lignin as a dispersant for a clay suspension was successfully analyzed by means of a photometric dispersion analyzer.

Keywords: kraft lignin, biopolymers, carboxymethylation, grafting, charge density, clay

## 2.2 Introduction

The gradual depletion and the availability of oil are major concerns these days [1]. As natural products are renewable, the production of natural based products and the replacement of these products for oil based products would help develop more sustainable society [2]. Lignin is the most abundant aromatic (phenolic) sustainable polymer in nature after cellulose [3, 4]. Due its large production worldwide, kraft lignin has been recognised as a potential raw material for preparing high valued products, such as phenols, carbon fibers and fuels [5, 6]. Kraft lignin is produced via acidification of black liquor (i.e. pulping spent liquor) that is generated in the kraft pulping process [7]. The industrial applications of kraft lignin are limited due to its poor water solubility [8], thus improving the water solubility of kraft lignin can widen its application in various industries including the mining, painting, oil and pulp and paper. In the past, various studies were conducted on preparing water soluble alkali lignin through chemical modifications such as sulfonation [9], oxidation [10], and copolymerization [2]. However, due to the rigorous reaction conditions, including high temperature and the use of expensive catalysts and organic solvents, the large scale production of carboxmethylated lignin following the previous reactions is not economically feasible [2, 9, 10].

Several modification reactions of lignin were reported in the literature [11, 12]. Carboxymethylation, which is one of the most effective chemical modification techniques, was applied in preparing water soluble carboxymethylated lignin from non-wood species [13]. Sugarcane bagasse based lignin generated by an organosolv (ethanol) pulping process was carboxymethylated by treating with monochloroacetic acid in order to produce carboxymethylated lignin (CML), which could be used as a stabilizing agent in aqueous ceramic suspensions [14]. Da Silva modified lignin obtained from the acid hydrolysis of sugarcane bagasse to prepare CML, which was used as an adsorbent for the removal of brilliant RED 2BE from effluent of the textile industry [15]. Additionally, alkali lignin from wheat straw was modified using monochloroacetic acid in order to prepare CML, which was applied as a dispersant in graphite aqueous suspensions [16]. Straw soda aqueous lignin was also modified to form chelating resins for binding to copper metals [17]. In another report, an acetone-based lignin model compound was carboxymethylated using bromoacetic acid to prepare carboxymethylated lignin, which was also used as dispersant for gypsum paste [18].

However, there is no report on the carboxymethylation of hardwood kraft lignin. Currently, there is a surplus production of hardwood kraft lignin in the pulping process, which could be separated from black liquor (i.e. spent pulping liquor), and functionalized to produce value-added chemicals. The main novelty of this work was the production of a dispersant from hardwood kraft lignin via carboxymethylation for clay suspensions. The impact of carboxymethylation on the charge density of the product, which is known to be an important parameter for dispersants (and basically polyelectrolyte systems) [19], is discussed for the first time. In this context, the influence of reaction parameters on the preparation of carboxymethylated lignin from hardwood kraft lignin using sodium chloroacetate under alkali conditions were studied in order to obtain carboxymethylated kraft lignin with a high charge density and solubility. The properties of carboxymethylated lignin were determined using NMR, TGA, FTIR, potentiometric titrator, charge density and elemental analyses. The dispersion performance of carboxymethylation lignin for a clay suspension was also studied using a particle dispersion analyzer (PDA).

## 2.3 Experimental

### 2.3.1 Materials

Mixed hardwood kraft lignin supplied by FPInnovations from its pilot scale facilities located in Thunder Bay, ON. Sodium hydroxide and sodium chloroacetate (SCA), tetrohydrofuran, acetyl

bromide and acetic acid were obtained from Sigma Aldrich and used as received. Sulphuric acid (98%) was obtained from Sigma Aldrich Company and diluted to 1 M prior to use. Cellulose acetate dialysis membrane (molecular weight cut off of 1,000 g/mol) was obtained from Spectrum Labs. Inc., USA. Polydiallyldimethylammonium chloride (PDADMAC) used in the study was obtained from Sigma Aldrich company and diluted to 0.005 M prior to use. Potassium polyvinyl sulfate (PVSK) was obtained from Wako Pure Chemical Industries Ltd, Japan. Trimethylsilyl propionic acid (TSP) was obtained from Sigma Aldrich Company.

### 2.3.2 Carboxymethylation

The carboxymethylation of kraft lignin was conducted as described in the literature on the carboxymethylation of other biomass [20]. A 1 g sample of hardwood kraft lignin was mixed with sodium chloroacetate under various reaction conditions. The reaction parameters were NaOH concentration (0.5-2.5 M), SCA/lignin ratio (1- 6 mol/mol), reaction temperature (30-70 °C), reaction time (1- 6 h) and lignin concentration (11-25 g/L).The reactions were carried out in a 100 mL three neck glass round bottom flask under a constant stirring at 150 rpm. Upon completion, the solution was cooled to room temperature and its pH was adjusted to 7 using a 1 M sulfuric acid solution. Unreacted reagents were separated with membrane dialysis having a molecular weight cut off of 1000 g/mol, while changing the water every 12 h for 2 days. The dialyzed samples were dried in an oven at 105 °C overnight and later stored at 4 °C until further use. The modified lignin, which was generated using a 0.15 M $NaOH_{(aq)}$, 0.33 mol/mol lignin/SCA ratio, at 40 °C for 4 h and a lignin concentration of 16.7 g/L, had the greatest charge density and solubility, and it was selected as the best sample for further characterization with TGA and FTIR.

### 2.3.3 Solubility measurement

To measure the solubility, 0.2 g of unmodified lignin (UL) or carboxymethylated lignin (CML) was suspended in 20 mL of deionized water stirring at 100 rpm for 1 h at 30 °C in a water bath shaker [21]. Each sample was then centrifuged at 1000 rpm for 5 min and subsequently the supernatant was dried in a 60 °C oven overnight. The concentration of the carboxymethylated lignin in the supernatants was determined using equation 2.1

$$\text{Solubility (wt. \%)} = \frac{\text{Mass of dissolved lignin}}{\text{Initial mass of lignin}} \times 100 \qquad (2.1)$$

To measure the solubility of samples at different pHs, 0.2 g of unmodified and carboxymethylated lignin samples was suspended in 20 mL of deionized water at different pHs ranging from 1 to 12 and incubated in a water bath shaker at for 30 min at 30 °C at 100 rpm. The solubility was determined as according to the previous section.

To measure the solubility of samples at different concentrations, different amounts of carboxymethylated lignin sample was mixed with water in order to make different concentrations of lignin in the range of 10 and 100 g/L. Afterwards, the solubility of lignin samples was determined as explained in the previous section.

All the solubility experiments were done in triplicates and average values were reported

### 2.3.4 Charge density and FTIR analysis

In preparing the samples for analysis, the carboxymethylated lignin was initially dried in a 100 °C oven overnight to remove moisture. A 0.2 g of sample was then suspended in 20 ml of deionized water and incubated for 1 h at 30 °C in a water bath shaker at 150 rpm. After incubation, the sample was centrifuged for 10 min. at 1000 rpm. The supernatant was used to determine the charge density using a particle charge detector (Mutek, PCD 04, Germany) against a PVSK standard solution (0.005M). All the experiments were repeated three times and average values were reported

FTIR (Fourier Transform Infrared Spectroscopy) analysis was conducted for both the unmodified and carboxymethylated kraft lignin samples. The samples were first dried in a 105 °C oven overnight and a 0.05 g of unmodified and carboxymethylated lignin samples were used for FTIR analysis using a Bruker Tensor 37, Germany, ATR accessory. The spectra were recorded in transmittance mode in the range 500 $cm^{-1}$ and 4000 $cm^{-1}$ with a 4 $cm^{-1}$ resolution.

### 2.3.5 pH determination during the reaction

To an alkali solution (pH 12), a 1 g sample of kraft lignin was mixed with sodium chloroacetate. The reaction was carried out in a 100 mL three neck round bottom glass flask at 50 °C for 6 h with constant stirring at 150 rpm. Samples were taken from the flask every 1 h time interval and the pH of the medium was determined using pH meter, HI 208 (HANNA Instruments).

### 2.3.6 Carboxylate group analysis

An aqueous potentiometric titration method was used for measuring the carboxylate group content of unmodified and carboxymethylated lignin samples using an automatic potentiometer,

Metrohm, 905 Titrado, Switzerland. 1 g samples of unmodified and carboxymethylated lignin were added to 100 mL of distilled water and the pH of the solution was adjusted to 10.5. The solution was then titrated with a cationic polymer, TEGO trant A100, to measure the amount of carboxylate groups. The degree of substitution was calculated based on equation 2.2 [22].

$$\text{Degree of substitution (DS)} = \frac{\mathrm{M} \times \mathrm{A}}{1 - 0.081 \times \mathrm{A}} \qquad (2.2)$$

where A is the total carboxylate group content (mmol/g), 0.081 (g/mmol) is the net increase in mass for each sodium carboxymethyl group attached to lignin [23] and M is the mass of the basic unit of lignin (g). All the measurements were repeated three times and average values were repeated.

### 2.3.7 Molecular weight analysis

Molecular weight analysis was performed for both unmodified and carboxymethylated lignin samples using a high performance liquid chromatography (HPLC) system, Agilent model 1200 (USA), equipped with Styragel HR4, HR4E and HR1 columns, UV and a multi angle laser light detector. Tetrohydrofuran was used as an eluent and conditions maintained were 1 mL/min flow rate, 35 °C and 50 min. Polystyrene was used as the standard solution. Samples were prepared via drying in a 105 °C oven overnight and then acetylating 0.01 g of dried lignin using 2.5 mL of acetyl bromide/acetic acid (8:92) at 50 °C for 2 h with gentle shaking. The acetylated samples were then dried under a reduced pressure to remove the acetic acid and then freeze dried until further use.

### 2.3.8 Elemental Analysis

Elemental analysis was performed for both unmodified and carboxymethylated lignin samples using an Elementar Vario EL Cube Elemental Analyzer by combustion method [24]. In preparing the samples for analysis, the samples were dried in a 105 °C oven overnight to remove any moisture. A 0.002 g sample of unmodified and carboxymethylated lignin samples were used for determining carbon, hydrogen, nitrogen and oxygen contents of the samples.

### 2.3.9 Thermogravimetric Analysis

The thermal analysis of carboxymethylated and unmodified lignin samples was conducted by using a thermogravimetric analyzer, TGA, i-1000 series, Instrument Specialist Inc. The samples were dried in an oven at 105 °C overnight and 7.5 mg of unmodified and carboxymethylated lignin samples were used for this analysis. The analysis was carried out under nitrogen at a

steady flow rate of 35 mL/min. Each sample was heated from room temperature to 800 °C at the rate of 10 °C/min

### 2.3.10 $^{1}$H-NMR analysis

The unmodified and carboxymethylated lignin samples were characterized by a Varian Unity, INOVA 500 MHz, spectrometer [25]. The samples were dried in an oven at 105 °C overnight and 60 mg of UL and CML was dissolved in 2 mL of $D_2O$ at 30 °C for 2 h and 170 rpm. The $^{1}$HNMR spectra were recorded at 21 °C after 16 scans. A 45° pulse flipping angle, a 4.6 μs pulse width, a 2.05 s acquisition time, and 1 s relaxation delay time were considered for this analysis.

The formation of a by-product, i.e. glycolic acid, of the carboxymethylation reaction was confirmed using a Varian Unity INOVA 500 MHz spectrometer [26]. The carboxymethylated reaction medium was centrifuged at 1000 rpm for 5 min after the reaction. To 1 mL of filtrate collected after the carboxymethylation reaction, 0.5 mL of $D_2O$ was added and incubated at 30 °C for 2 h at 150 rpm. Trimethylsilyl Propionic acid (TSP) was used as an internal reference standard for the NMR analysis. The $^{1}$H-NMR spectra of the samples were recorded at 21 °C after 8 scans. A 15° pulse flipping angle, a 4.6 μs pulse width, a 2.05 s acquisition time, and 1 s relaxation delay time were used in the NMR analysis. The peak at 3.93 ppm, which corresponded to methylene protons of glycolic acid, was considered to measure its concentration in the reaction medium [27].

### 2.3.11 Dispersion Analysis

A kaolin clay suspension of 100 g/L was used as a model sample in this study. The dispersion experiments were conducted using a photometric dispersion analyzer (PDA 3000, Rank Brothers Ltd), which was connected to a dynamic drainage jar (DDJ) fitted with a 70 mm mesh screen [28]. In the present study, 500 mL of distilled water was taken into the DDJ container and circulated from the DDJ to the PDA through a 3 mm plastic tube until a steady flow rate of 20 mL/min was achieved. The flow rate was regulated by peristaltic pump throughout the experiment. Then, 20 mL of a 100 g/L clay suspension was added into DDJ with a stirring speed of 100 rpm. This caused a decrease in the initial base DC voltage ($V_0$) to undispersed DC voltage ($V_i$). After 100 s, the carboxymethylated lignin (1 wt. %) produced under optimal conditions stated above was added to the suspension mixture at a dosage of 0.1 wt.% of a clay suspension. Unmodified lignin was also used as a control sample in this experiment. The increase in DC voltage was represented as a final suspension DC voltage ($V_f$). The pH of the clay suspensions

was maintained at 7.5 during the experiments. The dispersion performance of a kaolin clay suspension, which was represented by relative turbidity $\tau_r$, was measured from the variation in the direct current (DC) voltage of the PDA instrument [29]. The relative turbidity of the clay suspension was measured by using the following equation 2.3 [30]:

$$\text{Relative turbidity, } \tau r = \frac{\tau f}{\tau i} = \frac{ln(\frac{V0}{Vf})}{ln(\frac{V0}{Vi})} \quad (2.3)$$

Where $\tau_f$ is denoted as the final suspension turbidity, and $\tau_i$ is denoted as initial suspension turbidity.

## 2.4 Results and Discussion

### 2.4.1 Carboxymethylation of lignin

The reaction scheme for the carboxymethylation of lignin is shown in Figure 2.1. The carboxymethylation of lignin is performed using sodium chloroacetate as a carboxylate group donor (Figure 2.1a). Under alkali conditions, NaOH reacts with the hydroxyl group of the lignin's aromatic ring, generating a strong nucleophile. The alkoxide ion from the alkali lignin attacks the chloroacetate via a $S_N2$ reacting resulting in the ether methyl carboxylation of lignin. The degree of carboxymethylation depends on the number of hydroxyl group substitution with carboxymethyl groups. Furthermore, glycolic acid and NaCl could also be generated as by-products from sodium chloroacetate (Figure 1b) [16].

The hardwood lignin is made up of *p*-coumaryl alchol, sinapyl alcohol and coniferyl alcohol. Among them, sinapyl alcohol constitutes major percentage of hardwood lignin. In this context, sinapyl alcohol was chosen for representation [31].

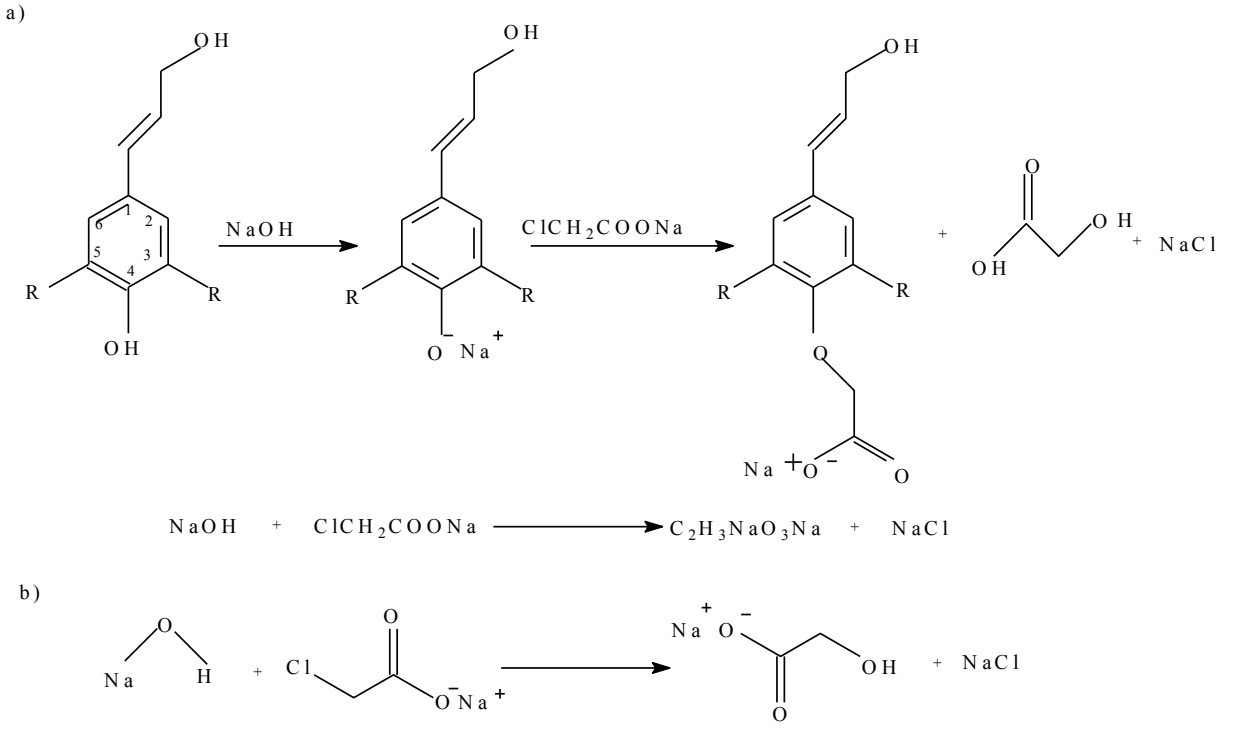


Figure 2.1. a) Carboxymethylation of lignin reaction scheme b) Possible undesired reactions. "R" can be OCH3 or H

### 2.4.2 Glycolic acid analysis

Figure 2.2 shows $^{1}$H-NMR spectrum of glycolic acid produced as a by-product of the reaction shown in Figure 1 during carboxymethylation of kraft lignin. The peak at 3.9 ppm corresponds to the methylene protons of glycolic acid, which confirms the presence of glycolic acid in the reaction mixture [27]. In a $^{1}$H-NMR study on the determination of glycolic acid, the presence of glycolic acid was confirmed by a single resonance peak at 3.9 ppm, which belongs to methylene protons of glycolic acid over a sweep width of 3800 Hz [25]. In another study on carboxymethylation of a xylan extracted from birch kraft pulp, the presence of peaks in the region of 4 and 4.3 ppm in the $^{1}$H-NMR analysis revealed the generation of glycolic acid as a by-product of the carboxymethylation reaction [49].

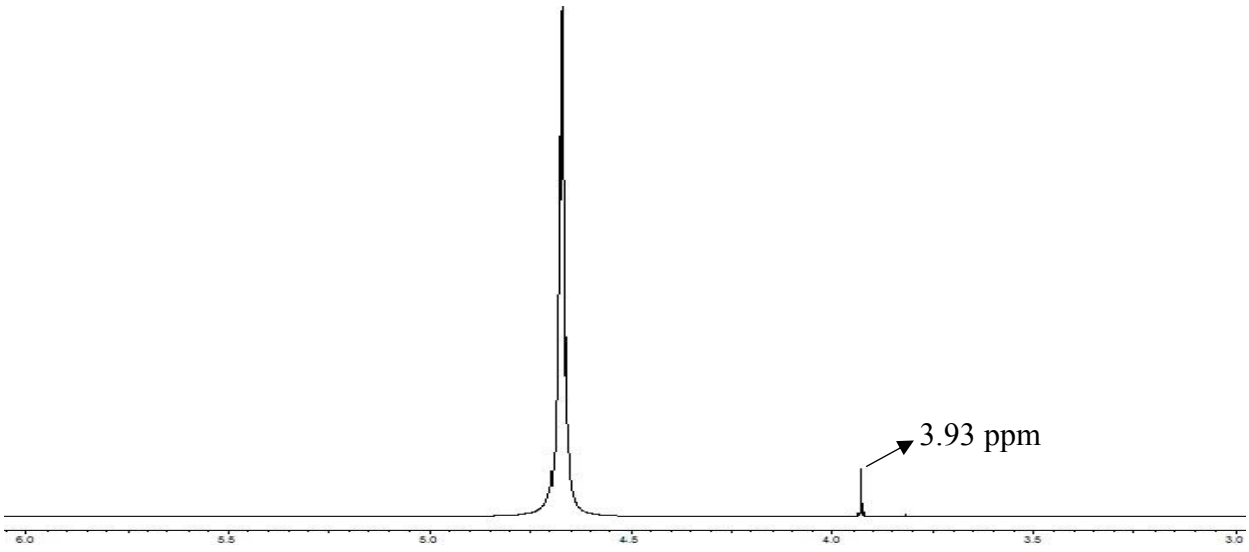


Figure 2.2. $^{1}$H-NMR spectrum of glycolic acid produced during carboxymethylation of lignin

### 2.4.3 Effect of NaOH concentration

The charge density and solubility of carboxymethylated kraft lignin as a function of NaOH concentration were shown in Figure 2.3. The maximum charge density (1.2 meq/g) and solubility (87 wt. %) were obtained using a 1.5 M of $NaOH_{(aq)}$ solution. This increase in solubility of the modified lignin is due to the greater affinity of nucleophilic substitution of hydroxyl group with a carboxylate group at a para position on the aromatic ring of the lignin [32]. Additionally, it was reported that NaOH was used for generating stronger nucleophiles in the aromatic ring of lignin, which further reacted with sodium chloroacetate to produce carboxymethylated lignin [16]. The Reaction efficiency is closely related to the affinity of nucleophilic substitution of the hydroxyl group with sodium methyl carboxylate and the production of by-products (as discussed in the previous section). The concentration of NaOH in solutions should be sufficient in order to promote the carboxymethylation process. However, sodium chloroacetate could react with sodium hydroxide to produce sodium glycolate at a higher concentration as shown in Figure 1b. In one study, a decrease in the carboxylate group of wheat straw alkali lignin was observed on the carboxymethylation of lignin at a high NaOH concentration [32, 33].

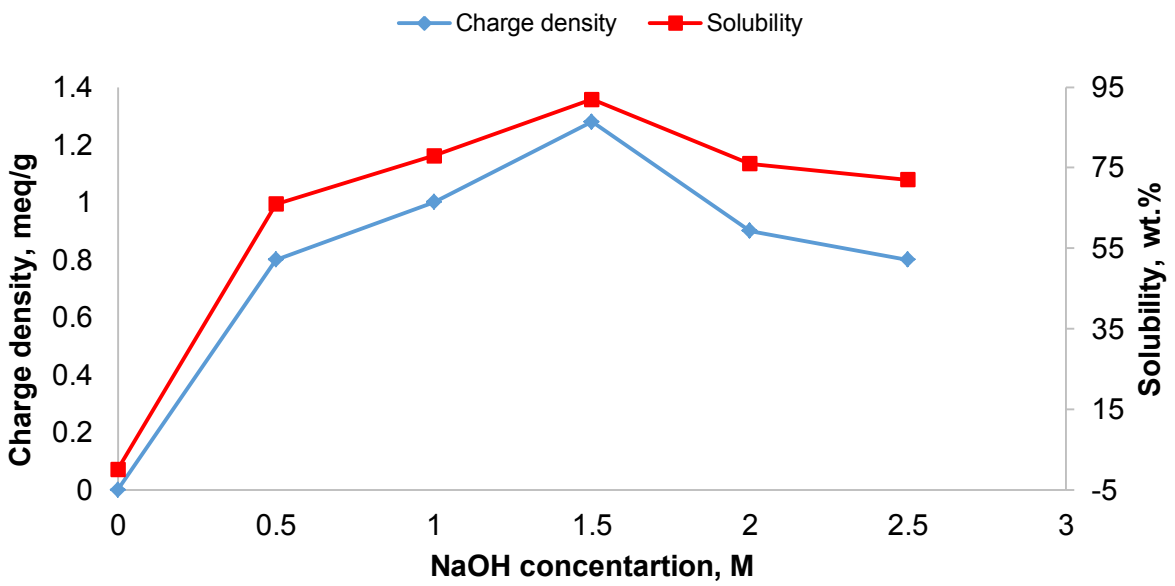


Figure 2.3. Effect of NaOH concentration on the charge density and solubility of carboxymethylated lignin under conditions of 14.3 g/L lignin concentration, 2 mol/mol ratio of SCA/lignin, 50 °C and 4 h

### 2.4.4 Effect of SCA/lignin mole ratio

The impact of SCA/lignin molar ratio on the charge density and solubility of modified lignin is shown in Figure 2.4. The charge density increased with the increase in the sodium chloroacetate until it reached the maximum of 1.8 meq/g at the molar ratio of 3. Similarly, the maximum solubility of 100 wt.% was obtained at SCA/lignin molar ratio of 3. Further increase in SCA concentration resulted in a decrease in both charge density and solubility. This can be attributed to the increase in the production of glycolic acid with the increase in SCA concentration as shown in Figure 4. Glycolic acid produced as a by-product of the reaction and acts as an inhibitor of the reaction [34]. In a study on the carboxymethylation of wheat straw alkali lignin using monochloroacetic acid, with the increase in the monochloroacetic concentration from 16 to 36 wt. % , the carboxylate group content was found to increase to 2.6 mmol/g, but further increase in the concentration of monocholoroacetic acid to 50 wt. % led to a decrease in the carboxylate group content [16]. In other reports, a higher SCA to lignin or starch molar ratio was claimed to lead to the production of sodium glycolate [1, 35, 36].

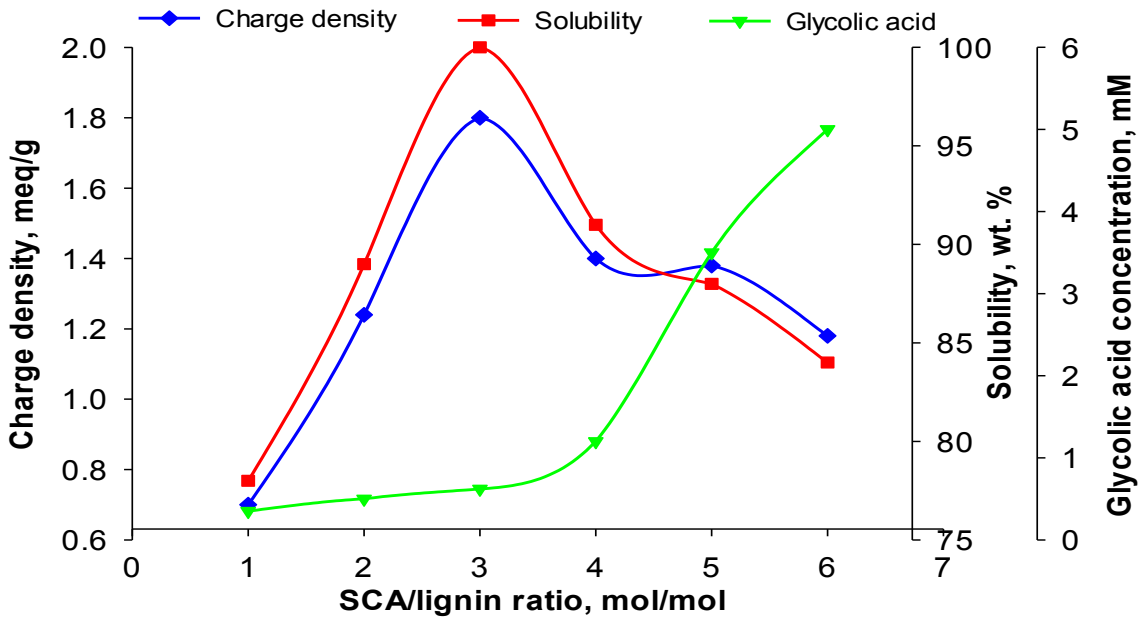


Figure 2.4.:Effect of molar ratio of SCA/lignin on glycolic acid concentration, charge density and solubility of carboxymethylated lignin under the conditions of 1.5 M NaOH concentration, 16.7 g/L lignin concentration, 40 °C and 4 h

### 2.4.5 Effect of Temperature

The changes in the charge density and solubility of the carboxymethylated lignin as a function of temperature are presented in Figure 2.5. By increasing the reaction temperature from 30 to 50 °C, the charge density of modified lignin increased to 1.3 meq/g. The maximum solubility of 89 wt.% was obtained at 40 °C. In a previous study on the carboxymethylation of sugarcane bagasse lignin, the maximum solubility was obtained at 50 °C [37]. Other reports have found that, with the increase in temperature, the degradation of reactants occurred, which in turn affected the pH of the reaction [38]. Further increase in the temperature resulted in a decrease in charge density and solubility of modified lignin (Figure 5). This may be due to the undesired alkaline hydrolysis of sodium monocholoroacetate. In one report on the carboxymethylation of peat by monochloroacetic acid, with an increase in temperature from 50 to 100 °C, the solubility and the amount of carboxymethyl groups increased from 40 to 80 wt.% and from 13.2 to 20.5 mol %, respectively [39].

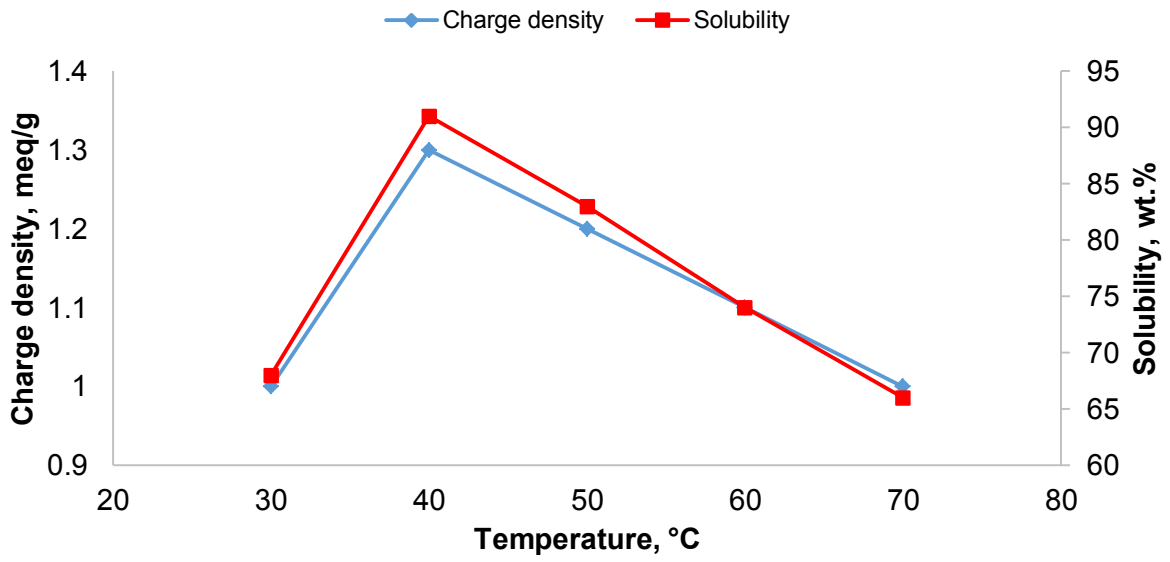


Figure 2.5. Effect of temperature on the charge density and solubility of carboxymethylated lignin under the conditions of 1.5 M NaOH concentration, 2 mol/mol SCA/lignin ratio, 14.3 g/L lignin concentration and 4 h

### 2.4.6 Effect of Time

The effect of time on the charge density and solubility of carboxymethylated lignin is shown in Figure 2.6. The maximum charge density (1.2 meq/g) and solubility (90 wt.%) were obtained at 4 h of reaction. By extending reaction time from 0.5 to 4 h, the charge density and solubility were both increased. The increases in the charge density and solubility are due to the progress of desired reaction. Further increase in time resulted in a decrease in the charge density and solubility. Similarly, as the reaction progresses, the end pH of the reaction mixture was decreased from 12.7 to 11.2. Thus, a decrease in charge density and solubility of lignin can be attributed to a decrease in pH due to consumption of NaOH as the reaction progress. Higazy and coworkers reported a similar result on the carboxymethylation of flax using monochloroacetic acid under alkali conditions [40]. In another study on carboxymethylation of cellulose, the reaction was optimized in 3 h [41].

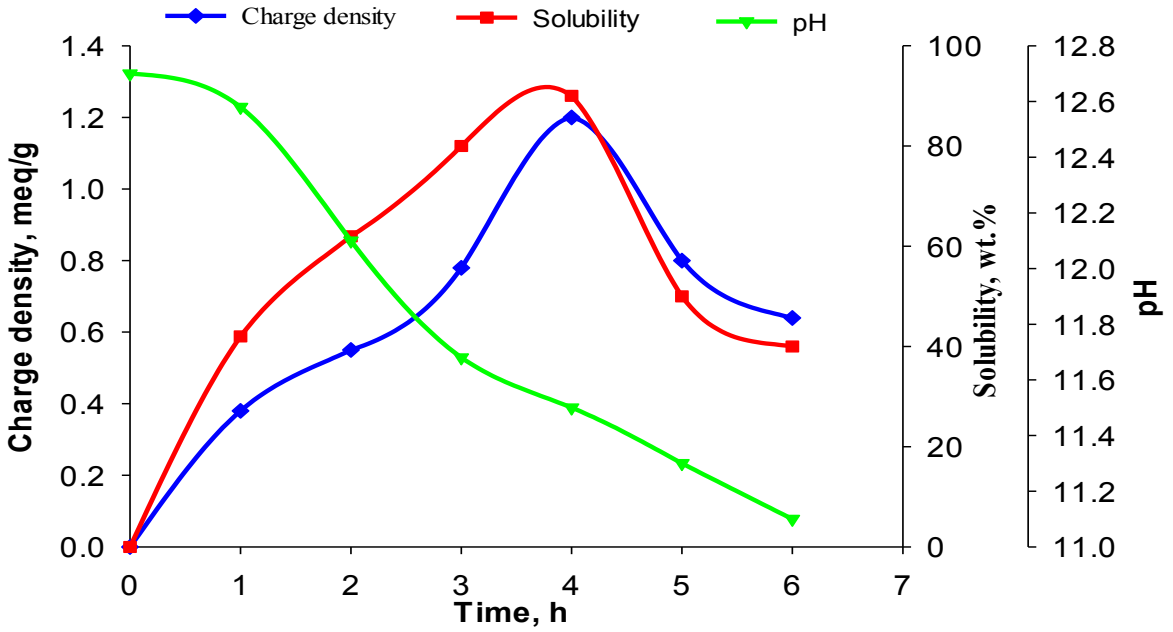


Figure 2.6. Effect of time on the pH, charge density and solubility of carboxymethylated lignin under the conditions of 1.5 M NaOH concentration, 2 mol/mol SCA/lignin ratio, 40 °C and 14.3 g/L lignin concentration.

### 2.4.7 Effect of lignin concentration

The charge density and solubility of the carboxymethylated lignin as a function of concentration is shown in Figure 2.7. By increasing the lignin concentration to 16.7 g/L, the charge density and solubility were increased to 1.24 meq/g and 90 wt.%, respectively. These increases are due to more frequent collisions of reagents in reaction media at higher concentrations [13]. Further increase in the concentration decreased the charge density and solubility, which could be due to the formation of undesirable by-products including glycolic and acetic acid. On the carboxymethylation of bran and husk rice powders, with an increase in the concentration from 10 to 40 g/L, the solubility was increased to 40% and 34%, respectively, which is due to introduction of carboxymethyl groups on the bran and husk rice powders, respectively [42].

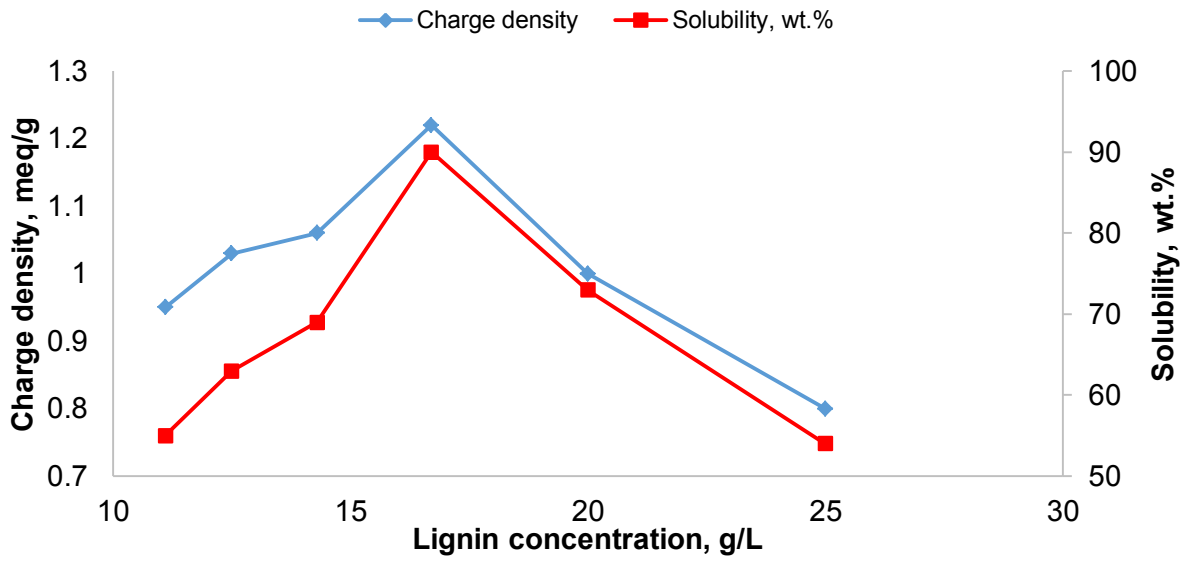


Figure 2.7. Effect of concentration of lignin on the charge density and solubility of carboxymethylated lignin under conditions of 1.5 M NaOH concentration, 2 mol/mol SCA/lignin ratio, 40 °C and 4 h

Results in Figures 2.3-2.7 generally show that the studied parameters significantly affected the production of carboxymethylated lignin in comparison with that of glycolic acid; and process optimization was an important factor in obtaining the product with desired properties.

### 2.4.8 Structural analysis of lignin

#### 2.4.8.1 Determination of carboxylate groups

The carboxymethylated lignin with the highest charge density and solubility, which was produced under the optimal conditions (1.5 M $NaOH_{(aq)}$, 3 mol/mol SCA/lignin ratio, 40 °C, 4 h and 16.7 g/L lignin) were selected for further analysis. Table 1 lists the properties of unmodified and carboxymethylated lignin samples. The carboxylate degree of unmodified and carboxymethylated lignin samples were found to be 0.15 mmol/g and 1.68 mmol/g, respectively (Table 2.1). This carboxylation degree would result in the degree of substitution of 0.03 and 0.36 for both unmodified and carboxymethylated lignin samples. The degree of substitution for unmodified lignin corresponds to carboxylate group that is already attached to lignin. In the past, the carboxymethylation of lignin obtained from spruce had a degree of substitution of 0.45 for water insoluble and 0.86 for water soluble lignin [22]. The carboxymethylation of hemicelluloses, which was conducted under alkaline conditions at 75 °C for 2 h using 0.005 mol sodium chloroacetate and 40% NaOH, led to a degree of substitution of 0.58 [43].

.

Table 2-1: Properties of unmodified and carboxymethylated lignin samples

| Sample | Elemental Analysis | | | | | COOH content, mmol/g | Degree of Substitution (DS) | Charge density, meq/g |
|---|---|---|---|---|---|---|---|---|
| | C, wt.% | H, wt.% | O, wt.% | N, wt. % | S, wt.% | | | |
| Unmodified lignin | 64.76 | 5.78 | 26.67 | 0.03 | 0.11 | 0.15 | 0.03 | 0.21 |
| Carboxymethylated lignin | 56.59 | 4.95 | 33.08 | 0.02 | 0.13 | 1.68 | 0.36 | 1.80 |

#### 2.4.8.2 .Characterization of carboxymethylated kraft lignin

The FTIR spectra of unmodified and carboxymethylated lignin samples are shown in Figure 2.8. The stretching band between 3400 and 3100 $cm^{-1}$ corresponds to the O-H band of aliphatic hydroxyl and phenolic hydroxyl groups. The absorption peaks at 2930 $cm^{-1}$ and 2300 $cm^{-1}$ correspond to C-H and C=C stretches of aldehyde groups [2]. There are three strong absorption peaks at 1600, 1510 and 1454 $cm^{-1}$ assigned to aromatic skeletal vibrations [31]. Furthermore, the band at 1263 $cm^{-1}$ belongs to guaiacyl assigned to C=O stretching, the band at 1209 $cm^{-1}$ belongs to aromatic ring assigned to C-O and C=O stretching and that at 1030 $cm^{-1}$ corresponds to aromatic C-H in plane deformation and C-O in primary alcohols [42]. Comparing the FTIR spectra of unmodified and carboxymethylated lignin, the change in O-H bond stretch between 3400 and 3100 $cm^{-1}$ is due to the decrease in hydroxyl groups in carboxymethylated lignin [32]. Similarly, an increase in peak intensity at 1600, 1263 and 1030 $cm^{-1}$ corresponds to the introduction of carboxylate group at the para position of aromatic rings in the modified lignin [18]. Thus, FTIR results confirm that there was an introduction of carboxylate group to the modified lignin due to the carboxymethylation of lignin with sodium chloroacetate.

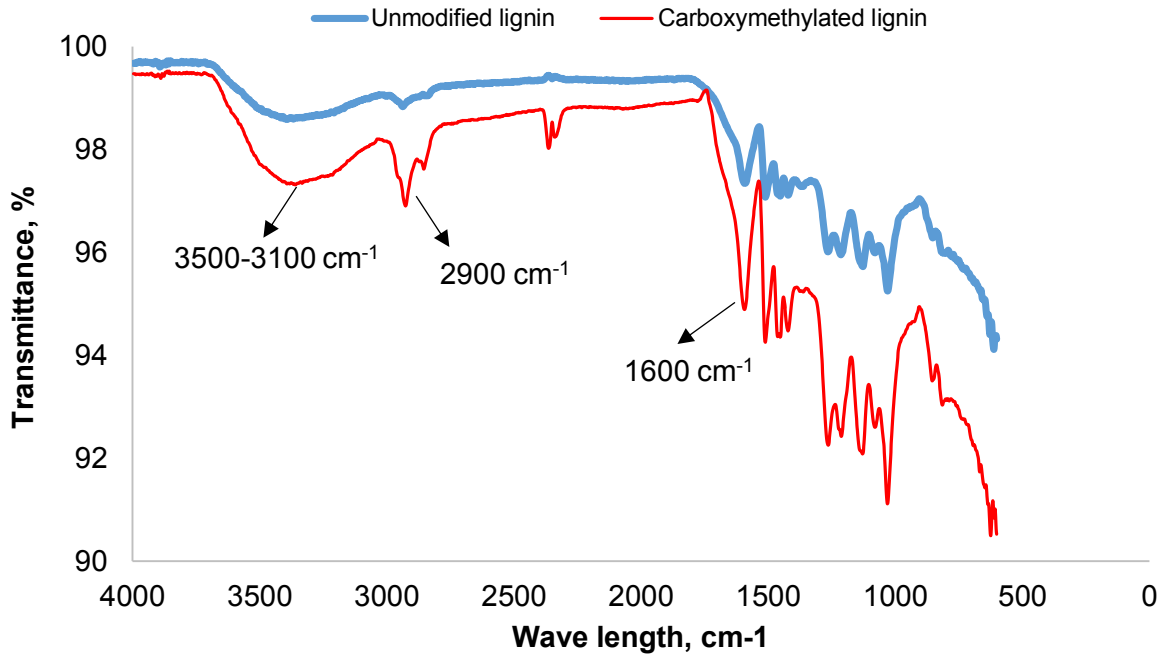


Figure 2.8. FTIR Spectra of unmodified and carboxymethylated lignin

### 2.4.8.3 Molecular weight determination

The results of molecular weight distribution of unmodified and carboxymethylated lignin samples are provided in Table 2.2. The carboxymethylated lignin had a slightly higher weight average molecular weight ($M_w$) of 29,960 g/mol and number average molecular weight $M_n$ of 22,820 g/mol compared to those of unmodified lignin ($M_w$ of 24,870 g/mol and $M_n$ of 17,985 g/mol). This increase in molecular weight can be attributed to the replacement of hydroxyl groups by carboxymethyl groups and the condensation of lignin during the carboxymethylation reaction [20]. The polydispersity ($M_w/M_n$) of lignin was slightly decreased from 1.38 to 1.31, which may be due to the alkaline degradation of lignin during carboxymethylation or the addition of carboxymthylate group to lignin structure [43].

Table 2-2: Molecular weight distribution of unmodified and carboxymethylated lignin

| Sample | $M_w$, g/mol | $M_n$, g/mol | $M_w/M_n$ |
|---|---|---|---|
| Unmodified lignin | 24,800 | 17,900 | 1.38 |
| Carboxymethylated lignin | 29,900 | 22,800 | 1.31 |

#### 2.4.8.4 . Chemical composition of kraft lignin

The results of elemental analysis for unmodified and carboxymethylated lignin samples are also provided in Table 2.1. The molecular formula was calculated to be $C_9H_{9.65}O_{2.78}S_{0.05}$ and $C_9H_{9.00}O_{3.82}S_{0.06}$ for unmodified and carboxymethylated lignin (nitrogen was removed from the formula due to its trace amount), respectively. It is evident that the amount of oxygen increased and the amount of hydrogen decreased in the modified lignin compared to unmodified sample confirming the carboxymethylation of kraft lignin [44]. The sulfur content of lignin may be attributed to attachment of sulfur groups during acidification of lignin in the kraft lignin production via LignoForce technology. No significant change in sulfur content of lignin was observed after carboxymethylation. In one study on the carboxymethylation of bagasse lignin using oxidation process, a decrease in the carbon and hydrogen contents and an increase in the oxygen content of lignin were reported [45].

#### 2.4.8.5 Thermogravimetric analyses (TGA)

The thermal characteristics of unmodified and carboxymethylated lignin samples are presented in Figure 2.9. It is seen that more weight loss was observed for carboxymethylated lignin compared to unmodified lignin, when the temperature was below 200 °C. Due to more hydrophilicity of carboxymethylated lignin than unmodified lignin, the carboxymethylated lignin might have absorbed more moisture at room temperature prior to analysis. This increase in hydrophilicity can be attributed to the introduction of carboxylate group to lignin during carboxymethylation of lignin [46]. The mass loss at a temperature higher than 200 °C corresponds to degradation of polymer backbone. Unmodified lignin showed about 55 wt.% loss between 220 °C and 380 °C. In the case of carboxymethylated lignin, approximately 35 wt.% loss was observed between 240 and 550 °C. Furthermore, 40 wt.% of carboxymethylated lignin was remained as ash at 700 °C, while unmodified lignin was completed decomposed. The high thermal stability of the carboxymethylated lignin with 40 % residue at 750 °C is due to ether bond linkages formed during carboxymethylation [47]. In a study conducted on the decomposition analysis of poly ether-ether ketone, it was reported that ether bonds started decomposing at 600 °C and remained 50 wt.% at 750 °C [48].

In this study, the ash that was generated during the incineration of modified kraft lignin could be most probably bottom ash (as it was heavy and stayed in the TGA container) with very low sulfur content and non-hazardous to environment.

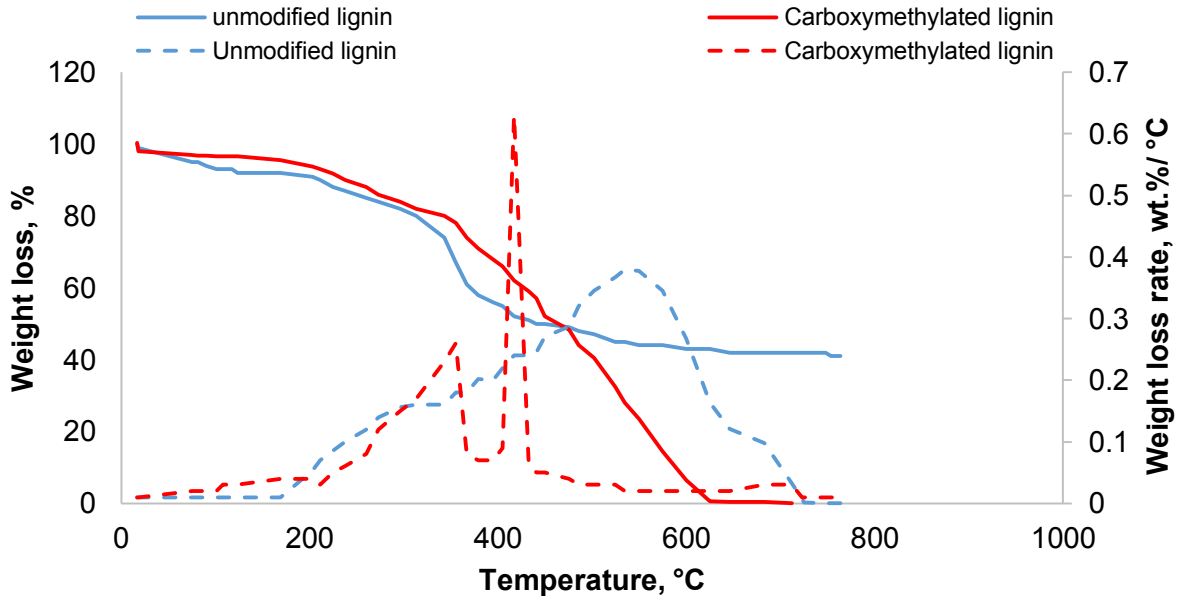


Figure 2.9. Weight loss and weight loss rate of unmodified and carboxymethylated lignin at 35 mL/min nitrogen flow rate

### 2.4.8.6 $^{1}$HNMR analysis

Figure 2.10 presents $^{1}$H-NMR spectra of unmodified and carboxymethylated lignin. The peaks at 8.0 and 6.5 ppm in unmodified lignin correspond to the protons of phenolic hydroxyl groups and aromatic ring, respectively [27]. The peak at 3.4 ppm corresponds to the protons of methoxyl groups. Compared to unmodified lignin, carboxymethylated lignin had a stronger peak at 8.1 ppm, which represents an increase in phenolic hydroxyl groups (due to demethylation and ether bond cleavage). Furthermore, the peaks at 6.5 and 3.5 ppm were significantly weaker in the carboxymethylated lignin, which might be due to the breakage of aromatic ring and methoxyl groups during carboxymethylation [1]. Furthermore, the peak at 3.8 ppm in carboxymethylated lignin corresponds to the protons of carboxymethyl groups attached to lignin, which is absent in unmodified lignin [49]. Thus, $^{1}$H-NMR analysis confirms that carboxymethyl groups were attached to lignin during modification. In the work reported by Gan and co-workers on the carboxymethylation of wheat straw alkali lignin using monochloroacetic acid, the attachment of

carboxymethyl groups in the lignin was determined by the peaks at 4.0 ppm in the H-NMR analysis [16].

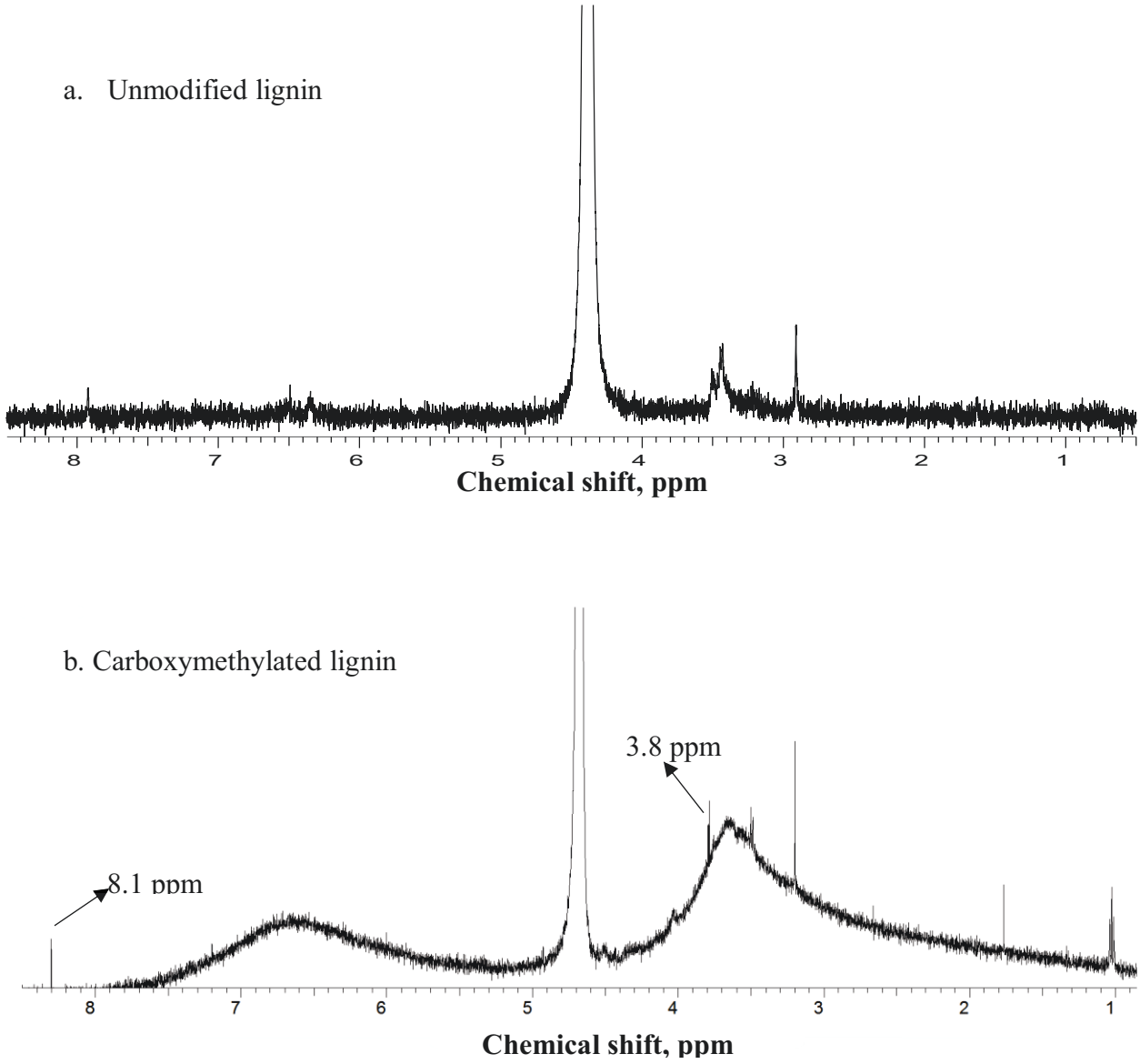


Figure 2.10. HNMR spectra of a) unmodified lignin b) Carboxymethylated lignin

As previously stated, the pH influences the solubility of lignin and its end use applications. Therefore, it is crucial to investigate the impact of pH on the solubility of carboxymethylated lignin. The dependence of the lignin solubility on the pH of solution is shown in Figure 2.11. The unmodified and carboxymethylated lignin samples are soluble at a pH higher than 11, but unmodified lignin was insoluble at a pH lower than 10, which has previously been reported [45].

The carboxymethylated lignin tended to become insoluble at pH 5. The pKa of carboxylate group is 4.76 and below this pH, the carboxylate groups become protonated, which decreases its solubility [50]. Furthermore, the maximum solubility of carboxymethylated lignin was found to be 80 g/L at pH 7.

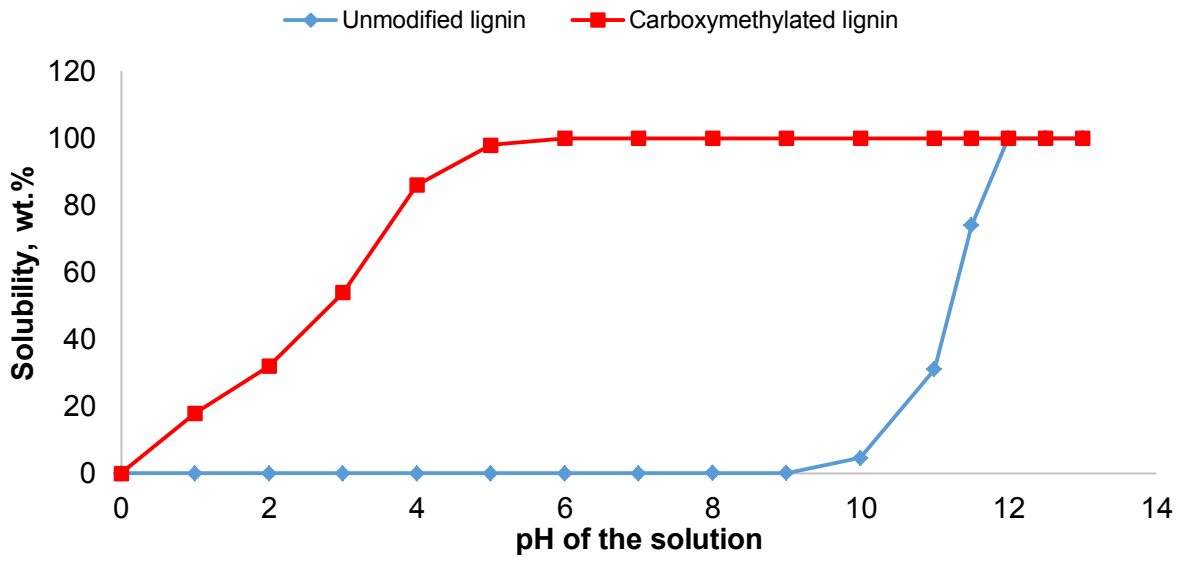


Figure 2.11. Effect of pH on the solubility of unmodified and carboxymethylated lignin under conditions of 10 g/L lignin concentration, 30 °C and 24 h

### 2.4.10 Dispersion analysis

Figure 2.12 represents the dispersion performance of unmodified and carboxymethylated lignin in aqueous clay suspensions at pH 7. The results showed that the clay suspension mixed with carboxymethylated lignin showed showed the high relative turbidity of 1.08 compared to the clay suspension mixed with unmodified lignin (0.99). By adding carboxymethylated lignin (with a charge density of -1.8 meq/g), the extra charges introduced by carboxymethylated lignin to the clay suspension improved repulsion between clay particles, and this increased the DC voltage and turbidity of the clay sample [51]. In a work conducted by Pawlik on coal aqueous slurries, anionic polymers were found to be better dispersants compared to non-ionic polymers because of their ability to generate electrostatic repulsion forces between the coal particles [52]. A similar work on the stabilization of ceramic particles using anionic polymeric dispersants, it was reported that the addition of poly acrylic acid and poly ethylene glycol improved the dispersion of ceramic particles in the suspension [53]. In addition, the produced carboxymethylated lignin

may also be used as a dispersant in the mining industry (ore suspensions), pesticide formulations, ceramic suspensions and cement admixture [14, 17, 54-55]

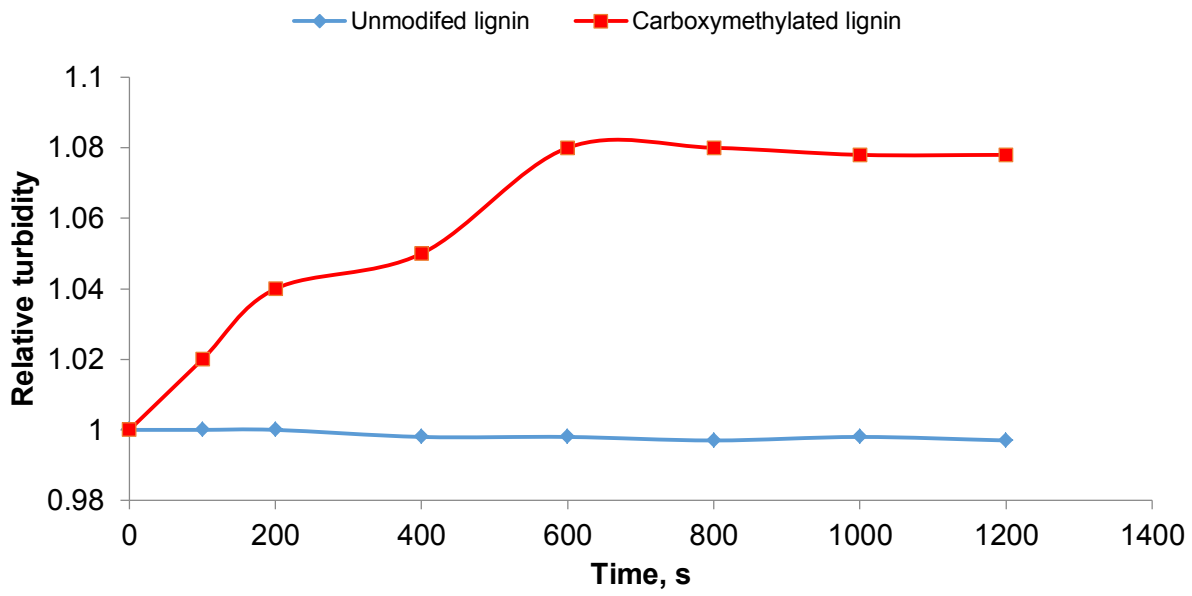


Figure 2.12. Relative turbidity of clay suspension (20 g/L) as a function of time in the treatment of clay suspension with 0.1 wt.% of carboxymethylated lignin or unmodified lignin at pH 7 and 100 rpm.

## 2.5 Conclusions

Carboxymethylated kraft lignin was successfully prepared in an aqueous medium by using sodium chloroacetate under alkali conditions. Sodium chloroacetate could promote carboxymethylation effectively by introducing carboxylate group on the aromatic ring (para position) of lignin. The FTIR, NMR and TGA analyses confirmed the addition of carboxylate group to the OH of phenolic group of lignin. The H-NMR analysis also confirmed the production of glycolic acid as a by-product in the carboxymethylation of kraft lignin. Carboxymethylated lignin with the highest carboxylate group and charge density was obtained under the conditions of 1.5 M NaOH concentration, 3 mol/mol of lignin/SCA ratio at 40 °C, 4 h and 16.7 g/L lignin concentration. Molecular weight analysis also confirmed an insignificant increase in the molecular weight of lignin after the carboxymethylation. The solubility of lignin was found to be pH dependent in that kraft lignin was insoluble at a pH below 10, whereas the carboxymethylated lignin was soluble at a pH higher than 5. The dispersion studies suggested that carboxymethylated lignin was an effective dispersant for a clay suspension. The results depicted that water soluble kraft lignin with a relatively high charge density and low molecular

weight can be obtained via carboxymethylation. The application of carboxymethylated lignin as a dispersant for various ore suspensions of the mining industry as well as cement and concrete admixtures will be assessed in future.

## 2.6 References


1. Gan L, Zhou D, Yang D, Qiu X. Aggregation and adsorption behaviours of carboxymethylated lignin (CML) in aqueous solution. Holzforschung, 2013, 67, 379-385.
2. Gan L, Zhou M, Yang D, Qiu X. Preparation and evaluation of carboxymethylated lignin as a dispersant for aqueous graphite suspension using Turbiscan Lab Analyzer. Journal of Dispersion Science and Technology, 2013, 34, 644-650.
3. Ishihara T, Miyazaki M. Oxidation of milled wood lignin by fungal laccase. Mokuzai Gakkaishi, 1972, 18, 415-419.
4. Leonowicz A, Szklarz G, Wojtas-Wasilewska M. The effect of fungal laccase on fractionated lignosulphonates (Peritan Na). Photochemistry, 1985, 24, 393-396.
5. Sarkanen KV, Ludwig CH. Lignins; Occurrence, Formation, Structure and Reactions. John Wiley & Sons, Inc: New York, 1971, pp. 250-255.
6. Fengel D, Weneger, G. Wood: Chemistry, Ultrastucture, Reactions. John Wiley & Sons, Inc: New York, 1983, pp. 304-310.
7. Wenbo Y, Huanzhen MU, Yanchu H. Treatment of black liquor from the paper making industry by acidification and reuse. Journal of Environmental Science, 2003, 15, 697-700.
8. Runcang S, Tomkinson F, Mao F, Sun X. Physicochemical characterization of lignin from rice straw by hydrogen peroxide treatment. Journal of Applied Polymer Science, 2001, 79, 719-732.
9. Gonclaves A, Benar P. Hydroxymethylation and oxidation of organosolv lignins and utilization of products. Bioresource Technology, 2001, 79, 103-111.
10. Maziero P, Neto MO, Machado D, Batista D, Cavalheiro CS. Structural features of lignin obtained at different alkaline oxidation conditions from sugarcane bagasse. Industrial Crops and Products, 2012, 35, 61-69.
11. Malutan T, Nicu R, Popa VI. Contribution to study of hydroxymethylation reaction of alkali lignin. BioResources, 2008, 3, 13-20.

12. Pang YX, Qing-Qui XD, Ming-Lou H. Influence of oxidation, hydroxymethylation and sulfomethylation on the physicochemical properties of calcium lignosulfonate. Colloids and Surfaces A: Physicochemical and Engineering Aspects, 2008, 312, 154-159.
13. Hon DNS, Chemical modification of lignocellulosic materials. Marcel Dekker, Inc: New York, 1996, pp. 129-135.
14. Cerrutti B, De Souza C, Castellan A, Ruggiero R, Frollini E. Carboxymethyl lignin as stabilizing agent in aqueous ceramic suspensions. Industrial Crops and Products, 2012, 36, 108-115.
15. Da Silva LG, Ruggiero R, Gontijo PM, Pinto RB, Royer B, Lima EC, Fernanades THM, Calvete T. Adsorption of Brilliant Red 2BE dye from water solutions by a chemically modified sugarcane bagasse lignin. Journal of Chemical Engineering, 2012, 168, 620-628.
16. Gan L, Zhou M, Qiu X. Preparation of water soluble carboxymethylated lignin from wheat straw alkali lignin. Advances in Material Research, 2012, 550-555, 1293-1298.
17. Hubbe MA, Hadi Hasan S, Ducoste JJ. Cellulosic substrates for removal of pollutants from aqueous systems: A review. 1. Metals. BioResources, 2011, 6, 2161-2287.
18. Matushita Y, Imai M, Tamura T, Fukushima K. Preparation and evaluation of a dispersant for gypsum paste from acid hydrolysis lignin. Journal of Applied Polymer Science, 2005, 98, 2508-2513.
19. Norgren M, Lindstrom B. Physico-Chemical characterization of a fractionated kraft lignin. Holzforschung, 2000, 54, 528-534.
20. Lange W, Schweers W. The carboxymethylation of organosolv and kraft lignin. Wood Science and Technology, 1980, 14: 1-7
21. Winowiski T, Lebo S, Gretland K, Gustafsson J. Characterization of sulfonated lignin dispersants by hydrophobic interactive chromatography. Journal of ASTM International, 2005, 2, 79-84.
22. Chien SN, Amidon TE, Lai YZ. Fractionation of wood polymers by carboxymethylation: Exploring the strategy. Tappi Journal, 2012, 11, 29-37
23. Peng XW, Ren JL, Zhong LX, Peng F, Sun RC. Xylan rich hemicelluloses- graft acrylic acid ionic hydrogels with rapid responses to pH, salt, and organic solvents. Journal of Agricultural Food Chemistry, 2012, 59,8208-8215.

24. Sarwar Jahan M, Liu Z, Wang H, Saeed A, Ni Y. Isolation and characterization of lignin from prehydrolysis liquor of kraft based dissolving pulp production. Cellulose Chemistry and Technology, 2012, 46, 261-267.
25. Males RG, Herring FG. A $^{1}$HNMR study of the permeation of glycolic acid through phosphoplipid membranes. Biochimca et Biophysica Acta, 1999, 1416, 333-338.
26. Yu G, Li B, Wang H, Liu C, Mu X. Preparation of concrete superplasticizer by oxidation-sulfomethylation of sodium lignosulfonate. Bioresources, 2013, 8, 1055-1063.
27. Dali S, Lefebvre H, Gharbi RE, Fradet A. Synthesis of poly(glycolic acid) in liquids. Journal of Polymer Science: Part A: Polymer Chemistry, 2006, 44, 3025-3035.
28. Zhang X, Liu W. Sodium titanium nanobelt as a microparticle to induce clay flocculation with CPAM. BioResources, 2010, 5, 1895-1907.
29. Xiao X, Liu Z, Wiseman N. Synergetic effect of cationic polymer microparticles and anionic polymer on fine clay flocculation. Journal of Colloid Interface Science, 1999, 216, 409-417.
30. Ovenden C, Xiao H. Flocculation behaviour and mechanisms of cationic inorganic microparticle/polymer systems. Colloids and Surfaces A: Physicochemical and Engineering Aspects, 2002, 197, 225-234.
31. Santos RB, Capanema EA, Balakshin MY, Chang HM, Jameel H. Lignin structural variation in hardwood species. Journal of Agriculture and Food Chemistry, 2012, 60, 4923-4930.
32. Deng Y, Feng X, Zhou M, Qian Y, Yu X, Qin X. Investigation of aggregation and assembly of alkali lignin using iodine as a probe. Biomacromolecules, 2011, 12, 1116-1125.
33. Jin Z, Yu Y, Shao S, Ye J, Lin L, Iiyama K. Lignin as a cross linker of acrylic acid grafted carboxymethyl lignocellulose. Journal of Wood Science, 2010, 56, 470-476.
34. Saghir S, Iqbal MS, Hussain MA, Koschella A, Heinze T. Structure characterization and carboxymethylation of arabinoxylan isolated from Ispaghula (Plantago ovata). Carbohydrate Polymers, 2008, 74, 309-317.
35. Lee S, Kim S, Pant BR, Kwen HD, Song HH, Lee SK, Nehete SY. Carboxymethylation of corn starch and characterization using asymmetrical flow field-flow fraction coupled with multi angle light scattering. Journal of Chromatography A, 2010, 1217, 4623-4628.
36. Peternele SW, Winkler-Hechenleitner AA, Gomez Pineda EA. Adsorption of Cd (II) and Pb (II) onto functionalized formic lignin from sugar cane bagasse. Bioresource Technology, 1999, 68, 95-100.

37. Barbara C, Montane D, Rinaudo M, Farriol X. Synthesis and characterization of carboxymethyl celluloses (CMC) from non-wood fibers I. Accessibility of cellulose fibers and CMC synthesis. Cellulose, 2002, 9, 319-326.
38. Efanov MV, Popova AA. Carboxymethylation of peat by monochloroacetic acid. Chemistry of Natural Compounds. Chemistry of Natural Compounds, 2011, 47, 498-499.
39. Higazy A, Hashem MM, Abou-Zeid NY, Hebeish A. Rendering flax fibre dyeable with basic dyes via partial carboxymethylation. Journal of the Society of Dyes and Colourists. Journal of the Society of the Dyers and Colourists, 1996, 112, 329-332.
40. Barai BKR, Singhal RS, Kulkarni PR. Optimization of process for preparing carboxymethyl cellulose from water hyacinth. Carbohydrate Polymers, 1997, 32, 229-231.
41. Choi OK, Yang CS, Kim ED, Kang WS, Shin M, Chaoi YH, Ko S. Improving solubility through carboxymethylation of different sized endosperm, bran and husk rice powders. Food Science and Biotechnology, 2009, 18, 1439-1446.
42. Ren JL, Sun RC, Peng F. Carboxymethylation of hemicelluloses isolated from sugarcane bagasse. Polymer Degradation and Stability, 2008, 93, 786-793.
43. Alekhina M, Mikkonen KS, Alen R, Tenkanen M, Sixta H. Carboxymethylation of alkali extracted xylan for preparation of bio-based packaging films. Carbohydrate Polymers, 2014, 100, 89-96.
44. Mousavioun P, Doherty WOS. Chemical and thermal properties of bagasse soda lignin. Industrial Crops and Products, 2010, 31, 52-58.
45. Pinkert A, Goeke DF, Marsh KN, Pang S. Extracting wood lignin without dissolving or degrading cellulose: Investigation on the use of food additive derived ionic liquids. Green Chemistry, 2011, 13, 3124-3136.
46. Liu X, Yu L, Liu H, Chen L, Li L. In situ thermal decomposition of starch with constant moisture in a sealed system. Polymer Degradation and Stability, 2008, 93, 260-262.
47. Nada AMA, Hassan ML. Ion exchange properties of carboxylated bagasse. 8th Arab International conference on polymer science and technology; Nov 27-30, 2005.
48. Patel P, Hull TR, McCabe RW, Flath D, Grasmeder J, Percy M. Mechanism of thermal decomposition of poly(ether ketone) from a review of decomposition. Polymer Degradation and Stability, 2010, 95, 709-718.

49. Li S, Lundquist, K. A new method for analysis of phenolic groups in lignins by $^{1}$HNMR. Nordiac Pulp and Paper Research Journal, 1994, 3, 191-195.
50. Riemenschneider W. Carboxylic acids, aliphatic in Ulmann's encyclopedia of industrial chemistry. Wiley-VCH: Weihelm, 2002.
51. Xu R, Zhuang W, He Q, Cai J, Hu B. Effects of chemical structure on the properties of carboxylate-type copolymer dispersant for coal water slurry. American Institute of Chemical Engineers Journal, 2009, 55, 2461-2467.
52. Pawlik M. Polymeric dispersants for coal water slurries. Colloids and Surfaces A: Physicochemical and Engineering Aspects, 2006, 266, 82-90.
53. Tyliszczak B, Sobczak-Kupiec A, BialikWas K, Kaspryzk W. Stabilization of ceramic particles with anionic polymeric dispersants. Journal of Nanoscience and Nanotechnology, 2012, 12, 9312-9318.
54. Li Z, Ge Y. Extraction of lignin from sugarcane bagasse and its modification into a high performance dispersant for pesticide formulations. Journal of Brazilian Chemical Society, 2011, 22, 1866-1871.
55. Darweesh HHM, EI-Meligy MG. Pulp white liquor waste as a cement admixture-part 1. American Journal of Mining and Metallurgy, 2014, 2, 88-93.

# **Chapter 3.** Production of water soluble hardwood kraft lignin via sulfomethylation using formaldehyde and sodium sulfite

Adapted from: Mohan K. R. Konduri, Pedram Fatehi*[a]

ACS Sustainable Chemistry and Engineering, 3(6), 2015, 1172-1182.

[a] Department of Chemical Engineering,

Lakehead University,

955 Oliver Road,

Thunder Bay, ON P7B 5E1, Canada

*Corresponding author

## 3.1 Abstract

Kraft lignin can be extracted from black liquor (i.e. spent liquor) from kraft pulping process to produce value-added chemicals, but its limited water solubility hampers its end-use applications. The main objective of this study was to investigate the sulfomethylation of kraft lignin to produce water soluble kraft lignin with an anionic charge density. In this work, hardwood kraft lignin was modified with formaldehyde and sodium sulfite under alkali conditions. The optimum conditions for sulfomethylation were 0.5 M $NaOH_{(aq)}$, 0.9 mol/mol sodium hydroxymethylsulfonate/lignin at 100 °C, for 3 h and 20 g/L lignin concentration. The resulting lignin had a charge density of -1.60 meq/g and sulfonated group content of 1.48 mmol/g. The molecular weight, structure, thermal behavior and elemental analyses of the product were also assessed. The modified lignin was used as a cement dispersant and the dispersibility of cement was increased from 60 mm to 155 mm by adding 1.2 wt.% sulfomethylated lignin (SML). However, unmodified lignin did not change the dispersibility of cement.

**Keywords**: Kraft lignin, Sulfomethylation, Sodium sulfite, TGA, Charge density, FTIR, Solubility

## 3.2 Introduction

Lignin is the most abundant renewable resource after cellulose. In chemical pulping processes, around 100 million tonnes of lignin is produced annually [1]. However, the majority of kraft lignin is incinerated in the recovery section of the kraft process for energy recovery. Kraft lignin can be recovered and used in the production of value-added products [2]. In this regard, lignosulfonate (LS), which is produced as a by-product of sulfite pulping process, has been used in various end-use applications including a dye dispersant, water reducing agent for cement admixture, or chelating agent [3]. The supply of LS is limited in the world and lignosulfonate from other technical lignins should be produced so that the market demand can be satisfied.

Sulfonated lignin with a high purity and quality can be produced from different lignin types and species. Studies were conducted on the preparation of water soluble sulfonated lignin from wood and non-wood lignin via sulfonation [4] and sulfomethylation [5]. In one study, sulfomethylated lignin (SML) was prepared by treating wheat straw lignin with formaldehyde and sodium sulfite [6]. Yasuda and coworkers [7] converted acid hydrolysed pinewood lignin model compound (cresol) to water soluble sulfonated lignin via sulfonation using sodium sulfite. Lignin has also been extracted from birch wood and converted to a water soluble product via sulfonation with

sodium sulfite under alkaline conditions [8]. However, the production of water soluble sulfonated hardwood kraft lignin has not been attempted in the past, and is the first objective of this study.

Several applications were suggested for sulfonated lignin. Sulfomethylated lignin obtained from treating sugarcane bagasse lignin with sodium sulfite and formaldehyde was used as a dispersant in pesticide formulations [9]. In another study, sulfomethylated lignin prepared from the sulfomethylation of esparto grass lignin with sodium sulfite and formaldehyde was used as a water reducer for cement admixture [10]. In another study, sulfonated lignin produced from treating softwood kraft lignin with sodium sulfite was found to be effective as a corrosion inhibitor for iron based materials [11]. Alternatively, lignosulfonate produced via sequential chemical modification of wood kraft lignin using aliphatic polyamine, aliphatic acyl chloride, formaldehyde and sodium sulfite served as a surfactant for crude oil [4]. In the past, sulfonated lignin prepared by treating low molecular weight pine (softwood) kraft lignin with sodium sulfite was used as a flocculant in water purification systems [12].

Due to the large production of hardwood lignin in kraft pulping process, the surplus amount of hardwood lignin could be used for the production of various value-added products. The sulfomethylation of hardwood kraft lignin offers an opportunity for producing water soluble products. The main novelty of this work is the optimization of parameters that influence sulfomethylation process during the production of lignosulfonate from hardwood kraft lignin by using Taguchi orthogonal design. Also, the impact of sulfomethylation on the charge density of the produced sulfonated lignin was discussed for the first time, which is known to be an important parameter of dispersants and flocculants in polyelectrolyte systems [13]. Nevertheless, the charge density of lignin can be directly related to its sulfonate groups [14].

The present study investigated the influence of reaction parameters on the preparation of sulfomethylated lignin from hardwood kraft lignin using formaldehyde and sodium sulfite. The characteristics of sulfomethylated lignin were determined by means of FTIR, potentiometric titrator, charge density and elemental analyses; meanwhile, the application of sulfomethylated lignin as a cement dispersant was studied.

## 3.3 Experimental

### 3.3.1 Materials

Mixed hardwood kraft lignin was supplied by FPInnovations from its pilot plant facilities located in Thunder Bay, ON [15]. Commercial cement was purchased from a retailer in Thunder Bay, Canada. Commercial lignosulfonate used in this study was obtained from Sigma and used as received. Sodium hydroxide, formaldehyde (37 wt.%), tetrohydrofuran (99.9 wt.%), acetyl bromide (99 wt.%), acetic acid (99.7 wt.%) and sodium sulfite used in this study were obtained from Sigma and used as received. Sulphuric acid (98 wt.%) obtained from Sigma Aldrich, and was diluted to 1 M concentration prior to use. Cellulose acetate dialysis membrane (molecular weight cut off of 1000 g/mol) was obtained from Spectrum Labs. Inc., USA. Polydiallyldimethyammonium chloride (PDADMAC) was obtained from Sigma-Aldrich Company and diluted to 0.005 M prior to use. Potassium polyvinyl sulfate (PVSK) was obtained from Wako Pure Chemical Industries Ltd., Japan, and diluted to 0.005 M prior to use.

### 3.3.2 Sulfomethylation

The sulfomethylation of kraft lignin was conducted as previously described in sulfomethylation of alkali corn stalk lignin [6]. A 1 g sample of hardwood kraft lignin (Mw,180 g/mol) was mixed with formaldehyde (37 wt.%) and sodium sulfite under various conditions. The reaction parameters investigated were NaOH concentration (0.25-1 molar concentration), sodium hydroxymethylsulfonate/lignin ratio (0.3-1.2 mol/mol), reaction temperature (80-140 °C), reaction time (1- 7 h) and lignin concentration (10-25 g/L). All the reactions were carried out in a 100 ml three-neck round bottom glass flask under constant stirring at 150 rpm. Upon completion, the solution was cooled to room temperature and then brought up to pH 7 using 1 M sulfuric acid. Unreacted sodium hydroxide, sodium sulfite and formaldehyde were separated from sulfonated kraft lignin by dialysis membranes, while changing the water every 12 h. The dialysed samples were then dried at 105 °C in an oven overnight and stored at 4 °C for further use. Based on charge density and solubility, the modified lignin, which was generated using of 0.5 M $NaOH_{(aq)}$, 0.9 mol/mol sodium hydroxymethylsulfonate/lignin ratio at 100 °C for 3 h, and a lignin concentration of 20 g/L, was selected as the best sample for further characterization using FTIR, TGA and elemental analysis. Hardwood kraft lignin (1 g) was mixed with formaldehyde (0.1 M) and sodium sulfite (0.1 M) under alkali conditions (pH 12). The reaction was carried out in a 100 ml three neck round bottom glass flask for at 100 °C for 8 h under constant stirring at

150 rpm. Samples were drawn from the flask every 1 h interval and pH of the medium was determined using pH meter, HI 208 (HANNA Instruments). This analysis determined the impact of reaction time on the pH of the reaction medium.

Taguchi's orthogonal array (OA) was used for obtaining the maximum charge density and solubility of sulphomethylated lignin under optimized conditions [16]. In this study, L16 orthogonal design with five factors (each at four levels) was used to investigate the effect of parameters on sulfomethylation reaction [17]. The conditions listed in Table 3.1 were selected for conducting optimization analysis using a L16 orthogonal design. In each experiment, three samples were prepared to minimize the errors. The standard deviation was determined based on the results and shown in Figures 2 to 7.

Table 3-1. Parameters considered for the optimization of sulphomethylation reaction based on Taguchi L16 orthogonal array design

| Run | Time, h | Temperature, °C | NaOH concentration, M | $CH_4NaO_4S$/lignin ratio, mol/mol | Lignin concentration, g/L |
|---|---|---|---|---|---|
| 1 | 1 | 80 | 0.25 | 0.3 | 10 |
| 2 | 1 | 100 | 0.5 | 0.6 | 15 |
| 3 | 1 | 120 | 0.75 | 0.9 | 20 |
| 4 | 1 | 140 | 1 | 1.2 | 25 |
| 5 | 2 | 80 | 0.5 | 0.9 | 25 |
| 6 | 2 | 100 | 0.25 | 1.2 | 20 |
| 7 | 2 | 120 | 1 | 0.3 | 15 |
| 8 | 2 | 140 | 0.75 | 0.6 | 10 |
| 9 | 3 | 80 | 0.75 | 1.2 | 15 |
| 10 | 3 | 100 | 1 | 0.9 | 10 |
| 11 | 3 | 120 | 0.25 | 0.6 | 25 |
| 12 | 3 | 140 | 0.5 | 0.3 | 20 |
| 13 | 4 | 80 | 1 | 0.6 | 20 |
| 14 | 4 | 100 | 0.75 | 0.3 | 25 |
| 15 | 4 | 120 | 0.5 | 1.2 | 10 |
| 16 | 4 | 140 | 0.25 | 0.9 | 15 |

Afterwards, the analysis of variance model (ANOVA) with *F*-test (Fisher test) was used to identify which process parameter significantly affected sulfomethylation reaction and which combination levels of process parameters produced a maximum response [17]. The definition of sample variance is shown in equation 3.1 [18]:

$$S^2 = \frac{1}{n-1} \Sigma (y_i - \bar{y}) \quad (3.1)$$

where $\boldsymbol{\Sigma}$ (yi - ȳ) refers to sum of squared (SS) deviation from the mean, 1/(n-1) refers to degrees of freedom (df), $S^2$ refers to mean squares (MS), which represents sum of squares divided by degrees of freedom used to quantify the error.

*F*-test refers to significance of variance or factor, which is quantified by the following equation 3.2 [18]:

$$F = \frac{MS_F}{MS_E} \quad (3.2)$$

where $MS_F$ is a mean square of the factor and $MS_E$ is a mean square of the error. Basing on the F test, if the variance caused by the factor ($MS_F$) is higher than the variance caused by the error ($MS_E$), the factor will have a significant effect on the response and thus, the higher the F test, the higher the significance effect would be [18].

### 3.3.3 Solubility

#### 3.3.3.1 Solubility determination

To measure the solubility of lignin samples, 0.2 g of unmodified lignin (UL) or sulfomethylated lignin was suspended in 20 ml of deionized water by stirring at 100 rpm for 2 h at 30 °C in a water bath shaker [19]. The samples were centrifuged at 1000 rpm for 5 min, and the supernatant was dried overnight in a 60 °C oven. As lignin has different structures and molecular weights, the sulphomethylation of lignin may not be able to solubilize all lignin segments. Therefore, reporting the solubility in wt.% would directly show how much of original lignin segments were solubilized. The solubility of lignin in the supernatants was determined according to equation 3.3.

$$\text{Water Solubility (wt.\%)} = \frac{\text{Mass of dissolved lignin}}{\text{Initial mass of lignin}} \times 100 \quad (3.3)$$

#### 3.3.3.2 Solubility vs pH

To measure the solubility of lignin samples at different pHs, 0.2 g of unmodified and sulfomethylated lignin samples was suspended in 20 ml of deionized water at different pHs ranging from 1 to 12. These samples were incubated in a water bath shaker for 2 h at 30 °C and 100 rpm. The solubility of these samples was determined according to equation 2.

#### 3.3.3.3 Solubility vs concentration

To measure the solubility of lignin samples at different concentrations, the sulfomethylated lignin sample was mixed with deionized water and was incubated in a water bath shaker at 100 rpm, pH 7 for 2 h at 30 °C.

### 3.3.4 Charge Density and FTIR Analyses

To measure the charge density of lignin samples, sulfomethylated lignin and commercial lignosulfonate were initially dried at 105 °C overnight to remove moisture. A 0.2 g sample of lignin samples was dissolved in 20 ml of deionized water and incubated for 1 h at 30 °C in a water bath shaker at 150 rpm. After the incubation, the samples were centrifuged at 1000 rpm for 10 min and supernatants were collected for the charge density analysis by using a particle charge detector (Mutek, PCD 04, Germany) and titrated against a PDADMAC standard solution (0.005 M).

To measure the charge density of cement particles, 0.2 g of cement was added into 20 ml of PVSK standard solution (0.005 M) and incubated for 2 h at 30 °C in a water bath shaker at 150 rpm. Simultaneously, a control sample (20 ml PVSK solution) without cement particles was also incubated under the same conditions. After the incubation, the samples were centrifuged at 1000 rpm for 10 min and collected supernatants were back titrated against a PDADMAC standard solution (0.005 M) in order to measure the charge density by using a particle charge detector. The difference between the blank and test samples were used to calculate the charge density of cement particles [20]. The Fourier Transform Infrared Spectrophotometer (FTIR) analysis was conducted on unmodified and sulfomethylated lignin samples. The samples were dried in a 105 °C oven overnight and 0.05 g of the sample was then used for structural characterization using FTIR (Bruker Tensor 37, Germany, ATR accessory). The spectra were recorded in transmittance mode in the range of 500 $cm^{-1}$ and 4000 $cm^{-1}$ with 4 $cm^{-1}$ resolution, while 32 scans per sample were conducted.

### 3.3.5 Zeta Potential Analysis

In this experiment, 0.2 g of cement was added to 20 ml of sulfomethylated lignin solution (lignin concentration is 10 g/L) and incubated in water bath shaker at 30 °C for 2 h at 150 rpm. Simultaneously, to measure the zeta potential of cement particles in the absence of sulfomethylated lignin, 0.2 g of cement was added to 20 ml of distilled water and incubated under the same conditions as described above. After the incubation, samples were analyzed for their surface zeta potential using compact automatic zeta meter (Laval labs Inc) [21]. All the measurements were carried out under room temperature with constant electric field (8.4 V/cm). Before and after each measurement, the micro-electrophoresis cell was washed with deionized water to prevent any cross contamination.

### 3.3.6 Sulfonated Group Analysis

The aqueous potentiometric titration method was used to measure the sulfonated group attached to unmodified and sulfomethylated lignin samples using an automatic potentiometer, Metrohm, 905 Titrado, Switzerland. In this experiment, a 1 g sample was added to 100 ml of distilled water and the pH of the solution was adjusted to 7.0 using 1M $H_2SO_4$. The solutions were then titrated against a cationic polymer, TEGO trant A 100, in order to determine the number of sulfonated groups. The degree of substitution was calculated based on equation 3.4 [22].

$$\text{Degree of Substitution (DS)} = \frac{\text{M} \times \text{A}}{1 - 0.117 \times A} \tag{3.4}$$

in which A is total sulfonated group content (mmol/g), 0.117 (g/mmol) is the net increase in mass for each sodium sulfomethyl group attached to lignin and M is mass of the basic unit of lignin (0.188 g/mmol for a $C_9$ unit of lignin) [23].

### 3.3.7 Molecular Weight Analysis

A 0.1 g sample of air dried unmodified lignin (UL) was dissolved in 4 ml of acetic anhydride/pyridine 1/1 (V/V) solution and was stirred for 30 min at 300 rpm at 25 °C. The solution was left for 24 h in the absence of light, and then it was poured in an excess (50 ml) of ice water and centrifuged/washed three times. The solvent was then removed from sample using freeze dryer. The acetylated UL was dissolved in 10 ml of tetrahydrofuran (THF) at 300 rpm for 30 min at room temperature and filtered with a PTFE filter (13 mm diameter and 0.2 µm pore size). The collected filtrate samples were used for molecular weight analysis. For sulfomethylated lignin (SML) and commercial lignosulfonate analysis, a 0.05 g of samples was

air dried and then dissolved in 10 ml of a 0.1 mol/l $NaNO_3$ solution and filtered with a nylon 0.2 µm filter (13 mm diameter). The filtered samples were used for molecular weight analysis.

The molecular weight analysis of the samples was carried out using size exclusion chromatography, Malvern GPCmax VE2001 Module + Viscotek TDA305 with RI and viscometer detectors. For UL measurements, the organic columns of PolyAnalytic PAS106M, PAS103 and PAS102.5 were used, and HPLC-grade tetrahydrofuran (THF) was used as solvent and eluent. The flow rate was set at 1.0 ml/min. For SML and commercial lignosulfonate measurements, the columns of PolyAnalytic PAA206 and PAA203 were used, and 0.1 mol/l $NaNO_3$ solution was used as solvent and eluent. The flow rate was set at 0.70 ml/min. The column temperature was set up at 35 °C for both systems. Polystyrene polymers were used as standards for the organic system and the polyethylene oxide for the aqueous system.

### 3.3.8 Elemental Analysis

The elemental analysis of lignin samples was performed using an Elementar Vario EL Cube elemental analyzer by combustion analysis method. The samples were first dried in a 105 °C oven overnight in order to remove any moisture. Approximately, 2 mg of unmodified and sulfomethylated lignin samples were weighed in silver vessels and loaded in the integrated carousel of elemental analyzer. Furthermore, the samples were automatically transferred into combustion tube and burnt at 1200 °C. Afterwards, the combustion gases were reduced and analyzed for carbon, hydrogen, nitrogen and oxygen content of the samples [24].

### 3.3.9 Thermogravimetric Analysis

The thermal analysis of sulfomethylated and unmodified lignin samples was conducted using a thermogravimetric analyzer, TGA, i-1000 series, Instrument Specialist Inc. The samples were dried in an oven at 105 °C overnight and 8 mg of unmodified and sulfomethylated lignin samples were used for this analysis. The analysis was carried out under nitrogen at a steady flow rate of 35 ml/min. Each sample was heated from room temperature to 800 °C at the rate of 10 °C/min.

### 3.3.10 Cement Fluidity

The fluidity of cement paste was determined according to the Chinese National Standard of GB 8077-2000. A 300 g sample of cement, 120 g water and 3 g sulfomethylated or unmodified lignin were added into paste blender and stirred for 4 min. The paste was then rapidly poured into the

truncated flow cone mold (base diameter of 60 mm, top diameter of 35 mm, and height of 60 mm) on a glass plate.

Once the cone was lifted, the cement paste collapsed and spread. The maximum diameter of the spread $d_1$ and the diameter perpendicular to it $d_2$ were measured. The mean value, $(d_1 + d_2)/2$, was considered as the fluidity of cement paste [25]. Three replicates for each sample were carried out, and the average was reported. Similarly, cement fluidity of commercial lignosulfonate was also measured using the same method described above and its results was compared with produced sulfomethylated lignin

## 3.4 Results and discussion

### 3.4.1 Reaction Scheme of Sulfomethylation of Lignin

The synthesis of the sulfonated kraft lignin is shown in Figure 3.1. In this reaction (under alkaline conditions) formaldehyde provides methyl group and sodium sulfite provides sulfonated group for sulfomethylation. This reaction proceeds through electrophilic substitution. Under alkali condition, the phenolic groups in lignin are converted to active electrophiles and the sodium sulfonate methyl derivative is formed by the nucleophilic addition of the sodium sulfite anion. There are possible competing side reactions including the production of sodium thiosulfate, which lowers the overall yield of the sulfonated lignin as shown in Figure 3.1b [26].

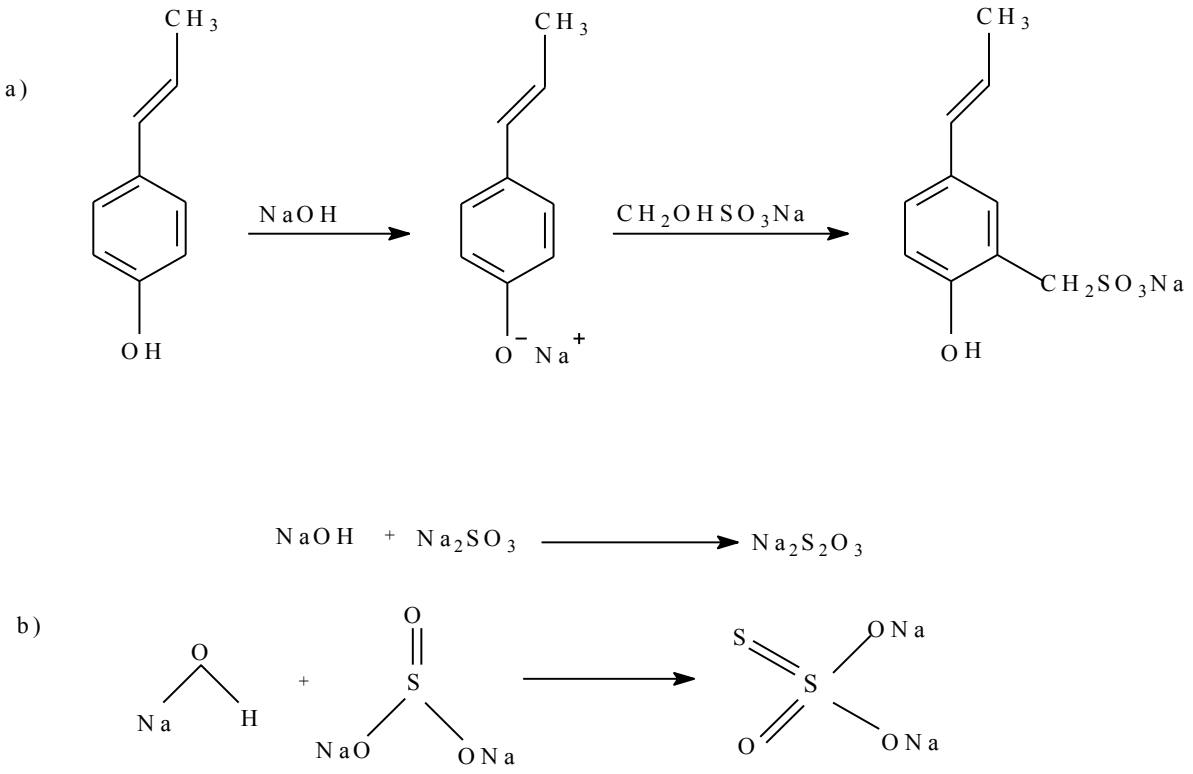


Figure 3.1. a) Sulfomethylation of lignin and b) undesired sodium thiosulfate production

### 3.4.2 Effect of NaOH Concentration

The sulfonation of alkali lignin is influenced by pH [6] and Figure 3.2 presents the impact of NaOH on the charge density and the solubility of sulfomethylated lignin. As is observable, a maximum charge density of 1.3 meq/g and solubility of 93 wt.% were obtained at 0.5 mole/l NaOH concentration. The increases in charge density and solubility were due to the impact of NaOH on the progress of sulfomethylation reaction (as shown in Figure 3.1a). The progress in the sulfomethylation of lignin is closely related to the ability of nucleophilic substitution of the hydroxyl group with sulfonated group under alkaline conditions. Thus, the concentration of NaOH in solutions should be sufficient to promote the sulfomethylation process. Below 0.5 M $NaOH_{(aq)}$, alkaline concentration was not sufficient for the reaction, and NaOH concentration that was higher than 0.5 M provided a suitable alkali environment for the undesired side reaction to progress. In the past, lignin obtained from stem of cotton plant showed an increase in solubility from 1 % (unmodified lignin) to 89 % due to sulfomethylation using sodium sulfite and formaldehyde at pH 8, which was th optimum pH in the range studied [26].

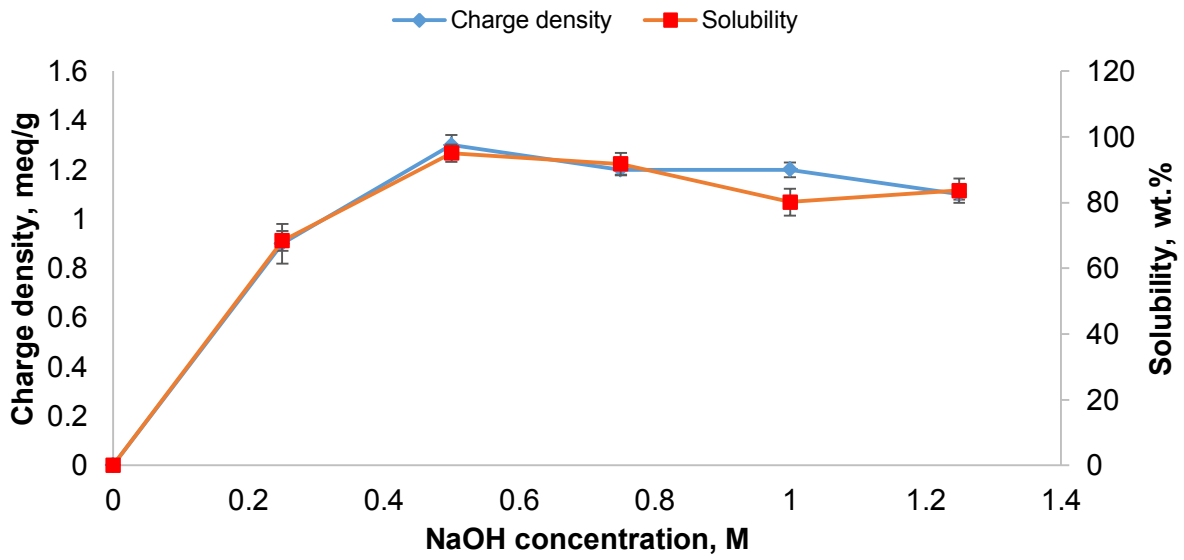


Figure 3.2. The effect of NaOH concentration on the charge density and solubility of sulfomethylated kraft lignin under conditions of 20 g/L lignin concentration, 0.2 mol/mol sodium hydroxymethylsulfonate /lignin ratio, 90 °C for 2 h.

### 3.4.3 Effect of Sodium Hydroxymethylsulfonate/lignin Mole Ratio

The charge density and solubility of sulfomethylated lignin as functions of lignin/sodium hydroxymethylsulfonate mole ratio were determined and are shown in Figure 3.3. The maximum charge density and solubility of SL lignin were 1.6 meq/g and 100 wt.% that was obtained at 0.9 mol ratio. The increase in the charge density and solubility of lignin (0.2-0.9 mol/mol ratio) was due to the increase in the amount of sodium hydroxymethylsulfonate in the solution, which improved the amount of sulfonate groups attached. The decreases in the charge density and solubility were probably due to undesirable side reactions as explained in section 3.1. In the past, the molar ratio of 0.6 sodium hydroxymethylsulfonate/lignin was found to be optimum for producing a dispersant for gypsum [27]. In another report on the sulfomethylation of alkali lignin from corn stalk, the maximum sulfonate group content of 1.29 mmol/g, which is directly related to its maximum charge density, was obtained at 1/1 weight ratio of lignin to sodium sulfite [6]. It is noted that the charge density of modified lignin is directly related to the change in the sulphomethylate group of lignin. Also, sulphomethylation reaction only affects the sulphomethylate groups attached to lignin, thus the charge density of modified lignin is directly related to the change in the sulphomethylate group of lignin. As the charge density is a property commonly used for analyzing the performance of a dispersant, charge density was selected as a

main property for assessing sulphomethylated lignin. In the previous work, only two process parameters (time and sodium sulfite/lignin ratio) were optimized to produce sulfomethylated lignin. In the current study, more process parameters were included for optimizing the sulphomethylation reaction. The inclusion of more process parameters and the alteration in lignin sources were probably the reasons for different charge densities reported in this work and the previous study.

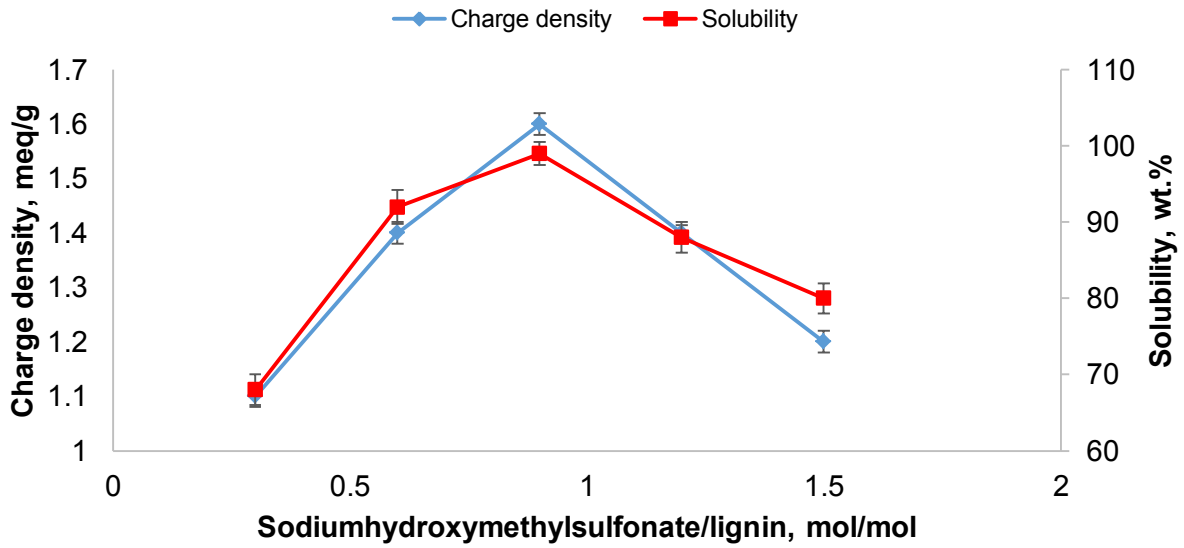


Figure 3.3. Effect of mole ratio of sodium hydroxymethylsulfonate/lignin on the charge density and solubility of sulfomethylated kraft lignin under the conditions of 0.5 mole/l NaOH concentration, 20 g/L lignin concentration, 100 °C, 3 h.

### 3.4.4 Effect of Time

The impact of reaction time on pH, charge density and solubility of sulfomethylated lignin are represented in Figure 3.4. The maximum charge density of 1.54 meq/g and solubility of 98 wt.% were obtained at 3 h. With the increase in time of reaction from 0 to 3 h, there was an increase in charge density and solubility. However, prolonging the time of reaction had a negative effect on the charge density of lignin, which could be due to the progress in the efficiency of side reaction (Figure 3.1b). In addition, as the reaction progressed a decrease in the pH from 12.7 to 11.2 was observed due to the consumption of NaOH [28]. In previous reports as the reaction time increased from 2 to 5 h during the sulfomethylation of alkali lignin from corn stalk, the charge density of lignin was increased from 0.2 to 0.7 meq/g and further extension of time had no effect on the reaction [6]. Yu and coworkers have also reported the oxidation and sulfomethylation of

sodium lignosulfonate and found that a reaction time for 3 h resulted in an increase in the sulfomethylation degree from 0.65 to 1.45 mmol/g, thus it can be inferred that its charge density was most probably at maximum after 3 h of reaction [29]. Similar results were also reported on the sulfonation of esparto grass lignin using sodium sulfite, in which a maximum sulfonation degree of 1.24 mmol/g was obtained in 4 h of reaction [10].

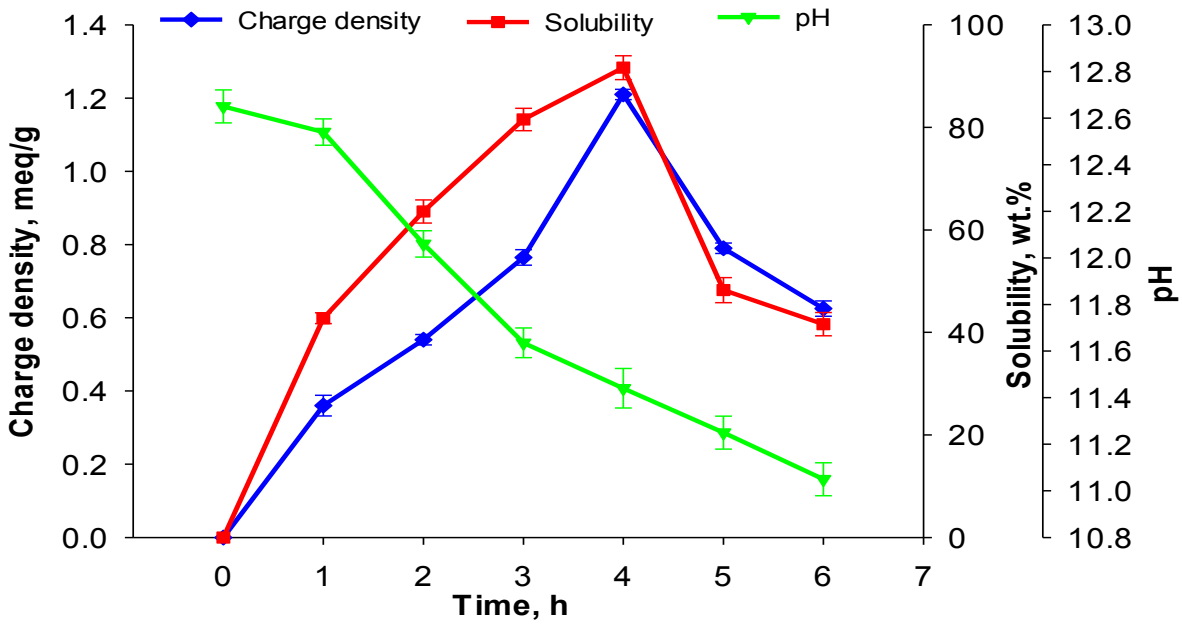


Figure 3.4. Effect of time on the charge density and solubility of sulfomethylated kraft lignin and the pH of reaction medium conducted under the conditions of 0.5 M NaOH concentration, 0.9 mol/mol sodium hydroxymethylsulfonate/lignin ratio, 100 °C, 20 g/l lignin concentration.

### 3.4.5 Effect of Temperature

The changes in charge density and solubility of the sulfomethylated lignin as a function of temperature are presented in Figure 3.5. By increasing the reaction temperature from 80 to 100 °C, the charge density and solubility of kraft lignin increased to 1.55 meq/g and 100 wt.% solubility, respectively. Pang and coworkers, [30] have reported the sulfomethylation of calcium lignosulfonate, the maximum sulfonation degree of 1.23 mmol/g was obtained at 90 °C. This initial increase in charge density and solubility was due to more frequent collisions between the reactants at a higher temperature [29]. Further increase in temperature did not result in an increase in charge density or solubility, possibly due to the formation of undesirable products, such as sodium thiosulfate at high temperatures [31]. These observations have also been

previously reported in the treatment of softwood kraft lignin with formaldehyde and sodium sulfite. The decrease in the sulfonation degree from 1.45 mmol/g to 1.05 mmol/g was accompanied by an increase in the production of sodium thiosulfate, when the temperature was increased from 100 to 150 °C [32]. Therefore, it may be inferred that the production of undesirable products was most probably the reason for the decrease in the charge density of the sulfomethylated lignin. Similar results were reported by Li and co-workers on the sulfonation of wheat straw hydroxymethyl ethanol lignin with sodium sulfite, in which with extending temperature from 60 to 80 °C, the sulfonated group content was increased from 0 to 1.22 mmol/g [33].

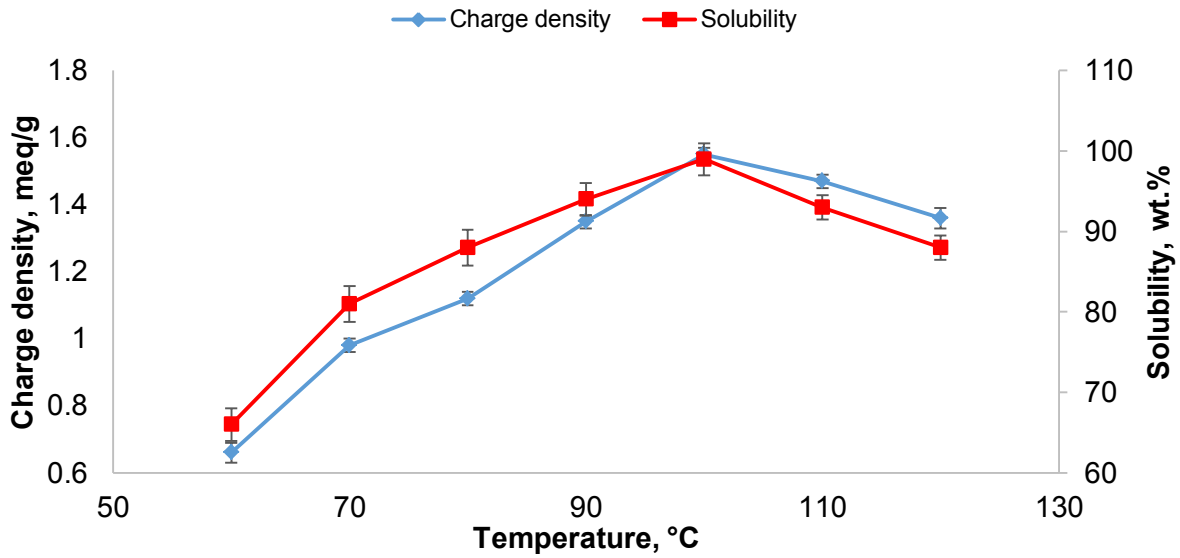


Figure 3.5. Effect of temperature on the charge density and solubility of sulfomethylated kraft lignin under the conditions of 0.5 mole NaOH concentration, 0.2 mol/mol sodium hydroxymethylsulfonate/lignin, 20 g/L lignin concentration, 3 h.

### 3.4.6 Effect of Lignin Concentration

The effect of lignin concentration on the charge density and solubility of sulfomethylated lignin are plotted in Figure 3.6. The maximum charge density of 1.6 meq/g and solubility of 98.8 wt.% were obtained at 20 g/L lignin concentration. The reason for the increase in the charge density and solubility is that lignin is a complex molecule and has very few reaction sites to react with reagents. Thus, with the increase in the lignin concentration, the frequent and effective collisions between the reaction sites and reagents were mostly probably increased, which improved the sulfomethylation reaction [34]. However, further analysis is needed to identify the reason for this

behavior, which is out of the scope of this study. Further increase in the concentration decreased charge density and solubility, which could be due to the limitation in stirring the solution with a magnetic bar (i.e. mechanical constrains) in the reaction setup in this study. A similar trend was reported on the production of surface active agents from beech wood lignin obtained from organosolv pulping process, in which the initial increase in lignin concentration increased the solubility up to 90%, and further increase caused a decrease in solubility [35].

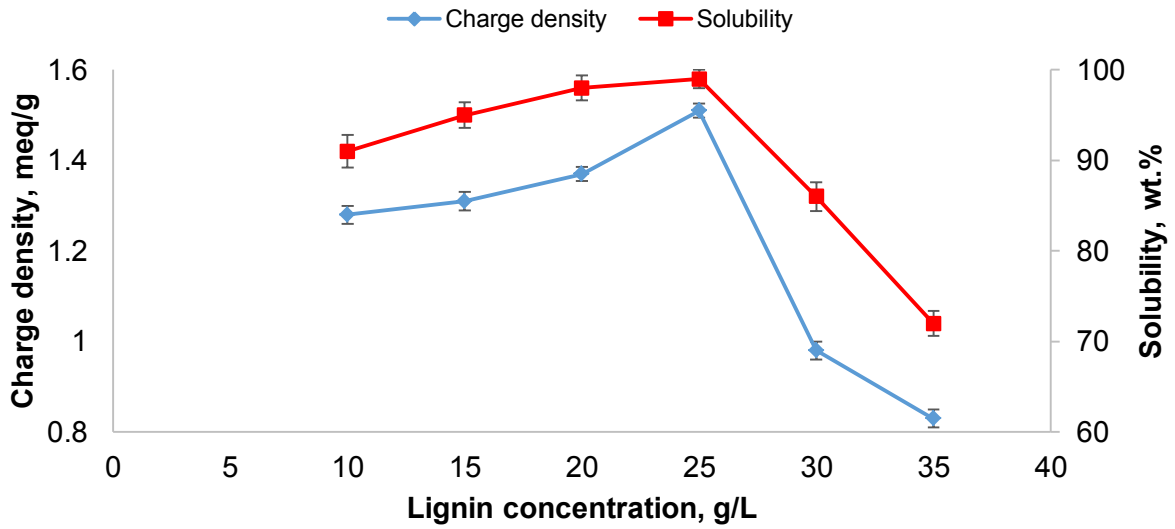


Figure 3.6. Effect of concentration of lignin on the charge density and solubility of sulfomethylated kraft lignin under conditions of 0.5 M NaOH concnentration, 0.9 mol/mol sodium hydroxymethylsulfonate/lignin ratio, 100 °C, 3 h.

### 3.4.7 Orthogonal Design Analysis

The purpose of the orthogonal design is to investigate which process parameter significantly affects the charge density and solubility of sulfomethylated lignin. Table 3.2 lists sum of squared deviation (SS), mean squares (MS) and *F*-test (F). It is apparent that sum of squares, mean squared and F test were the maximum for time. When F is large, the variation within the process parameter has a significant effect on the results [36]. Based on the results in Table 3.2, time has the maximum and NaOH concentration has the minimum effect on the charge density of the resultant sulfomethylated lignin. Time with the F value of 32.80 has the maximum and NaOH concentration with the F value of 0.65 has the minimum effects on the charge density. Similarly, time has the maximum (F value of 70.38) and temperature has the minimum effect (F value of 0.7) on the solubility of the sulphomethylated lignin. These reports indicated that, the time of the

reaction was the most influential factor on the charge density and solubility of sulfomethylated lignin. Based on the ANOVA analysis, the optimal processing conditions for obtaining the maximum charge density and solubility were 0.5 M NaOH concentration, 0.9 mol/mol sodium hydroxymethylsulfonate/lignin ratio, temperature of 100 °C, time of 3 h and lignin concentration of 20 g/L, which was consistent with the optimized conditions obtained on Figures 2 to 6.

Table 3-2. Parameters for investigating the impact of sulphomethylatation reaction on the charge density and solubility of sulphomethylated lignin

| Factor | Sum of squares | | Mean square | | F value | |
|---|---|---|---|---|---|---|
| | Charge density, meq/g | Solubility, wt.% | Charge density, meq/g | Solubility, wt.% | Charge density, meq/g | Solubility, wt.% |
| Time, h | 0.98 | 1988.25 | 0.33 | 662.75 | 32.80 | 70.38 |
| Temperature, °C | 0.03 | 28.25 | 0.007 | 9.42 | 0.73 | 0.70 |
| NaOH concentration, g/L | 0.02 | 40.25 | 0.006 | 13.42 | 0.65 | 1.42 |
| Sodium Hydroxymethylsulfonate/lignin, mol/mol | 0.16 | 156.25 | 0.053 | 52.08 | 5.37 | 5.53 |
| Lignin concentration, g/L | 0.03 | 42.75 | 0.01 | 14.25 | 1.53 | 1.51 |

### 3.4.8 FTIR Analysis

The FTIR spectra of unmodified and modified lignins are presented in Figure 3.7. The strong and broad band at around 3431 $cm^{-1}$ is the characteristic of OH or phenolic groups [37]. The peaks at 2361 and 2336 $cm^{-1}$ are associated with C-H stretching of methyl or methylene groups. The increase in absorption peaks at 1593 and 1510 $cm^{-1}$ is attributed to the aromatic functionality in lignin and benzene ring skeletal vibration [28]. The increase in absorption peaks at 1460 and 1423 $cm^{-1}$ corresponds to C-H bending and C-H stretching of methylene groups [9]. The peak at 1200 $cm^{-1}$ can be attributed to C=O stretching of guaiacyl unit and to C-O and C=O stretching of the aromatic ring [38]. The absorption peak at 1032 $cm^{-1}$ on sulphomethylated lignin is attributed to sulfonated acid groups, which is not present in unmodified lignin and confirms the grafting of sulfonated groups to the modified lignin in the sulfomethylation reaction [9]. In the previous

work, sulfonate groups attached to lignin was confirmed by the increase in absorption peak at 1040 $cm^{-1}$ in the FTIR spectrum of sulfomethylated sodium lignosulfonate [9].

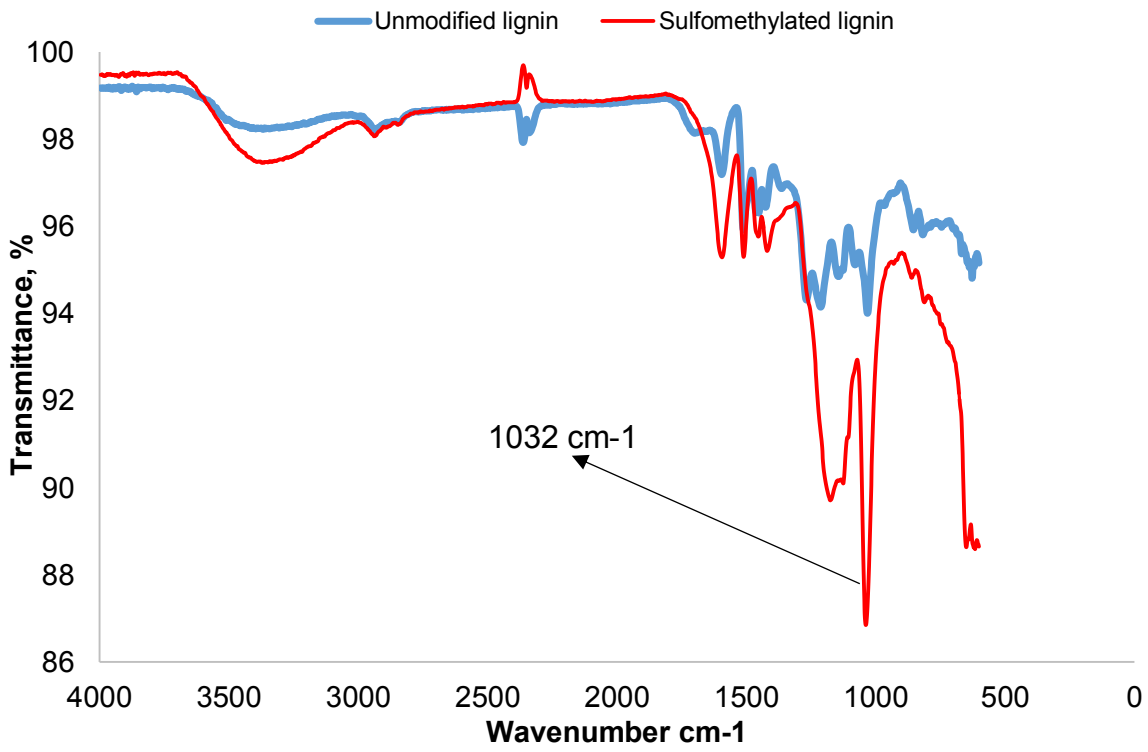


Figure 3-7 : FTIR spectra of unmodified and sulfomethylated kraft lignin produced under conditions of 0.5 M $NaOH_{(aq)}$, 0.9 mol/mol sodium hydroxymethylsulfonate/lignin ratio, 100 °C, 3 h, 20 g/l lignin concentration.

### 3.4.9 Properties of Sulfonated Lignin

The sulfomethylated lignin with highest charge density and solubility, which was produced under the conditions of 0.5 M NaOH concentration, 0.9 mol/mol ratio of sodium hydroxymethylsulfonate/lignin ratio, 100 °C, 3 h and 20 g/L lignin concentration, were selected for further analysis. Table 3.3 shows the properties of unmodified and sulfomethylated lignins. The number of sulfonated groups in kraft lignin was increased from 0.03 on unmodified lignin to 1.48 on modified (sulfomethylated) lignin, which corresponded to a degree of substitution (DS) of 0.005 and 0.33 for unmodified and sulfomethylated lignin, respectively. The degree of substitution for unmodified lignin corresponds to sulfonated group that is already attached to lignin or present in the kraft lignin as impurities (as kraft lignin was separated from black liquor via sulfuric acid treatment in the process of kraft lignin isolation) [39]. In the past, the degree of substitution of sulfonated group was increased from 0.02 to 0.18 by reacting sugarcane bagasse

lignin with sodium sulfite under the conditions of 5% NaOH, 37 wt.% formaldehyde, 1.2 g sodium sulfite for 150 min at 95 °C [40].

Table 3-3: Properties of unmodified and sulfomethylated lignin.

| Sample | Elemental Analysis | | | | | Sulfonated group, mmol/g | Degree of Substitution (DS) | $M_W$, g/mol | Cement fluidity, mm |
|---|---|---|---|---|---|---|---|---|---|
| | C, wt.% | H, wt.% | O, wt.% | N, wt.% | S wt.% | | | | |
| Unmodified lignin | 64.76 ± 0.02 | 5.78 ± 0.5 | 26.67 ± 0.8 | 0.03 ± 0.002 | 1.05 ± 0.7 | 0.03 ± 0.004 | 0.005 | 22,700 ± 124 | 60 ± 2 |
| Sulfomethylated lignin | 53.76 ± 0.02 | 4.94 ± 0.5 | 33.81 ± 0.8 | 0.04 ± 0.002 | 3.21 ± 0.6 | 1.48 ± 0.02 | 0.33 | 53,300 ± 316 | 155 ± 4 |

The results from the molecular weight analysis for unmodified and sulfomethylated kraft lignin samples are provided in Table 3.3. The sulfomethylated lignin (53,360 g/mol) had a higher molecular weight than unmodified lignin (22,746 g/mol). This increase in molecular weight was due to the replacement of hydroxyl groups with sulfomethyl groups in sulfomethylated lignin [19]. Previously, the oxidation and sulfomethylation of lignosulfonate with $FeSO_4$, formaldehyde and sodium sulfite showed an increase in molecular weight (20,650 g/mol for modified lignin compared to 2,378 g/mol for unmodified lignin) [28]. In another report, the sulfonation of wheat straw kraft lignin with sodium sulfite increased its molecular weight to 55,700 g/mol compared to unmodified lignin (1,900 g/mol) [24]. As the lignin sources were different in the present study and previous reports, [23, 29] the structure and molecular weight of produced lignin as outcomes of pulping processes would be different. It is also possible that lignin segment would condense under alkaline conditions, which would increase the molecular weight of lignin.

The elemental analysis of unmodified lignin and sulfomethylated kraft lignin are also provided in Table 3.3. The sulfur and oxygen contents of lignin were increased and the hydrogen content decreased in the modified lignin compared with unmodified lignin, which proved the sulfomethylation of kraft lignin [25]. Similar results were reported by Matushita and coworkers on the sulfomethylation of acid hydrolysed pine wood lignin with sodium hydroxymethylsulfonate [25]. The sulfomethylation of wheat straw alkali lignin with sodium sulfite showed an increase in sulfonated group content from 0 to 1.48 mmol/g [19]. Based on the

results tabulated in Table 3.3, the chemical formulas of unmodified and sulfomethylated lignin were $C_9H_{9.65}O_{2.78}S_{0.05}$ and $C_9H_{9.92}O_{4.23}S_{0.20}$, respectively (Nitrogen was omitted due to its trace amount).

### 3.4.10 Thermogravimetric (TGA) Analysis

Figure 3.8 shows the results of TGA analysis for unmodified and sulfomethylated lignin samples. At a low temperature (lower than 300 °C), the unmodified lignin decomposed faster than sulfomethylated lignin. The increase in the thermal stability of lignin could be an advantage for its end-use applications in composites or as a dispersant and flocculant [6]. This increase was due to the introduction of sulfomethylated groups in the modified lignin during sulfomethylation [41]. The unmodified lignin decomposed continuously above 200 °C and was completely degraded at 650 °C. In the case of sulfomethylated lignin, the degradation began at 250 °C and there was only 70% weight loss at 650 °C, which was due to the introduction of methyl and sulfonate groups in sulfomethylation. It was reported that methyl groups will be decomposed mostly between 700 and 800 °C [42]. The TGA analysis clearly confirmed that the introduction of sulfonated and methyl groups into lignin increased its thermal stability when compared to unmodified lignin.

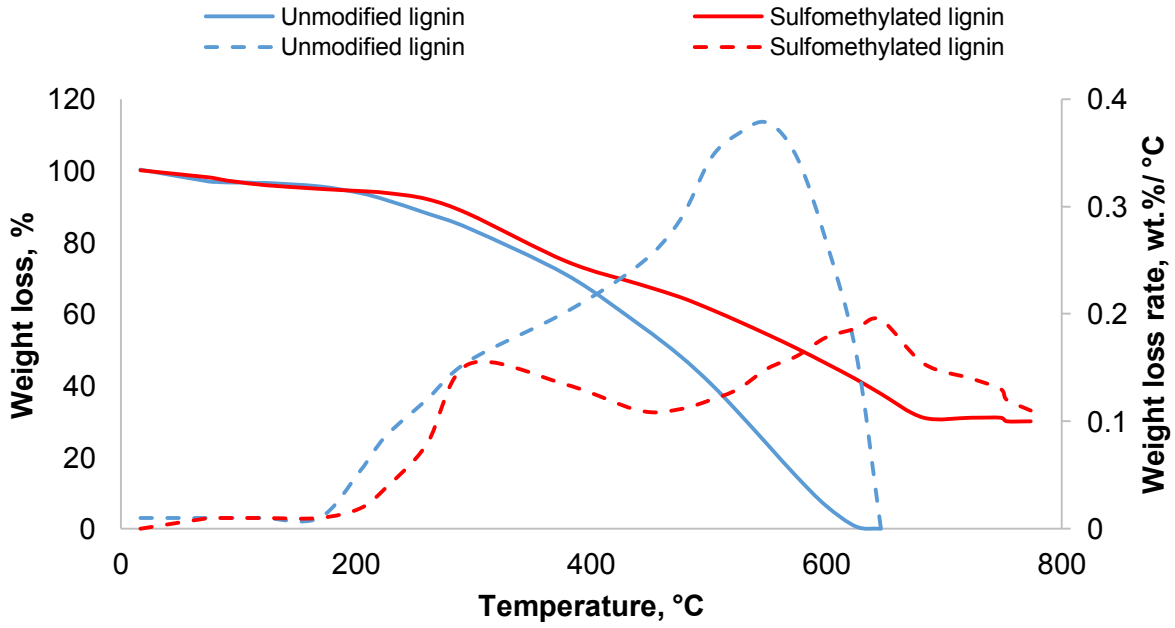


Figure 3.8. Weight loss (solid line) and weight loss rate (dash line) of unmodified and sulfomethylated lignin produced under the conditions of 0.5 M $NaOH_{(aq)}$, 0.9 mol/mol sodium

hydroxymethylsulfonate/lignin ratio, 100 °C, 3 h, 20 g/L lignin concentration at 35 ml/min nitrogen flow rate.

### 3.4.11 Impacts of pH and Concentration on Solubility of Lignin

As pH influences the solubility of lignin, its end-use application will also be affected. Therefore, it is crucial to investigate the impact of pH on the solubility of sulfomethylated lignin. The dependency of the lignin solubility on the pH is shown in Figure 3.9. The unmodified and sulfomethylated lignin are soluble at a high pH; however, decreasing the pH to 10 led to its insolubility [43]. The sulfomethylated lignin became insoluble at pH 6 and its solubility was dramatically reduced at pH 3. The pKa of sulfonic acid group was 2.8. Thus, the sulfonated group was in its protonated form below pH 2.8 and this decreased the solubility of lignin. It is claimed that, the sulfonated group deprotonates above pH 2.8, which improves the hydrophilicity and thus the water solubility of lignin [44]. The high solubility of sulfomehylated lignin was due to the introduction of sulfonated groups via sulfomethylation, as discussed earlier.

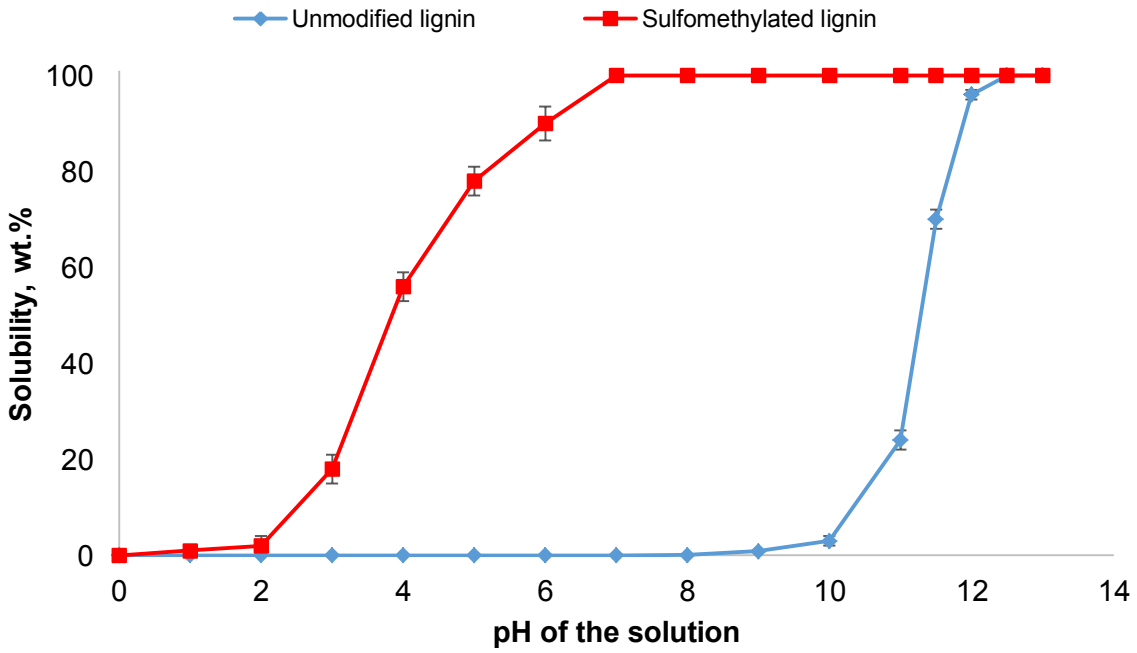


Figure 3.9. Effect of pH on the solubility of unmodified and sulfomethylated lignin under conditions of 10 g/L lignin concentration, 30 °C, 2 h.

The effects of concentration of sulfomethylated lignin on its solubility under a neutral condition are presented in Figure 3.10. It can be understood that, with the increase in the concentration of lignin from 10 to 40 g/L, sulfomethylated lignin exhibited 100 wt.% solubility. Lignin reached the saturation concentration of 40 g/L in this experiment [44]. This decrease in solubility of

lignin was probably due to hydrogen bonding (and self-assembly) of lignin molecules in solution at a high concentration [45].

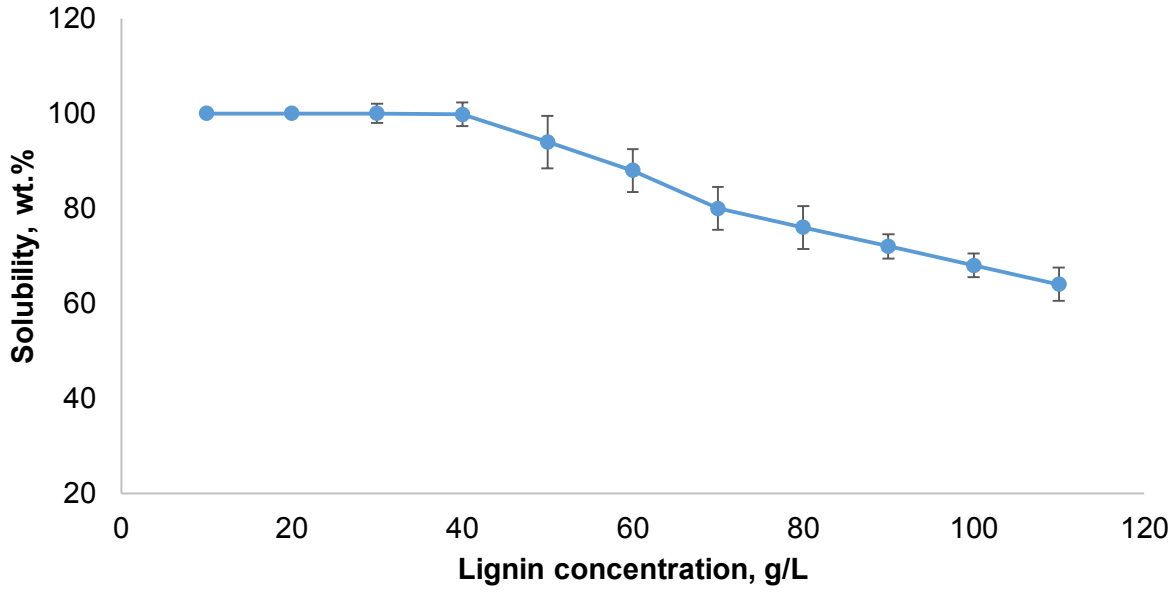


Figure 3.10. Effect of sulfomethylated lignin concentration on its solubility under the conditions of pH 7, 30 °C, 2 h.

### 3.4.12 Effect of Sulfomethylated Lignin on Cement Fluidity

In order to improve the strength and durability of fresh concrete, additives such as lignosulphonates are usually mixed with cement admixtures [46]. These additives can improve the workability and fluidity of the cement admixture, as they make the cement flow better. In this study, sulfomethylated lignin produced under optimal conditions was tested as an additive to improve the fluidity of cement admixture [47]. The results of cement fluidity analysis are also shown in Table 3.3. In the presence of sulfomethylated lignin, cement fluidity was found to increase to 155 mm compared to cement fluidity in the absence of lignin (60 mm). However, unmodified lignin didn't show any increase in cement fluidity (60 mm). This behaviour was due to the introduction of sulfonated group to the lignin via sulfomethylation and its water soluble nature [23]. The sulfomethylated lignin with the charge density (-1.6 meq/g) adsorbed strongly to the cement particles with a positive charge density (+0.13 meq/g). Considering the charge densities of sulphomethylated lignin and cement, as well as the dosage of sulphomethylated lignin, it is estimated that the overall charge density of cement paste would change to –1.79 meq/g, which imposed strong electrostatic repulsion force between the cement particles, and

thereby the dispersibility of cement particles was improved [48]. Furthermore, change in the charge density of the cement particles before and after adsorption with sulfomethylated lignin was also confirmed by zeta potential results. The surface zeta potential of the cement particles was found to decrease from + 3.25 mV (before adsorption) to – 8.2 mV (after adsorption). In the previous work [15], sulfomethylated lignin had a high sulfonated group content (-1.5 mmol/g) and a low molecular weight (9688, g/mol) compared to sulfonated group content (-1.48 mmol/g) and molecular weight (53,360 g/mol) of sulfomethylated lignin in the present work. A comparison may suggest that sulfonated lignin with a lower molecular weight and a high sulfonated degree would be more effective in dispersing cement particles. In the past, sulfonated lignin prepared by treating wheat straw alkali lignin with sodium sulfite showed a cement fluidity of 216 mm compared to that (65 mm) of unmodified lignin [20]. In the previous work, sulfomethylated lignin had a high sulfonated group content (-1.5 mmol/g) and a low molecular weight (9688, g/mol) compared to sulfonated group content (-1.48 mmol/g) and molecular weight (53,360 g/mol) of sulfomethylated lignin in the present work. A comparison may suggest that a lower molecular weight and high sulfonated group content would be more effective for cement dispersion. Furthermore, the cement fluidity of sulfomethylated lignin was compared with that of commercial lignosulfonate (215 mm). A higher fluidity of cement using commercial lignosulfonate (than using sulfonated lignin) was due to its low molecular weight (9,243 g/mol) and high charge density (-1.8 meq/g) compared to those of sulfomethylated lignin.

### 3.5 Conclusions

Sulfomethylated hardwood kraft lignin was successfully prepared in an aqueous medium by using sodium sulfite and formaldehyde under alkali conditions. The experimental design results showed that the optimal conditions for sulfomethylation were 0.5 M of $NaOH_{(aq)}$, 0.9 mol/mol of sodium hydroxymethylsulfonate/lignin ratio, 100 °C, 3 h reaction time with lignin concentration of 20 g/L. The sulfonated lignin had 1.48 mmol/g of sulfonated group, while unmodified lignin had 0.03 mmol/g of sulfonated group. Molecular weight analysis confirmed that the molecular weight of lignin increased via sulfomethylation from 22,746 to 53,360 g/mol. Solubility analysis confirmed the high solubility (40 g/L) of sulfomethylated lignin at neutral pH, whereas unmodified lignin was insoluble at pH 7. The solubility was pH dependent in that kraft lignin was insoluble at pH below 10, but sulfomethylated lignin was insoluble at pH below 3. The FTIR analysis also confirmed the structural changes, while TGA analysis showed an increase in the

thermal stability of the lignin via sulfomethylation. Also, the fluidity of cement was improved to 155 mm via adding sulfomethylated lignin, while that of cement was improved to 60 mm via adding unmodified lignin.

### 3.6 References


1. Windt M, Meier D, Marsman JH, Heeres HJ, De Koning S. Micropyrolysis of technical lignins in a new modular rig and product analysis by GC-MS/FID and GCXGC-TOFMS/FID. Journal of Analytical and Applied Pyrolysis, 2009, 85, 38-46.
2. Voitl T, Von Roh PR. Demonstration of process for the conversion of kraft lignin into vanillin and methyl vanillate by acidic oxidation in aqueous methanol. Industrial Engineering and Chemistry Research, 2010, 49, 520-525.
3. Gooselink RJA, Snijder MHB, Kranenbarg A, Keijsers ERP, De Jong E, Stigsson LL. Characterization and application of NovaFiber lignin. Industrial Crops and Products, 2014, 20, 191-203.
4. Yanhua J, Weihong Q, Zongshi Li, Lubai C. A study on the modified lignosulfonate from lignin. Energy Sources, 2004, 26, 409-414.
5. Maziero P, Neto MO, Machado D, Batista D, Cavalheiro CS. Structural features of lignin obtained at different alkaline oxidation conditions from sugarcane bagasse. Industrial Crops and Products, 2012, 35, 61-69.
6. Wu H, Chen F, Feng Q, Yue X. Oxidation and sulfomethylation of alkali extracted lignin from corn stalk. Bioresources, 2012, 7, 2742-2751.
7. Yasuda S, Hamaguchi E, Matsushita Y, Goto H, Imai T. Ready chemical conversion of acid hydrolysis lignin into water soluble lignosulfonate II: hydroxymethylation and subsequent sulfonation of phenolized lignin model compounds. Journal of Wood Science, 1998, 44, 116-124.
8. Watanabe M, Meshitsuka G, Ishizu A. Radical sulfonation of lignin II: water solubilisation of acid hydrolysis lignin. Journal of Japan Wood Research Society, 1990, 306, 876-882.
9. Li Z, Ge Y. Extraction of lignin from sugarcane bagasse and its modification into a high performance dispersant for pesticide formulations. Journal of Brazilian Chemical Society, 2011, 22, 1866-1871.

10. Kamoun A, Jelidi A, Chaabouni M. Evaluation of the performance of the sulfonated esparto grass lignin as a plasticizer- water reducer for cement. Cement and Concrete Research, 2003, 33, 995-1003.
11. Abu-Dalo MA, Al-Rawashdeh NAF, Ababneh A. Evaluating the performance of sulfonated kraft lignin agent as corrosion inhibitor for iron based materials in water distribution systems. Desalination, 2013, 313, 105-114.
12. Bolto B, Gregory J. Organic polyelectrolytes water treatment. Water Research, 2007, 41, 2301-2324.
13. Norgren M, Lindstrom B. Physiochemical characterization of a fractionated kraft lignin. Holzforschung, 2000, 54, 528-534.
14. Liimatainen H, Visanko M, Sirvio J, Hormi O, Niinimaki J. Sulfonated cellulose nanofibrils obtained from wood pulp through regioselective oxidative bisulfite pre-treatment. Cellulose, 2013, 10, 1007-1015.
15. Kouisni L, Holt-Hindle P, Maki K, Paleologou M. The LignoForce system: a new process for the production of high-quality lignin from black liquor**.** Journal of Science and Technology for Forest Products and Processes**,** 2012, 2, 6-10.
16. Darghai M, Kazemian H, Soltanieh M, Hosseinpour M, Rohani S. High temperature synthesis of SAPO-34: Applying an L9 Taguchi orthogonal design to investigate the effects of experimental parameters. Powder Technology, 2012, 217, 223-230.
17. Sun W, Zhang G, Pan L, Li H, Shi A. Synthesis, characterization, and flocculation properties of branched cationic polyacrylamide. International Journal of Polymer Science, 2013, 10, 1155-1166.
18. Mason RL, Gunst RF, Hess JL. Statistical design and analysis of experiments. John Wiley & Sons, Inc: New Jersey, 2003.
19. Ouyang X, Ke L, Qiu X, Guo Y, Pang Y. Sulfonation of alkali lignin and its potential use in dispersant for cement. Journal of Dispersion Science and Technology, 2009, 30, 1-6.
20. Teranishi T. Encyclopedia of surface and colloid science; Marcel Dekker: New York, 2002.
21. Plank J, Hirsch C. Impact of zeta potential of early cement hydration phases on superplasticizer adsorption. Cement and Concrete Research, 2007, 57, 537-542.
22. Chien S.N, Amidon TE, Lai YZ. Fractionation of wood polymers by carboxymethylation: Exploring the strategy. Tappi Journal, 2012, 11, 29-37.

23. Peng XW, Ren JL, Zhong LX, Peng F, Sun RC. Xylan rich hemicelluloses- graft acyclic acid ionic hydrogels with rapid responses to pH, salt, and organic solvents. Journal of Agriculture and Food Chemistry, 2011, 59, 8208-8215.
24. Sarwar Jahan M, Liu Z, Wang H, Saeed A, Ni Y. Isolation and characterization of lignin from prehydrolysis liquor of kraft based dissolving pulp production. Cellulose Chemistry and Technology, 2012, 46, 261-267.
25. Lou H, Lai H, Wang M, Pang Y, Yang D, Qiu X, Wang B, Zhang H. Preparation of lignin-based superplasticizer by graft sulfonation and investigation of the dispersive performance and mechanism in a cementitious system. Industrial and Engineering Chemistry and Research, 2013, 52, 16101-16109.
26. Madzhidova VE, Dalimova GN, Abduazimov KA. Sulfomethylation of lignins. Chemistry and Natural Compounds, 1998, 34, 179-181.
27. Matsushita Y, Yasuda S. Preparation and evaluation of lignosulfonates as a dispersant for gypsum paste from acid hydrolysis lignin. Bioresource Technology, 2005, 96, 465-470.
28. Gan L, Zhou M, Qiu X. Preparation of water soluble carboxymethylated lignin from wheat straw alkali lignin. Advances in Material Research, 2012, 550-553, 1293-1298.
29. Yu G, Li B, Wang H, Liu C, Mu X. Preparation of concrete superplasticizer by oxidation-sulfomethylation of sodium lignosulfonate. BioResources, 2013, 8, 1055-1063.
30. Pang XY, Qiu XQ, Yang DJ, Lou HM. Influence of oxidation, hydroxymethylation and sulfomethylation on the physicochemical properties of calcium lignosulfonate. Colloids and Surfaces A: Physiochemical and Engineering aspects, 2008, 312, 154-159.
31. Bruden S, Schoenmakers P. Analytical Methodology for sulfonated lignins. Journal of Separation Science, 2010, 33, 439-452.
32. Hu TQ. Chemical modification, properties, and usage of lignin; Kluwer Academic / Plenum Pulishers: New York, 2002.
33. Li G, Huang Y, Chen C. Preparation of cement water reducer by sulfonation modifying of wheat straw hydroxymethyl ethanol lignin. Advances in Material Research, 2011, 250-253, 1011-1016.
34. Elkin VV, Shorygina NN. Reactions of some lignin models with sodium bisulfite. Russian Chemical Bulletin, 1966, 15, 1726-1731.

35. Sharma P, Verma A, Sidhu RK, Pandey, OP. Process Parameter selection for strontium ferrite sintered magnets using Taguchi L9 orthogonal design. Journal of Materials Processing Technology, 2005, 168, 147-151.
36. Kosikova B, Duris M, Demianova V. Conversion of lignin biopolymer into surface active derivatives. European Polymer Journal, 2000, 36, 1209-1212.
37. Ibrahim MNM, Chuah SB, Wan Rosli WD. Characterization of lignin precipitated from the soda black liquor of oil palm empty fruit bunch fibers by various mineral acids. ASEAN Journal of Science and Technology for Development, 2004, 21, 57-67.
38. Malutan T, Nicu R, Popa VI. Contribution to study of hydroxymethylation reaction of alkali lignin. BioResources, 2008, 3, 13-20.
39. Ikeda T, Tomimura Y, Magara K, Hosoya S. Sulfuric acid bleaching of kraft pulp II: Behaviour of lignin and carbohydrate during sulfuric acid bleaching. Journal of Wood Science, 1999, 45, 313-318.
40. Ouyang X, Lin Z, Yang D, Qiu X. Chemical modification of lignin assisted by microwave irradiation. Holzforschung, 2011, 65, 697-701.
41. Liu Q, Wang S, Zheng Y, Luo Z, Cen K. Mechanism study of wood lignin pyrolysis by using TG-FTIR analysis. Journal of Analytical and Applied Pyrolysis, 2008, 82, 170-177.
42. Xiao B, Sun XF, Sun RC. Chemical structural, and thermal characterizations of alkali soluble lignins and hemicelluloses, and cellulose from maize stems, rye straw and rice straw. Polymer Degradation and Stability, 2001, 74, 307-319.
43. Pinkert A, Goeke DF, Marsh KN, Pang S. Extracting wood lignin without dissolving or degrading cellulose: Investigation on the use of food additive derived ionic liquids. Green Chemistry, 2011, 13, 3124-3136.
44. Wang Q, Chen K, Li J, Yang G, Liu S, Xu J. The solubility of lignin from bagasse in a 1, 4-butanediol/water system. BioResources, 2011, 6, 3034-3043.
45. Reid ID, Paice MG. Effect of manganese peroxidase on residual lignin of softwood kraft pulp. Applied Environmental Microbiology, 1998, 64, 2273-2274.
46. Maruya E, Ichinose R, Sakai E. Influence of mineral admixtures on the paste fluidity of cement with high aluminium phase content. Concrete International, 2009, 262, 347-356.

47. Agullo L, Toralles-Carbonari B, Gettu R, Aguado A, Fluidity of cement paste with mineral admixtures and superplasticizer - A study based on the Marsh cone test. Material Structures, 1999, 32, 479-485.
48. Pouteau C, Dole P, Cathala B, Averous L, Boquillon N. Antioxidant properties of lignin in polypropylene. Polymer Degradation Stability, 2003, 81, 9-18.

# **Chapter 4.** Synthesis and characterization of carboxymethylated xylan and its application as a dispersant

Adapted from: Mohan K. R. Konduri, Pedram Fatehi*[a]

Carbohydrate Polymers, 146, 2016, 26-35.

[a] Department of Chemical Engineering,

Lakehead University,

955 Oliver Road,

Thunder Bay, ON P7B 5E1, Canada

*Corresponding author

## 4.1 Abstract

In this study, carboxymethylated beechwood xylan was produced under alkali conditions using sodium chloroacetate. Taguchi orthogonal design was used to explore the influence of the process parameters, i.e. NaOH concentration, time, temperature, molar ratio of sodium chloroacetate to xylan and the concentration of the reaction medium on the charge density and degree of substitution (DS) of xylan. Carboxymethylated xylan (CMX) with the maximum charge density of 1.62 meq/g and DS of 0.21 was produced under the optimal conditions of 0.75 M NaOH concentration, 1.0 mol/mol sodium chloroacetate (SCA)/xylan ratio, 2 h reaction time, 70 °C and 15 g/L xylan concentration. The carboxylate group of the product was 1.48 mmol/g. The attachment of the carboxymethylate group to xylan was confirmed by Fourier transform infrared spectroscopy (FTIR) and proton nuclear magnetic resonance ($^1$H-NMR) spectroscopy. The molecular weight of xylan increased and its thermal stability was improved via carboxymethylation. The dispersion performance of the carboxymethylated xylan in clay suspensions was determined by photometric dispersion analyzer (PDA). CMX showed better dispersion performance than sodium carbonate-polyacrylic acid ($Na_2CO_3$-PAA) system. The unmodified xylan did not show any dispersion performance.

Keywords: Xylan, Carboxymethylation, Charge density, Degree of substitution, Dispersant, Orthogonal design

## 4.2 Introduction

Today, there is a strong intensive for replacing oil-based chemicals with green chemicals [1]. Xylan is a polysaccharide polymer with a similar structure to cellulose. It constitutes 25-35 wt.% of woody biomass and approximately 50 wt.% of non-woody plants [2]. The polymeric backbone of xylan is made of xylose repeating units that are linked with β-1-4 linkage [3]. Recently, xylan gained interests as a functional biopolymeric material because of its abundant hydroxyl group and large availability in hardwood species [4, 5].

Xylan can be chemically modified to produce value-added products [6]. These chemical modifications include carboxymethylation [7], cationization [8, 9], laurolyation [10], acetylation [11] and oleoylation [12]. Among these chemical modifications, carboxymethylation is the most versatile modification for producing biobased materials that can be used in paper, textile, pharmaceutical and paint industries [13, 14, 15]. This is because carboxymethylation excludes

the use of extreme modification conditions and solvents (e.g. ethanol), which makes it industrially attractive.

In the past, studies were conducted on the carboxymethylation of non-wood and wood based xylan in solvent media [16, 17]. In one study, arabinoxylan isolated from *Plantago ovata* seed husk was carboxymethylated using sodium monochloroacetate (SMCA) in an ethanol medium [18]. In another study, xylan-rich hemicelluloses extracted from wheat straw biomass was carboxymethylated using SMCA in an ethanol/water medium under microwave irradiation [19]. Ren and coworkers produced a carboxymethylated product by modifying sugarcane bagasse xylan using monochlroacetic acid in an isoproponal medium [20]. Xylan isolated from birchwood was converted into a carboxymethylated product using sodium monochloroacetate in an isopropanol medium [21]. However, there are very few studies reported on the carboxymethylation of hardwood xylan in aqueous conditions [22]. The first objective of this study was to produce carboxymethylated xylan in aqueous media (under alkaline conditions).

Modified hemicelluloses were proposed to be used in various applications [1]. In one study, carboxymethylated hemicelluloses were reported to be used as an emulsifying or binding agent in the pharmaceutical industry [23], oil drilling, metal binding, papermaking and medicine [24] or packaging film [25]. In another study, sugarcane based carboxymethylated hemicellulose was used as a strength agent for papermaking [26]. However, the use of carboxymethylated xylan as a dispersant has not been reported and was, in fact, the second objective of this work.

According to the literature, the stabilization of clay suspensions with minimum water loss is critical to drilling process; therefore, this study intended to produce a biobased dispersant for this application [27]. Natural polyelectrolytes, e.g. starch, cellulose, guar gum, are considered to be used as dispersants. These polyelectrolytes can adsorb onto clay particles and introduce steric and electrostatic repulsions between the particles resulting in the stabilization of colloidal suspensions [28]. The availability of guar gum is limited, starch is mainly used as a food product and cellulose is widely used in the paper production. However, xylan is not presently utilized effectively, and therefore, can be converted to a dispersant for clay suspensions.

The main novelties of this work were the production of carboxymethylated xylan in an aqueous medium and the use of the product as a dispersant for clay suspensions. The impact of carboxymethylation on the charge density of xylan was also discussed for the first time in this

work. In the present work, the carboxymethylation of beechwood xylan was conducted using sodium chloroacetate in order to obtain carboxymethylated xylan with a high charge density and degree of substitution. The chemical, physical and structural properties of carboxymethylated xylan were also determined. The application of carboxymethylated xylan as a dispersant in clay suspensions was also discussed for the first time in this study.

## 4.3 Experimental

### 4.3.1 Materials

Beechwood xylan, sodium hydroxide, sodium chloroacetate (SCA), 3-(Trimethylsilyl) propionic-2,2,3,4-$d_4$ acid sodium salt (TSP), sodium nitrate, acrylic acid (99 %), sodium carbonate, potassium persulphate ($K_2S_2O_8$) and kaolin clay were obtained from Sigma Aldrich Company and used as received. Acetic acid (99%) was obtained from Sigma-Aldrich Company and diluted to 80 wt.% prior to use. Ethanol (99 %) obtained from Sigma Aldrich Company and was used as received or diluted to 80 wt. % prior to use. Sulphuric acid was obtained from Sigma-Aldrich Company and diluted to 0.1 M prior to use. Cellulose acetate dialysis membrane (molecular weight cut off of 1,000 g/mol) was purchased from Spectrum Labs. Inc., USA. Polydiallyldimethylammonium chloride (PDADMAC) was obtained from Sigma Aldrich Company and diluted to 0.005 M prior to use. Potassium polyvinyl sulfate (PVSK) was obtained from Wako Pure Chemical Industries Ltd., Japan.

### 4.3.2 Carboxymethylation

The carboxymethylation of xylan was conducted as described in the literature on the carboxymethylation of alkali lignin extracted from sugarcane bagasse [20]. In this study, 1 g sample of xylan was dissolved in 50 mL of NaOH solution (0.25 – 1.25 M) by stirring at 200 rpm for 15 min at room temperature. Sodium chloroacetate solution of varying concentration ratios to xylan (0.25 to 2 mol/mol) was added, and the reaction was carried out at designated times and temperatures under a constant stirring at 200 rpm. After completion, the solution was cooled to room temperature and its pH was adjusted to 7 using an 80 wt. % acetic acid solution. The polymer present in the solution was precipitated using 150 mL of 99.5 % ethanol. Then, the precipitated polymer was washed thrice using an 80 wt.% ethanol solution and dried at room temperature overnight and then stored at 4 °C until further use.

### 4.3.3 Experimental design and statistical analysis

The effect of reaction parameters on the charge density and degree of substitution (DS) of carboxymethylated xylan were studied using Taguchi Orthogonal design [29]. In this experiment, $L_{16}$ orthogonal design with five factors (each at four levels) was used to investigate the effect of parameters on the carboxymethylation reaction. The factors and their levels were time (1, 2, 3 and 4 h), temperature (50, 60, 70 and 80 °C), NaOH concentration (0.5, 0.75, 1.0 and 1.25 M), xylan concentration (10, 15, 20 and 25 g/L) and SCA/xylan (0.5, 1.0, 1.5 and 2.0 mol/mol). The experiments were repeated three times, and the average values were reported in this work. The carboxymethylated xylan (CMX) that was produced under the conditions of 0.75 M $NaOH_{(aq)}$, 1.0 mol/mol SCA/xylan ratio at 70 °C for 2 h and xylan concentration of 15 g/L had the maximum charge density and DS was selected for further characterization with TGA, FTIR and $^{1}$HNMR.

### 4.3.4 Orthogonal design

A total of 16 runs were conducted based on Taguchi orthogonal design ($L_{16}$) to determine the optimum conditions for producing carboxymethylated xylan with the maximum charge density and DS. The experimental conditions conducted in the orthogonal design are listed in Table 4.1. The models for producing maximum charge density and DS of carboxymethylated xylan are depicted in equation 4.1. The number of terms in the models depends on the main effects and their degrees of freedom.

$$Y = b_0 + b_1A[1] + b_2A[2] + b3A[3] + b_4B[1] + b_5B[2] + b_6B[3] + b_7C[1] + b_8C[2] + b_9C[3] + b_{10}D[1] + b_{11}D[2] + b_{12}D[3] + b_{13}E[1] + b_{14}E[2] + b_{15}E[3] \ldots\ldots \quad (4.1)$$

In this equation, Y is charge density or DS, $b_0$ is the intercept, $b_i$ represents the model coefficients, A, B, C, D and E represent primary dimensionless factors for time, temperature, NaOH concentration, xylan concentration and SCA/xylan ratio. The numbers in brackets represent the first, second and third levels of each primary factor.

Table 4-1. The Taguchi Orthogonal parameters and levels ($L_{16}$)

| Run | Time (A), h | Temperature (B), °C | NaOH concentration (C), M | Xylan concentration (D), g/L | SCA/xylan (E), mol/mol |
|---|---|---|---|---|---|
| 1 | 1 | 50 | 0.5 | 10 | 0.5 |
| 2 | 1 | 60 | 0.75 | 15 | 1 |
| 3 | 1 | 70 | 1.0 | 20 | 1.5 |
| 4 | 1 | 80 | 1.25 | 25 | 2 |
| 5 | 2 | 50 | 0.75 | 20 | 2 |
| 6 | 2 | 60 | 0.5 | 25 | 1.5 |
| 7 | 2 | 70 | 1.25 | 10 | 1 |
| 8 | 2 | 80 | 1.0 | 15 | 0.5 |
| 9 | 3 | 50 | 1.0 | 20 | 1 |
| 10 | 3 | 60 | 1.25 | 20 | 0.5 |
| 11 | 3 | 70 | 0.5 | 15 | 2 |
| 12 | 3 | 80 | 0.75 | 10 | 1.5 |
| 13 | 4 | 50 | 1.25 | 15 | 1.5 |
| 14 | 4 | 60 | 1.0 | 10 | 2 |
| 15 | 4 | 70 | 0.75 | 25 | 0.5 |
| 16 | 4 | 80 | 0.5 | 20 | 1 |

### 4.3.5 Preparation of Polyacrylic acid (PAA) homo polymer

PAA was synthesized according to the procedure described elsewhere [30]. In this study, 2 g of acrylic acid monomer (0.56 mol/L) was dissolved in 50 ml of deionized water at specific temperature by stirring at 200 rpm and pH was adjusted to 3 using 0.1 M $H_2SO_4$. The solution was then charged with initiator, $K_2S_2O_8$ solution (0.002 mol/L) and the reaction was carried out at 50 °C for 60 min with nitrogen purging (20 min). After the reaction, the solution was neutralized with 0.1 M NaOH and dialyzed for 2 days using dialysis membrane to remove salts and acrylic acid monomers by changing water twice a day. After the dialysis, the solution was dried at 105 °C overnight and sample was later stored at 4 °C until further use.

### 4.3.6 Charge density analysis

In preparing the samples for analysis, the carboxymethylated xylan and PAA were initially dried in a 105 °C in an oven overnight to remove moisture. A 0.2 g of sample was then suspended in 20 mL of deionized water and incubated for 1 h at 30 °C in a water bath shaker at 150 rpm. After incubation, the sample was centrifuged for 10 min at 1000 rpm. The supernatant was used for determining the charge density using a particle charge detector (Mutek, PCD 04, Germany) with a PDADMAC standard solution (0.0056M). All the experiments were performed in triplicates, and the average values were reported.

### 4.3.7 Carboxylate group analysis and degree of substitution (DS)

The aqueous potentiometric titration method was used for measuring the carboxylate group content of unmodified and carboxymethylated xylan samples, by using an automatic potentiometer, Metrohm, 905 Titrado, Switzerland. A 1 g sample of unmodified xylan (UX) and carboxymethylated xylan (CMX) was added to 100 mL of distilled water, and the pH of the solution was adjusted to 10.5. The solution was then titrated with a cationic polymer, TEGO trant A100, in order to measure a number of carboxylate groups. The degree of substitution was calculated using equation 4.2 [31]:

$$\text{Degree of Substitution (DS)} = \frac{\text{M} \times \text{A}}{1 - 0.081 \times \text{A}} \qquad (4.2)$$

where A is the total carboxylate group content (mmol/g), 0.081 (g/mmol) is the mass of sodium carboxymethyl group attached and M is the mass of the primary unit of xylan (0.132 g/mmol).

### 4.3.8 Molecular weight analysis

A molecular weight analysis was performed for unmodified xylan (UX), carboxymethylated xylan (CMX) that were produced under the conditions of 70 °C, 2 h, 0.75 M NaOH, 1.0 mol/mol SCA/xylan and 15 g/L xylan concentration and PAA homopolymer was synthesized under the conditions of 0.56 mol/L acrylic acid, 0.002 mol/L $K_2S_2O_8$ solution, 50 °C and 60 min, using Malvern GPCmax VE2001 Module + Viscotek TDA305 (RI and viscometer detectors). Polyethylene oxides were used as standards. The samples were oven dried at 105 °C before analysis and about 100 mg of UX or CMX were dissolved in 10 mL of 0.1 mol/L $NaNO_3$ solution and filtered with a nylon 0.2 µm filter (13 mm diameter). The filtered solutions were used for molecular weight analysis. PolyAnalytic columns, PAA206 and PAA203 were

used with column temperature at 35 °C. The flow rate of GPC was set at 0.70 mL/min and 0.1 mol/L $NaNO_3$ solution was used as solvent and eluent.

### 4.3.9 FTIR analysis

The Fourier Transform Infrared Spectrophotometer (FTIR) analysis was conducted on UX and CMX samples. The samples were dried at 105 °C overnight, and 0.05 g of the sample was then used for structural characterization using FTIR (Bruker Tensor 37, Germany, ATR accessory). The spectra were recorded in the transmittance mode in the range of 500 $cm^{-1}$ and 4000 $cm^{-1}$ with a 4 $cm^{-1}$ resolution, and 32 scans per sample were conducted.

### 4.3.10 Thermogravimetric analysis

The thermal decomposition analysis of UX and CMX was carried out using a thermogravimetric analyzer, TGA, i-1000 series, Instrument Specialist Inc. 7.5 mg of UX and CMX samples were dried in an oven at 105 °C overnight and used for this analysis. The analysis was carried out under nitrogen at a steady flow rate of 35 mL/min. Each sample was heated from room temperature to 800 °C at the rate of 10 °C/min

### 4.3.11 $^{1}$H NMR analysis

The UX and CMX samples were characterized by a Varian Unity, INOVA 500 MHz, spectrometer [32]. The samples were dried in an oven at 105 °C overnight, and 50 mg of UX and CMX was dissolved in 2 mL of $D_2O$ containing 1 wt.% TSP at 50 °C for 2 h and 150 rpm. The $^{1}$HNMR spectra were recorded at 21 °C after 16 scans. A 45° pulse flipping angle, a 4.6 µs pulse width, a 2.05 s acquisition time, and 1 s relaxation delay time were considered for this analysis.

The formation of a by-product, i.e. glycolic acid, in the carboxymethylation reaction was confirmed using a Varian Unity INOVA 500 MHz spectrometer [33]. In this set of experiments, the carboxymethylated reaction medium generated under the conditions of 0.75 M NaOH concentration, 1.0 mol/mol SCA/xylan (anhydroxylose unit), 2 h, 70 °C and 15 g/L xylan concentration was adjusted to pH 7 using 80 wt. % acetic acid and the medium was centrifuged at 1000 rpm for 5 min. To 1 mL of supernatant, 0.5 mL of $D_2O$ was added and incubated at 30 °C for 2 h at 150 rpm. TSP was used as an internal reference standard for the NMR analysis. The $^{1}$H-NMR spectra of the samples were recorded at 21 °C after 8 scans. A 15° pulse flipping angle, a 2.05 s acquisition time, and 1 s relaxation delay time were used in the NMR analysis. As

reported earlier, glycolic acid was measured by the integration of the peak in the NMR spectrum at 4 ppm, which corresponded to the methylene protons of glycolic acid [34, 29].

### 4.3.12 Elemental analysis

An elemental analysis was performed for both UX and CMX samples using an Elementar Vario EL Cube elemental analyzer by the combustion method [35]. The samples were first dried in a 105 °C oven overnight in order to remove any moisture. Approximately, 2 mg of UX or CMX samples were weighed in silver vessels and loaded in an integrated carousel of the elemental analyzer. The samples were automatically transferred into a combustion tube and burnt at 1200 °C. Afterwards, the combustion gases were reduced and analyzed for carbon, hydrogen, nitrogen and oxygen content of the samples.

### 4.3.13 Dispersion analysis

A kaolin clay suspension of 100 g/L was used as a model sample in this study. The dispersion experiments were conducted using a photometric dispersion analyzer (PDA 3000, Rank Brothers Ltd), which was connected to a dynamic drainage jar (DDJ) fitted with a 70 mm mesh screen [36]. In the present study, 500 mL of distilled water was taken into the DDJ container and circulated from the DDJ to the PDA through a 3 mm plastic tube until a steady flow rate of 20 mL/min was achieved. The flow rate was regulated by peristaltic pump throughout the experiment. Then, 10 mL of a 100 g/L clay suspension was added into DDJ (2 g/L clay concentration) at 500 rpm. This caused a decrease in the initial base DC voltage ($V_0$) to a new DC voltage ($V_i$). After 100 s, 8 mg/g of UX or CMX, which was produced under optimal conditions as stated in section 2.3 or PAA (8 mg/g), produced under conditions as stated in section 2.5 was added to clay suspension. Similarly, in another experiment 8 mg/g of $Na_2CO_3$-PAA system (4 mg/g each) was added after 100 s under the conditions described above. The increase in DC voltage was represented as the DC voltage ($V_f$) of final suspension. The pH of the clay suspensions was maintained at 7.0 during the experiments. The dispersion performance of the clay suspension, which was represented by relative turbidity $\tau_r$, was measured from the variation in the direct current (DC) voltage of the PDA instrument [37]. The relative turbidity of the clay suspension was measured using equation 4.3 [38]:

$$\text{Relative turbidity, } \tau r = \frac{\tau f}{\tau i} = \frac{ln(\frac{V_0}{V_f})}{ln(\frac{V_0}{V_i})} \qquad (4.3)$$

where $\tau_f$ is denoted as the final suspension turbidity, and $\tau_i$ is denoted as initial suspension turbidity.

## 4.4 Results & Discussion

### 4.4.1 Carboxymethylation of xylan

The carboxymethylation reaction of xylan is shown in Figure 4.1. The carboxymethylation of xylan is performed using sodium chloroacetate as a carboxylate group donar (Figure 4.1a). Under alkali conditions, NaOH reacts with the hydroxyl group of xylan and generates a strong nucleophile. The alkoxide ion from the alkali xylan attacks the chloroacetate through $S_N2$, results in the carboxymethylation of xylan. The degree of carboxymethylation depends on the number of hydroxyl group substituted with carboxymethyl groups. Furthermore, glycolic acid and NaCl could be generated as by-products at high concentrations of sodium chloroacetate and NaOH (Figure 4.1b) [20].

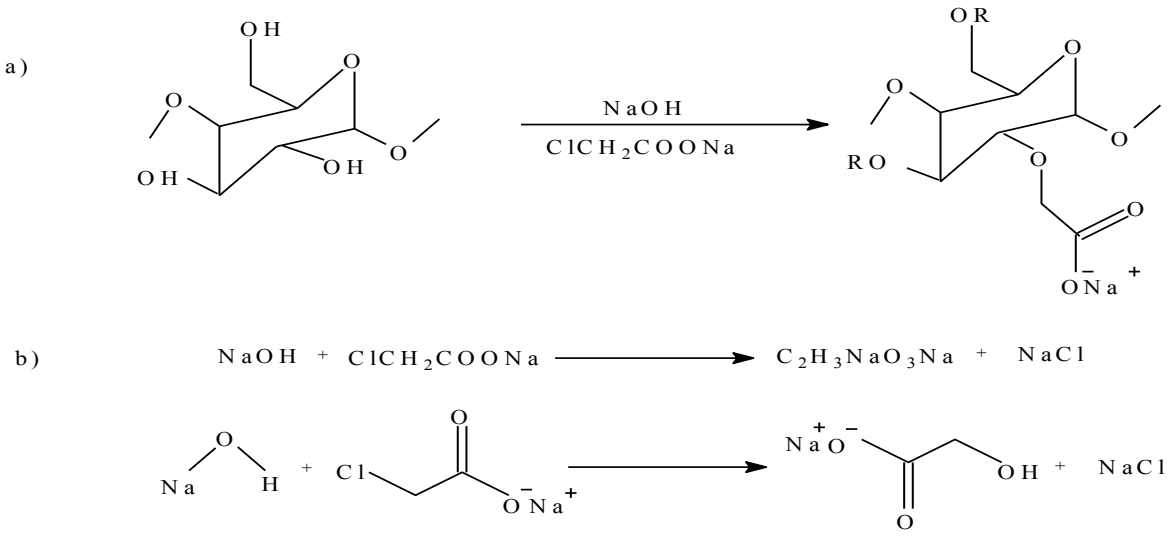


Figure 4.1. a) Carboxymethylation of xylan b) undesired side reaction, R may be H or $CH_2COONa$

### 4.4.2 Effect of reaction conditions

#### 4.4.2.1 NaOH concentration

Figure 4.2a represents the influence of NaOH concentration on the charge density and degree of substitution of CMX. An increase in NaOH concentration from 0.25 to 0.75 M increased the charge density and DS from 1.02 to 1.49 meq/g and from 0.1 to 0.19, respectively. Further increase in NaOH concentration resulted in a decrease in both charge density and DS. This initial increase in the reaction efficiency is due to a higher nucleophilic reactivity generated by the

availability of sufficient NaOH concentration [39]. In contrast, higher concentrations of NaOH inhibited the reaction efficiency by generating sodium glycolate via undesired side reaction as reported in section 3.1. A similar result was reported on the microwave induced carboxymethylation of wheat straw hemicelluloses using sodium monochloroacetate, in which an increase in NaOH concentration from 0.4 to 1.4 M increased the DS of carboxymethylated hemicellulose from 0.44 to 0.91. Further increase in NaOH concentration to 1.6 M decreased the DS to 0.79 [19].

#### 4.4.2.2 Time

The effect of time on the charge density and DS of carboxymethylated xylan are shown in Figure 4.2b. It is clear that with the time extension, the charge density and DS were increased. The maximum charge density (1.42 meq/g) and DS (0.18) were obtained at 2 h reaction time. Prolonging the reaction time to 4 h resulted in a decrease in the charge density and DS. The initial increase in the charge density and DS were due to favourable conditions for carboxymethylation (i.e. better contact between the etherifying agent and xylan). In the work conducted by Hebeish and co-authors on the preparation of carboxymethylated rice starch using monochloroacetic acid, with a time extension from 0.5 to 4 h, the DS was found to increase from 0.25 to 0.40 [40]. In contrast, a decrease in the charge density and DS beyond 2 h reaction in Figure 2b was due to the progress in the production of the undesired product shown in Figure 4.1b [18].

#### 4.4.2.3 Temperature

Figure 4.2c represents the influence of temperature on the charge density and DS of CMX. A maximum charge density (1.52 meq/g) and DS (0.2) were obtained at 70 °C. There was an increase in the charge density and DS with the temperature increase, which was due to the existence of more favorable conditions for the mobility of reactants, swellability of xylan and compatibility of reactants [17]. A decrease in the charge density and DS were due to the degradation of xylan and generation of undesired products. The deterioration of CMX at high temperatures was confirmed by the molecular weight analysis of CMX. The molecular weight ($M_w$) was found to decrease from 32,573 to 6,916 g/mol. In the carboxymethylation of amaranth and corn starch using sodium monochloroacetate, an optimum temperature was found to be 65 °C for both amaranth and corn starch [41]. In another work performed by Bi and co-authors on

the carboxymethylation of potato starch using monochloroacetic acid, the optimum temperature was found to be 50 °C [39].

#### 4.4.2.4 Xylan concentration

The effect of xylan concentration on the charge density and DS of CMX are depicted in Figure 2.2d. It is clear that with an increase in the xylan concentration from 5 to 15 g/L, an increase in the charge density and DS was obtained from 1.25 to 1.56 meq/g and from 0.14 to 0.2, respectively. The increase in the xylan concentration favours the accessibility of xylan to sodium chloroacetate [17]. In contrast, a decrease in the charge density and DS of carboxymethylated xylan was observed with the increase in xylan concentration beyond 15 g/L. This decline in the charge density and DS may be due to precipitation or gelation of xylan at high concentrations [42]. It was reported that the optimum concentration for the carboxymethylation of amaranth and corn starch was 66.7 g/L in order to achieve the maximum DS of 0.21 [41].

#### 4.4.2.5 Ratio of SCA/xylan

The effects of SCA/xylan on the charge density, DS of CMX, as well as on glycolic acid production are presented in Figure 2.2e. Both the charge density and DS increased with a rise in the SCA/xylan molar ratio. The maximum charge density (1.62 meq/g) and DS (0.21) were obtained at 1.0 SCA/xylan molar ratio. Furthermore, with the increase in SCA/xylan molar ratio from 0.25 to 2.0, glycolic acid production was found to rise from 0.01 to 1.8 mM. Similar trends were observed in the carboxymethylation of corn, rice starch and birch xylan using sodium monochloroacetate in the past [41, 40, 43].

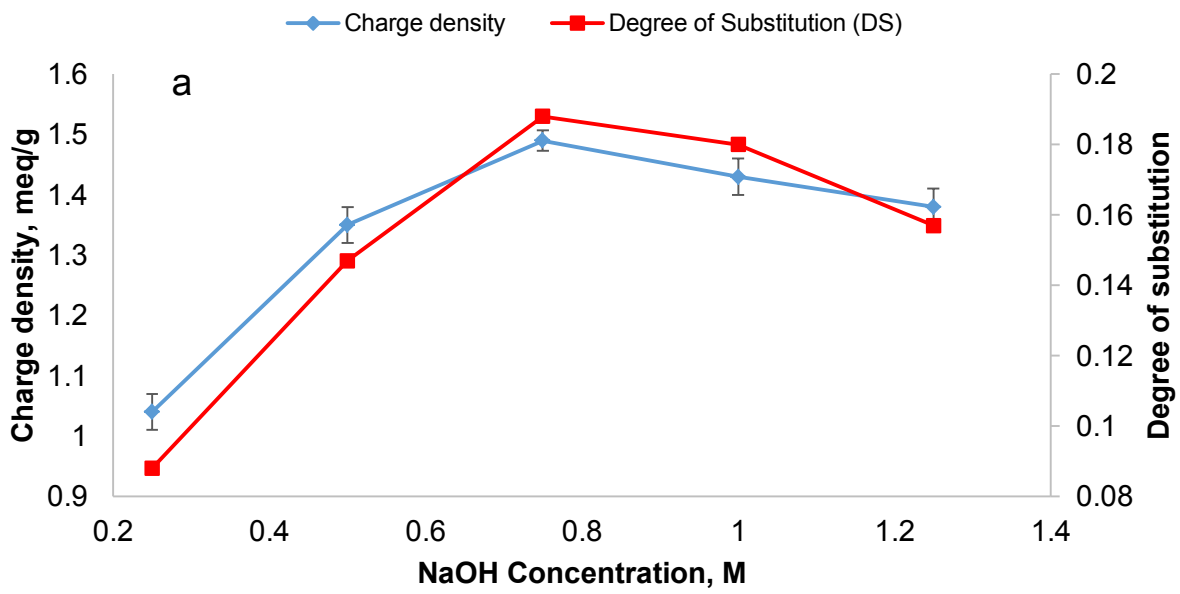
Charge density
Degree of Substitution (DS)
a
Charge density, meq/g
Degree of substitution
NaOH Concentration, M
1.6
1.5
1.4
1.3
1.2
1.1
1
0.9
0.2
0.18
0.16
0.14
0.12
0.1
0.08
0.2
0.4
0.6
0.8
1
1.2
1.4

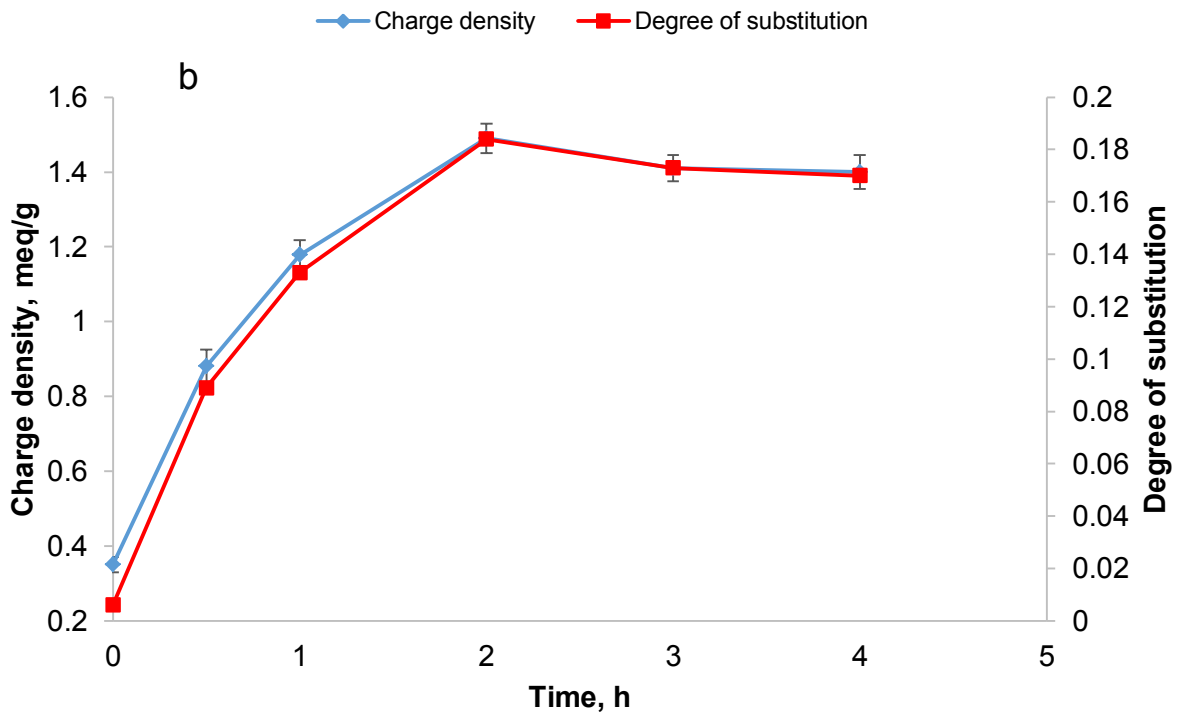
Charge density
Degree of substitution
b
Charge density, meq/g
Degree of substitution
Time, h
1.6
1.4
1.2
1
0.8
0.6
0.4
0.2
0.2
0.18
0.16
0.14
0.12
0.1
0.08
0.06
0.04
0.02
0
0
1
2
3
4
5

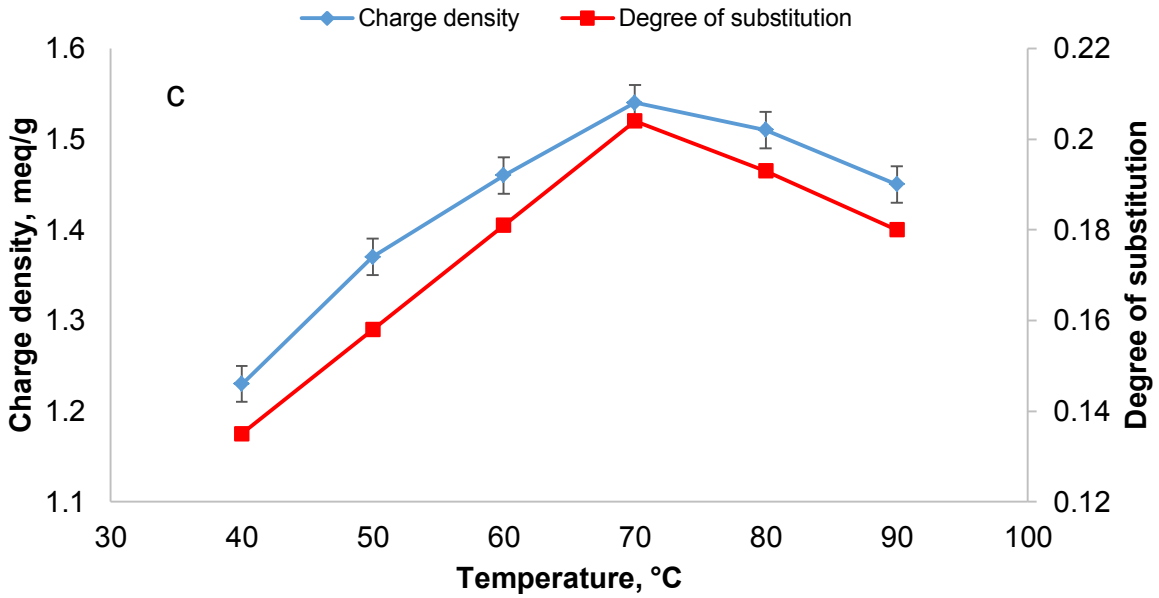
Charge density
Degree of substitution
c
Charge density, meq/g
Degree of substitution
Temperature, °C
1.6
1.5
1.4
1.3
1.2
1.1
0.22
0.2
0.18
0.16
0.14
0.12
30
40
50
60
70
80
90
100

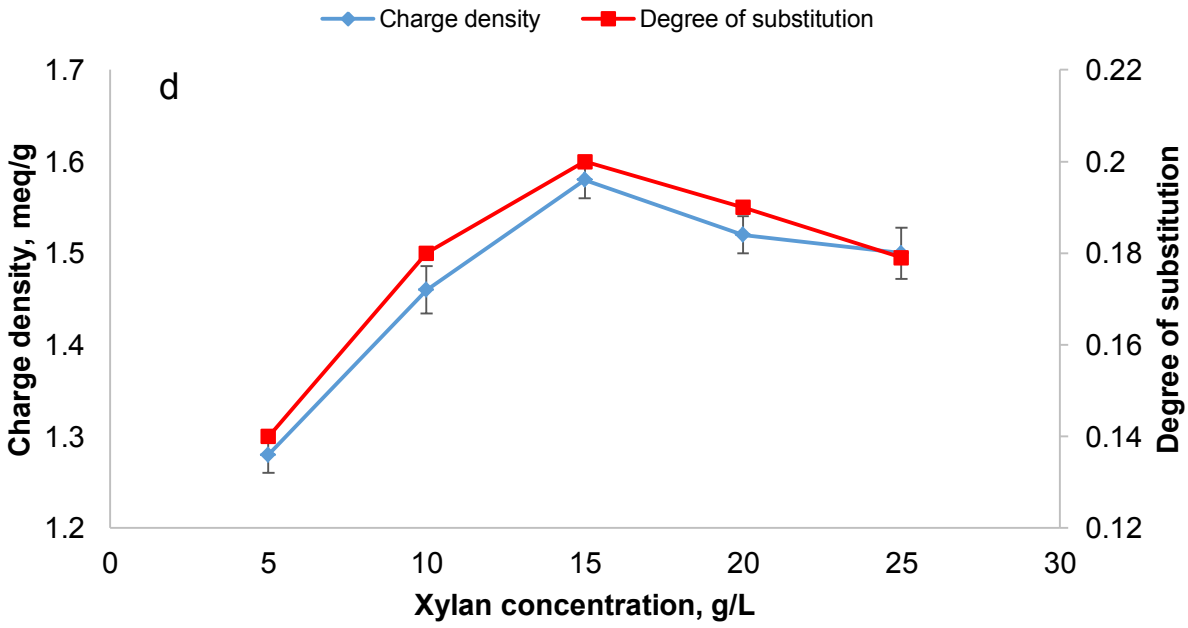
Charge density
Degree of substitution
d
Charge density, meq/g
Degree of substitution
Xylan concentration, g/L
1.7
1.6
1.5
1.4
1.3
1.2
0.22
0.2
0.18
0.16
0.14
0.12
0
5
10
15
20
25
30

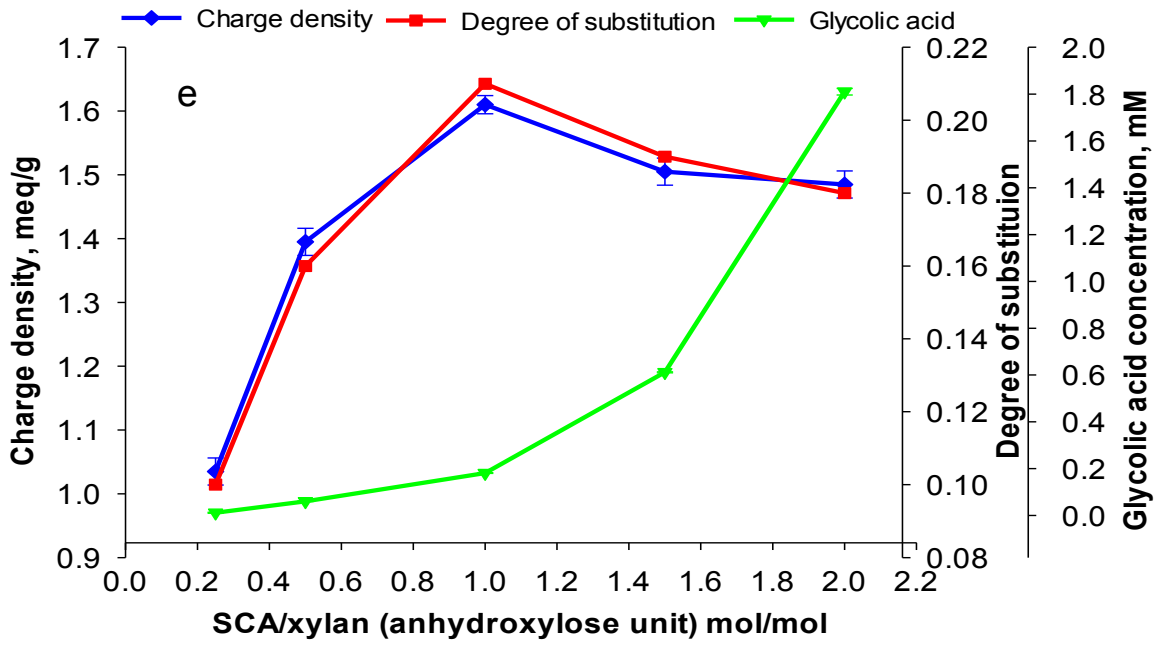


Figure 4.2. Effect of (a) NaOH, (b) Time, (c) Temperature, (d) Xylan concentration and (e) Molar ratio of SCA/xylan (anhydroxylose unit) on the charge density and DS of CMX

### 4.4.3 Analysis of variance (ANOVA)

The results in Figures 4.2a to 4.2e do not show which reaction parameters had the most significant impact on the charge density and DS of the CMX. The relationship among experimental factors and the generated results as well as the contribution of experimental factors can be determined by the ANOVA statistical technique [29]. Table 4.2 contains the predicted data generated by the models and the regression coefficients ($R^2$). The factor with a high F-value would have a more significant contribution (i.e. more influence) in producing the maximum charge density and DS [44]. Among all five factors studied, time had the highest F-value for both charge density (169.39) and DS (64.20). This indicates that the time of reaction is the most contribution factor in producing the maximum response.

Table 4-2. ANOVA analysis for charge density and DS of carboxymethylated lignin

| Source | Sum of Squares | | Mean Square | | F-value | | P-value | | Significant | |
|---|---|---|---|---|---|---|---|---|---|---|
| | Charge density, meq/g | DS | Charge density, meq/g | DS | Charge density, meq/g | DS | Charge density, meq/g | DS | Charge density, meq/g | DS |
| Model | 0.45 | 0.015 | 0.038 | 0.0012 | 54.71 | 30.9 | 0.0035 | 0.0082 | Yes | Yes |
| Time, min | 0.35 | 0.008 | 0.121 | 0.0026 | 169.39 | 64.2 | 0.0008 | 0.0032 | | |
| Temperature, °C | 0.03 | 0.0001 | 0.011 | 0.00004 | 16.33 | 0.078 | 0.0231 | 0.0495 | | |
| SCA/xylan, mol/mol | 0.04 | 0.0042 | 0.015 | 0.0014 | 21.24 | 33.8 | 0.0160 | 0.0082 | | |
| Xylan concentration, g/L | 0.03 | 0.0017 | 0.008 | 0.0006 | 11.89 | 13.8 | 0.0358 | 0.0292 | | |
| NaOH concentration, mol | 0.002 | 0.0014 | 0.0007 | 0.0005 | 0.071 | 11.8 | 0.0457 | 0.0362 | | |
| | Standard deviation | | Coefficient of variation, % | | $R^2$ | | Adjusted $R^2$ | | Predicted $R^2$ | |
| | Charge density, meq/g | DS | Charge density, meq/g | DS | Charge density, meq/g | DS | Charge density, meq/g | DS | Charge density, meq/g | DS |
| Model Fitting | 0.026 | 0.006 | 1.91 | 4.07 | 0.9955 | 0.992 | 0.9773 | 0.9599 | 0.8706 | 0.7717 |

The P-value denotes the probability of occurring F-value as noise, and if P-value is less than 0.05, the factors used in the design are considered to be significant. All the factors were found to have P-values less than 0.05 for both the charge density and DS. Similarly, the factor with a smaller P-value would have a more significant contribution to increasing the charge density and DS [45]. Thus, the time of reaction with the smallest P-value for both charge density (0.0008) and DS (0.0032) had the maximum effect compared to other factors. The smaller values of standard deviation (SD) and coefficient of variation (CV) for the charge density (0.03 meq/g and 1.91 %) and DS (0.006 and 4.07 %) revealed that the experimental results obtained are reliable

[46]. The reliability of results was further confirmed by the regression coefficients ($R^2$) values for the charge density (0.995) and DS (0.992). Both predicted $R^2$ and adjusted $R^2$ determined how well the model fit to the experimental data. The former assumed that all the independent variables impacted the dependent variables, and the latter considered that only the independent variables affectet the dependent variable [45]. The predicted $R^2$ values of charge density and DS were found to be in agreement with adjusted $R^2$ values. The regression analysis was employed to fit experimental data (Table 4.1) to the first order polynomial (equation 1) using Taguchi orthogonal model. The results obtained were shown in Table 4.3.

Table 4-3. Model coefficients estimated by regression analysis

| Term | Charge density, meq/g | | | | DS | | | |
|---|---|---|---|---|---|---|---|---|
| | Coefficient estimate | Standard Error | 95% CI Low | 95% CI High | Coefficient estimate | Standard error | 95% CI Low | 95% CI High |
| Intercept | 1.38 | 0.007 | 1.36 | 1.40 | 0.16 | 0.002 | 0.15 | 0.16 |
| A[1] | -0.26 | 0.011 | -0.29 | -0.22 | -0.034 | 0.003 | -0.043 | -0.025 |
| A[2] | 0.099 | 0.011 | 0.063 | 0.13 | 0.024 | 0.003 | 0.015 | 0.033 |
| A[3] | 0.074 | 0.011 | 0.038 | 0.11 | -0.006 | 0.003 | -0.015 | -0.003 |
| B[1] | -0.026 | 0.011 | -0.062 | 0.01 | 0.001 | 0.010 | 0.001 | 0.005 |
| B[2] | -0.016 | 0.011 | -0.052 | 0.020 | 0.004 | 0.010 | 0.001 | 0.007 |
| B[3] | 0.079 | 0.011 | 0.043 | 0.11 | -0.001 | 0.010 | -0.006 | -0.001 |
| C[1] | 0.019 | 0.043 | -0.086 | 0.12 | -0.016 | 0.003 | -0.025 | -0.007 |
| C[2] | -0.001 | 0.043 | -0.11 | 0.1 | 0.004 | 0.003 | -0.005 | 0.013 |
| C[3] | -0.011 | 0.043 | -0.12 | 0.093 | 0.004 | 0.003 | -0.005 | 0.013 |
| D[1] | 0.009 | 0.011 | -0.027 | 0.045 | 0.009 | 0.003 | 0.0001 | 0.018 |
| D[2] | 0.034 | 0.011 | -0.002 | 0.070 | -0.014 | 0.003 | -0.023 | -0.005 |
| D[3] | -0.066 | 0.011 | -0.10 | -0.030 | -0.006 | 0.003 | -0.015 | 0.003 |
| E[1] | -0.081 | 0.011 | -0.12 | -0.045 | -0.009 | 0.003 | -0.018 | 0.0001 |
| E[2] | 0.064 | 0.011 | 0.028 | 0.100 | 0.021 | 0.003 | 0.012 | 0.030 |
| E[3] | 0.019 | 0.011 | -0.017 | 0.055 | 0.009 | 0.003 | -0.0001 | 0.018 |

It is clear that time had a major effect on the charge density and DS with maximum coefficient values at each level, while NaOH concentration and temperature had the minimum effects on the charge density and DS, respectively. Small standard errors of regression indicated that the experimental data was well fitted into the first order polynomial equation. The coefficient values

predicted for the terms also found to be in the 95 % confidence interval (CI) range. These results suggested that the models can be used to predict the charge density and DS of carboxymethylated xylan.

The predicted charge density and DS results were plotted against experimental results in Figure 4.3. As can be seen, the predicted results were in good agreement with the experimental data [47]. Based on the ANOVA analysis, the optimal conditions to produce carboxymethylated xylan with the maximum charge density and DS were found to be 0.75 M NaOH concentration, time of 2 h, the temperature of 70 °C, 15 g/L xylan concentration and 1.0 mol/mol SCA/xylan ratio.

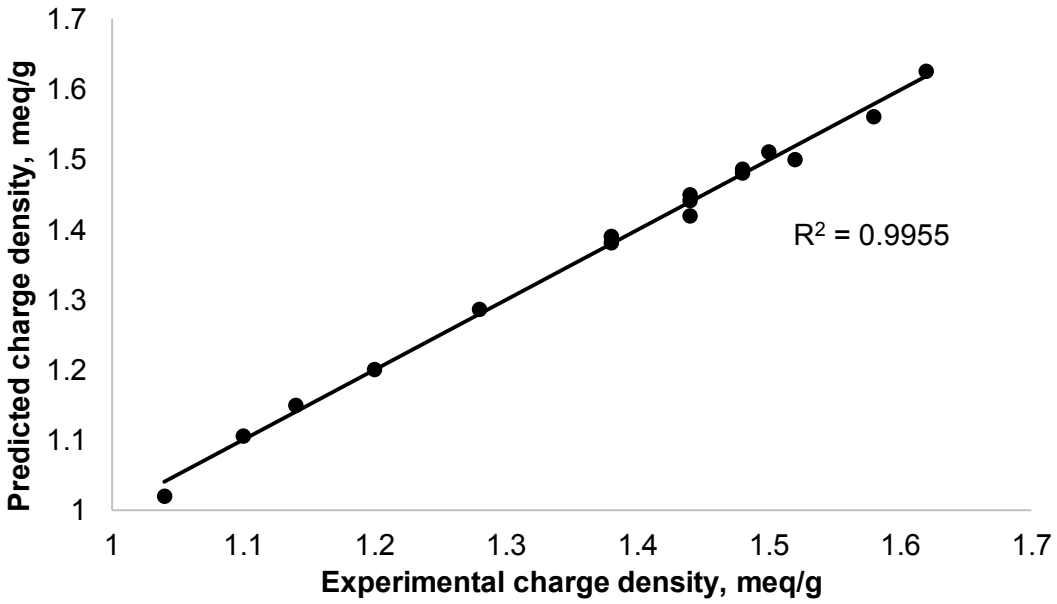

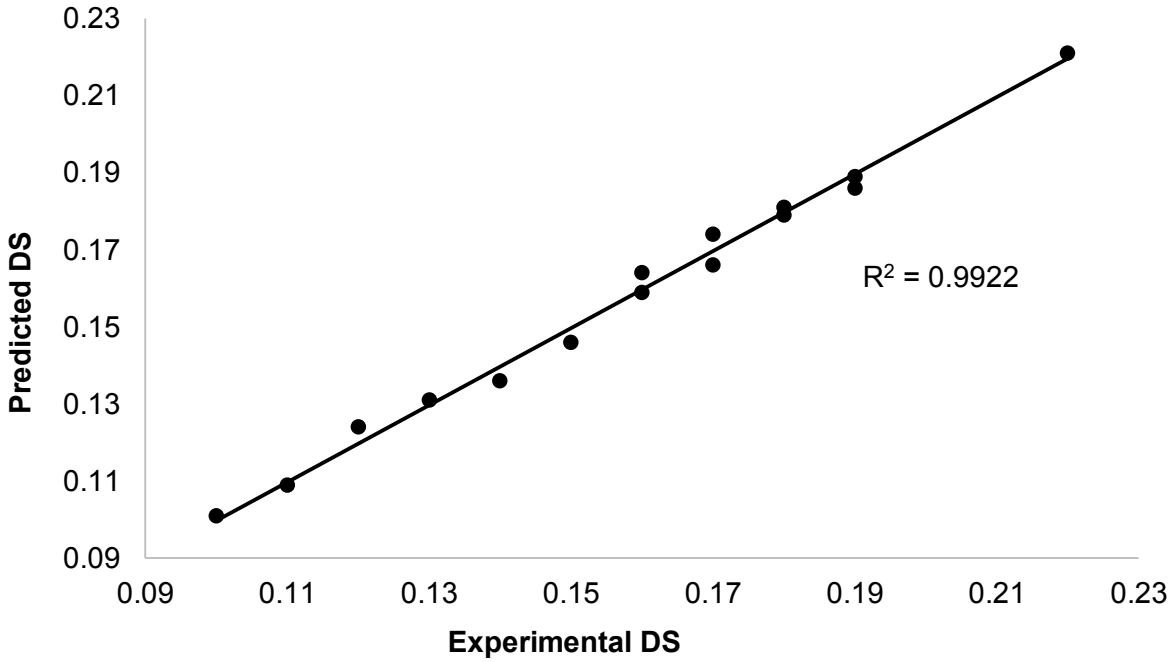


Figure 4.3. Relationship between the predicted values and experimental values for 1) charge density and 2) DS based on Taguchi orthogonal design

### 4.4.4 Properties of UX and CMX

The carboxymethylated xylan with the charge density of 1.62 meq/g and DS of 0.21 produced under the optimal conditions of 0.75 M $NaOH_{(aq)}$, 1.0 mol/mol SCA/xylan (anhydroxylose unit) ratio, 70 °C, 2 h and 15 g/L xylan concentration was selected for further analysis. Table 4.4 lists the properties of UX and CMX produced under these conditions. The carboxylate group of UX and CMX samples were found to be 0.32 mmol/g and 1.48 mmol/g, respectively. It is evident that the oxygen and hydrogen contents were higher for CMX than for UX confirming the success of carboxymethylation. In one study on the carboxymethylation of bagasse lignin using oxidation process, a decrease in the carbon and hydrogen contents and an increase in the oxygen of lignin were obtained as a result of carboxymethylation [48]. Based on these findings, the chemical formulas for UX and CMX were determined to be $C_5H_{8.592}O_{4.352}S_{0.001}$ and $C_5H_{8.960}O_{5.936}S_{0.002}$, respectively.

The carboxylate degree of CMX would correspond to the level of substitution of 0.04 and 0.21 for both UX and CMX as listed in Table 4.4. The carboxylate group attached to UX is attributed to glucuronic acid attached to the backbone of xylan [49]. Previously, the carboxymethylation of birch xylan with sodium monochloroacetate in isoproponal medium showed an increase in the

degree of substitution from 0 to 1.09 at 75°C for 70 min [43]. In another study, the carboxymethylation of xylan from birch wood in the isopropanol medium, which was conducted under the conditions of 25 wt. % NaOH, 4/1 Sodium monochloroacetate/xylan (anhydroxylose unit), 75 °C, 70 min, showed an increase in the DS from 0 to 1.13 [25]. Furthermore, CMX was found to have a higher $M_w$ of 24,127 g/mol and $M_n$ of 19,254 g/mol than UX ($M_w$ of 20,840 g/mol and $M_n$ of 15,852 g/mol, respectively). Based on the degree of substitution (Table 4.4), the molecular weight ($M_w$) of CMX was calculated to be 23,511 g/mol. The increase in the molecular weight can be attributed to the introduction of carboxymethyl groups in the modified xylan. Furthermore, CMX showed slightly lower polydispersity (1.25) compared to UX (1.31). This decrease in polydispersity may be due to alkaline degradation of xylan during carboxymethylation as explained earlier. It was reported that the carboxymethylation of xylan from birch wood with sodium choloroacetate in isopropanol medium increased its molecular weight from 11,700 to 17,100 g/mol, but reduced its polydispersity from 1.79 to 1.62, [25].

The properties of polyacrylic acid homopolymer synthesized under the conditions of 0.5 mol/L acrylic acid, 0.002 mol/L $K_2S_2O_8$ solution, 50 °C and 60 min were also listed in Table 4.4. PAA had a negative charge density of 11.2 meq/g. The weight average molecular weight (Mw) and number average molecular weight (Mn) of PAA were measured to be 31,151 g/mol and 26,647 g/mol respectively. The polydispersity of PAA was found to be 1.17.

Table 4-4. Properties of unmodified, carboxymethylated beechwood xylan and PAA homopolymer

| Sample | Unmodified Xylan (UX) | Carboxymethylated xylan (CMX) | Polyacrylic acid (PAA) |
|---|---|---|---|
| Carbon, wt.% | 41.0 (±1) | 32.0 (±1) | - |
| Oxygen, wt.% | 47.2 (±1) | 58.1 (±1) | - |
| Hydrogen, wt.% | 6.1 | 4.5 | - |
| Sulfur, wt% | 0.02 | 0.03 | - |
| Charge density, meq/g | 0.38 (± 0.05) | 1.62 (±0.02) | 11.2 (±0.07) |
| Carboxylic group content, mmol/g | 0.36 (±0.05) | 1.48 (±0.02) | - |
| DS | 0.04 | 0.21 | - |
| $M_w$, g/mol | 20,840 | 24,127 | 31,151 |
| $M_n$, g/mol | 15,852 | 19,254 | 26,647 |
| $M_w/M_n$ | 1.31 | 1.25 | 1.17 |

### 4.4.5 FTIR analysis

The FTIR spectra of UX and CMX are presented in Figure 4.4. The broad stretch between 3400-3100 $cm^{-1}$ represents hydroxyl groups on the backbone of xylan [10]. The peaks at 1640 and 1043 $cm^{-1}$ present in UX corresponded to C=C and C-O bond stretching, respectively [26]. The peak at 918 $cm^{-1}$ was attributed to β-glycosidic linkages between the sugars units, indicating that xylose residues forming the backbone of xylan polymer were bonded by β linkages [50]. In the spectrum of CMX, the peak between 2936 and 2993 $cm^{-1}$ was attributed to C-H bending and C-H stretching of methylene groups [35]. A strong peak at 1601 $cm^{-1}$ was ascribed to carboxyl groups present in CMX. The strong signal at 1401 $cm^{-1}$ corresponded to $CH_2$ stretching of methylene groups attached to xylan. Previously, the attachment of carboxyl group to xylan was confirmed by the generation of the peak at 1601 $cm^{-1}$ for the carboxymethylation of wheat straw hemicelluloses in solvent media [19]. Thus, FTIR analysis confirmed the presence of carboxymethyl groups on CMX.

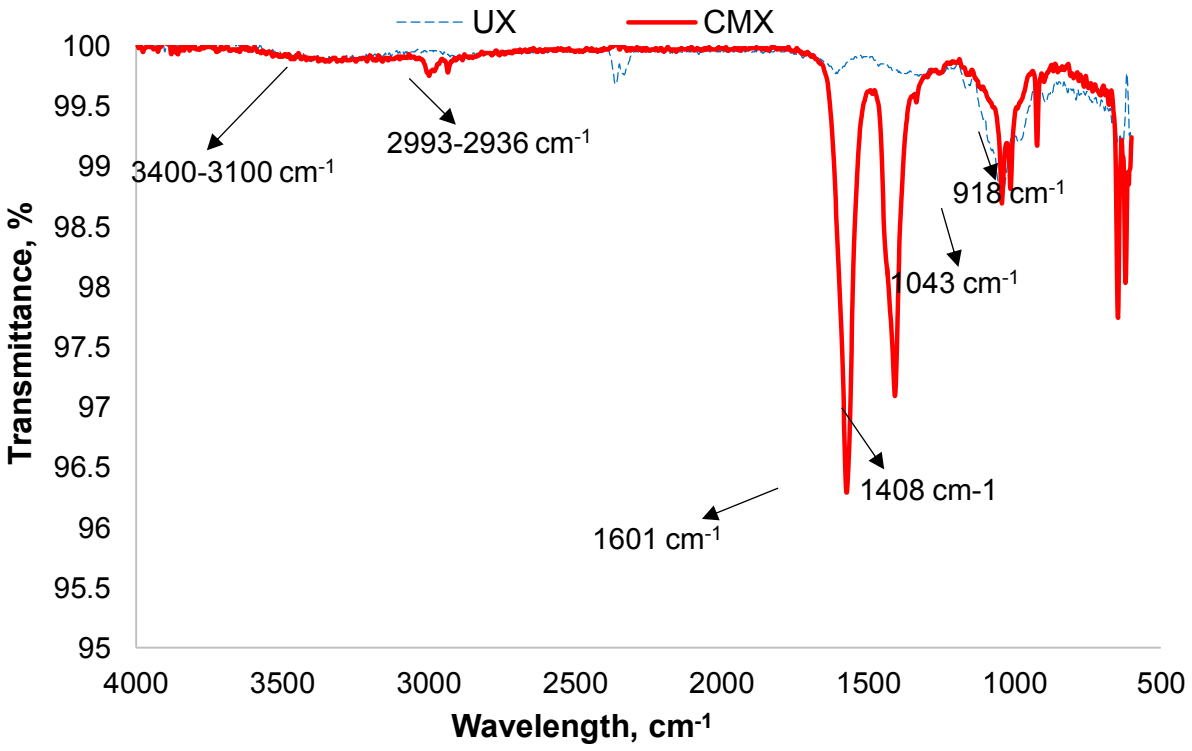


Figure 4.4. FTIR spectra of UX and CMX

### 4.4.6 $^{1}$HNMR analysis

Figure 4.5 shows the $^{1}$HNMR spectra of UX and CMX produced under optimized conditions. The peaks at 4.0-4.4 ppm and 3.0 to 3.9 ppm corresponded to equatorial and axial protons of

xylan anhydroxylose unit [51]. The peak at zero ppm corresponded to TSP (internal standard) and peaks at 0.6, 1.2 and 2.8 ppm corresponded to acetyl and methyl groups of 4-O-methyl-D-glucuronic acid, respectively [18]. The sharp peaks at 3.95 and 4.05 ppm in the CMX corresponded to the protons of carboxymethylate groups attached to anhydroxylose unit. In the H-NMR analysis of a carboxymethylated birch xylan, the carboxymethylate groups were found to be attached to either O-2 or O-3 positions of anhydoxylose units [43]. The $^{1}$HNMR analysis also confirmed the attachment of carboxymethyl groups to xylan in the carboxymethylation reaction.

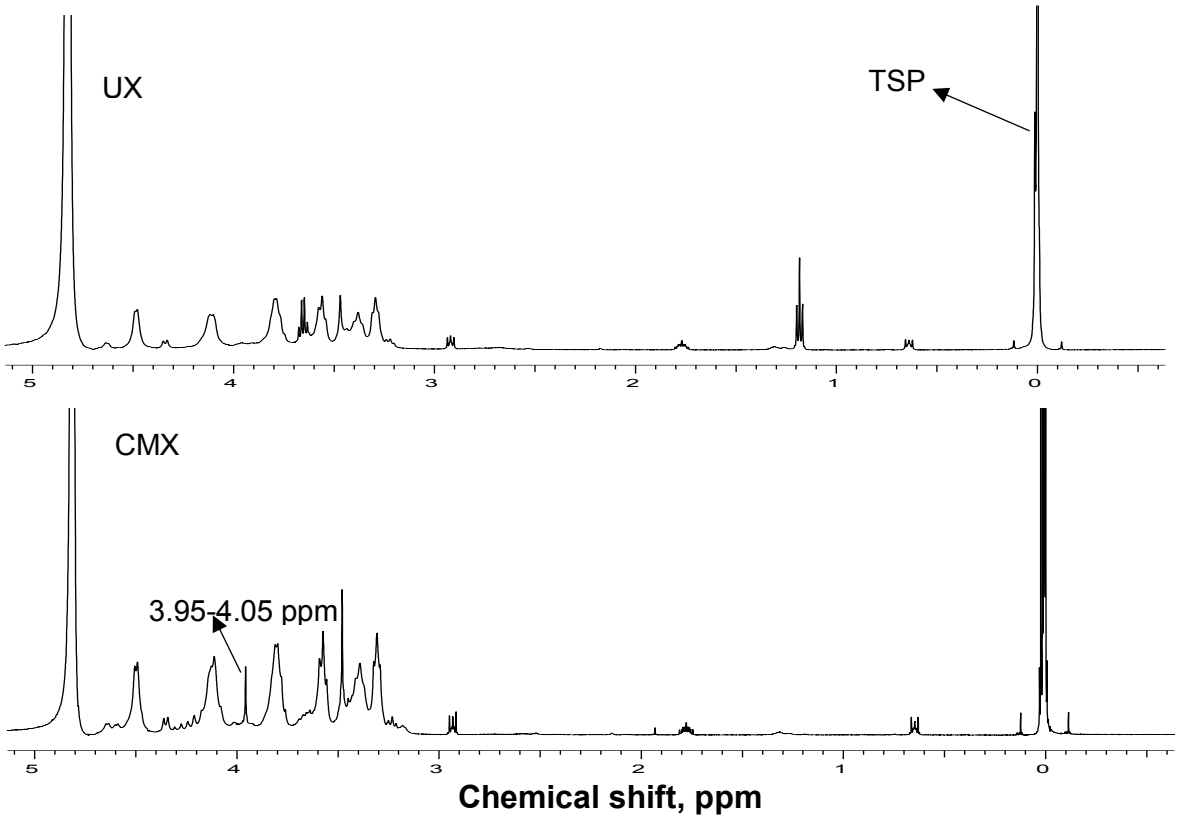


Figure 4.5. HNMR spectra of UX and CMX

### 4.4.7 Thermogravimetric (TGA) analysis

The thermal decomposition behavior of UX and CMX is presented in Figure 4.6. The weight loss of CMX was more than UX when the temperature increased to 200 °C. Generally, CMX is more hydrophilic than UX due to the presence of carboxylate group [7]. Due to more hydrophilicity of CMX, more moisture is presumably attached to the carboxymethylated xylan [51]. UX showed

about 55 wt.% weight loss between 220 to 380 °C. CMX showed approximately 35 wt.% weight loss between 240 to 550 °C. CMX had 40 wt.% residues as ash, while UX contained 20 wt.% as ash at 800 °C. This was mostly due to the introduction of methyl groups in the carboxymethylation of xylan [25]. Fang and co-authors reported a high thermal stability of methylated wheat straw hemicelluloses compared to unmodified one, which was due to the attachment of methyl groups [52].

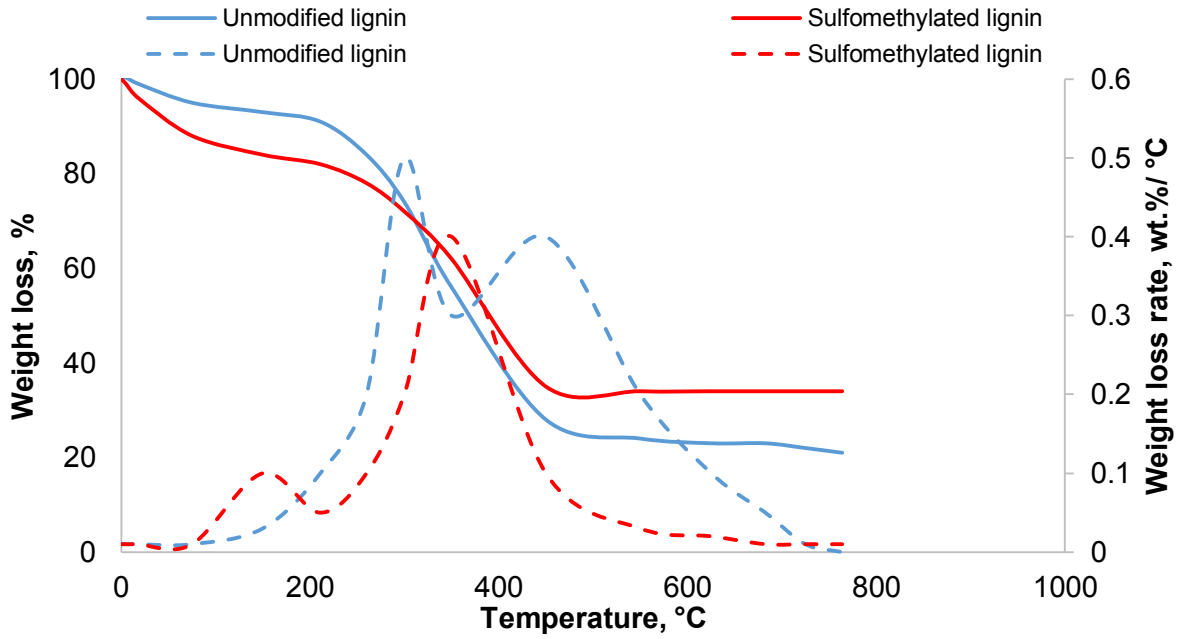


Figure 4.6. Weight loss and weight loss rate of UX and CMX produced under the conditions of 0.75 M NaOH, 1.0 mol/mol SCA/xylan (anhydroxylose unit), 2 h, 15 g/L xylan concentration and temperature of 70 °C. The TGA analysis was conducted at 35 mL/min nitrogen flow rate.

### 4.4.8 Dispersion analysis

Figure 4.7 presents the relative turbidity of clay suspension in the presence of UX or CMX (produced under optimal conditions), PAA and sodium carbonate-PAA system at pH 7.0. The addition of CMX (8 mg/g) to the clay suspension resulted in an increase in the relative turbidity from 0.99 to 1.27 within 200 s of treatment. PAA (8 mg/g) increased the relative turbidity of clay suspension from 0.99 to 1.26, which implies that the effectiveness of CMX and PAA were very similar. The increase in relative turbidity of clay suspension in the presence of CMX or PAA was due to their negative charge density, which induced repulsion between the clay particles by introducing extra negative charges on their surface [53, 29]. Kakui and Kamiya claimed that large electrostatic repulsion was generated between coal particles via introducing anionic

polymers to the coal suspension, which improved the dispersibility of the slurry [54]. In another report on the stabilization of ceramic suspensions using polyacrylic acid or polyethylene glycol, the dispersibility of ceramic suspension was increased after addition of anionic polymers [55]. Biodegradability and environmental friendly nature of CMX compared to PAA also make CMX more industrially attractive. The addition of sodium carbonate-PAA system (4 mg/g each to generate the total of 8 mg/g) caused an increase in the relative turbidity of the clay suspension from 0.99 to 1.2, which was lower than that of CMX or PAA. In this case, the increase in the relative turbidity of the clay suspension was due to the stabilization of clay particles via replacement of $Ca^{2+}$ ions present on the clay surface with $Na^{+}$ ions, which resulted in a decrease in screening of surface charge [56] and also due to introduction of negative charges by PAA on clay surface. The lower performance of sodium carbonate-PAA system than PAA was possibly due to the interaction of $Ca^{2+}$ ions in the suspension with the negative charges of PAA and thereby reduced its efficiency to impart negative charge to clay surface. In one report on the adsorption of polyacrylamide on calcite surface, it was reported that the interaction of polyacrylic acid on calcite surface was decreased in the presence of $Ca^{2+}$ ions, which screened the carboxylate groups of polyacrylic acid [57]. UX did not show any significant increase in relative turbidity (0.99 to 1.02). It is inferred from this figure that CMX exhibited better performance than sodium carbonate-PAA system, which suggest that CMX can be the best alternative for polyacrylic acid-sodium carbonate system in stabilizing clay suspensions.

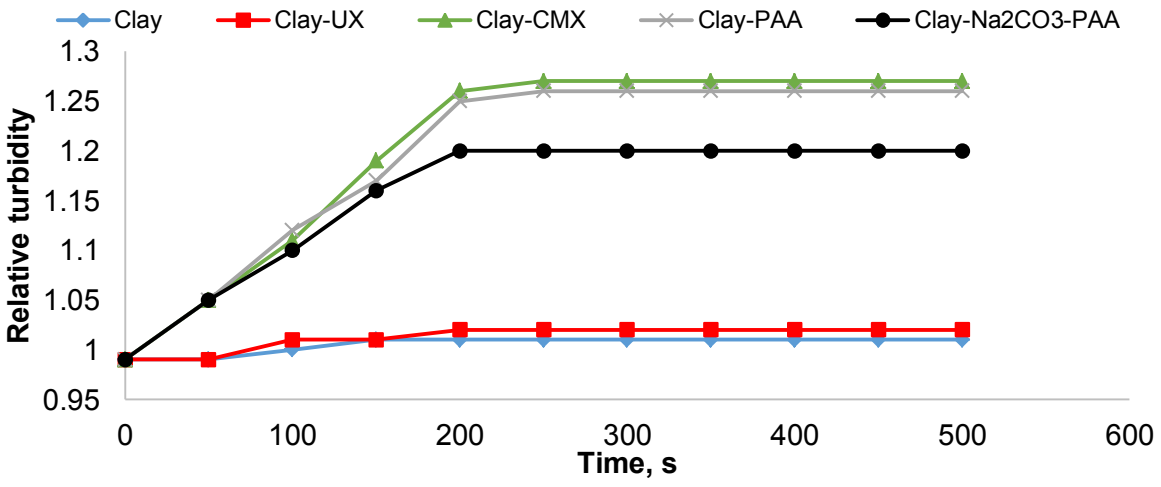


Figure 4.7. Relative turbidity of clay suspension in the presence of UX/CMX/PAA/sodium carbonate-PAA system under the conditions of pH 7.0, 2 g/L clay dosage, 500 rpm, 8 mg/g of CMX or PAA or sodium carbonate-PAA system.

Xylan can be carboxymethylated to higher DS compared to cellulose, because xylan is more reactive than cellulose due to absence of an OH group at C6, which makes cellulose chemically stable by forming hydrogen bonds [58, 59]. Also cellulose has numerous other applications (bioethanol production, synthesis of nanofibers, cellulose acetate membranes) making it more expensive; whereas, xylan has no effective application and can be cheaply available for synthesis of CMX. On the other hand, cellulose is a high molecular weight polymer and can generate comparatively high molecular weight products than xylan upon modification.

## 4.5 Conclusions

In the present work, the carboxymethylated xylan was successfully prepared in an aqueous medium. The experimental and modeling analyses confirmed that CMX with the maximum charge density of -1.62 meq/g, carboxylate group of 1.48 mmol/g and DS of 0.21 could be generated under the conditions of 0.75 M NaOH, 1.0 mol/mol SCA/xylan (anhydroxylose unit) ratio, 2 h reaction time, temperature of 70 °C and 15 g/L xylan concentration. The molecular weight of xylan was increased from 20,840 g/mol to 32,573 g/mol after carboxymethylation. The attachment of carboxymethyl groups to UX was confirmed by both FTIR and $^{1}$HNMR analyses. PAA with molecular weight 34,151 g/mol and charge density 11.2 meq/g was prepared under the conditions of 0.56 mol/L acrylic acid, 0.002 mol/L $K_2S_2O_8$ solution, 50 °C and 60 min under constant nitrogen purging (20 min). The dispersion analysis confirmed that CMX could be an effective dispersant compared to sodium carbonate-PAA system for clay suspension as the relative turbidity of the clay suspension was increased from 0.99 to 1.27 in the presence of CMX. Meanwhile, sodium carbonate-PAA system increased the relative turbidity of clay suspension from 0.99 to 1.25. However, UX did not show any significant effect on dispersibility of clay suspensions.

## 4.6 References


1. Hansen NML, Plackett, D. Sustainable films and coatings from hemicelluloses: A Review. Biomacromolecules, 2008, 9, 1493-1505.
2. Sjostrom E. Wood chemistry: Fundamentals and applications (2nd ed.). Academic press: San Diego, CA, 1993, (Chapter 1).
3. Mueller-Harvey I, Hartley RD. Linkages of p-coumaroyl and feruloyl groups to cell wall polysaccharides of barley straw. Carbohydrate Research, 1986, 148, 71-85.

4. Adinugraha MP, Marseno DW, Haryadi M. Synthesis and characterization of sodium carboxymethylcellulose from Cavendish banana pseudo stem. Carbohydrate Polymers, 2005, 62, 164-169.
5. Heinze T, Liebert T, Heinze U, Schwikal K. Starch derivatives of high degree of functionalization; Carboxymethyl starches. Cellulose, 2004, 11, 239-245.
6. Schmorak J, Adams GA. The preparation and properties carboxymethylated xylan. Tappi Journal, 1957, 40, 378-383.
7. Petzold K, Schwikal K, Gunther W, Heinze T. Carboxymethyl xylan-control of properties by synthesis. Macromolecular Symposium, 2006, 232, 27-36.
8. Schwikal K, Heinze T, Ebringerova A, Petzold K. Cationic xylan derivarives with high degree of functionalization. Macromolecular Symposium, 2006, 232, 49-56.
9. Wang S, Hou Q, Kong F, Fatehi P. Production of cationic xylan-METAC copolymer as a flocculant for textile industry. Carbohydrate Polymers, 2015, 124, 229-236.
10. Ren JL, Xu F, Sun RC, Peng P, Sun JX. Studies of the lauroylation of wheat straw hemicelluloses under heating. Journal of Agriculture and Food Chemistry, 2008, 56, 1251-1258.
11. Ren JL, Sun RC, Liu CF, Cao ZN, Luo W. Acetylation of wheat straw hemicelluloses in ionic liquid using iodine as a catalyst. Carbohydrate Polymers, 2007, 70, 406-414.
12. Sun XF, Sun RC, Sun JX. Oleoylation of sugarcane bagasse hemicelluloses using N-bromosuccinimide as a catalyst. Journal of Science and Food and Agriculture, 2004, 84, 800-810.
13. Chen SY, Zou Y, Yan ZY, Shen W, Shi SK, Zhang X, Wang HP. Carboxymethylated-bacterial cellulose for copper and lead ion removal. Journal of Hazardous Materials, 2009, 161, 1355-1359.
14. Heinze T, Koschella A. Carboxymethylesters of cellulose and starch-A review. Macromolecular Symposium, 2005, 223, 13-40.
15. Methacanon P, Chaikumpollert O, Thavorniti P, Suchiva K. Hemicellulosic polymer from veitver grass and its physicochemical properties. Carbohydrate Polymers, 2003, 54, 335-342.
16. Hebeish A, Khalil MI, Hasheem A. Carboxymethylation of starch and oxidised starches. Starch, 1990, 42, 185-191.

17. Togrul H, Aralan N. Production of carboxymethyl cellulose from sugar beet pulp cellulose and rheological behaviour of carboxymethyl cellulose. Carbohydrate Polymers, 2003, 54, 73-82.
18. Saghir S, Iqbal MS, Hussain MA, Koschella A, Heinze T. Structure characterization and carboxymethylation of arabinoxylan isolated from Isphagula (*Plantago ovata*) seed husk. Carbohydrate Polymers, 2008, 74, 309-317.
19. Peng XW, Ren JL, Zhong LX, Cao XF, Sun, RC. Microwave-induced synthesis of carboxymethyl hemicelluloses and their rheological properties. Journal of Agriculture and Food Chemistry, 2011, 59, 570-576.
20. Ren JL, Sun RC, Peng F. Carboxymethylation of hemicelluloses isolated from sugarcane bagasse. Polymer Degradation and Stability, 2008, 93, 786-793.
21. Petzold-Welcke K, Schwikal K, Daus S, Heinze T. Xylan derivatives and their application potential – Mini review of our results. Carbohydrate Polymers, 2014, 100, 80-88.
22. Simkovic I, Kelnar I, Uhliarikova I, Mendichi R, Mandalika A, Elder T. Carboxymethylated-, hydroxypropylsulfonated- and quarternized xylan derivative films. Carbohydrate Polymers, 2014, 110, 464-471.
23. Ogaji IJ, Nep EI, Audu-Peter JD. Advances in natural polymers as pharmaceutical excipients. Pharmaceutica Analytica Acta, 2011, 3, 146-162.
24. Goksu EI, Karamanlioglu M, Bakir U, Yilmaz L, Yilmazer U. Production and characterization of films from cotton stalk xylan. Journal of Agricultural and Food Chemistry, 2007, 55, 10685-10691.
25. Alekhina M, Mikkonen KS, Alen R, Tenkanen M, Sixta H. Carboxymethylation of alkali extracted xylan for preparation of biobased packaging films. Carbohydrate Polymers, 2014, 100, 89-96.
26. Ren JL, Peng F, Sun RC, Kennedy JF. Influence of hemicellulosic derivatives on the sulfate kraft pulp strength. Carbohydrate Polymers, 2009, 75, 338-342.
27. Zhoumei L, Xhuexin Z, Zhiming X, Yuhui H. Structure-property relationship of polyelectrolytes and its application in stabilizing drilling–mud in presence of salts. Chinese Journal of Polymer Science, 1990, 8, 204-210.

28. Bimal PS, Menchavez R, Takai C, Fujy M, Takahaschi M. Stability of dispersion of colloidal alumina particles in aqueous suspensions. Journal of Colloid and Interface Science, 2005, 291, 181-186.
29. Konduri M, Fatehi P. Production of water soluble hardwood kraft lignin via sulfomethylation using formaldehyde and sodium sulfite. ACS Sustainable Chemistry and Engineering, 2015, 3, 1172-1182.
30. Kong F, Wang S, Price J, Konduri M, Fatehi P. Water soluble kraft lignin-acrylic acid copolymer: synthesis and characterization. Green Chemistry, 2015, 17, 4355-4367.
31. Peng XW, Ren JL, Zhong LX, Peng F, Sun RC. Xylan rich hemicelluloses- graft acyclic acid ionic hydrogels with rapid responses to pH, salt, and organic solvents. Journal of Agricultural and Food Chemistry, 2011, 59, 8208-8215.
32. Shen J, Singh R, Konduri M, Fatehi P. Cationic hemicellulose as a product of dissolving pulp based bioefinery. Industrial Engineering and Chemistry Research, 2015, 54, 1426-1432.
33. Sarwar Jahan M, Liu, Z, Wang H, Saeed A, Ni Y. Isolation and characterization of lignin from prehydrolysis liquor of kraft based dissolving pulp production. Cellulose Chemistry and Technology, 2012, 46, 261-267.
34. Lou H, Lai H, Wang M, Pang Y, Yang D, Qiu X, Wang B, Zhang H. Preparation of lignin-based superplasticizer by graft sulfonation and investigation of the dispersive performance and mechanism in a cementitious system. Industrial Engineering Chemistry Research, 2013, 52, 16101-16109.
35. Peng X, Ren J, Peng F, Sun R. Rapid carboxymethylation of xylan-rich hemicelluloses by microwave irradiation. Advanced Materials Research, 2011, 236-238, 292-296.
36. Zhang X, Liu W. Sodium titanium nanobelt as a microparticle to induce clay flocculation with CPAM. BioResources, 2010, 5, 1895-1907.
37. Xiao X, Liu Z, Wiseman N. Synergetic effect of cationic polymer microparticles and anionic polymer on fine clay flocculation. Journal of Colloid Interface Science, 1999, 216, 409-417.
38. Ovenden C, Xiao H. Flocculation behaviour and mechanisms of cationic inorganic microparticle/polymer systems. Colloids and Surfaces A: Physiochemical Engineering Aspects, 2002, 197, 225-234.

39. Bi YH, Liu MZ, Wu L, Cui DP. Synthesis of carboxymethyl potato starch and comparison of optimal reaction conditions from different sources. Polymers for Advanced Technologies, 2008, 19, 1185-1192.
40. Hebeish A, Khalil MI. Chemical factors affecting preparation of carboxymethyl starch. Starch, 1988, 40, 147-150.
41. Bhattacharya D, Singhal RS, Kulkarni PR. A comparative account of conditions for synthesis of carboxymethyl starch form corn and amaranth starch. Carbohydrate Polymers, 1995, 27, 247-253.
42. Qi H, Liebert T, Meister F, Heinze T. Homogenous carboxymethylation of cellulose in the NaOH/urea aqueous solution. Reactive and Functional Polymers, 2009, 69, 779-784.
43. Petzold K, Schwikal K, Heinze, T. Carboxymethyl xylan-synthesis and detailed structure characterization. Carbohydrate Polymers, 2006, 64, 292-298.
44. Bi Y, Liu M, Wu L, Cui D. Optimization of preparation conditions of carboxymethyl potato starch through orthogonal experimental design. Journal of Applied Polymer Science, 2009, 113, 24-39.
45. Kosikova B, Duris M, Demianova V. Conversion of lignin biopolymer into surface active derivatives. European Polymer Journal, 2000, 36, 1209-1212.
46. Zhang GL, Zhang L, Deng H, Sun P. Preparation and characterization of sodium carboxymethyl cellulose from cotton stalk using microwave heating. Chemical Technology and Biotechnology, 2011, 86, 584-589.
47. Sasmal S, Goud VV, Mohanty K. Optimization of the acid catalysed pretreatment of areca nut husk fibre using the Taguchi design method. Biosystems Engineering, 2011, 110, 465-472.
48. Mousavioun P, Doherty WOS. Chemical and thermal properties fractionated soda bagasse lignin. Industrial Crops and Products, 2010, 31, 52-58.
49. Ban L, Chai X, Guo, J, Ban W, Lucia LA. Chemical response of hardwood oligosaccharides as a statistical function of isolation protocol. Journal of Agricultural and Food Chemistry, 2008, 56, 2953-2959.
50. Ren H, Omori S. Comparison of hemicelluloses isolated from soda cooking black liquor with commercial and bacterial xylan. Cellulose Chemistry and Technology, 2014, 48, 675-681.

51. Liu X, Yu L, Liu H, Chen L, Li L. Insitu thermal decomposition of starch with constant moisture in a sealed system. Polymer Degradation and Stability, 2008, 93, 260-262.
52. Fang JM, Fowler P, Tomkinson J, Hill, CAS. Preparation and characterization of methylated hemicelluloses from wheat straw. Carbohydrate Polymers, 2002, 47, 285-293.
53. Singh BP, Menchavez R, Takai C, Fuji M, Takahashi M. Stability of dispersions of colloidal alumina particles in aqueous suspensions. Journal of colloid and Interface Science, 2005, 291, 181-186.
54. Kakui T, Kamiya H. Effect of sodium aromatic sulfonate group in anionic polymer dispersant on the viscosity of coal-water mixtures. Energy & Fuels, 2004, 18, 652-658.
55. Tyliszczak B, Sobczak-Kupiec A, Bialik-Was K, Kaspryzk W. Stabilization of ceramic particles with anionic polymeric dispersants. Journal of Nanoscience and Nanotechnology, 2012, 12, 9312-9318.
56. Yuan J, Garforth WL, Preutt RJ. Influence of dispersants on the solubility of calcined kaolin. Applied Clay Science, 1998, 13, 137-147.
57. Sparks DJ, Romero-Gonalez ME, El-Taboni E, Freeman CL, Hall SA, Kakonyi G, Swanson L, Banwart SA, Harding JH. Adsorption of poly acrylic acid onto the surface of calcite: an experimental and simulation study. Physical Chemistry Chemical Physics, 2015, 17, 27357-27365.
58. Sjostrom E. Cellulose*:* Structural and functional aspects (Kennedy, J.F, Philips, G.O & Williams, P. A, eds.), Ellis Horwood, Chichester, 1989; (p.239).
59. Hon, DNS. Chemical modification of lignocellulosic materials, New York, USA, Marcel Dekker Inc, 1996, (p.64).

# **Chapter 5.** Dispersion of kaolin particles with carboxymethylated xylan

Adapted from: Mohan K. R. Konduri, Pedram Fatehi*[a]

Applied Clay Science, 137, 2017, 183-191.

[a] Department of Chemical Engineering,
Lakehead University,
955 Oliver Road,
Thunder Bay, ON P7B 5E1, Canada

*Corresponding author

## 5.1 Abstract

In this work, the performance of carboxymethylated xylan (CMX) as a dispersant in kaolin dispersions (20 g/L) was systematically investigated. The influence of process parameters, such as dispersion pH and CMX dosage on the kaolin dispersions was also determined. Adsorption studies revealed that CMX had a maximum adsorption of 2.48 mg/g on kaolin particles under the treatment conditions of pH 6, 15 mg/g CMX/kaolin, 30°C and 30 min. The minimum zeta potential of -33 mV and the highest stability for the kaolin dispersions were found under the same treatment conditions using photometric dispersion, vertical scan analysis and turbidimetry. Isotherm and kinetic studies revealed that the adsorption of CMX on kaolin particles tended to significantly impact the zeta potential and relative turbidity of the kaolin dispersion, but the zeta potential did not necessarily predict the high stability of the kaolin dispersion. CMX improved the stability of the kaolin dispersions more than unmodified xylan (UX) and mechanical stirring.

**Keywords:** Dispersion, Carboxymethylated xylan, Kaolin, Zeta potential, Biorefining

## 5.2 Introduction

The stabilization of kaolin slurries is a crucial step in the production of cosmetics, ceramics, paints and coating formulas in order to obtain stable and homogenous colloidal systems [1, 2]. Dispersants have been widely used in the stabilization of kaolin dispersions [3]. The surface of kaolin particles is usually heterogeneous consisting of positive charges at the edges and negative charges on the basal face, and the interaction of these charges with surrounding environment promotes the aggregation of particles [4]. Dispersants prevent the aggregation of kaolin particles by inducing electrostatic/steric repulsion between them via adsorbing on their surface [5].

Numerous inorganic and synthetic dispersants are currently used in the stabilization of clay slurries. Sodium silicate [6, 7], sodium carbonate [8] and sodium pyrophosphate [9] have been used as dispersants for stabilizing clay and clay mineral dispersions in the mining and oil industries. In one study, the sodium salt of poly acrylic acid (1 wt.%) improved the fluidity of highly concentrated (12-15 wt.%) kaolin dispersions by 30% [10]. Poly acrylic acid, poly methacrylic acid and sodium silicate mixtures were used as dispersants for the stabilization of porcelain dispersions (40 vol%) [11]. Similarly, a water soluble non-ionic polyethylene oxide (4,000 g/mol) served as an effective dispersant for bentonite dispersions [12]. Although synthetic dispersants are effective, there are concerns about their non-biodegradable nature and health impacts, and as such, there is a strong incentive for producing green dispersants.

In the past, the utilization of polysaccharide based dispersants in colloidal dispersions was reported [13, 14]. The addition of 0.8 wt.% carboxymethylated cellulose to a kaolin dispersion increased its stability by 20% at pH 6 [15]. In another study on the stabilization of dolomite dispersions using carboxymethylated cellulose (CMC), an increase in the dosage of CMC from 8 to 100 mg/L increased the turbidity of the dolomite dispersion from 20 to 90% [16]. The addition of starch (0.8 wt.%) to red kaolin based ceramic dispersions (at pH 7) increased the fluidity of dispersions by decreasing the kaolin particle size from 2.8 to 1.5 μm [17]. On the stabilization of coal dispersions, the addition of a lignin based dispersant (1 wt.%) increased the turbidity of the dispersion by 68% [18]. However, starch is mainly used as a food product and cellulose is widely used in the paper production, thus they may have limited availability to be used for other purposes including dispersant production. On the other hand, xylan currently has limited industrial applications (e.g. xylitol, ethanol) but available in plentiful and can be produced in the hydrolysis stage of kraft based dissolving pulp production process [19]. To widen the application of xylan based products, in the previous study, carboxymethylated xylan was produced in aqueous conditions via modifying xylan with sodium chloroacetate [20]. In the present study, the first objective was to evaluate the dispersion performance of CMX in a kaolin dispersion under varied process conditions.

The stability of kaolin particles in dispersions is affected by many factors. The behaviour of kaolin particles is affected by the chemistry of the dispersions, the properties of particles in the dispersions and process conditions, such as shear rates [21, 22]. These factors significantly influence the repulsive and attractive inter-particle forces, which should be controlled in order to stabilize kaolin particles in dispersions [23]. The increase in repulsive/attraction force depends on the dielectric properties and compositions of kaolin particles and medium [24]. To overcome the attraction force and to have a well-stable dispersion, one approach is to introduce charges with sufficient magnitude on the surface of kaolin particles by adsorbing dispersants on them. Alternatively, the agglomeration of particles can be prevented by introducing shear rates [25, 26]. In this study, the impact of CMX as a dispersant will also be compared with that of shear rates for stabilizing kaolin particles in a dispersion.

The main novelty of this work was the investigation on the dispersion performance of CMX in kaolin dispersions by monitoring the adsorption of CMX on kaolin particles and its resultant

impacts on the properties of the dispersion. The impact of dispersant dosage, time and pH on the stability of kaolin particles was fundamentally studied. The effect of shear rates on the dispersion performance of CMX was also determined and compared with that of CMX treatment.

## 5.3 Experimental

### 5.3.1 Materials

Beechwood xylan, sodium chloride (97.0%), sodium hydroxide, sodium chloroacetate and kaolin were purchased from Sigma Aldrich Company and used as received. Potassium chloride and sulfuric acid (95-98%) were received from Fisher scientific, USA. All of the chemicals were analytical grades. Polydiallyldimethylammonium chloride (PDADMAC) was obtained from Sigma Aldrich Company and diluted to 0.005 M prior to use. Polyacrylic acid (PAA, 35 wt.%)) used in the study was obtained from sigma aldrich. Potassium polyvinyl sulfate (PVSK) was obtained from Wako Pure Chemical Industries Ltd., Japan. Cellulose acetate dialysis membrane (molar mass cut-off of 1,000 g/mol) was obtained from Spectrum Labs., USA. The TEGO trant A100 polymer was also received from Metrohm, Canada, and used as received.

### 5.3.2 Surface area analysis

The surface area of kaolin particles was determined by using Quantachrome surface area analyzer, Nova2200e. In this set of experiments, the samples were initially dried in an oven at 105°C overnight and approximately 0.05 g of sample was pretreated for 4 h at 250°C prior to analysis. The specific surface area of the samples was then analyzed according to Branuer-Emmett-Teller (BET) method via adsorption-desorption isotherms using nitrogen gas at -180°C in the relative pressure range of 0.01 to 0.99 [27].

### 5.3.3 Charge density analysis

The surface charge density of kaolin was determined via a back titration method with a particle charge detector (Mutek, PCD 04, Germany). In this set of experiments, 0.2 g of kaolin was dispersed in 50 mL of PDADMAC (0.005 M) solution and incubated for 2 h at 150 rpm and 30°C. After the incubation, the samples were filtered using Whatman#1 filter paper and the filtrates were titrated against PVSK (0.005 M) solution. In another experiment, 0.2 g of kaolin sample was dispersed in 50 ml of PVSK (0.0025 M) solution and incubated for 2 h at 150 rpm and 30 °C. After the incubation, the samples were filtered as described above and filtrates were titrated with 0.005 M PDADMAC solution. Similarly, the titration analysis was conducted for

control sample (i.e. PDADMAC and PVSK solutions) and the difference was employed to quantify the anionic and cationic surface charge density of kaolin particles.

The charge density of UX and CMX was determined using the same particle charge detector via titrating with PDADMAC (0.005 M). In this set of experiments, the UX and CMX were initially dried in an oven at 105°C overnight and 0.2 g of each of the samples was mixed with 20 mL of deionized water and incubated for 2 h at 30°C and 150 rpm. After incubation, the samples were titrated with PDADMAC to determine the surface charge density.

### 5.3.4 Chemical and mineralogical analysis of kaolin

The chemical composition of kaolin was determined using scanning electron microscopy (SEM), Hitachi Su-70, Schotty in tandem with energy dispersive X ray spectroscopy (EDX) [28]. In this experiment approximately 0.2 g of kaolin was dispersed in 20 ml of acetone under ultrasonic vibrations for 5 min and allowed to air dried for 24 h. After drying, the sample was coated with carbon using Edward Auto 306 system (Edward International Corp, UK) under vaccum ($3*10^{-5}$ mbar) for 10 minutes, and later subjected to SEM.

The mineralogical analysis of kaolin was carried out using spinning stage PANalytical X'pert-PRO diffractometer (XRD), PW1050-3710 with a Cu Kα (λ =1.5405 Å) radiation source [28]. A 0.5 g of kaolin sample was air dried and loaded on the spinner stage of XRD. The sample was then scanned from 6 to 43° with a step of 0.02° per second for 2 minutes. The X'pert High Score software linked with a reference database was used to determine the mineral composition of kaolin [29]. Due to limitations of the instrument, the kaolin sample was scanned up to 43°.

### 5.3.5 Carboxymethylation of xylan (CMX) preparation and analysis

The CMX was synthesized according to the method described in the previous study under the conditions of 0.75 M NaOH concentration, 1.0 mol/mol sodium chloroacetate (SCA)/xylan ratio, 2 h reaction time, 70°C and 15 g/L xylan concentration to obtain the CMX with the charge density of 1.6 mmol/g [20]. The properties of UX and CMX were reported in Table 5.1.

Table 5-1. Properties of UX, CMX and PAA [20]

| Sample | UX | CMX | PAA |
|---|---|---|---|
| Charge density, mmol/g | 0.38 (± 0.05) | 1.62 (±0.02) | 13.5 (±0.3) |
| Carboxylate group content, mmol/g | 0.36 (±0.05) | 1.48 (±0.02) | - |
| $M_w$, g/mol | 20,800 | 24,100 | 100,100 |
| $M_n$, g/mol | 15,800 | 19,200 | 30,200 |
| $M_w/M_n$, g/ml | 1.31 | 1.25 | 3.3 |

The carboxylate content of UX/CMX was measured using an automatic potentiometer, Metrohm, 905 Titrado, Switzerland. In this set of experiments, 1 g of UX/CMX sample was added to 100 mL of deionized water and the pH of the solution was adjusted to 10.5. The solution was then titrated with a cationic polymer, TEGO trant A100, in order to identify the carboxylate content of UX or CMX [20].

The weight average molar mass ($M_w$), number average molar mass ($M_n$) and polydispersity ($M_w/M_n$) of UX/CMX samples were determined using a Malvern GPCmax VE2001 Module + Viscotek TDA305 (RI and viscometer detectors) with polyethylene oxide standards. About 100 mg of UX or CMX was dissolved in 10 mL of 0.1 mol/L $NaNO_3$ solutions and filtered with a nylon 0.2 μm filter (13 mm diameter). The filtered solutions were subjected to molar mass analysis by passing though PolyAnalytic columns, PAA206 and PAA203, with column temperature of 35°C. A 0.1 mol/L $NaNO_3$ solution was used as a solvent and eluent at a flow rate of 0.70 mL/min in this analysis.

### 5.3.6 Adsorption studies

In this set of experiments, the adsorption of CMX/UX on kaolin particles at varying pH (2, 6 and 10) and dosages (2.5 – 25 mg/g) was studied. UX or CMX of varying dosages (2.5 to 25 mg/g of kaolin) was added to the kaolin dispersions (20 g/L) at pH 2, 6, 10 and stirred at 250 rpm and 30°C for 30 min. The pH of the dispersions was adjusted using 0.1 M NaOH or 0.1 M $H_2SO_4$. After mixing UX or CMX with the kaolin dispersion, the mixture was filtered using Whatmann#1 filter paper and the concentration of UX or CMX in the filtrates before and after mixing with dispersions was determined [30]. In another set of experiments, UX or CMX were

mixed with the kaolin dispersions at the dosage of 5 mg/g and pH 6, but at different time intervals between 0 and 30 min, and UX or CMX was separated from the dispersion using the Whatmann filter papers. To determine the concentration of UX or CMX in the solutions, all of the filtrates were hydrolysed with 4 wt.% $H_2SO_4$ in a 600 mL pressurized reactor (Parr Instruments, 4838) for 1 h at 121°C. The concentration of UX or CMX present in the filtrates was measured based on the concentration of their monomeric sugars in the filtrates after the acid hydrolysis with an ion chromatography, ICS 5000+, Thermo Scientific, equipped with an electrochemical detector. 1 mM KOH solution was used as a mobile phase and all the filtered samples were allowed to pass through a Dionex Carbopac$^{TM}$ SA 10 column at a flow rate of 1.2 mL/min. The temperature of the column was maintained at 30°C. All of the experiments were performed in triplicates and the average values were reported in the study.

### 5.3.7 Zeta potential analysis

The zeta potential analysis of the kaolin particles was performed using a NanoBrook Zeta PALS (Brookhaven Instruments Corp, USA). In this study, UX/CMX with varying dosages (2.5 – 25 mg/g) were added to 50 mL of the kaolin dispersion (20 g/L) at pH 2, 6 and 10 and stirred at 250 rpm and 30°C for 30 min. After mixing, 1 mL of the sample was added to 20 mL of KCl solution (1 mM) prior to the zeta potential analysis. In another set of experiments, UX or CMX (5 mg/g of kaolin) was mixed with the kaolin dispersions (20 g/L) at 300 rpm and pH 6. The samples were withdrawn at desired time intervals between 2 and 30 min and subjected to zeta potential analysis as described above. 0.1 M of $H_2SO_4$ or 0.1 M of NaOH was used to adjust the pH of kaolin dispersions. The experiments were carried out three times and the mean values were reported in this study.

### 5.3.8 Dispersion analysis under dynamic conditions

The dispersion experiments were conducted using a photometric dispersion analyzer (PDA 3000, Rank Brothers Ltd), which was connected to a dynamic drainage jar (DDJ) fitted with a 70 mm mesh screen [31]. The dispersion of the kaolin particles in the suspension was measured from the variation in the direct current (DC) voltage of the PDA instrument [32]. In this present study, 450 mL of distilled water was poured into the DDJ container and circulated from the DDJ to the PDA through a 3 mm plastic tube until a steady flow rate of 20 mL/min was achieved. The flow rate was regulated by peristaltic pump throughout the experiment. Then, 50 mL of a 200 g/L kaolin dispersion was added into DDJ (to make a 20 g/L kaolin concentration) at varying rpms

(between 50 and 1000 rpm). This caused a decrease in the initial base DC voltage ($V_0$) to a new DC voltage ($V_i$). After 200 s, UX/CMX of varying dosages (1 to 25 mg/g of kaolin) was added to the dispersion mixture in the DDJ. The increase in DC voltage was represented as the DC voltage ($V_f$) of the final dispersion. All of the tests were carried out at three different pH (2, 6 and 10) of kaolin dispersions, which was controlled by adding 0.1 M NaOH or 0.1 M $H_2SO_4$. In another set of experiments, UX or CMX (5 mg/g) were added into DDJ containing 500 mL of the kaolin dispersions (20 g/L) at 300 rpm and pH 6. The increase in DC voltage ($V_i$ to $V_f$) was recorded at different desired time intervals (between 2 and 30 min). The relative turbidity of the kaolin dispersion was measured using equation 5.1[33]:

$$\text{Relative turbidity} = \frac{\tau f}{\tau i} = \frac{ln(\frac{V0}{Vf})}{ln(\frac{V0}{Vi})} \quad (5.1)$$

where $\tau_f$ is denoted as the final dispersion turbidity, and $\tau_i$ is denoted as the initial dispersion turbidity.

### 5.3.9 Dispersion analysis under static conditions

The turbidity of the kaolin particles in the dispersion under static conditions was also determined in the presence of UX or CMX with a turbidity meter, Hatch, 2100 AN. In one set of experiments, 100 mL of kaolin dispersions (20 g/L) with or without UX/CMX (5 mg/g of kaolin) was prepared by stirring at 250 rpm. Then, 35 mL of the mixture was withdrawn at desired time intervals (between 0 and 30 min) and subjected to turbidity measurements. In another set of experiments, altered dosages (1-25 mg/g) of CMX was added to 100 mL of kaolin dispersions (20 g/L) at different pH (2, 6 and 10) and mixed at 250 rpm for 30 min. After mixing, 35 mL of the mixture was collected as described above and subjected to turbidity analysis. The turbidity of deionised water at varying pH and time intervals before addition of kaolin was also measured. The relative turbidity of the kaolin dispersions was determined by following equation 5.2 [34].

$$\text{Relative turbidity} = \frac{ln(\frac{T0}{Tf})}{ln(\frac{T0}{Ti})} \quad (5.2)$$

where, $T_0$ is turbidity of deionised water, $T_i$ is the turbidity of kaolin dispersion and $T_f$ is the turbidity of the kaolin dispersion after addition of CMX.

### 5.3.10 Stability analysis

The stability of the kaolin dispersion in the presence and absence of UX/CMX was investigated using a vertical scan analyzer, Turbiscan Lab Expert, Formulaction, France. This analysis was conducted in the past to study the stability of emulsions and concentrated colloidal dispersions [35]. In this analysis, light beams pass through a dispersion. The light passes through a transmission zone of the samples, while it cannot pass through the sediment zone of the samples [36]. Two synchronous optical sensors receive light transmitted through the sample (180° from the incident light, transmission sensor) and light backscattered by the sample (45° from the incident radiation, backscattering detector). The higher transmission zone implies less stable kaolin dispersions due to the sedimentation of kaolin particles. In one set of experiments, UX/CMX (5 mg/g of kaolin) was added to the kaolin dispersions (20 g/L) at pH 6 and 20 mL of the mixture was transferred to cylindrical tubes of the instrument and then analyzed by the instrument at desired time intervals (between 2 and 30 min). In another set of experiments, kaolin dispersions (20 g/L) CMX mixtures (dosage between 1 and 25 mg/g) at varying pH of 2, 6 and 10 were prepared. After 30 min of mixing at 200 rpm, 20 mL of the dispersions was transferred to a cylindrical tube and analyzed by instrument. The dispersions were vertically scanned at 880 nm wavelength every 2 sec by the instrument at 30ºC. The transmission zone percentage data was calculated by turbisoft 2.1 software by comparing the transmittance signals generated by the sample with those generated by a silicon oil that is used as a calibration chemical for the instrument [37]. These transmittance signals were recorded as a percentage of transmittance signals with respect to that of the silicon oil.

The size of kaolin particles in the dispersed state (i.e. not settled) and their volume fractions can be obtained based on the backscattering data collected. Based on the Mie theory [38], the back scattering data measured by the instrument can be expressed as a function of photo transport mean free path, I* in equation 5.3.

$$BS = \frac{1}{\sqrt{I^*}} \qquad (5.3)$$

In addition, the photo transport mean free path, I*, could be obtained via following equation 5.4

$$I^*(d, \theta) = \frac{2d}{3\theta\,(1-g)Q_s} \qquad (5.4)$$

where, d is the particle mean diameter, θ is the particle volume fraction, g and Qs are the scattering efficiency factors, which depend on the particle diameter (d), wave length of light (λ), refractive index of dispersed kaolin particles ($n_p$) and the refractive index of continuous phase ($n_f$). In this work, the refractive indices of kaolin particles and water were considered to be 1.54 and 1.33 [33].

According to Eqs. 2 and 3, back scattering data is directly dependent on the particle mean diameter, d, and their volume fraction, θ [39]. By providing refractive indices of kaolin and water, the turbisoft 2.1 software would generate a correlation between the size of kaolin particles and their volume fraction in the dispersion from the backscattering data. The size and volume fraction analysis was conducted for all the samples analyzed in this work.

## 5.4 Results & Discussion

### 5.4.1 Characterization of kaolin

The average particle size and surface area of kaolin particles were 7.5 μm and 38.43 $m^2/g$, respectively. The anionic and cationic surface charge density of kaolin particles are found to be -6.3 μmol/g and 2.0 μmol/g respectively, which is probably due to the presence of oxide anions and associated polyvalent metal ions, such as $Si^{4+}$ and $Al^{3+}$ on their surface [40].

The chemical and mineralogical composition of kaolin was shown in Table 5.2. Silica (22.94 wt.%) and alumina (20.91 wt.%), and their corresponding oxides (54.12 and 42.25 wt,%) were found to be the major elements of kaolin. While the other elements that constitute kaolin, Ti, Fe, Mn, P, Na and Cu, are in very limited proportions. The presence of high content of alumina and silica is also confirmed by mineralogical data. Aluminosilicate rich minerals such as, Kaolinite (34 wt.%), Dickite (29 wt.% and Narcite (29 wt.%) were found to be present in large amounts (Table 4.2). Tridymite (a silicate quartz), hematite and magnetite are the other minerals observed in kaolin in limited amounts (4, 2 and 2 wt.% respectively) [28].

Table 5-2. Chemical and mineral composition of kaolin

| Chemical composition | | | | Mineral composition | |
|---|---|---|---|---|---|
| Element | Wt.% | Calculated oxides | Wt.% | Mineral | wt.% |
| O | 49.88 | | | kaolinite | 34 |
| Al | 21.54 | $Al_2O_3$ | 40.71 | Dickite | 29 |
| Si | 25.94 | $SiO_2$ | 55.49 | Narcite | 28 |
| Ti | 0.65 | $TiO_2$ | 1.09 | Tridymite | 4 |
| Fe | 0.51 | $FeO_2$ | 0.66 | Hematite | 2 |
| Cu | 0.60 | CuO | 0.75 | Magnetite | 2 |
| Mn | 0.33 | MnO | 0.61 | | |
| P | 0.18 | $P_2O_5$ | 0.42 | | |
| Na | 0.21 | $Na_2O_8$ | 0.28 | | |

### 5.4.2 Properties of UX/CMX

The charge density of xylan was increased from 0.38 to 1.62 mmol/g after carboxymethylation. UX and CMX had carboxylate group contents of 0.32 mmol/g and 1.48 mmol/g, respectively. Furthermore, the $M_w$ (24,127 g/mol) and $M_n$ (19,254 g/mol) of CMX was found to be larger than those of UX ($M_w$ of 20,840 g/mol and $M_n$ of 15,852 g/mol, respectively). The higher molecular weight of CMX was due to the attachment of carboxyl groups in carboxymethylation. The polydispersity of xylan was reduced after carboxymethylation, which was due to alkaline degradation of xylan in carboxymethylation [20].

### 5.4.3 Adsorption analysis

Figure 5.1 represents the adsorption of CMX on the kaolin particles as a function of CMX dosage at pH 2, 6 and 10. The CMX had no significant adsorption under acidic conditions (pH 2). At pH 6, the maximum adsorption of 2.4 mg/g was obtained on the kaolin particles at the dosage of 10 mg/g. The higher adsorption of CMX at pH 6 than pH 2 was due to the ionization of carboxylate groups at pH 6 (pKa 4.7), which causes the CMX to adsorb on kaolin particles on positive sites via electrostatic interaction [41]. Under basic conditions, the maximum adsorption of 1.52 mg/g was obtained at a 10 mg/g CMX dosage. At pH 10, the particles possess negative charges, and thus their adsorption efficiency was lower than that at pH 6 for CMX [42]. The

studies on the stabilization of kaolinite particles using polyacrylic acid exhibited that the adsorption of polyacrylic acid on kaolinite was decreased from 125 to 90 µmol/g with an increase in the pH from 7 to 9 [43]. The adsorption of UX on kaolin was found to be negligible irrespective to pH and dosage. This is because, UX has neglizable charge as shown in Table 1 [27].

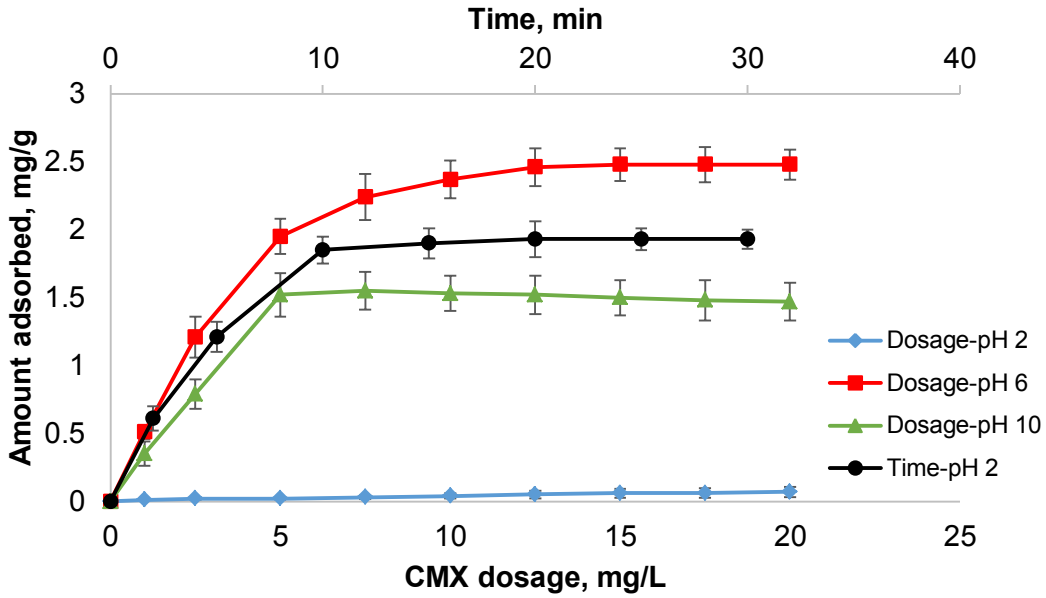


Figure 5.1. Adsorption of CMX on kaolin particles as a function of CMX dosage at pH 2, 6 and 10 under the conditions of 20 g/L kaolin, 30°C and 30 min and the adsorption of CMX on kaolin particles as a function of time at pH 6, 20 g/L kaolin, 5 mg/g CMX dosage and 30°C.

### 5.4.4 Zeta potential analysis

Figure 5.2 presents the impact of CMX dosage on the zeta potential of kaolin particles at pH 2, 6 and 10. The zeta potential of kaolin particles was close to zero at pH 2 and found to remain unchanged in the presence of CMX or UX. The insignificant change in the zeta potential of particles at pH 2 is due to the weak adsorption of CMX on their surface (as represented in Figure 1). An increase in the dosage of CMX from 1 to 20 mg/g reduced the zeta potential of particles from -20 to –33 mV at pH 6. In the dispersion studies of kaolinite particles using sodium silicate dispersant, an increase in the dosage of dispersant from 0.1 to 0.8 wt.% led to a drop in the zeta potential of the dispersion from -20 to -41.2 mV at pH 7 [6]. In another study on the stabilization of ceramic dispersions using carboxymethylated lignin, an increase in the dosage of the polymer

from 0.1 to 0.6 mg/L reduced the zeta potential of the dispersion from -20 to -30 mV at pH 6 [44]. The kaolin dispersion exhibited the minimum zeta potential of -40 mV at a 5 mg/g CMX dosage. Under alkaline pH, the zeta potential of the dispersion was more negative due to the presence of more hydroxyl ions in the dispersion. However, the decrease in the zeta potential of the kaolin dispersion was more significant at pH 6 than at pH 10, which is attributed to the adsorption of more CMX on the kaolin particles at pH 6. No significant change in the zeta potential of kaolin dispersion was noted with UX at any pH studied.

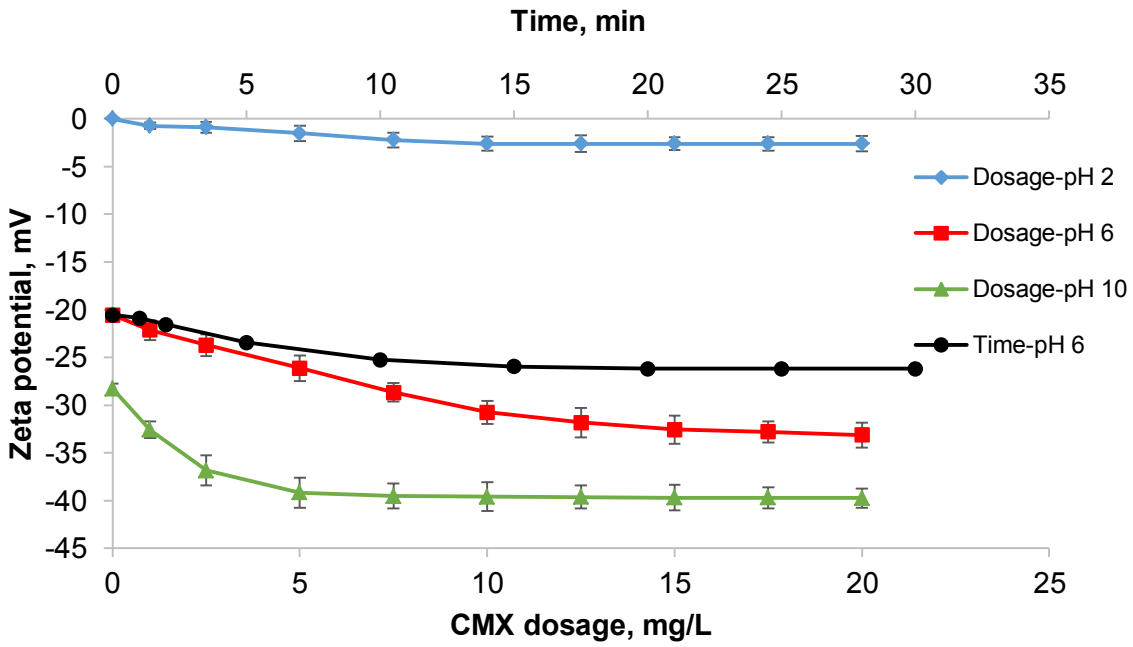


Figure 5.2. Effect of CMX dosage on the zeta potential of the kaolin dispersion at pH 2, 6 and 10 under the conditions of 20 g/L kaolin, 30 min and 30°C and the impact of time on the zeta potential of the kaolin dispersion under the conditions of 20 g/L kaolin, pH 6, 5 mg/g CMX dosage and 30°C.

To understand if the zeta potential of kaolin particles is affected by the adsorbed amounts of CMX or diffused CMX layers surrounding the particles in the dispersion, the adsorbed amounts of CMX was plotted against the zeta potential of particles at pH 2, 6 and 10 [27]. Figure 5.3 represents the change in the zeta potential of kaolin particles as a function of adsorbed amount of CMX at varying pH. The zeta potential of kaolin particles was negligible at pH 2 implying that the zeta potential of dispersion remained unchanged when the adsorption of CMX was limited. At pH 6 or 10, the zeta potential of the kaolin dispersion was decreased to -33 or -40 mV with

the increase in adsorbed amounts of CMX to 2.48 and 1.53 mg/g, respectively. This reveals that the adsorbed amounts indeed influenced the zeta potential of the kaolin particles. The last points on each curve (point S in Figure 5.3) represents the zeta potential of kaolin particles at the maximum adsorption amount (i.e. saturation adsorption in Figure 5.1). For these points, the adsorption amount on particles was close, but the amounts of unadsorbed CMX remained in the kaolin dispersions were different (Figure 5.1). These results confirm that the amount of unadsorbed CMX in the kaolin dispersions did not play a major role on the zeta potential of the kaolin particles.

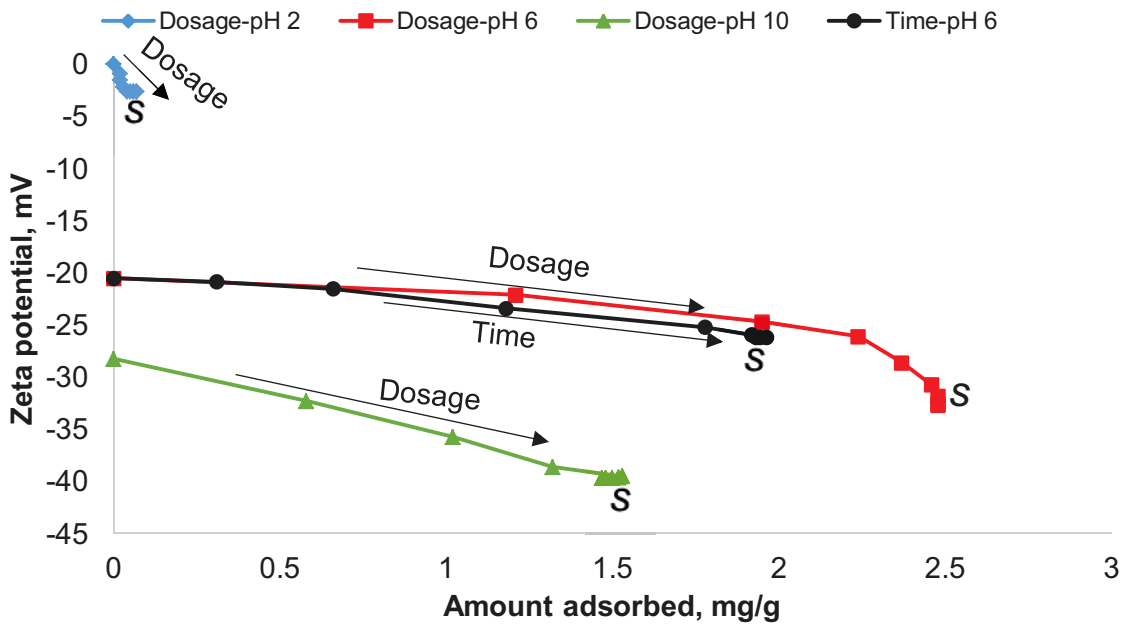


Figure 5.3. Effect of adsorbed amount of CMX on the zeta potential of kaolin particles at pH 2, 6 and 10 under the conditions of 20 g/L kaolin dispersion, 30 min and 30°C and the effect of adsorbed amount of CMX on the zeta potential at different time intervals under conditions of pH 6, 5 mg/g CMX dosage and 20 g/L kaolin.

### 5.4.5 Stability analysis

#### 5.4.5.1 Impacts of dosage and pH on the relative turbidity under dynamic conditions

The effect of CMX dosage on the relative turbidity of kaolin dispersions at pH 2, 6 and 10 is shown in Figure 5.4. The CMX was ineffective in improving the stability of kaolin dispersions at pH 2. This is because most of the carboxylate groups of CMX are protonated at this pH (pKa 4.7), which results in negligible adsorption of CMX on the kaolin surface (Figure 5.1) and thus

an insignificant change in the relative turbidity. At pH 6, the relative turbidity of the kaolin dispersion was increased to 1.25 as CMX increased from 1 to 15 mg/g of kaolin. The increase in the relative turbidity of the kaolin dispersions is due to the adsorption of CMX on the kaolin surface (Figure 5.1), which in turn increased the electrostatic repulsion between the kaolin particles. At saturation adsorption level, the relative turbidity did not change [8, 26]. At pH 10, the relative turbidity was increased from 1.08 to 1.27 as CMX dosage increased from 1 to 10 mg/g of kaolin. In the past, the stability of polyacrylic acid and poly (acrylic acid-*co*-maleic acid) titanate dispersion (0.2 wt.%) was increased to 50% with the pH increased from pH 4 to 10 [45].

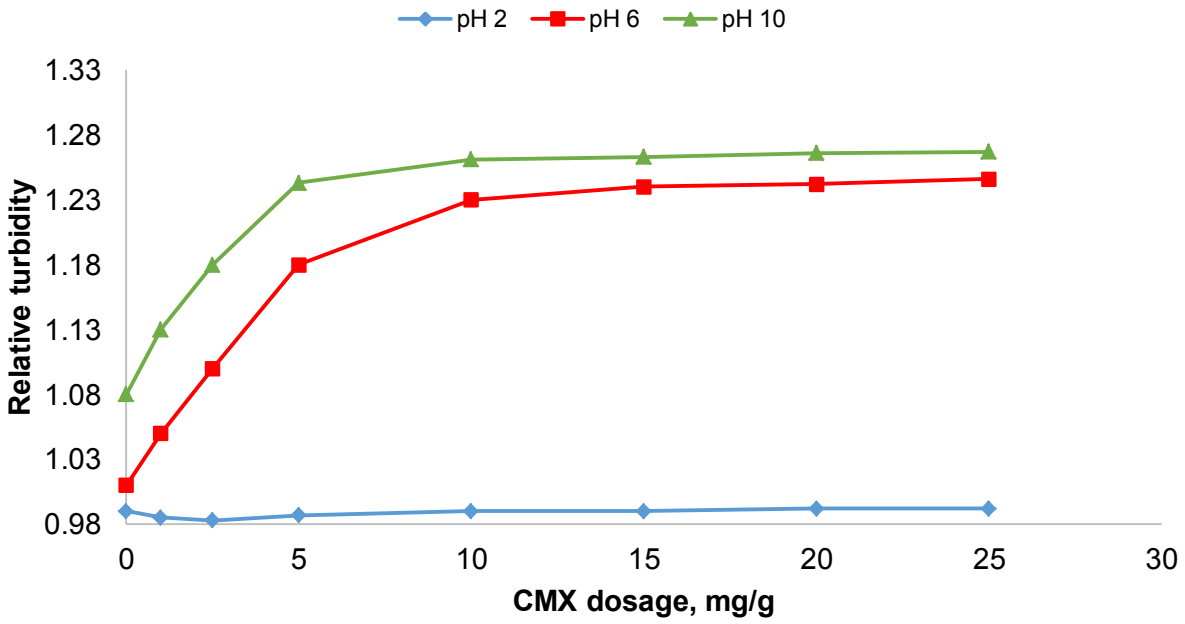


Figure 5.4. Effect of CMX dosage on the relative turbidity of kaolin dispersions at pH 2, 6 and 10 under the conditions of 20 g/L kaolin at 25°C and 30 min.

To understand if the zeta potential of kaolin particles is affected by the adsorbed amounts of CMX or diffused CMX layers surrounding the particles in the dispersion, the adsorbed amounts of CMX was plotted against the zeta potential of particles at pH 2, 6 and 10 [27]. Figure 5.5 depicts the change in the zeta potential of kaolin particles as a function of adsorbed amount of CMX at varying pH. The zeta potential of kaolin particles was negligible at pH 2 implying that the zeta potential of dispersion remained unchanged when the adsorption of CMX was limited. At pH 6 or 10, the zeta potential of the kaolin dispersion was decreased to -33 or -40 mV with

the increase in adsorbed amounts of CMX to 2.48 and 1.53 mg/g, respectively. This reveals that the adsorbed amounts indeed influenced the zeta potential of the kaolin particles. The last point on each curve (point S in Figure 5.3) represents the zeta potential of kaolin particles at the maximum adsorption amount (i.e. saturation adsorption in Figure 5.1). For these points, the adsorption amount on particles was close, but the amounts of unadsorbed CMX remained in the kaolin dispersions were different (Figure 5.1). These results confirm that the amount of unadsorbed CMX in the kaolin dispersion did not play a major role on the zeta potential of the kaolin particles.

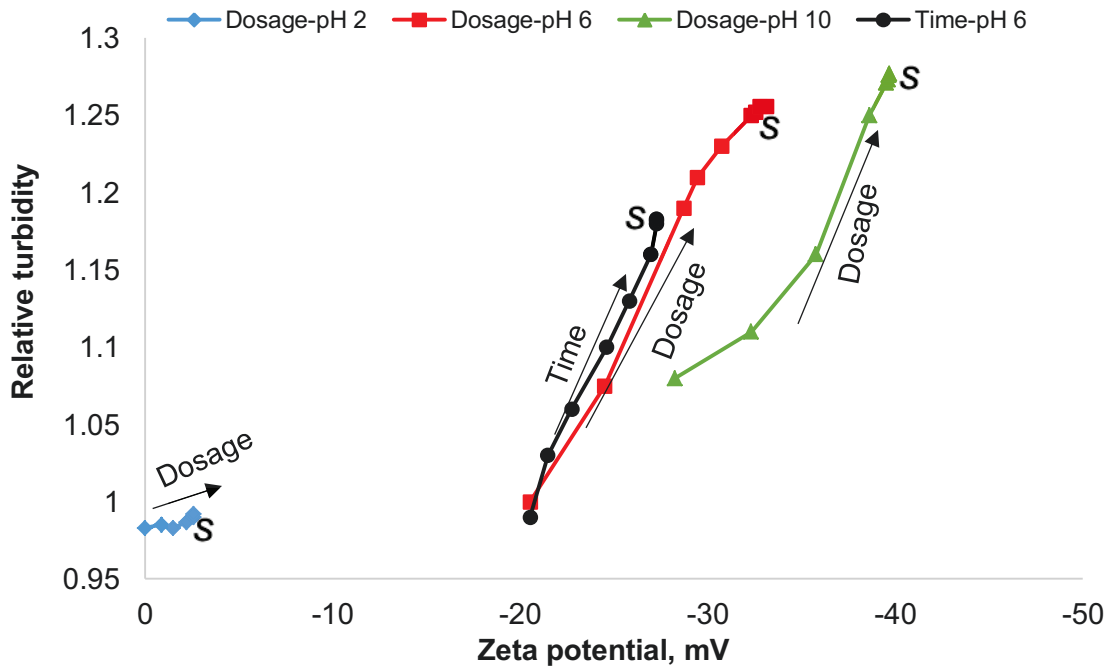


Figure 5.5. Effect of zeta potential of kaolin particles on the relative turbidity of kaolin dispersions at pH 2, 6 and 10 under the conditions of 0.5 h, 25°C, 30 min and 20 g/L of kaolin concentration.

### 5.4.5.2 Effect of dosage and pH on the stability under static conditions

The influence of CMX dosage on the relative turbidity and transmission zone of kaolin dispersions at pH 2, 6 and 10 is shown in Figure 5.6. In the absence of CMX, the transmission zone of kaolin particles was low (0.3%), and the relative turbidity of kaolin dispersions (i.e. control samples) was higher at pH 10 than other pH (results not shown in this figure), which is due to stronger electrostatic repulsion force between the kaolin particles at a high pH of 10 (as seen as a high negative zeta potential in Figure 5.2). The addition of 25 mg/g of CMX to the

kaolin dispersions at pH 2 had no significant effect on the transmission zone and relative turbidity of the dispersions implying that it was poorly stabilized. This behaviour is due to the aggregation of kaolin particles as the dispersions were overall neutral at acidic pH (Figure 5.2) and to the insignificant adsorption of CMX on kaolin particles at pH 2 (Figure 5.1). At pH 6, the addition of CMX to the kaolin dispersions increased the stability of particles, which is evident from a decrease in the transmission zone (from 71% to 2.2%) and an increase in the relative turbidity (from 2.2 to 4.8). This increase in the stability was due to the adsorption of CMX on kaolin particles [46]. At pH 10, the transmission zone of the kaolin dispersion was decreased from 20 to 0.3%, while the relative turbidity was increased from 4.4 to 5.0 with the increase in the CMX dosage. In the past, the stability of kaolin dispersions (30 wt.%) was achieved at a high pH of 10 in the presence of wheat straw alkali lignin as a dispersant [47].

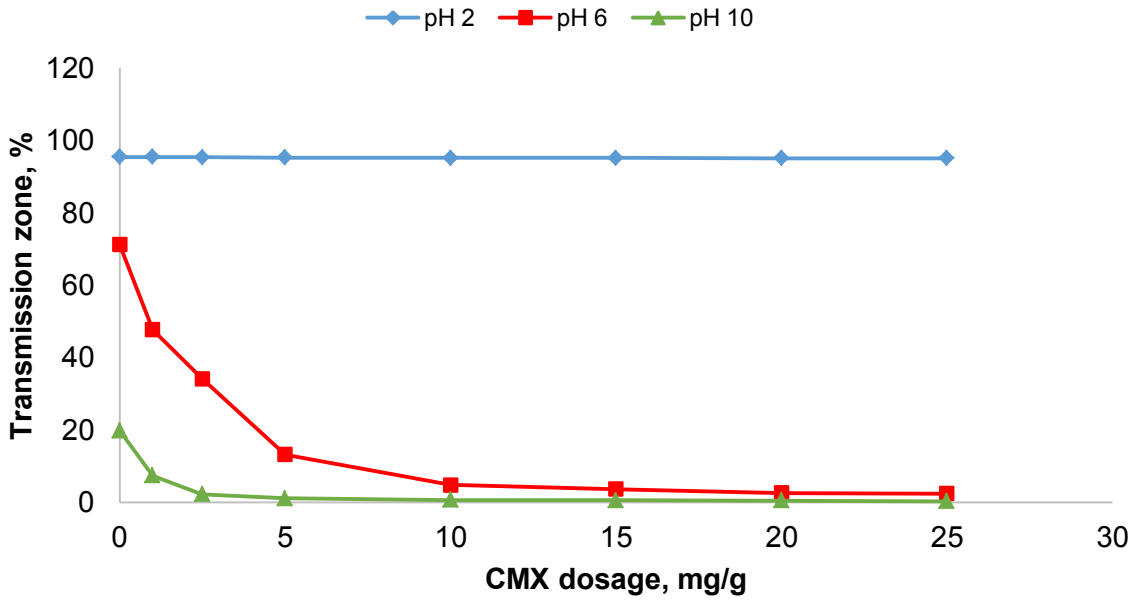

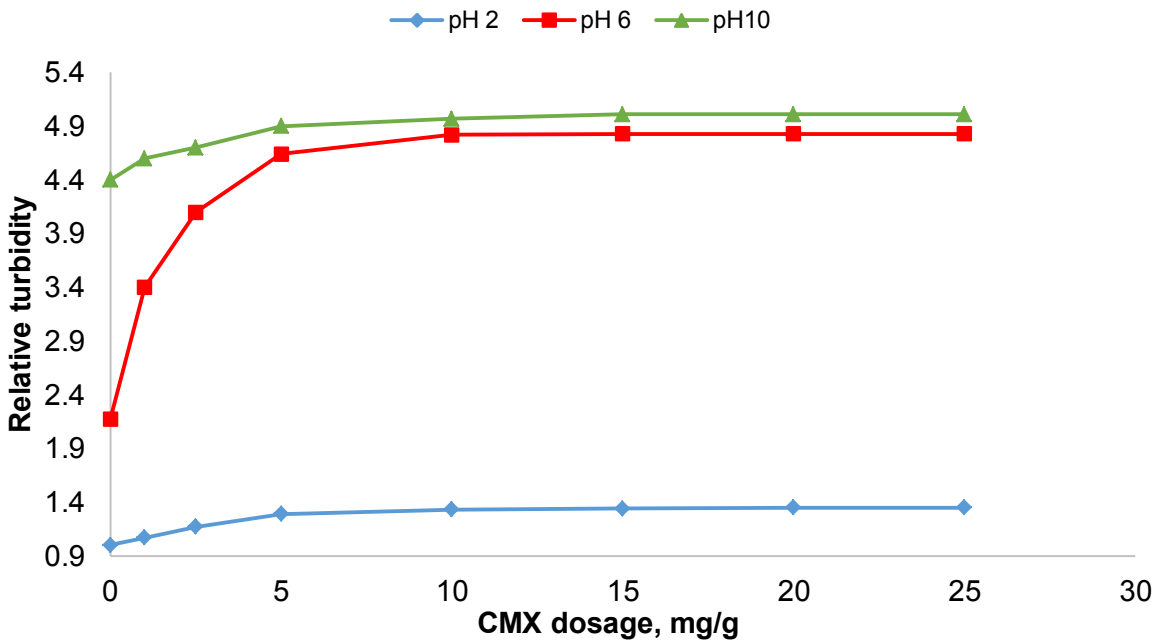


Figure 5.6. The effect of CMX dosage on transmission zone and the relative turbidity of kaolin dispersions at pH 2, 6 and 10 under the conditions of 20 g/L kaolin at 25°C and 30 min.

Figure 5.7 presents the size of the kaolin particles and their volume fraction present in the dispersions at varying pH (2, 6 and 10) as a function of CMX dosage under static conditions. Regardless of the CMX use, the kaolin particles with the size range between 0.2 and 15 µm tended to precipitate (i.e., negligible volume fraction in the dispersion) at pH 2 (Figure 5.7a). This is due to an insignificant adsorption of CMX on kaolin particles (Figure 5.1). In the absence of CMX (control), the kaolin particles settled with negligible volume fraction in the dispersed state at pH 6. With the increase in the CMX dosage to 20 mg/g, the volume fraction of particles (0.2 to 8 µm size range) increased in the dispersion at pH 6 (Figure 5.7b). This increase in the volume fraction of particles in the dispersions can be attributed to the electrostatic repulsion developed between them. Due to existing electrostatic repulsion forces between the kaolin particles under alkali conditions (pH 10), the particles tended to stay in the dispersed state even in the absence of CMX. The addition of CMX further increased the volume fraction of dispersed particles due to adsorption of CMX. The UX had no substantial effect on stability of the kaolin particles. These results also confirm that the CMX acted as an effective dispersant under static conditions.

Interestingly, the results also exhibited that by increasing the dosage of CMX, the fraction of large particles increased; particles with the size of 8 µm had the highest volume fraction in the kaolin dispersions; and larger particles than these settled from the dispersions. The results confirmed that the largest particles that could remain dispersed in the dispersions was those with the size of 8 µm, and large ones settled, regardless of the dosage of CMX and pH of dispersions.

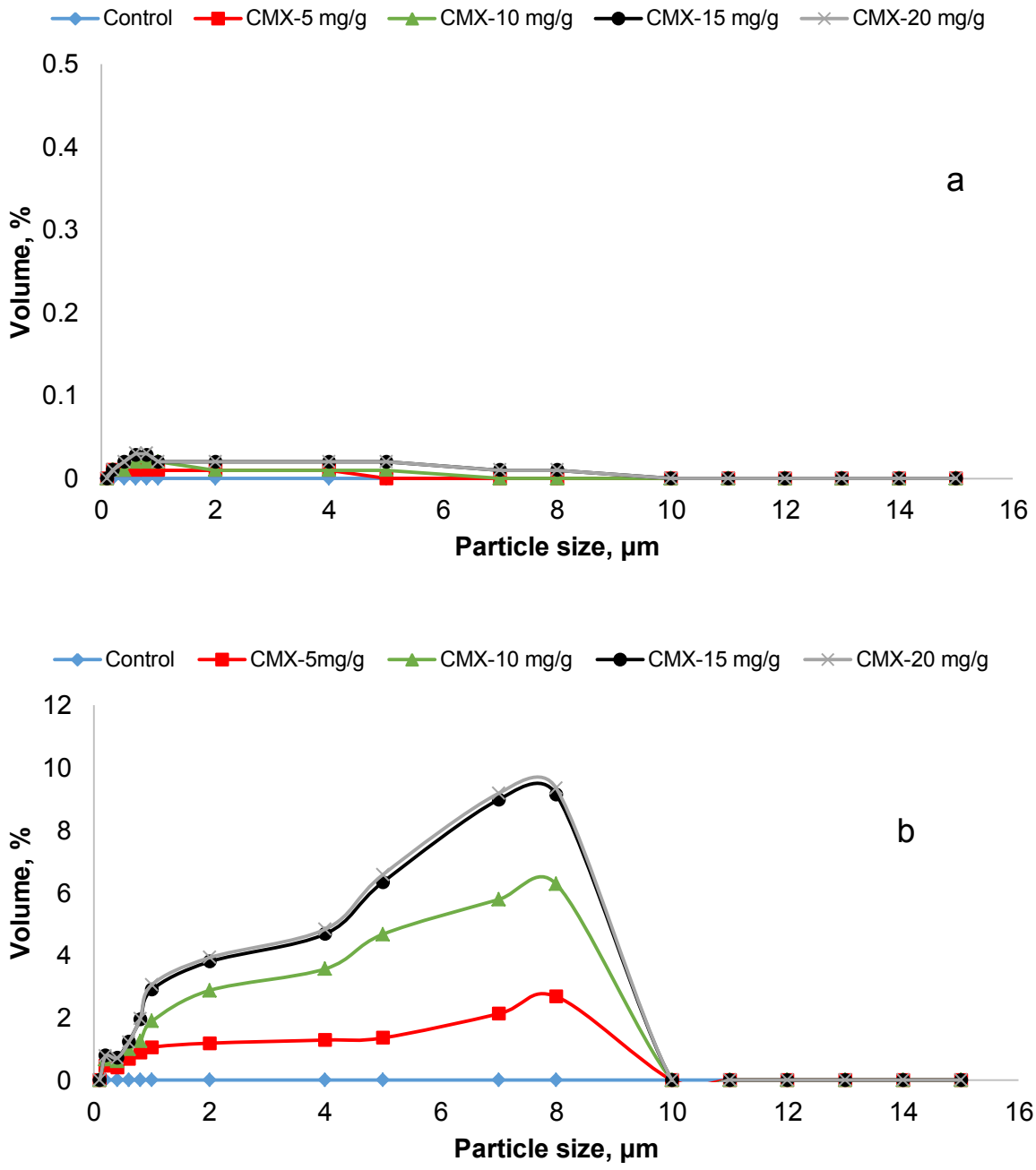

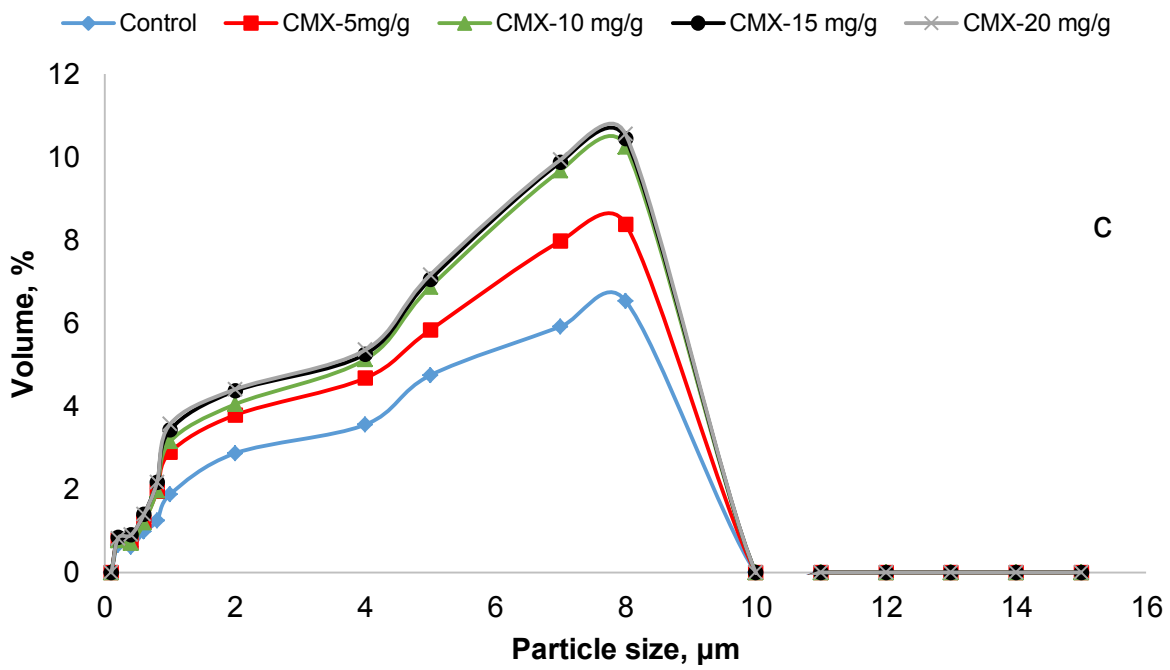


Figure 5.7. Size of kaolin particles in the presence or absence of UX/CMX at a) pH 2, b) pH 6 and c) pH 10 under the conditions of 20 g/L kaolin at 25°C and 30 min.

### 5.4.6 Kinetic studies

To further understand the importance of adsorption on the zeta potential and relative turbidity of the kaolin dispersions, the kinetics of adsorption, zeta potential, relative turbidity and transmission zone for the system of CMX and kaolin dispersions was studied. Included in Figure 5.1 were also the results for the adsorption of CMX on kaolin particles as a function of time. As found, a time extension to 30 min increased the adsorption of CMX from 0.61 to 1.93 mg/g on kaolin particles. The adsorption of UX on kaolin surface was found to be minimal. Figure 5.2 also presents change in the zeta potential of kaolin dispersion with CMX as a function of mixing time. The zeta potential of the particles was found to decrease from -21 to -28 mV with the time of treatment extended to 30 min in the presence of CMX. This decrease in the zeta potential can be attributed to negative charges imparted on the kaolin surface due to the adsorption of CMX on particles as shown in Figure 5.3. These results also confirmed that only adsorbed CMX (and not the unadsorbed CMX) influenced the zeta potential of kaolin particles.

The impact of time on the kaolin dispersion stability under dynamic and static conditions was represented in Figure 5.8. The kaolin dispersion (control sample) exhibited an insignificant increase in the relative turbidity from 0.99 to 1.01 as time elapsed to 30 min in the absence of

UX/CMX under dynamic conditions. Also, the UX had no effect on the relative turbidity of the kaolin dispersion. The addition of CMX increased the relative turbidity to 1.18 within 10 min of analysis (Figure 5.8a), but further time extension had no impact on relative turbidity. This increase in the relative turbidity with time is due to a decrease in the zeta potential of kaolin particles as shown in Figure 5.5 The relative turbidity was found to increase to 1.18 with a decrease in the zeta potential from -20 to -27 mV. Similarly, in the absence of CMX, the transmission zone of the kaolin dispersions increased to 71% (Figure 5.8b) within 10 min due to the settling of kaolin particles under static conditions. Furthermore, the UX had no significant effect on the transmission zone. In the presence of CMX, the kaolin particles were well stable in the dispersions with an increase in transmission zone from 0 to 10%. The relative turbidity studies under static conditions (Figure 5.8c) also exhibited a similar trend. In the absence of CMX, no significant increase in the relative turbidity of kaolin dispersions was found, while the relative turbidity increased to 5.4 after 30 min in the presence of CMX. Although, the overall surface charge of kaolin particles is negative, kaolin particles possess both negative and positively charged sites as reported in section 5.4.1 and elsewhere [48]. The kaolin particles generally possess both negative and positive charges on their surface causing them to aggregate under natural conditions. Previously, the turbidity of clay dispersion was increased by 75% with the time extension to 45 min at pH 5.5 in the stability analysis of bentonite dispersions (10 wt.%) using anionic polystyrene sulfonate (50 mg/L) [49].

The results in Figures 5.1 inform that the adsorption of CMX on kaolin particles was increased via following two methods of dosage and time. Figures 5.1 to 5.8 reveal that the adsorption of CMX on kaolin particles significantly impacted the zeta potential and relative turbidity of the kaolin dispersions. Regardless of the time or dosage effect, the adsorption tailored the zeta potential and relative turbidity very similarly. However, an increase in the zeta potential did not necessarily improve the relative turbidity of kaolin dispersions significantly.

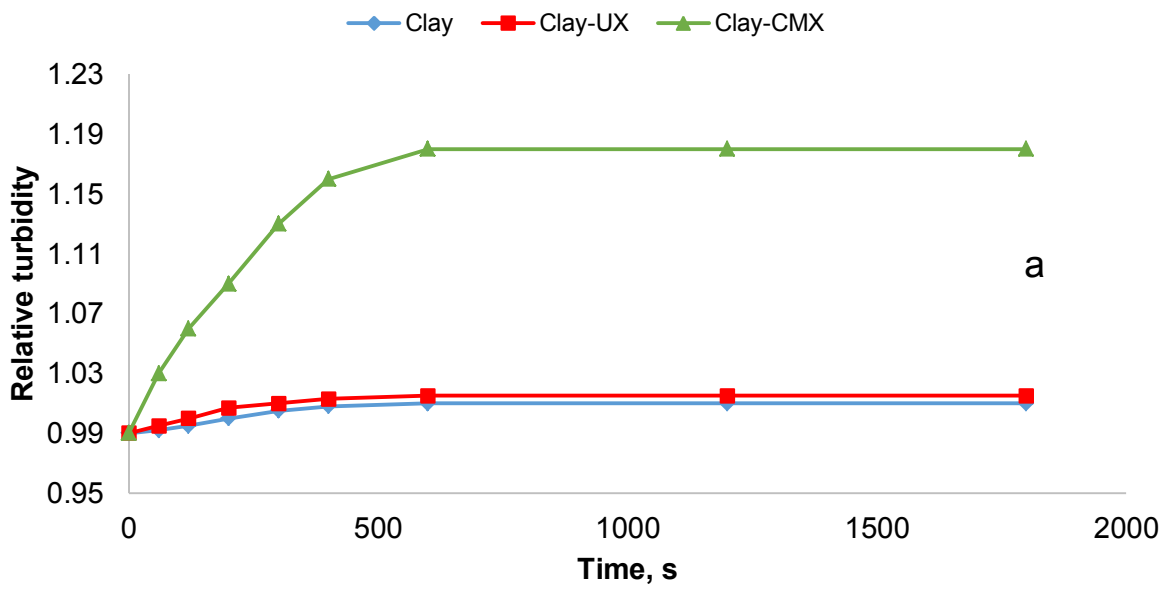
Clay
Clay-UX
Clay-CMX
1.23
1.19
1.15
1.11
1.07
1.03
0.99
0.95
Relative turbidity
a
0
500
1000
1500
2000
Time, s

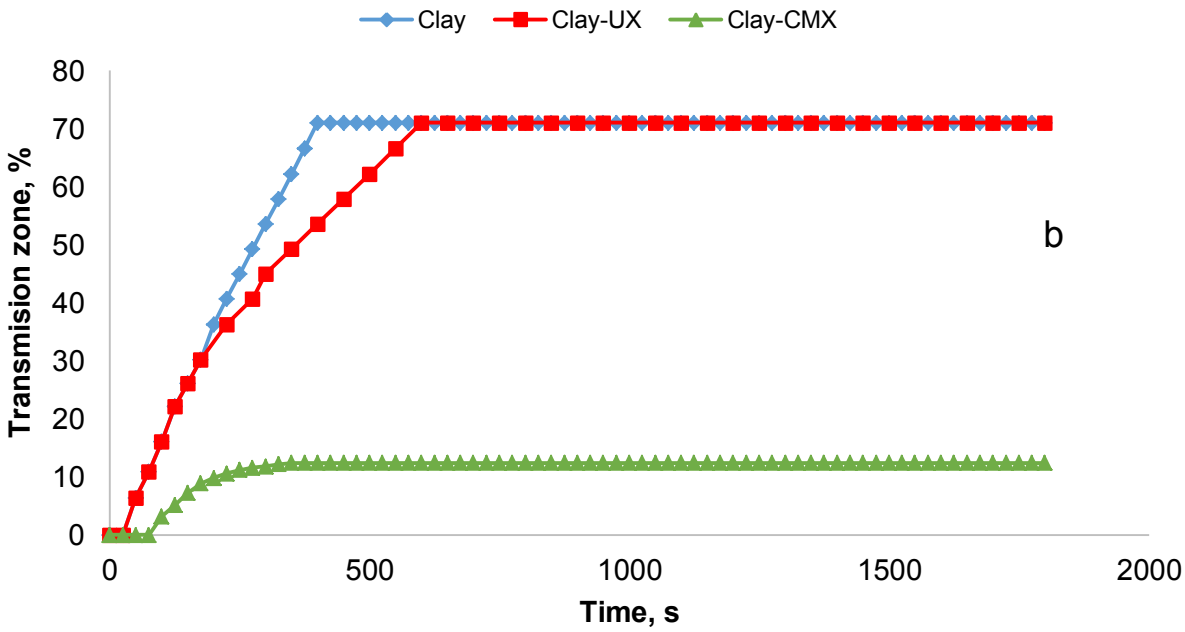
Clay
Clay-UX
Clay-CMX
80
70
60
50
40
30
20
10
0
Transmision zone, %
b
0
500
1000
1500
2000
Time, s

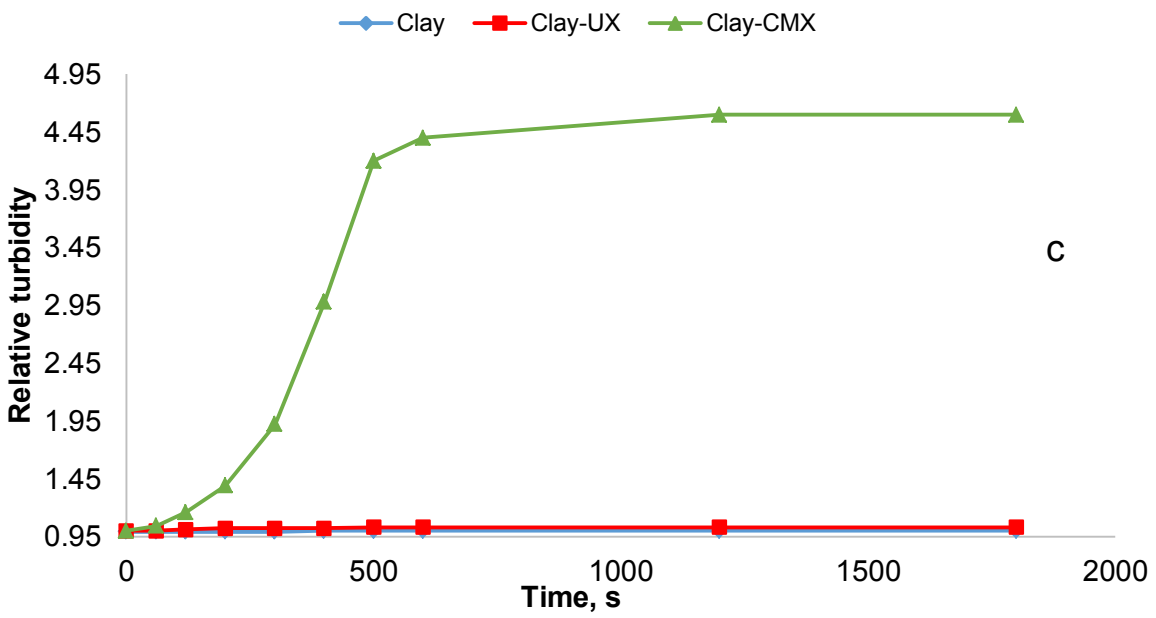


Figure 5.8. a) Effect of time on the relative turbidity under dynamic conditions; b) transmission zone and c) relative turbidity under static conditions for kaolin dispersions in the absence and presence (5 mg/g) of CMX or UX at pH 6, 20 g/L kaolin and 30°C.

### 5.4.7 Impact of shear rate

The kaolin particles tend to aggregate due to weak electrostatic repulsion between the particles and thereby possess complex flow behavior at neutral pH [50]. The increase in the shear rate of dispersion is one way to prevent or break the formation of aggregates and thus to increase the stability of kaolin dispersions [51]. As noted earlier, the addition of CMX was able to improve the dispersion of kaolin particles under static and dynamic states. The influence of shear rate and dispersant dosages on the relative turbidity of kaolin dispersions was compared at pH 6 in Figure 5.9. The results exhibit that the relative turbidity of kaolin dispersions was increased from 1.12 to 1.25 with an increase in shear rate from 50 to 300 rpm in the presence of CMX. In the absence of CMX, the acceleration of shear rate from 50 to 1000 rpm marginally rose the relative turbidity of the kaolin dispersions from 1 to 1.08. These results states that the dispersion of kaolin particles were improved significantly by CMX (i.e. chemical addition), and this high performance was not achieved with shear rate increase (i.e. mechanical stirring). The results also depicted that 10 mg/g of CMX at 100 rpm or 5 mg/g at 300 rpm was able to reach the relative turbidity that was obtained at 800 rpm in the absence of CMX. Furthermore, the relative turbidity of clay suspension in the presence of CMX (1.23) is higher than commercial PAA (1.2). As

mechanical stirring is costly, the addition of CMX might be an option to reduce the cost of maintaining kaolin particles in the dispersions.

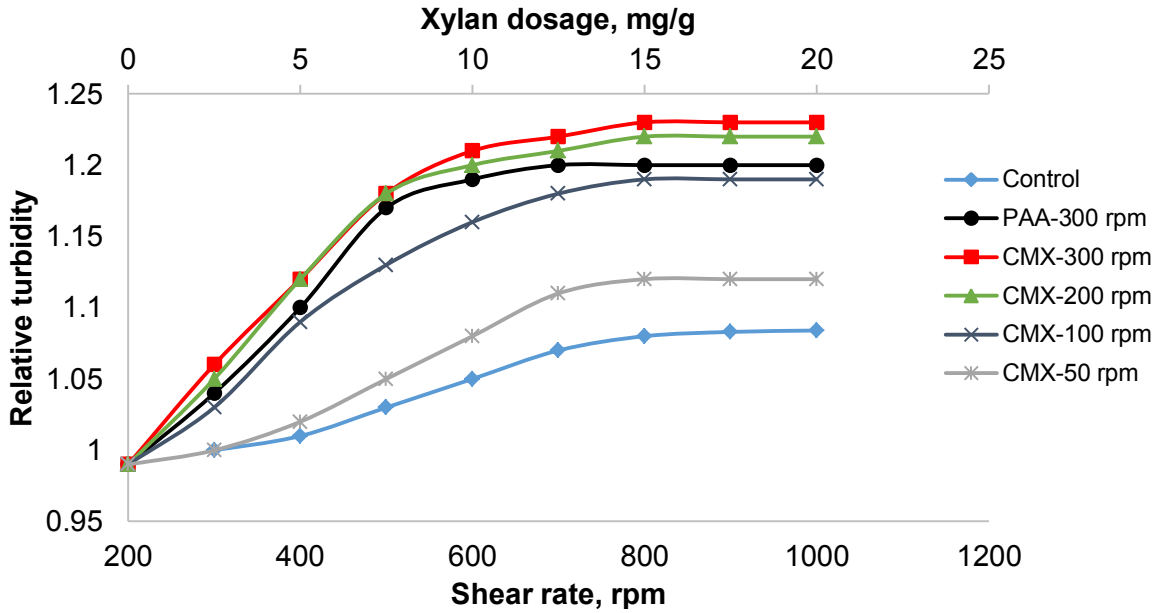


Figure 5.9. Effect of shear rate on the relative turbidity of kaolin dispersions in the absence of CMX and effect of CMX and PAA dosage on the relative turbidity of kaolin dispersions at varying shear rates under the conditions of pH 6, 0.5 h, 25°C and 20 g/L of kaolin concentration

## 5.5 Conclusions

CMX having a charge density of 1.6 mmol/g and molar mass of 24,122 g/mol was used as an effective dispersant for the stabilization of kaolin dispersions. CMX exhibited the maximum adsorption of 2.48 mg/g on kaolin particles at pH 6, which was higher than that of UX (0.08 mg/g). The stability of kaolin dispersion was increased quickly in the presence of CMX and increased with increase of pH and CMX dosage. The maximum relative turbidity of 1.25 was obtained at pH 6 at 25 mg/g CMX in the kaolin dispersions under dynamic conditions. The amount of CMX adsorbed directly affected the zeta potential and relative turbidity of dispersions under static and dynamic states, and the zeta potential of kaolin particles was not an indicative of their dispersion. The results suggested that CMX dosage, pH of kaolin dispersion and mixing time had great influence on the stabilization of kaolin particles. An increase in the stability of kaolin dispersions with CMX dosage under static conditions was also confirmed by a reduction in the transmission zone, increase in the volume fraction of kaolin particles in the dispersed state and in the relative turbidity of kaolin dispersion. The addition of CMX was found to be more effective in stabilizing kaolin dispersions than a shear rate increase.

## 5.6 References


1. Brady PV, Cygan RT, Nagy KL. Molecular controls on kaolinite surface charge. Journal of Colloid Interface Science, 1996, 183, 356-364.
2. Zaman AA, Tsuchiya R., Moudgil BM. Adsorption of a low-molecular weight polyacrylic acid on silica, alumina and kaolin. Journal of Colloid Interface Science, 2002, 256, 73-78.
3. Yuan J, Garforth WL, Preutt RJ. Influence of dispersants on the solubility of calcined kaolin. Applied Clay Science, 1998, 13, 137-147.
4. Nuntiya A, Prasanphan S. The rheological behaviour of kaolin suspensions. Chaing Mai Journal of Science, 2006, 33, 271-281.
5. Boisvert JP, Persello J, Castaing JC, Cabane B. Dispersion of alumina coated $TiO_2$ particles by adsorption of sodium polyacrylate. Colloids and Surfaces A: Physiochemical Engineering Aspects, 2001, 178, 187-198.
6. Amoros JL, Beltron V, Sanaz V, Jarque JC. Electrokinetic and rheological properties of highly concentrated kaolin dispersions: Influence of particle volume fraction and dispersant concentration. Applied Clay Science, 2010, 49, 33-43.
7. Ma M. The dispersive effect of sodium silicate on kaolinite particles in process water: Implications for iron ore processing. Clay and Clay Minerals, 2011, 59, 233-239.
8. Eygi MS, Atesok G. An investigation on utilization of poly-electrolytes as dispersant for kaolin slurry and its slip casting properties. Ceramics International, 2008, 34, 1903-1908.
9. Qin W, Wei Q, Jiao F, Li N, Wang P, Ke L. Effect of sodium pyrophosphate on the flotation separation of chalcopyrite from galena. International Journal of Mining Science and Technology, 2012, 22, 345-349.
10. Loginov M, Larue O, Lebvoka N, Vorobeiv E. Fluidity of highly concentrated kaolin suspensions: Influence of particle concentration and presence of dispersant. Colloids and Surfaces A: Physiochemical Engineering Aspects, 2008, 325, 64-71.
11. Garcia OA, Vazquez SB, Medina JZ. Mixture design to optimize the amount of deflocculants in aqueous porcelain suspensions. Journal of Ceramic Processing Research, 2009, 10, 125-128.
12. Ece OI, Alemdar A, Gungor N, Hayashi S. Influence of non-ionic poly (ethylene glycol) polymer PEG on electrokinetic and rheological properties of bentonite suspensions. Journal of Applied Polymer Science, 2002, 86, 341-346.

13. Conceicao SI, Velho JL, Ferreira JMF. Influence of deagglomeration and carboxymethylcellulose binders on rheological behaviour of kaolin suspensions. Applied Clay Science, 2003, 23, 257-264.
14. Laskowski JT, Liu Q, O'Connor CT. Current understanding of the mechanism of polysaccharide adsorption at the mineral/aqueous solution interface. International Journal of Mineral Processing, 2007, 84, 59-68.
15. Penkavova V, Guerreiro M, Tihan J, Teixeira JAC. Deflocculation of kaolin suspensions – The effect of various electrolytes. Applied Rheology, 2015, 25, 24151-24165.
16. Pawlik M, Laskowski JS, Ansari A. Effect of carboxymethyl cellulose and ionic strength on stability of mineral suspensions in potash ore flotation systems. Journal of Colloid Interface Science, 2003, 260, 251-258.
17. Umaran MVA, Menchavez RL. Aqueous dispersion of red clay based ceramic powder with the addition of starch. Materials Research, 2013, 16, 375-384.
18. Li Z, Pang Y, Lou H, Qiu X. Influence of lignosulfonates on the properties of dimethomorph water-dispersible granules. Bioresources, 2009, 4, 589-601.
19. Schild G, Sixta H. Sulfur free dissolving pulps and their application for viscose and lyocell. Cellulose, 2011, 18, 1113-1125.
20. Konduri MKR, Fatehi P. Synthesis and characterization of carboxymethylated xylan and its application as a dispersant. Carbohydrate Polymers, 2016, 146, 26-35.
21. Zaman AA, Mathur S. Influence of dispersing agents and solution conditions on the solubility of crude kaolin. Journal of Colloid and Interface Science, 2004, 271, 124-130.
22. Guillemet B, Faatz M, Grohn F, Wegner G, Gnanou Y. Nanosized calcium carbonate stabilized by poly (ethylene oxide)-b-poly (acrylic acid) block copolymers. Langmuir, 2006, 22, 1875-1879.
23. Li X, Li Q. YAG ceramic processed by slip casting via aqueous slurries. Ceramics International, 2008, 34, 397-401.
24. Gregorova E, Pabst W. Process control and optimized preparation of porous alumina ceramics by starch consolidation casting. Journal of European Ceramic Society, 2011, 31, 2073-2081.

25. Papo A, Piani L, Ricceri R., 2002. Sodium tripolyphosphate as dispersing agents for kaolin suspensions: rheological characterization. Colloids and Surfaces A: Physiochemical Engineering Aspects, 2002, 201, 219-230.
26. Konduri M.K.R, Kong F, Fatehi P. Production of water soluble kraft lignin via carboxymethylation using sodium chloroacetate. European Polymer Journal, 2015, 70, 371-383.
27. Wang S, Konduri M.K.R, Hou Q, Fatehi, P. Cationic xylan-METAC copolymer as a flocculant for clay suspensions. RSC Advances, 2016, 6, 40258-40269.
28. Senoussi H, Osmani H, Courtois C, Bourahli M.H. Minerological and chemical charcaterization of DD3 kaolin from the east of Algeria. Journal of Spanish Ceramic Glass Society, 2016, 55, 121-126.
29. Mcintosh A, Lawther S.E.M, Kwasny J, Soutsos M.N, Cleland D, Nanukuttan S, 2015 Selection and characterization of geological materials for use as geopolymer precursors. Advances in Applied Ceramics, 2015, 114, 378-385.
30. Marco P, Llorens J. Surface charge and rheological properties of raw porcelain gres suspension with acrylic copolymers bearing carboxylic groups. Journal of European Ceramic Society, 2009, 29, 559-564.
31. Ramphal SR, Sibiya MS. Optimization of coagulation-flocculation parameters using a photometric dispersion analyzer. Drinking Water Engineering and Science, 2014, 7, 73-82.
32. Xiao F, Huang JCH, Zhang BJ, Cui CW. Effect of low temperature on coagulation kinetics and floc surface morphology using alum. Desalination, 2009, 237, 201-213.
33. Wang LJ, Wang JP, Zhang SJ, Chen YZ, Yuan SJ, Sheng GP, Yu HQ. 2009. A water soluble cationic flocculant synthesized by dispersion polymerization in aqueous salts solution. Separation Purification and Technology, 2009, 67, 331-335.
34. Ovenden C, Xiao H. Flocculation behaviour and mechanisms of cationic inorganic microparticle/polymer system. Colloids and Surfaces A: Physiochemical Engineering Aspects, 2002, 197, 225-234.
35. Vie R, Azema N, Quantin JC, Touraud E, Fouletier M. Study of suspension settling: A approach to determine suspension classification and particle interactions. Colloids and Surfaces A: Physiochemical Engineering Aspects, 2007, 298, 192-200.

36. He W, Zhang Y, Fatehi P. Sulfomethylated kraft lignin as a flocculant for cationic dye. Colloids and Surfaces A: Physiochemical Engineering Aspects, 2016, 503, 19-27.
37. Mengual O, Menuier G, Cayre I, Puech K, Sanbre P. Characterization of instability of concentrated dispersions by a new optical analyzer: the Turbiscan MA 1000. Colloids and Surfaces A: Physiochemical Engineering Aspects, 1999, 152, 111-123.
38. Breitung-Faes S, Kwade A. Production of transparent suspensions by real grinding of fused corundum. Powder Technology, 2011, 212, 383-389.
39. Celia C, Trapasso E, Cosco D, Paolino D, Fresta M . Turbiscan lab expert analysis of the stability of ethosomes and ultradeformable liposomes containing a bilayer fluidizing agent. Colloids Surfaces B: Biointerfaces, 2009, 72, 155-160.
40. Loginov M, Larue O, Lebvoka N, Vorobeiv E. Fluidity of highly concentrated kaolin suspensions: Influence of particle concentration and presence of dispersant. Colloids and Surfaces A: Physiochemical Engineering Aspects, 2008, 325, 64-71.
41. Ryan JN, Gschwend PM. Effect of solution chemistry on clay colloid release from an iron oxide-coated aquifer sand. Environmental Science and Technology, 1994, 28, 1717-1726.
42. James AE, Nasser MS. The effect of polyacrylamide charge density and molecular weight on the flocculation and sedimentation behaviour of kaolin suspensions. Separation Purification Technology, 2006, 52, 241-252.
43. Sastry NV, Sequaris JM, Schwuger M.J. Adsorption of polyacrylic acid and sodium dodecylbenzenesulfonate on kaolinite. Journal of Colloid Interface Science, 1995, 171, 224-233.
44. Cerrutti BM, De-souza CS, Castellan A, Ruggiero R, Frollini E. Carboxymethyl lignin as stabilizing agent in aqueous ceramic suspensions. Industrial Crop Products, 2012, 36, 108-115.
45. Traiphol N, Suntako R, Chanthornship K. Roles of polymeric dispersant charge density on lead zirconate titanate aqueous processing. Ceramics International, 2010, 36, 2147-2153.
46. Shin YJ, Su CC, Shen YH. Dispersion of aqueous nano sized alumina suspensions using cationic polyelectrolyte. Materials Research Bulletin, 2006, 41, 1964-1971.
47. Gan L, Zhou M, Yang D, Qiu X. Preparation and evaluation of carboxymethylated lignin as dispersant for aqueous graphite suspension using Turbiscan lab analyzer. Journal of Dispersion Science and Technology, 2013, 34, 644-650.

48. Tombac E, Szekeres M, Surface charge heterogeneity of kaolinite in aqueous suspension in comparison with montmorillonite. Applied Clay Science, 2006, 34, 105-124.
49. Mostafa BA, Assad FF. Rheological and electrical properties of bentonite in anionic polystyrene sulfonate and non-ionic poly (vinyl alcohol). Journal of Applied Polymer Science, 2007, 104, 3886-3894.
50. Gareche M, Arzil N, Saoudi L, Dupin J. C, Allal A, Zeraibi N. Colloidal behaviour of montmorillonite suspensions in the presence of non-ionic polymer. Journal of Hydraulic Engineering, 2015, 1, 60-66.
51. Yukselen MA, Gregory J, 2004. The effect of rapid mixing on the break up and reformation of flocs. Journal of Chemical Technology and Biotechnology, 2004, 79, 782-788.

# Chapter 6. Influence of charge density and molecular weight of anionic kraft lignin on dispersibility of kaolin suspensions

Mohan K. R. Konduri, Pedram Fatehi[a]

[a] Department of Chemical Engineering,

Lakehead University,

955 Oliver Road,

Thunder Bay, ON P7B 5E1, Canada

## 6.1 Abstract

To generate an effective dispersants for concentrated kaolin slurries, it is important to study, how the properties of polyelectrolytes affect their performance. In this study, kraft lignin was modified via oxidation using nitric acid under varied conditions to produce oxidised lignin (OL) products with different charge densities and molecular weights. Then, the effect of anionic charge density (CD) and molecular weight (MW) of the lignin based products on the relative turbidity, destabilization index, particle size and zeta potential of kaolin suspension was investigated under neutral conditions (pH 7). One set of lignin based products had a similar molecular weight around 26,000 g/mol, while their charge densities varied between 1.2 and 3.6 meq/g. Another set of lignin based products had a similar charge density of 3.6 meq/g, but altered molecular weight range of 11,000-80,000 g/mol. Adsorption of OLs on kaolin surface increased with charge density, while molecular weight had no influence on OLs adsorption. Zeta potential of kaolin particles is affected by charge density of OLs. Dispersion studies with OLs under dynamic and static conditions suggests that, both charge density and molecular weight had a great influence on stability of kaolin particles. OL8 with charge density, 3.6 meq/g and molecular weight, 30,243 g/mol improved the relative turbidity of kaolin suspension, maximum up to 1.31, and reduced stabilization index to 0.06 at 16 mg/L concentration.

## 6.2 Introduction

Kaolin suspensions have been used as raw materials in mineral, ceramic, paper and other chemical industries [1, 2]. In these processes, the fluidity of kaolin suspensions is crucial to produce final products with acceptable properties while maintaining the production and energy costs low [3]. The stability of kaolin suspensions depends on the size and interaction between the kaolin particles [4]. The fluidity of kaolin suspensions can be enhanced using dispersants [5]. When a dispersant is added to aqueous suspensions, it adsorbs on the particle surface and induces electrostatic or steric repulsion between them. As a result, the particles do not agglomerate and become stabilized in the suspensions [6]

Numerous synthetic polymers have been proposed as dispersants for kaolin suspensions [7,8]. However, their non-biodegradable and toxic nature is their main barrier for practical useskaolin [9]. Alternatively, the use of natural or semi-natural polymers have been proposed to address this challengekaolin [3,10]. In one study, the use (0.2 wt.%) of anionic lignin-based product

produced via chemical modification of hardwood kraft lignin improved the relative turbidity of a kaolin suspension (20 g/L) to 1.1 [11]. In another work, carboxymethylated lignin produced via treatment of wheat straw alkali lignin with chloroacetic acid was applied as a dispersant for graphite aqueous suspensions [12]. Calcium lignosulfonate (1.0 wt.%), obtained from spent liquor of sulfite pulping process of pine wood improved the stability of graphite suspension by 70 %, while a commercial dispersant, Reax-85A improved it only by 50% [10]. Currently, in this work, hardwood kraft lignin is oxidised with nitric acid under various reaction conditions to produce anionic lignin products with varied molecular weights and charge densities to be used as dispersants for kaolin suspensions.

Kaolin particles tend to aggregate due to interactions between positively charged edges and negatively charged basal plane over a wide pH range [13]. As kaolin contains heterogeneously charged edges, it has intricate surface chemistry. To develop an efficient dispersant for kaolin, its interaction with kaolin should be well understood [4]. The adsorption of anionic polymers on kaolin alters the surface charge density of kaolin particles, which in turn reduces the aggregation of particles [14]. Factors such as, polymer concentration, pH and ionic strength of the suspensions are known to affect the adsorption behaviour of polymers significantly [15,16]. Previously, an increase in sodium polyacrylate concentration from 0.1 to 0.4 wt.% increased the adsorption of polymer on kaolin particles to 0.05 mg/m$^2$ [17]. Studies by Deng and co-authors demonstrated that the adsorption of anionic polyacrylamide on kaolinite improved up to 0.6 mg/g with an increase in polymer concentration from 0.2 to 1.2 mg/L, and the adsorbed polymer altered the surface charge of kaolinite particles [18]. In this work, the impact of the adsorption of anionic lignin on the surface chemistry of kaolin is studied.

The dispersion of colloidal suspensions is a complex process, and is influenced by the adsorption of polymers and the characteristics of adsorbed polymers [19, 20]. The characteristics of polymer such as charge density and molecular weight are known to affect the adsorption of polymers [3, 21] . In a study on the stabilization of $TiO_2$ suspensions, an increase in the molecular weight of lignosulfonates from 1000 to 30,000 g/mol improved the dispersion stability by 50 % [3]. In another study on the stabilization of kaolin suspensions using carboxymethylated cellulose (CMC), an increase in molecular weight from 35,000 to 125,000 g/mol decreased the turbidity of kaolin suspension by 50 % [22]. Poly (acrylic acid-co-maleic acid) exhibited high dispersion

performance in lead zirconate titanate aqueous suspensions (60 wt.%)[5]. However, the relationship between structural and chemical properties of oxidized kraft lignin as a dispersant for colloidal suspensions has not been studied yet [23]. In this work, the impact of molecular weight and charge density of oxidized lignin as a dispersant for kaolin suspensions was studied under both dynamic and static conditions.

In this work, the oxidation of kraft lignin with nitric acid under various conditions was studied to produce anionic lignin samples with different molecular weights and charge densities. The primary novelty of this work is the investigation on the influence of charge density and molecular weight of anionically charged lignin products on the stability of kaolin suspensions.

## 6.3 Materials & Methods

### 6.3.1 Materials:

Mixed hardwood lignin was supplied by FPInnovations from its pilot plant facilities located in Thunder Bay, ON [24]. Sodium nitrate (99 %), potassium nitrate (99.99 %), kaolin, potassium hydroxide (> 85 wt.%), sodium hydroxide and para hydroxybenzoic acid (PHBA) were obtained from Sigma Aldrich Company and used as received. Nitric acid was obtained from Sigma Aldrich company and diluted to 30 wt.% prior to use. Standard hydrochloric acid (HCl) solution (30-35 wt.%) was obtained from Fluka analytical and used as received. Sulphuric acid (95-98 %) was obtained from Sigma Aldrich Company and diluted to 0.1 M prior to use. Cellulose acetate dialysis membrane (molecular weight cut off of 1,000 g/mol) was obtained from Spectrum Labs. Inc, USA. Polydiallyldimethylammonium chloride (PDADMAC) was obtained from Sigma Aldrich Company and diluted to 0.005 M prior to use. Potassium polyvinyl sulfate (PVSK) was obtained from Wako Pure Chemical Industries Ltd., Japan and diluted to 0.005 M prior to use.

### 6.3.2 Oxidation

The oxidation of kraft lignin was performed as described previously [25]. A 5 g sample of hardwood lignin was treated with nitric acid at different temperatures for different time intervals as shown in Table 1. After the reaction, the mixture was cooled to room temperature and its pH was adjusted to 7 using 0.1 M NaOH. Unreacted nitric acid was separated using the dialysis membrane, while changing water every 12 h for two days. The dialyzed samples were oven dried at 105 °C and stored at 4 °C until further use.

### 6.3.3 Charge density analysis

The charge density of unmodified lignin (UL) and oxidized lignin samples (OL1 to OL 10) was determined using a particle charge detector (Mutek, PCD 04, Germany). The samples were initially dried at 105 °C overnight to remove moisture. A 0.2 g sample of oxidized lignin samples was dissolved in 20 mL of deionized water and incubated for 2 h at 30 °C in a water bath shaker (Classic C76, New Brunswick Scientific, Edison, NJ, USA) at 150 rpm. After the incubation, the samples were centrifuged at 1000 rpm for 10 min and supernatants were collected for the charge density analysis. A 1 mL of supernatant was titrated against 0.005M PDADMAC using a Mutek, PCD 04 particle charge detector (Germany) to measure the charge density according to Equation 6.1[26].

$$\text{Surface charge density (meq/g)} = \frac{C_T \times V_S}{W_S} \qquad (6.1)$$

where $C_T$ is the concentration of titrant or PDADMAC (0.005 mol/L), $V_S$ is the volume of the PDADMAC used for titrating the sample (mL) and $W_S$ is the weight of the sample (g).

To determine the surface charge density of particles, 0.2 g of kaolin was suspended in 50 mL of PDADMAC (0.005M) solution and the suspension was incubated at 30 °C for 2 h at 150 rpm. After the incubation, the samples were filtered using Whatmann#1 filter membranes and the filtrates were titrated against PVSK (0.0055 M) solution with the titrator. Similarly, the titration analysis was conducted for control sample (i.e. PDADMAC solution before mixing with kaolin) and the difference was considered for quantifying the surface charge density of kaolinkaolin particles.

### 6.3.4 Surface area analysis of kaolin particles

The surface area of kaolin particles was determined by using Quantachrome surface area analyzer, Nova 2200e, instrument. In this set of experiments, the samples were initially dried in an oven at 105 °C overnight and approximately 0.05 g of sample was pretreated for 4 h at 250 °C prior to analysis. The specific surface area of the samples was then analyzed according to Branuer-Emmett-Teller (BET) method via adsorption-desorption isotherms using nitrogen gas at -180 °C with relative pressure range of 0.01 to 0.99 [27].

### 6.3.5 Carboxylate group analysis

The aqueous conductometric titration method was used to measure the amount of carboxylate groups attached to unmodified or oxidized lignin samples using an automatic conductometric

titrator, Metrohm, 785 DMP Titrino, Switzerland. In this set of experiments, a 0.06 g sample was added to 100 mL of deionized water containing 1 mL of 0.8 M potassium hydroxide in a 200 mL beaker and stirred at 500 rpm for 10 min. To this mixture, 4 mL of 0.5 wt.% PHBA solution was added as an internal standard and titrated against a standard 0.1 M hydrochloric acid solution. The volume of HCl consumed to decrease the pH of the sample solution to specific end points are noted as $V_2'$ (pH 7) and $V_3'$ (pH 3) and their corresponding end points for blank solutions (without sample) are noted as $V_2$ and $V_3$. While $V_1'$ and $V_1$ correspond to volume of HCl consumed to decrease the pH of sample to 10 for sample and control solutions. The carboxylate group content of the samples was calculated according to Equation 6.2 [28].

$$\text{Carboxylate group content (mmol/g)} = \frac{\{(V_3' - V_2') - (V_3 - V_2)\} \times C_{HCl}}{W_s} \qquad (6.2)$$

where Ws is the weight of the sample (0.06 g), $C_{HCl}$ is the concentration of the HCl (0.1 M), V is the volume of the titrant (ml) consumed to reach the end points of titration. Three replicates were performed and the average values were reported.

### 6.3.6 Molecular weight analysis

To determine the molecular weight of the samples, they were first dried in an oven at 105 °C. Approximately, 50 mg sample of UL or OL was dissolved in 5 mL of 0.1 mol/L $NaNO_3$ solution and filtered with a nylon 0.2 µm filter (13 mm diameter). The filtered solutions were used for the molecular weight analysis. The molecular weight of unmodified lignin (UL) and oxidized lignin (OL) samples were assessed using a gel permeation chromatograph instrument (Malvern GPCmax VE2001 Module + Viscotek TDA305) equipped with refractive index and viscometer detectors. PolyAnalytic columns, PAA206 and PAA203, were used at the column temperature of 35 °C. Polyethylene oxide was used as standards. 0.1 mol/L $NaNO_3$ solution was used as solvent and eluent with flow rate of 0.70 mL/min.

### 6.3.7 Hydrodynamic diameter analysis

A static light scattering instrument (Brookhaven Instruments, BI-200SM, USA) equipped with a laser light at a wavelength of 637 nm was used to determine the hydrodynamic diameter of UL and OL samples [29]. All the samples were oven dried at 105 °C overnight to remove the moisture content prior to analysis. In this set of experiments, 0.1 g of samples was dissolved in 100 mL of deionized water at pH 7 and incubated in water bath shaker at 30 °C for 2 h and 150 rpm. Subsequently, 3.2 mL of potassium nitrate (0.4 M) solution was added to the samples and

stabilized for 24 h. 20 mL of each sample was prepared by filtering with 0.45 µm disposable syringe filters and measured at 90° scattering angle for 2 min and 25 °C. Three replicates were performed for each experiment and average values were reported.

### 6.3.8 Contact angle measurement

An optical tensiometer instrument, Theta lite (Biolin Scientific, Finland) equipped with camera was used to determine the wettability of OL samples. All samples (OL1-OL10) including UL were oven dried, and a 0.2 g of each sample was dissolved in 20 mL of deionized water (10 g/L) and incubated in water bath for 2 h at 30 °C. After incubation, 2 mL of sample was loaded on to microscopic glass slides and allowed to dry using a spin coater, WS-650 (Laurell Technologies Corp) under vacuum with 60 Psi pressure, 250 rpm for 60 s. The contact angle of water with OL or UL samples coated on microscopic slides was determined using the sessile drop method, by fitting the data to young laplace equation (Eq 6.3) [30]. Approximately, droplets containing 5 µL of water was placed on the coated slides and the contact angles of the droplet and the slides were determined using optical tensiometer. Three replicates were performed for each experiment and average values were reported.

$$\gamma_{lv}\, cos\theta_Y = \gamma_{sv} - \gamma_{sl} \qquad (6.3)$$

where, $\gamma_{lv}$, $\gamma_{sv}$ and $\gamma_{sl}$ represent the interfacial tenstions of liquid vapour, solid vapour and solid liquid, respectively, and $\theta_Y$ is the contact angle of water with OL sample coated on glass slide.

### 6.3.9 Adsorption studies

The adsorption of UL or OL samples onto kaolin particles was studied as a function of polymer dosage. In this experiment, UL or OL concentrations of 2 to 256 mg/L were provided into 250 mL glass flask containing 50 mL of a kaolinkaolin suspension (2 g/L) and incubated at 30 °C for 1 h and 150 rpm. After the incubation, the mixture was centrifuged at 2500 rpm for 10 min to separate thekaolin particles from the suspensions. The concentration of UL or OL samples in the supernatants was measured using UV-Vis Spectrophotometer at a wavelength of 205 nm [31]

### 6.3.10 Zeta Potential Analysis

The zeta potential analysis of kaolin particles was performed using a NanoBrook Zeta PALS (Brookhaven Instruments Corp, USA). In this study, 2 g of kaolin suspension (100 g/L) was added to 100 mL of deionized water and stirred at 150 rpm for 1 h at room temperature. After mixing, 1 mL of sample was subjected to instrument for zeta potential analysis. Similarly, the

zeta potential of kaolin particles in the presence of UL or OLs was measured at different polymer dosages (2 to 256 mg/L) under the same conditions as described above. The experiments were carried out three times and the mean values were reported in this study.

### 6.3.11 Particle size analysis

In this study, 2 mL of kaolinkaolin suspension (100 g/L) was added to 100 mL of deionized water and incubated in water bath shaker at 30 °C and 150 rpm. After the incubation, the samples were transferred to a MasterSizer 2000 particle size analyzer (Malvern Instruments) equipped with a light scattering detector to measure the particle size distribution of the kaolin kaolinparticles. Similarly, the particle size analysis of kaolinkaolin suspensions was carried out as a function of UL or OL dosage from 2 to 256 mg/L under the conditions described above. All the measurements were carried out at room temperature. Three measurements were carried out for each sample and average values were reported.

### 6.3.12 Dispersion Analysis

The dispersion affinity of OL samples in kaolin suspensions was studied using a photometric dispersion analyzer (PDA 3000, Rank Brothers Ltd) that was connected to a dynamic drainage jar (DDJ) fitted with a 70 mm mesh screen[32]. The degree of dispersion or flocculation of the kaolin suspension was presented by relative turbidity, $\tau_r$, which was quantified from the variation in the direct current (DC) voltage signals of the PDA instrument [33]. In this set of experiments, 500 mL of deionised water was transferred into the DDJ container and allowed to circulate from the DDJ to the PDA through a 3 mm plastic tube until a steady flow rate of 20 mL/min was achieved using a peristaltic pump. Then, 10 mL of a 100 g/L kaolin suspension was added into DDJ (2 g/L kaolin concentration) at a constant stirring rate of 300 rpm and allowed to circulate through PDA. A decrease in the initial base DC voltage ($V_0$) to a new DC voltage ($V_i$) was recorded. Different dosages (2 to 256 mg/L) of UL or OL (10 g/L) in the suspension mixture were prepared in the DDJ, and the increase or decrease in DC voltage was represented as the DC voltage ($V_f$) of the final suspension. The pH of the kaolin suspensions was maintained at 7 during the experiments. The relative turbidity of the kaolin suspension, $\tau_r$, was measured according to equation 6.4 [34].

$$\text{Relative turbidity, } \tau_r = \frac{\tau_f}{\tau_i} = \frac{ln(\frac{V_0}{V_f})}{ln(\frac{V_0}{V_i})} \qquad (6.4)$$

where $\tau_f$ is denoted as the final suspension turbidity, and $\tau_i$ is denoted as initial suspension turbidity.

### 6.3.13 Stability analysis

The stability of the kaolin suspension in the presence OLs was investigated using a Turbiscan Lab Expert, Formulaction, France. This analysis was conducted in the past to study the stability of emulsion and concentrated colloidal dispersions. In this set of experiments, kaolin suspensions (2 g/L) in the presence of OLs (OL1-OL10) at varying dosages (2-256 mg/L) were prepared and changes in the suspension stability was analyzed for 1 h (single scans were collected every 2 sec) by the instrument at 30 ºC. The transmission and backscattering zone percentage data was determined by turbisoft 2.1 software by comparing the transmittance signals generated by the sample with those generated by the standard silicon oil, which is used as a calibration chemical by the instrument [35]. These transmittance and backscattering signals were recorded as a percentage of transmittance signals in regard to that of the silicon oil.

The transmission and backscattering data was used for determining the destabilization index (DSI) and average particle diameter using the turbisoft software by equations 6.5 and 6.6[36].

$$\mathrm{DSI} = \Sigma_i \frac{\Sigma_h |scan_i(h) - scan_{i-1}(h)|}{H} \qquad (6.5)$$

Where $scan_i$ (h) and $scan_{i-1}$ (h) are the transmission signals for two consecutive time intervals at a given height and H is the total height of sample.

Correlation between the particle migration velocity and the properties of the suspensions can be determined using equation 4.

$$V(\Phi, \mathrm{d}) = \frac{|p_p - p_c| g d^2}{18 v p_c} \times \frac{[1-\Phi]}{\left[1 + \frac{4.6\,\Phi}{(1-\Phi)^2}\right]} \qquad (6.6)$$

Where $V$ is the particle migration velocity, $p_c$ is the continuous phase density, $p_p$ is the particle density, d is the particle mean diameter, $v$ is the continuous phase dynamic viscosity and $\Phi$ is the volume fraction of dispersed particles (i.e. kaolin particles).

## 6.4 Results & Discussion

### 6.4.1 Preparation of oxidized lignin and kaolin

Kaolin found to have a surface area and particle size of 25.65 $m^2/g$ and 7.2 µm, respectively. The surface charge density of kaolin particles was -6.3 µmol/g, which is probably due to the presence of oxide anions on its surface [37]. Oxidized lignin samples were produced via nitric acid treatment of kraft lignin under different conditions as listed in Table 6.1. The reaction was carried out at high temperatures and acidic conditions due to limited reactivity of hardwood kraft lignin [38].

Table 6-1. Reaction conditions and properties of produced anionic lignin polymers and kaolin particles

| Sample | Conditions | | | | Charge density, meq/g | $M_w$, g/mol | $M_n$, g/mol | Carboxylate group content, mmol/g | $h_y$ | Contact angle, ° |
|---|---|---|---|---|---|---|---|---|---|---|
| | Time, h | Temperature, °C | $HNO_3$ concentration, wt.% | $HNO_3$/lignin, wt./wt. | | | | | | |
| UL | - | - | - | - | 0.2 | 28,200 | 19,100 | 0.16 | 3.72 | 28.3 |
| OL1 | 1 | 100 | 20 | 4 | 1.22 | 26,700 | 18,600 | 1.05 | 3.65 | 5.2 |
| OL2 | 1 | 100 | 20 | 6 | 1.80 | 25,800 | 18,800 | 1.63 | 3.61 | 4.8 |
| OL3 | 1 | 100 | 20 | 8 | 2.45 | 26,200 | 18,400 | 2.28 | 3.66 | 4.7 |
| OL4 | 1 | 100 | 20 | 10 | 3.06 | 25,100 | 18,200 | 2.86 | 3.62 | 4.6 |
| OL5 | 1 | 100 | 20 | 12 | 3.63 | 26,400 | 19,300 | 3.46 | 3.67 | 4.6 |
| OL6 | 1 | 100 | 30 | 8 | 3.58 | 11,600 | 3,200 | 3.45 | 2.21 | 4.5 |
| OL7 | 1 | 100 | 20 | 8 | 3.64 | 21,800 | 11,100 | 3.46 | 3.57 | 4.8 |
| OL8 | 1 | 100 | 25 | 8 | 3.68 | 30,200 | 22,800 | 3.47 | 3.81 | 4.6 |
| OL9 | 1 | 100 | 35 | 10 | 3.57 | 42,500 | 35,100 | 3.43 | 4.06 | 4.7 |
| OL10 | 1 | 100 | 35 | 12 | 3.62 | 83,500 | 52,500 | 3.47 | 7.33 | 4.8 |

The OLs were all soluble in water at 10 g/L concentration, but UL had a limited solubility of 2 wt.% at this concentration. The OL1 to OL5 had a similar molecular weight of 26,000 g/mol, but altered charge densities. The OL6 to OL10 had a similar charge density of 3.6 meq/g, but varied molecular weights. The carboxylate group content of the OL samples followed the same trend as

their charge densities. As expected, this phenomenon describes that the main source of anionic charge density of OLs was carboxylate group. Previously, an increase in the carboxylate group was well associated with the increase in the charge density in the oxidation of softwood kraft lignin with nitric acid [25]. The hydrodynamic diameter of OL1-OL5 was approximately 3.6 nm, while that of OL6-OL10 was in the range of 2.2-7.3 nm. A comparison between the contact angles of water droplet on the glass slides coated with OLs samples reveals that 1) the contact angle of water droplet was significantly small (4 °) for OL samples compared with that for UL (28 ° confirming the increased water solublity and hydrophilicity of the OL samples, 2) the contact angles of all OL samples were similar confirming similar water hydrophilicity of OL samples.

### 6.4.2 Adsorption of OLs

Figures 6.1 present the adsorption of OLs on kaolin as a function of OL dosage. Although, kaolin particles exhibit an overall negative charge density (section 6.4.1), the basal surface of kaolin carry constant positive charges over a wide pH range [13]. Thus, the adsorption of OLs on the kaolin surface occurs via electrostatic interaction between the cationic sites present on the surface of kaolin particles and carboxylate groups of OLs [39]. Upon adsorbing OLs, the surface charge density of kaolin particles was enhanced, which improved the repulsion of particles [5]. In a similar work, Wisniewska and his co-authors reported that the alumina suspension was electrostatically stabilized by polyacrylamide dispersants due to adsorption of anionic polyacrylamide on the alumina surface [40]. As shown in Figure 1a, the higher concentration of OLs led to their higher adsorption on kaolin surface. However, the higher the charge density (negative charge) of OL, the more the OL adsorbed on kaolin surface [41]. On the other hand, the molecular weight of OLs showed an insignificant influence on the adsorption of OLs on kaolin surface (Figure 6.1b). OL6 with the charge density of 3.6 meq/g and molecular weight of 11,654 g/mol exhibited maximum adsorption of 0.81 mg/g,

Based on the amount of UL or OLs adsorbed on kaolin particles (Figure 6.1a and 6.1b) and the charge density of UL and OLs (Table 6.1), the surface charge density of kaolin can be theoretically calculated. Figures 6.1c and 6.1d depict the impact of adsorbed UL or OLs on the theoretical surface charge density of kaolin particles. In these figures, the surface charge density of unmodified kaolin was experimentally determined as described in section 6.3.3, but it was not possible to experimentally measure the surface charge density of kaolin particles after OLs

adsorption. As expected, the negative surface charge density of kaolin particles was increased with the increase in adsorption of OLs. An increase in the charge density of OLs induced kaolin particles with more negative surface charge density, while increase in molecular weight of OLs had a marginal impact on the surface charge density of kaolin particles.

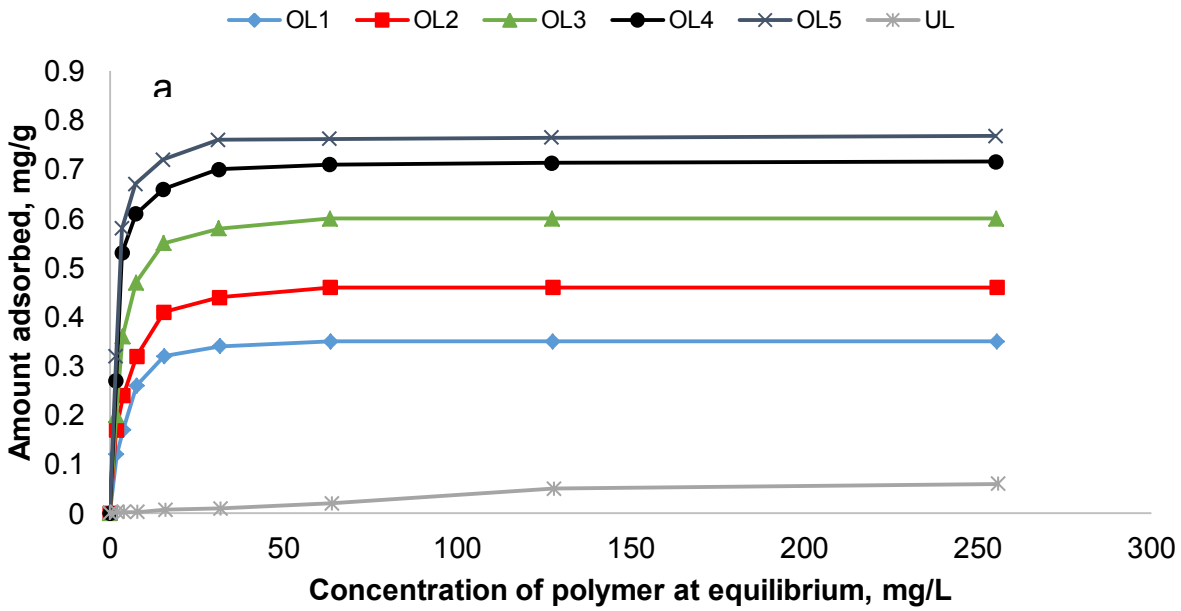

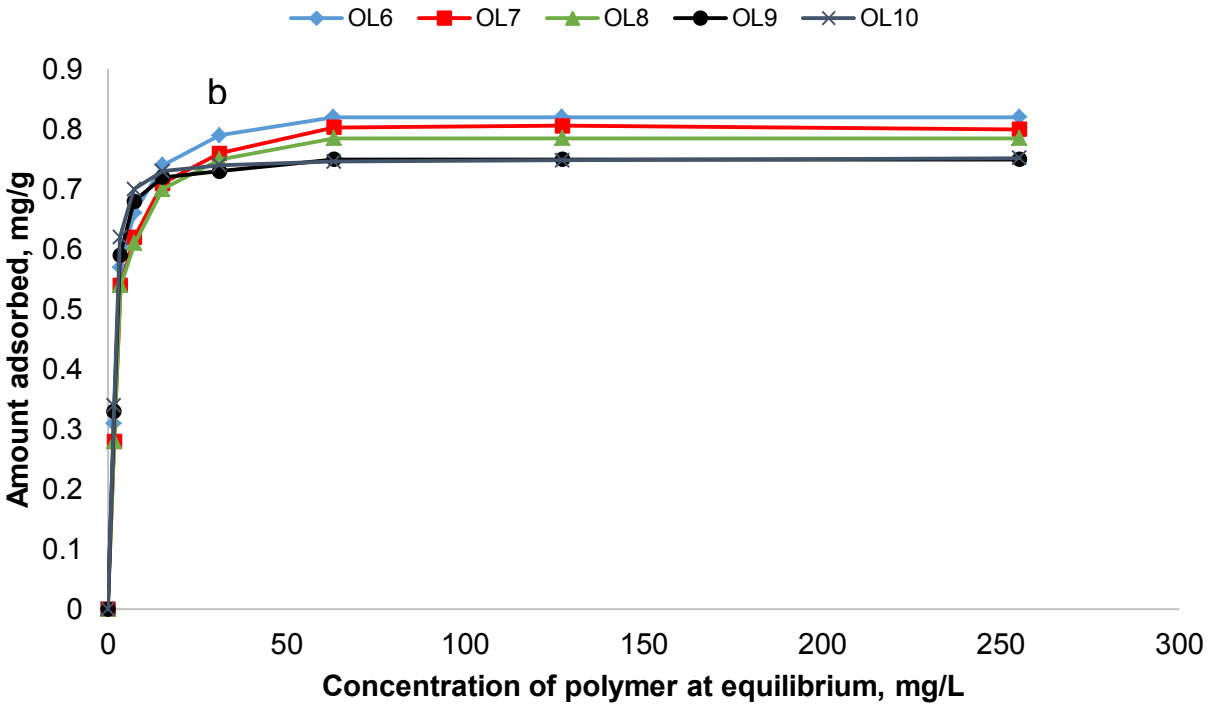
OL6
OL7
OL8
OL9
OL10
b
Amount adsorbed, mg/g
0.9
0.8
0.7
0.6
0.5
0.4
0.3
0.2
0.1
0
0
50
100
150
200
250
300
Concentration of polymer at equilibrium, mg/L

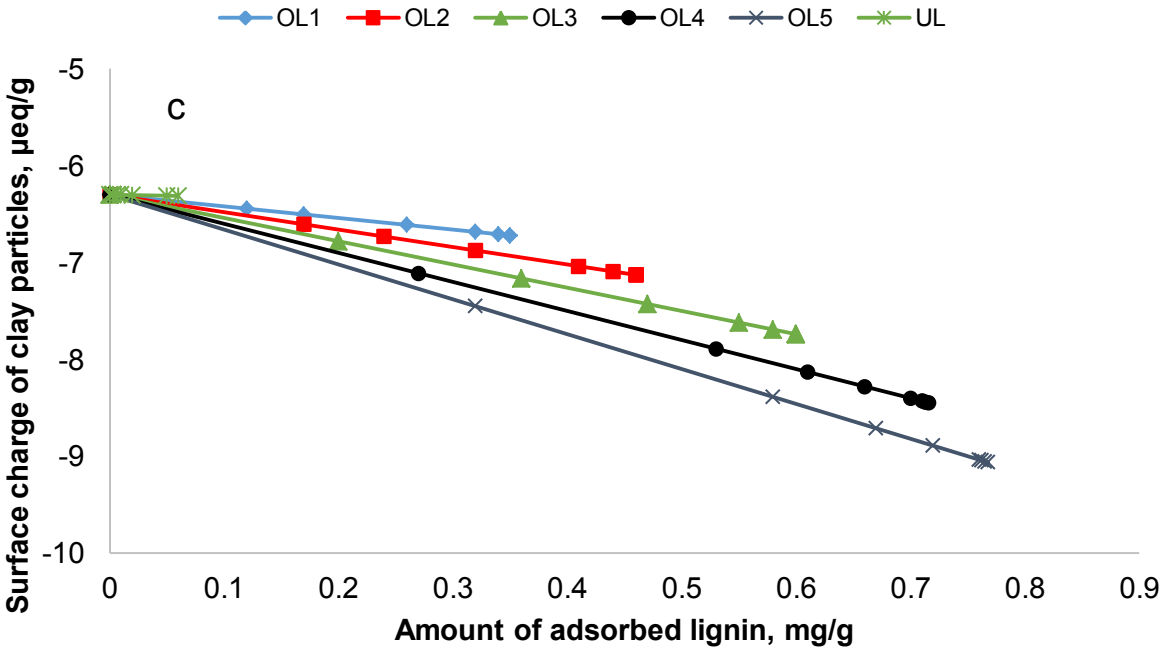
OL1
OL2
OL3
OL4
OL5
UL
c
Surface charge of clay particles, µeq/g
-5
-6
-7
-8
-9
-10
0
0.1
0.2
0.3
0.4
0.5
0.6
0.7
0.8
0.9
Amount of adsorbed lignin, mg/g

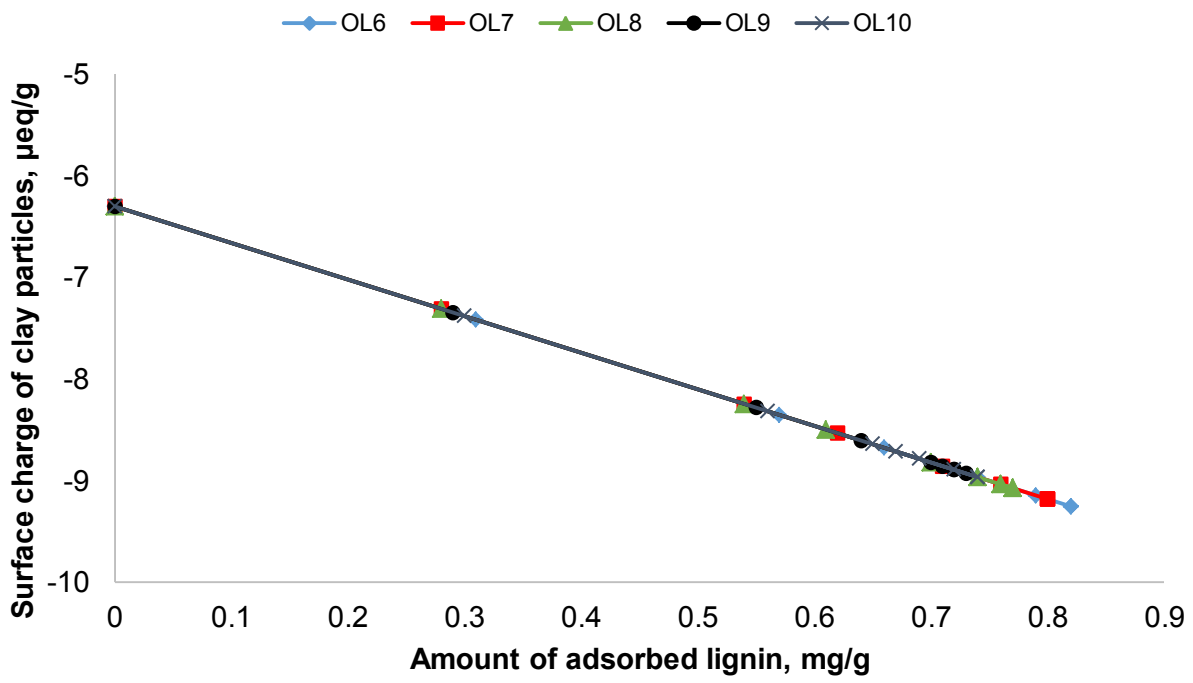


Figure 6-1: Adsorption isotherms of OLs as a function of OL or UL concentration in the presence of a) OLs with molecular weight of 26,000 g/mol but with different charge densities, b) OLs with a charge density of 3.6 meq/g but with different molecular weights. Theoretical surface charge density of kaolin particles as a function of adsorbed amounts of lignin in the presence of c) OLs with a molecular weight of 26,000 g/mol but with different charge densities, d) OLs with a charge density of 3.6 meq/g but with different molecular weights studied under the conditions of 30 °C, pH 7 and 2 g/L kaolin dosage.

### 6.4.3 Zeta potential analysis

Figures 6.2a and 6.2b present the effect of polymer dosage on the zeta potential of kaolin particles in the absence and presence of UL and OLs. The zeta potential of kaolin suspension was reduced as the dosage of OL was increased in the suspensions. The effect of UL was found to be insignificant on zeta potential of the suspensions. OL6 with the charge density of 3.6 meq/g and molecular weight of 11,654 g/mol led to the maximum decrease in the zeta potential of kaolin particles from -22 to -56 mV. This behavior is due to its maximum adsorption on the kaolin surface (Figures 6.1a and 6.1b). An increase in the charge density of OLs resulted in a significant decrease in zeta potential. OLs have more carboxylate group when their charge density was higher (Table 6.1) causing the OLs to introduce more negative charges on kaolin

surface. In the past, Boisvert and co-authors reported that the reduction in zeta potential of titanium dioxide particles was attributed to the increased adsorption of sodium polyacrylate on titanium dioxide particles [42]. In another study on the stabilization of raw porcelain suspensions using acrylic copolymers, the zeta potential of the suspension was reduced to -60 mv with an increase in dispersant dosage from 1 to 250 mg/L [4]. It is also observable that OL with different molecular weights did not alter the zeta potential of the suspensions (Figure 6.2) as their adsorption amounts were similar (Figure 6.1).

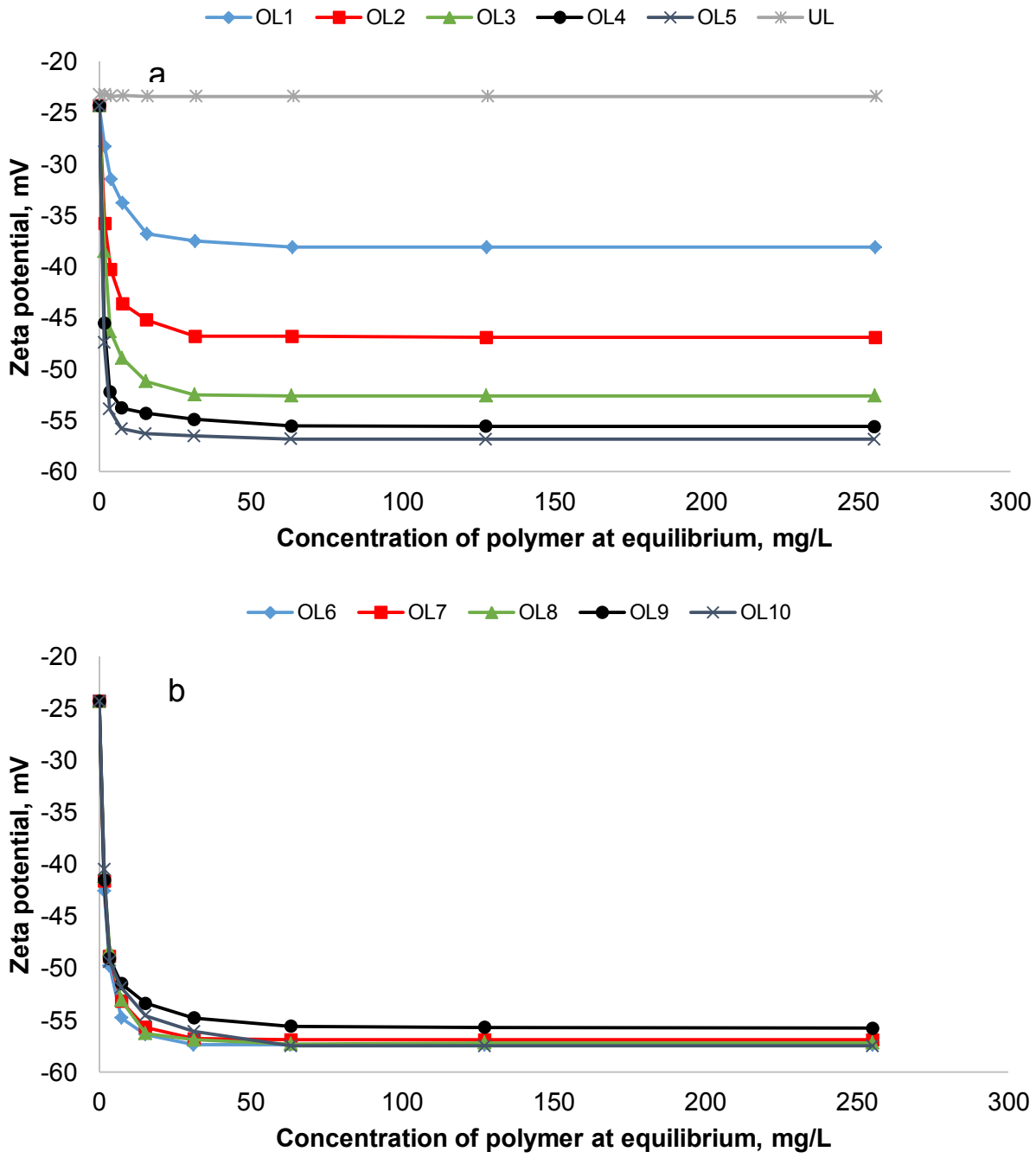


Figure 6-2: Zeta potential of kaolin suspension as a function of polymer concentration in the presence of a) OLs with varied charge densities but with 26,000 g/mol molecular weight, b) OLs with varied molecular weights but with 3.6 meq/g charge density studied under the conditions of 30 °C, pH 7 and 2 g/L kaolin dosage.

To understand if the zeta potential of kaolin particles is affected by the charges of particles or by diffused OL layer surrounding the particles in the suspension, the zeta potential of kaolin

suspension can be plotted against the theoretical surface charge of kaolin particles. Figures 6.3a and 6.3b shows the zeta potential of the kaolin suspension as a function of the theoretical surface charge density of kaolin particles in the presence of OLs. The zeta potential of kaolin particles was -24 mV when its surface charge density was -6 µeq/g (kaolin particles with no OLs adsorption) at pH 7. With decreasing the surface charge density of kaolin particles, as a result of more OL adsorption on positive sites on kaolin surface, the zeta potential of kaolin particles was also found to decrease. OL with a more negative charge density decreased the zeta potential of particles to a greater extent, as it adsorbed more. However, OL with different molecular weights impacted the zeta potential and theoretical charge density of particles similarly. The results depict that the charge density and molecular weight of OLs minimally affected the surface charge-zeta potential correlation, but OLs with more adsorption affinity had a greater influence on the surface charge density and zeta potential of kaolin particles. Furthermore, points "*s*" on Figure 6.3a and 6.3b represents that the zeta potential of kaolin particles depends on surface charge introduced by the adsorbed amount of OLs, and not by the unadsorbed OLs that were present in the suspension. This indicates that both zeta potential and surface charge density of kaolin particles were interrelated and only depend on adsorbed amount of OLs.

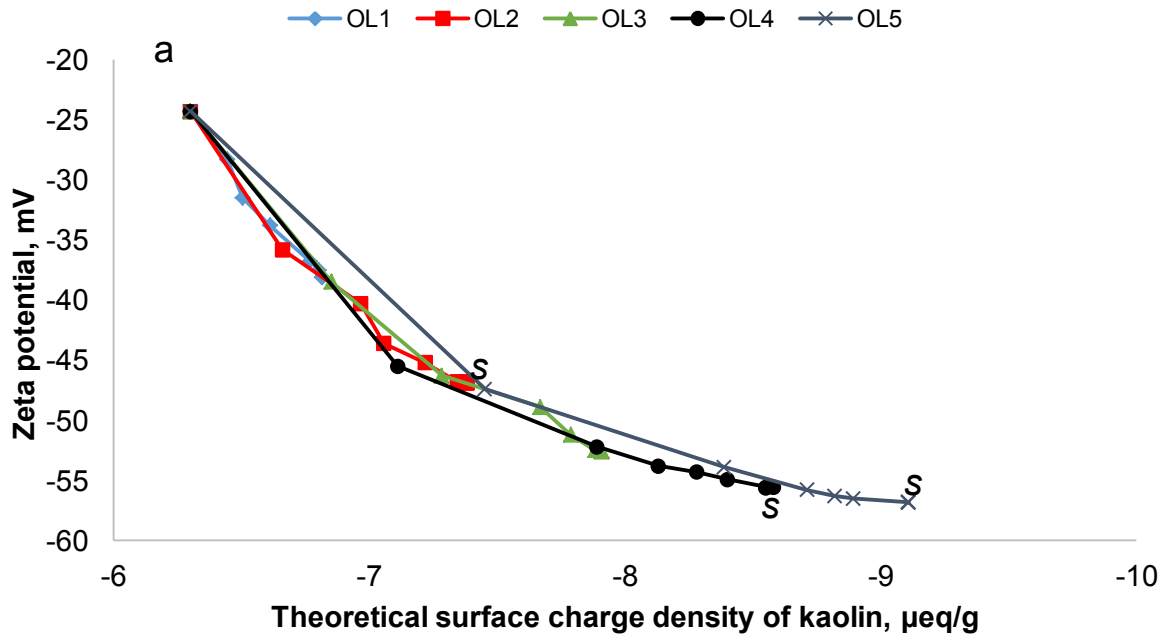

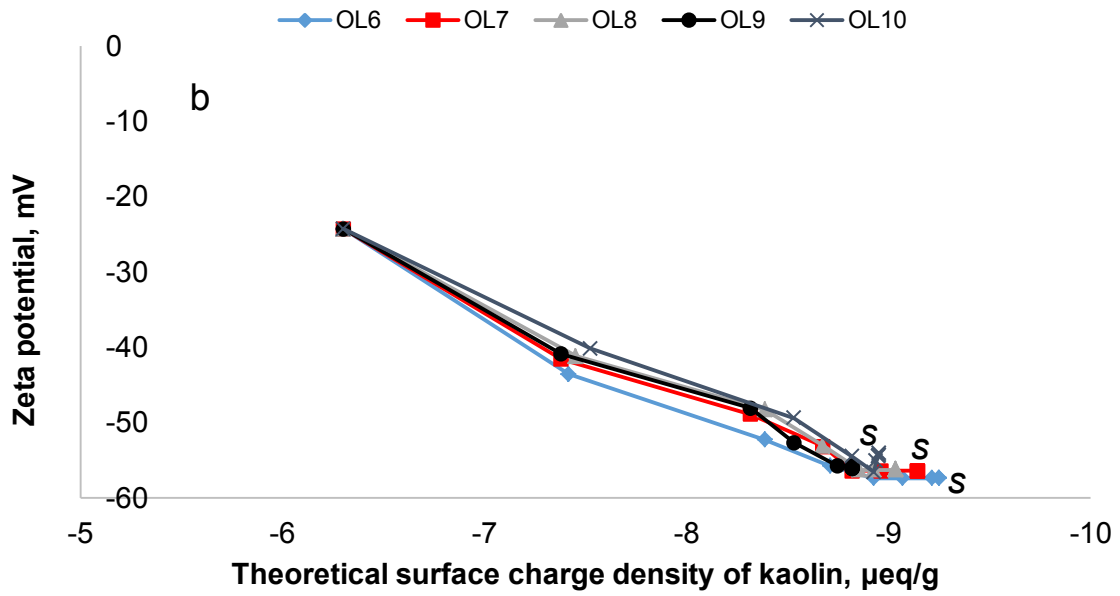


Figure 6-3: Zeta potential of kaolin suspension as a function of theoretical surface charge density of kaolin particles in the presence of a) OLs with varied charge densities but molecular weight of 26000 g/mol, and b) OLs with varied molecular weights but a charge density of 3.6 meq/g studied under the conditions of 30 °C, pH 7 and 2 g/L kaolin dosage.

### 6.4.4 Dispersion studies

#### 6.4.4.1 Impact of OLs charge density and molecular weight on the relative turbidity of kaolin suspensions under dynamic conditions

Figure 6.4 presents the relative turbidity of kaolin suspensions as a function of OL dosage. The relative turbidity of the kaolin suspension was improved as the charge density of OL increased (Figure 6.4a). Kaolin suspensions containing OL5 exhibited the maximum relative turbidity of 1.3 at 16 mg/g dosage. This is because, OL5 with high charge density induced more electrostatic repulsion between the kaolin particles by adsorbing more on the kaolin particles (Figures 6.1a and 6.1b). Figure 4a also depicts that low charged OLs (e.g. OL2) needed a higher dosage to improve the relative turbidity. Jiang and co-authors also stated that sodium poly(acrylic acid-co-maleic anhydride-co-itaconic acid) with a higher charge density (-6.6 meq/g) produced a more stable ceramic dispersion [43].

In Figure 6.4b, the dosage increase from 1 to 16 mg/L of OL6, OL7, and OL8 amplified the relative turbidity of kaolin suspensions containing polymers to 1.28, 1.3 and 1.31, respectively. This is possibly due to increase in steric repulsion between the particles as they adsorbed on

kaolin particles. In one study, the dispersibility of $TiO_2$ suspensions was increased with an increase in the molecular weight of sodium lignosulfonate (4 g/L) to 30,000 g/mol, which was ascribed to increase in steric repulsion forces [3]. Interestingly, OLs with a higher molecular weight (e.g. OL9 and OL10) increased the relative turbidity at a low dosage, but the improvement in relative turbidity was hampered at a high dosage. As these OLs had a relatively higher molecular weight and thus sizes (Table 6.1), they could interact with more than one kaolin particles via bridging upon adsorption. The higher adsorption of these OLs improved the possibilities for this interaction. Therefore, the less improvement in relative turbidity at a higher dosage of these OLs is most likely due to the bridging and thus flocculation affinity of these OLs on kaolin particles at a high dosage. A similar phenomenon was observed on the dispersion of coal water slurries (CWS) using sodium polystyrene sulphonate (SPS), CWS, where the maximum stability was obtained for SPS at a concentration of 64 mg/L [44].

These results suggest that charge density, molecular weight and concentration of OLs significantly affected the relative turbidity and thus the dispersibility of OLs in kaolin suspensions.

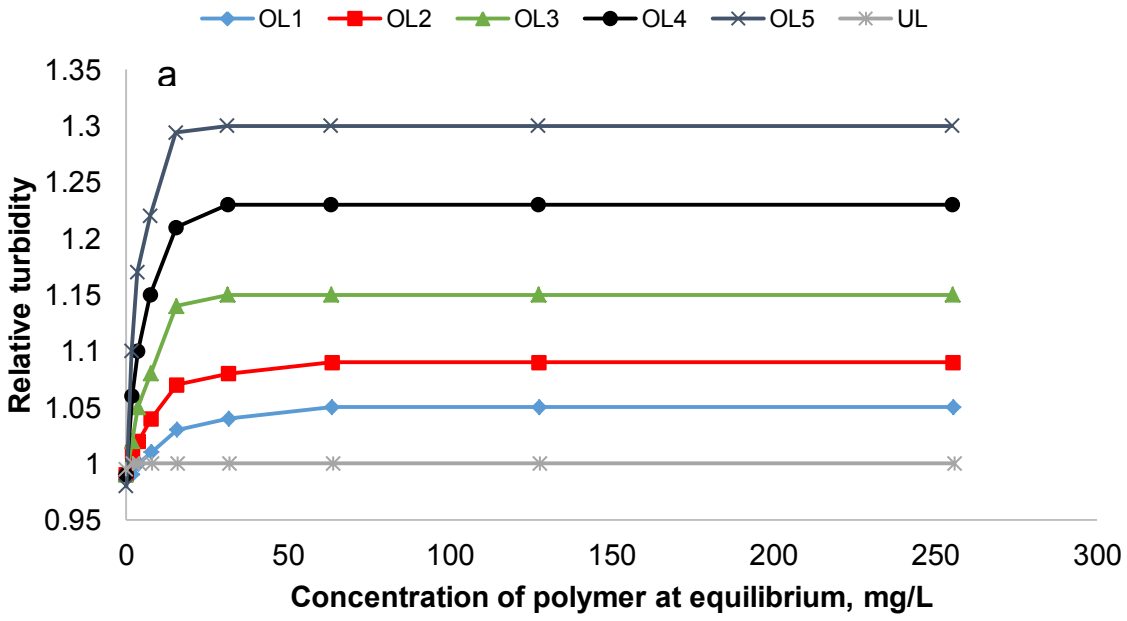

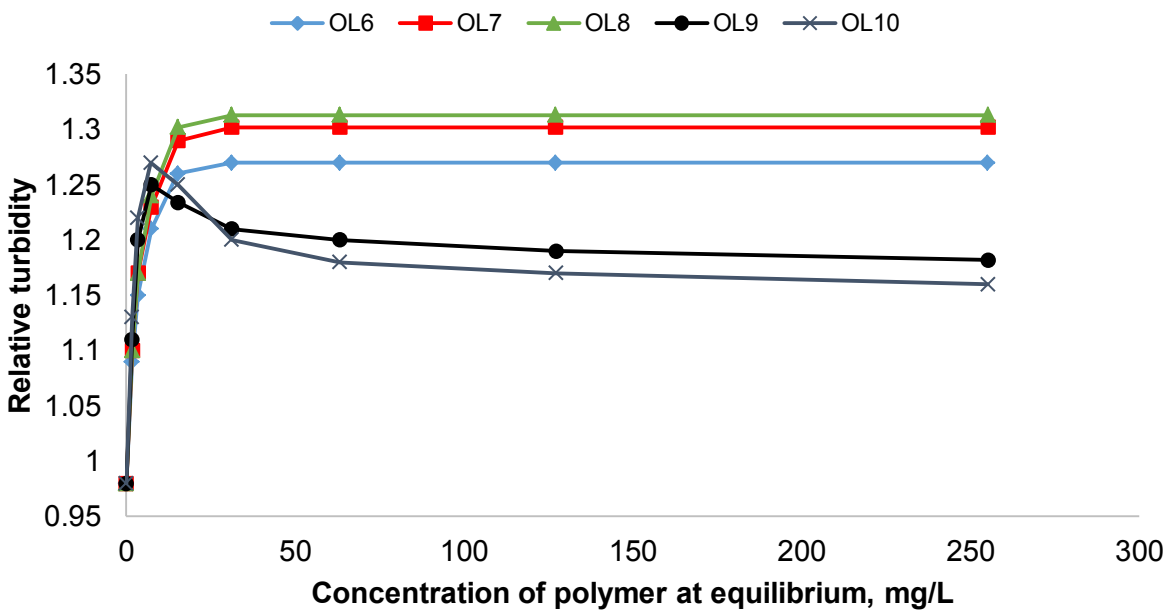


Figure 6-4: Relative turbidity of kaolin suspension as a function of OL concentration in the presence of a) OLs with varied charge densities and 26,000 g/mol molecular weight and b) OLs with varied molecular weights and 3.6 meq/g charge density studied under the conditions of 30 °C, pH 7 and 2 g/L kaolin dosage.

#### 6.4.4.2 Impact of OLs charge density and molecular weight on the size of kaolin particles under dynamic conditions

The addition of dispersants to colloidal solutions causes a dramatic decrease in size of particles by minimizing the aggregation of particles [45]. Analysis of kaolin particle size in the suspensions is crucial in determining the dispersibility of colloidal suspensions. Figures 6.5 show the impact of charge density and molecular weight of OLs on the size of kaolin particles as a function of OL dosage. The results showed that by increasing the dosage of OLs the size of kaolin particles was reduced. With increasing the charge density (OL1 to OL5), the size of kaolin particles decreased significantly. The size of particles dropped the most via adding OL with the highest charge density of 3.6 meq/g (OL5). The decrease in size of kaolin particles may provide evidence for improvement in the dispersion of kaolin particles. In one study, the dispersion of red kaolin based ceramic suspensions decreased with increasing the dosage of starch from 0.1 to 0.8 wt.% as evidenced by particle size changes from 2.8 to 1.5 µm at pH 7 [46].

Figure 6.5b presents the influence of OLs molecular weight on the size of kaolin particles. Interestingly, a dosage of 16 mg/g OL was sufficient to reduce the size of particles, and a higher dosage (specially for OL9 and OL10) had a negative impact on the size of particles. These

results also support the trend observed in the relative turbidity analysis in Figure 6.4. In a study on the stabilization of kaolin suspensions using polyacrylic acid (PAA) PAA with the molecular weight of 1800 g/mol was effective in dispersing particles [47].

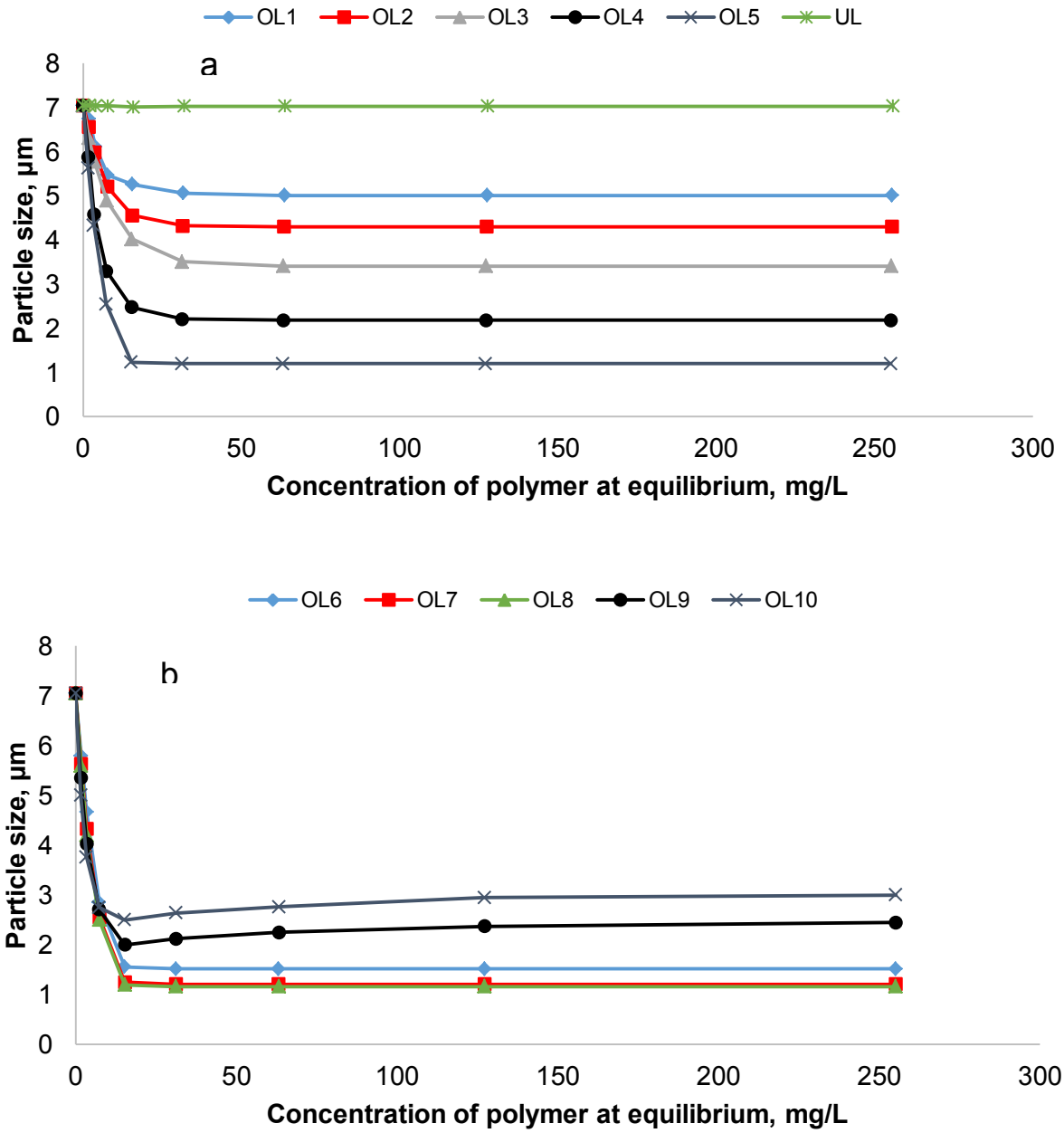


Figure 6-5:a) Effect of concentration of OLs having a similar molecular weight of 26,000 g/mol but with different charge densities and b) effect of concentration of OLs having a similar charge density of 3.6 meq/g but with different molecular weights on the particle size of kaolin conducted under the conditions of 30 °C, pH 7 and 2 g/L kaolin dosage

Figure 6.6 present the relative turbidity of the kaolin suspension as a function of theoretical surface charge density of particles. As seen in Figure 6.6a, the decrease in surface charge density of kaolin particles led to an increase in the relative turbidity. At the same amount of OL adsorption, the OL with the higher charge density improved the relative turbidity of the suspension more greatly. As the theoretical surface charge density of kaolin particles increased, more repulsion was introduced between particles, which increased the relative turbidity of the suspension.

Figure 6.6b depicts the relative turbidity of kaolin suspension as a function of theoretical surface charge density of kaolin particles. It is observable that the increase in the surface charge density of particles increased the repulsion force between the particles and in turn improved the relative turbidity. As these OLs had a similar charge density, they modified the surface charge density f the particles in a similar fashion, which resulted in a similar relative turbidity behavior. This is a confirmation that the change in the surface charge density of particles was indeed a crucial factor in relative turbidity change of the suspension. However, with the molecular weight of OLs were high (and thus their hy was larger), the increase in the relative turbidity of the particles was hampered when the dosage of OL was higher than 0.7 mg/g. This indicates that the larger OLs may also develop bridging that hampered their affinity in dispersing kaolin particles.

These results indicate that the performance of OL9 and OL10 was dosage dependent. At the adsorbed amount of 0.7 mg/g, the amount of OL polymers on kaolin particles was sufficiently high to bridge kaolin particles. The last points on each curve show the relative turbidity of kaolin suspensions when the maximum adsorption amount (i.e. saturation adsorption) was achieved (Figure 6.1). For these points (point *s* on Figure 6.6a ad 6.6b), the total adsorption amount was similar, but the amounts of unadsorbed OLs remained in the suspensions were different. These results confirm that, the amount of adsorbed OLs (and not the amount of unadsorbed OLs in suspensions) played a major role in the relative turbidity of kaolin suspension.

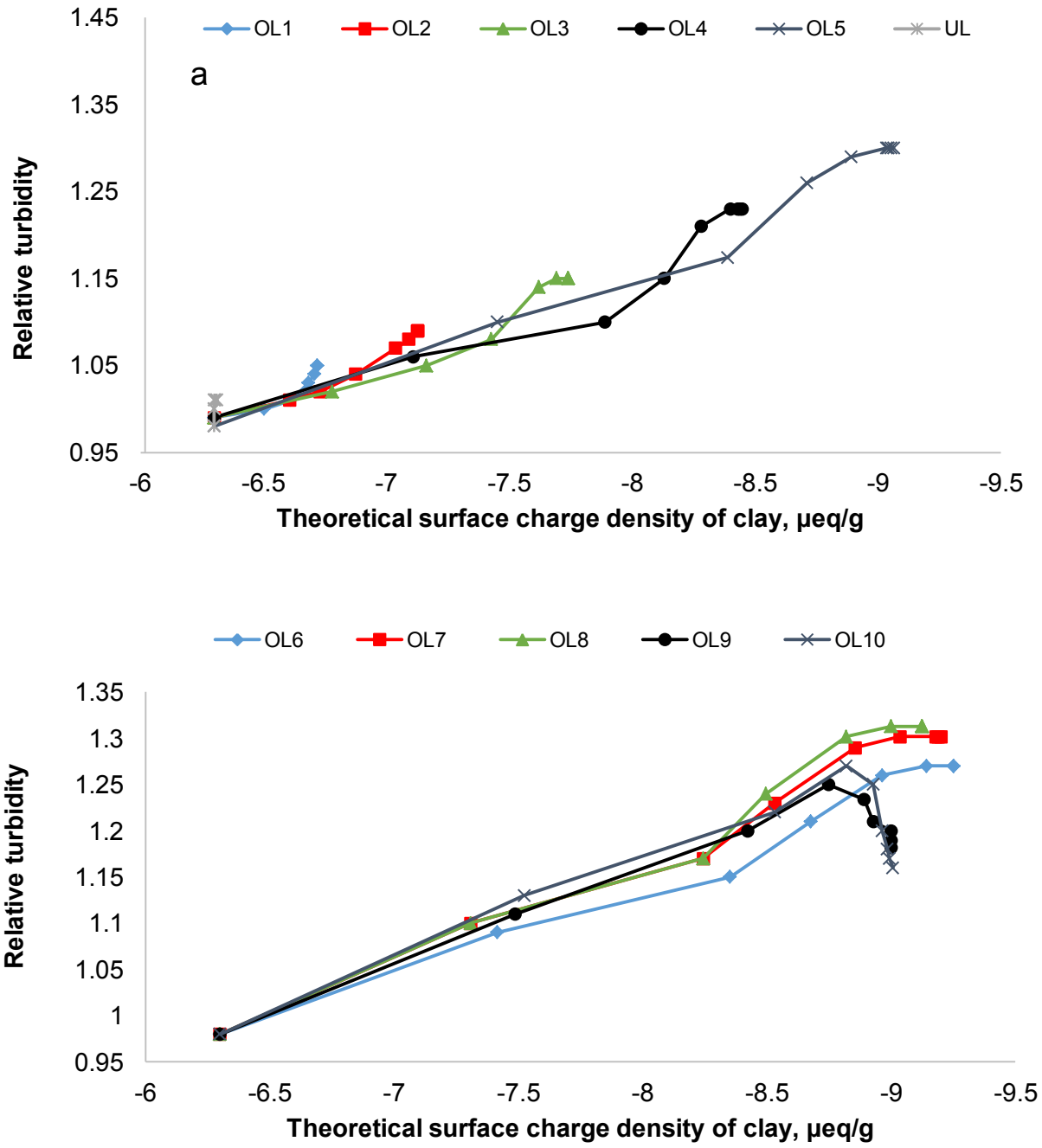


Figure 6-6: Relative turbidity of kaolin suspension as a function of adsorbed amount of lignin in the presence of a) OLs with varied charge densities and a molecular weight of 26,000 g/mol and b) OLs with varied molecular weights and a charge density of 3.6 meq/g studied under the conditions of 30 °C, pH 7 and 2 g/L kaolin dosage.

To further determine the mechanism of OLs in dispersing kaolin suspensions, the relative turbidity of kaolin suspension was studied as a function of zeta potential in Figure 6.7. For OLs

with different charge densities (Figure 6.7a), the relative turbidity of the kaolin suspensions found to increase continuously with the reduction in zeta potential of kaolin suspension, which indicates that these OLs dispersed kaolin particles via charge repulsion mechanism. As similar trend was observed for OL6, OL7 and OL8 with different molecular weights (Figure 6.7b). In case of OL9 and OL10, the increase in zeta potential change did not improve the relative turbidity. This means that the increase in the repulsion between particles was not sufficiently high to overcome the bridging effect of OL9 and OL10. Therefore, within the range studied, both charge density and molecular weight play significant roles in dispersion of kaolin suspensions.

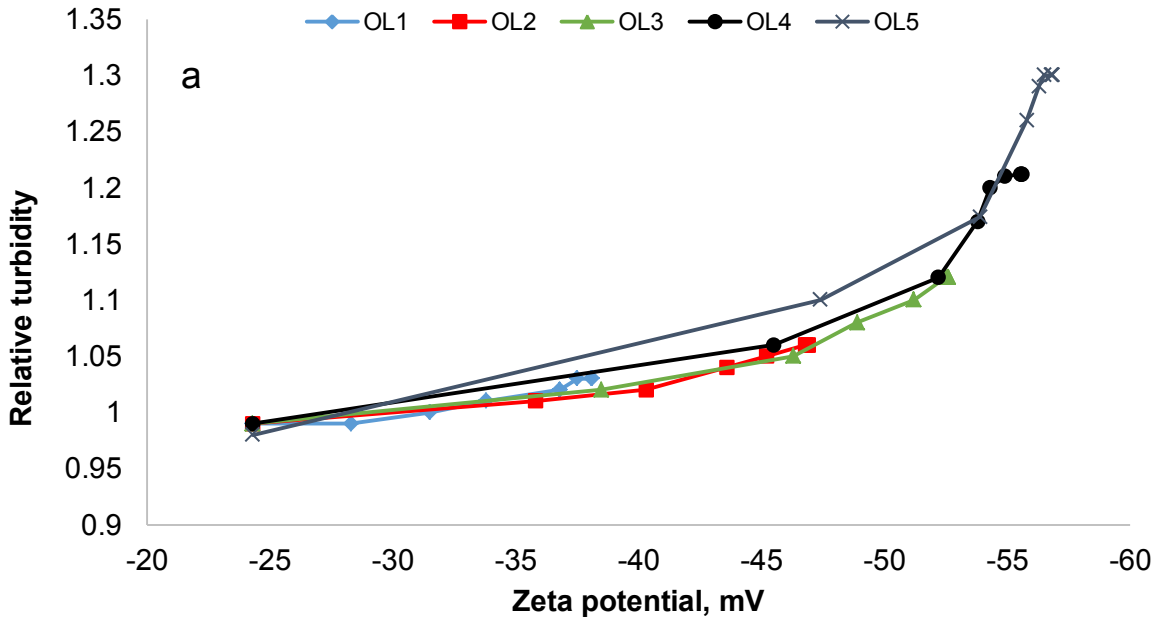

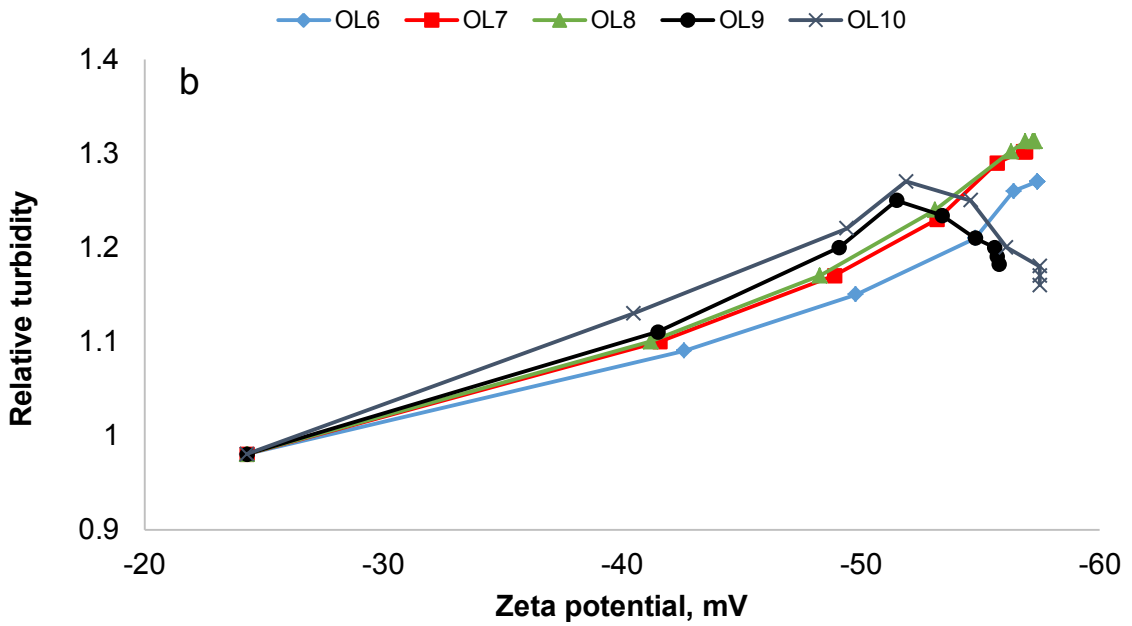


Figure 6-7: Relative turbidity of kaolin suspension as a function of zeta potential in the presence of a) OLs with varied charge densities and a molecular weight of 26,000 g/mol, and b) OLs with varied molecular weights and a charge density of 3.6 meq/g studied under the conditions of 30 °C, pH 7 and 2 g/L kaolin dosage.

#### 6.4.4.3 Impact of OLs charge density and molecular weight on the stability of kaolin particles under static conditions

Figure 6.8 shows the destabilization index of clay suspension in the presence of OLs. Increase in charge density of OL improved the stability of clay particles, which is evident from reduction in destabilization index (Figure 6.8a). OL5 with high charge density exhibited maximum reduction in destabilization index up to 0.2 at 16 mg/L dosage. As can be seen, OLs with low charge density need high dosage to increase the stability of clay particles. These results lead to postulate that, stabilization of clay particles may followed electrostatic repulsion mechanism due to introduction of negative charges by the OLs. UL has no effect on stability of clay particles, because of low charge density. Previously, anionic polyacrylamide (APAM), with high charge density (-4.2 meq/g) stabilized kaolin particles better than APAM with low charge density (-1.8 meq/g), which was attributed to maximum adsorption of high charge APAM on clay surface [19].

Figure 6.8b represents influence of molecular weight of OLs on destabilization index. All OLs (OL6-OL10) exhibited increase in stability of clay particles with dosage up to 16 mg/L. The clay

particles tend to stabilize more with molecular weight, possibly due to increased steric repulsion forces. OL6, OL7 and OL8 with increasing molecular weights stabilized the clay particles effectively, which is evident from reduction in destabilization index to 0.07. In case of high molecular weight OLs (OL9 and OL10), the destabilization index is lower than OL8 at 8 mg/L polymer concentration. However, high concentrations resulted in lower stability (increase in destabilization index up to 2.5 and 3.3 respectively) Similar trend was also observed under dynamic conditions with decreased relative turbidity of clay suspensions at higher dosages of OL9 and OL10. Lentz and co-authors demonstrated that, the efficacy of clay particles stabilization decreased with increasing molecular weight of anionic polyacrylamide (10 mg/L) [48]. These results suggest that, both molecular weight and charge density of OLs has a strong influence on stabilization of clay particles

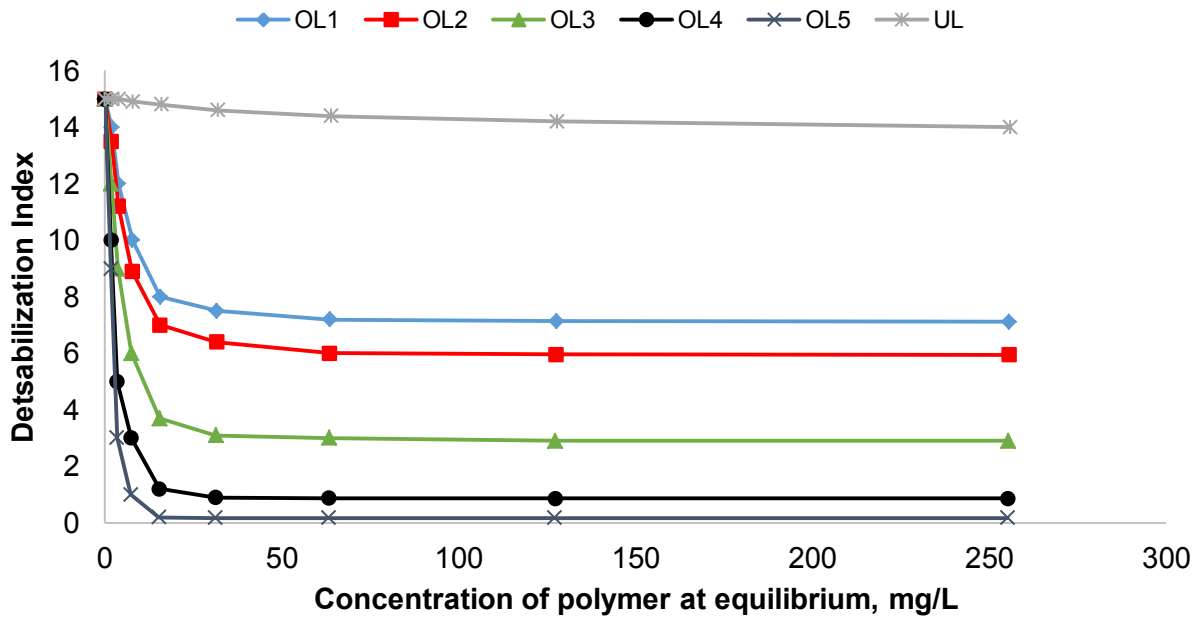

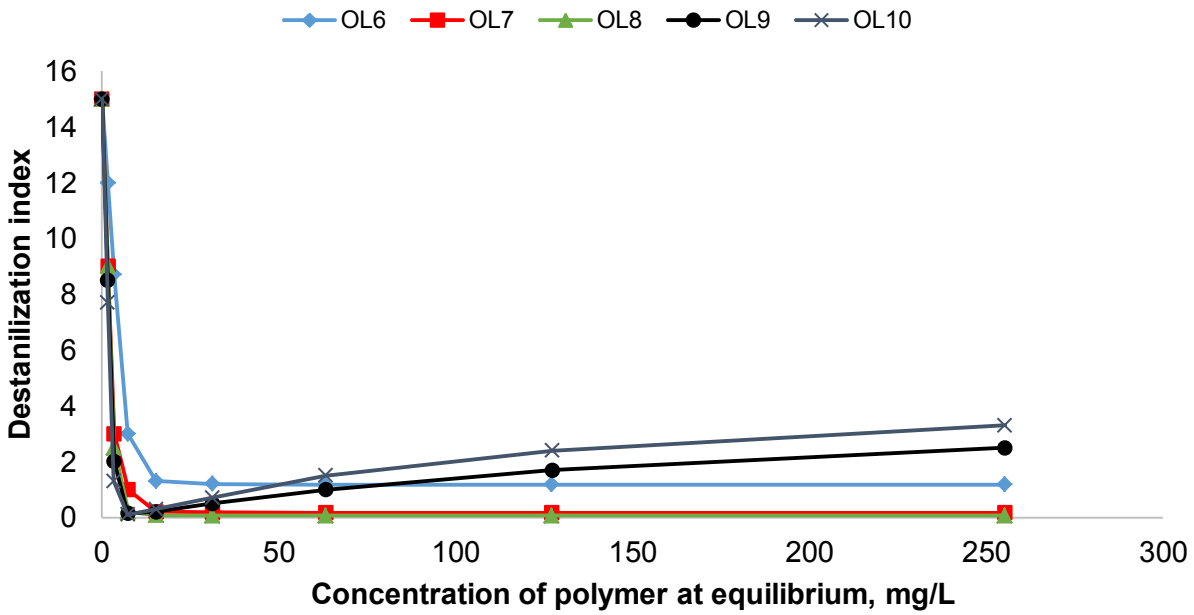


Figure 6-8: Destabilization index of kaolin suspension as a function of polymer concentration in the presence of a) OLs with varied charge densities and a similar molecular weight and b) OLs with varied molecular weights and a similar charge density studied under the conditions of 30 °C, pH 7 and 2 g/L kaolin dosage.

#### 6.4.4.4 Impact of OLs charge density and molecular weight on the size of kaolin particles under static conditions

Figures 6.9 presents influence of OLs dosage on size of kaolin particles. The reduction in kaolin particle size is observed with increase in OLs concentration up to 16 mg/L. As shown in Figure 6.9a, a higher charge density of OLs (OL1-OL5) leads to a decreased size of kaolin particles. However, UL with negligible charges exhibited insignificant reduction in particle size. This reduction in kaolin particle size can be attributed to improved dispersion of particles with OLs charge density. OL5 exhibited a maximum reduction in particle size up to 1.6 µm. Studies by Li and co-authors also confirmed that the charge of the polycarboxylate copolymer is significant in contributing to the dispersion of kaolin particles [49].

Figure 6.9b presents the impact of OLs molecular weight on size of kaolin particles. OL6, OL7 and OL8 are found to reduce the particle size up to 1.6, 1.2 and 1.0 µm, respectively, at 16 mg/L. While, OL9 and OL10 reduced the particles size up to 1.3 and 1.1 µm at 8 mg/L concentration. It is clear that, the kaolin particles dispersed more with increase in OLs molecular weight and dosage. However at higher dosages, size of kaolin particles is increased (specially with large

molecular weight polymers, OL9 and OL10). This increase in kaolin particle size is possibly due to aggregation of particles by the configuration of large size polymers at solid/liquid interface [50]. These results also supports the trend reported under dynamic conditions (Figure 6.5c).

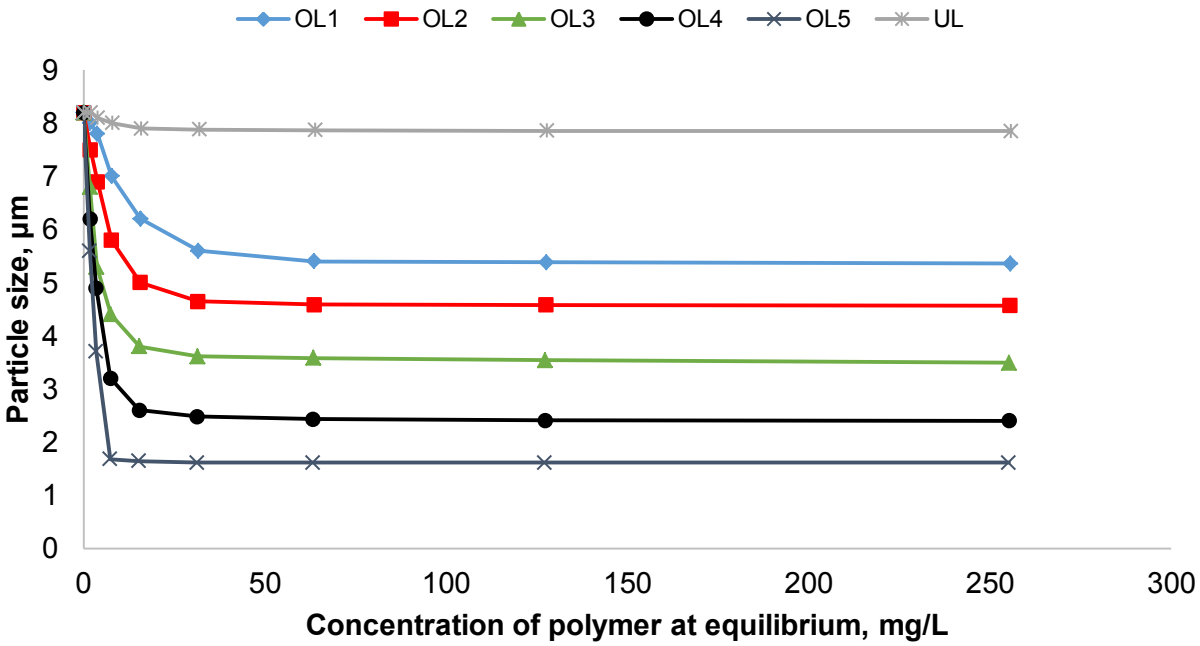

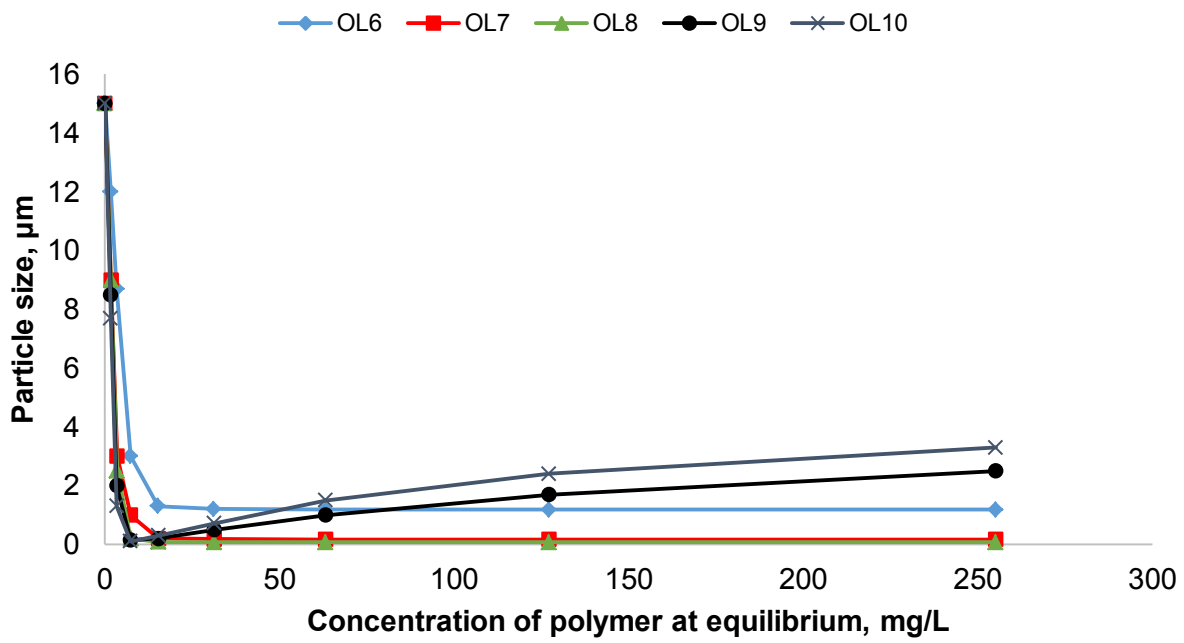


Figure 6-9: a) Effect of concentration of OLs having a similar molecular weight of 26,000 g/mol but with different charge densities and b) effect of concentration of OLs having a similar charge density of 3.6 meq/g but with different molecular weights on the particle size of kaolin conducted under static conditions of 30 °C, pH 7 and 2 g/L kaolin dosage.

### 6.4.5 Kinetic studies

To further understand the effect of charge density and molecular weight of OLs on dispersion of kaolin particles, the kinetics of kaolin particle size in the presence of OLs is studied under static conditions. Figure 6.10 presents the influence of charge density and molecular weight of OLs (128 mg/L) on kaolin particle size as a function of time. The kaolin suspension exhibited insignificant decrease in kaolin particle size as time elapsed to 60 min in the presence of UX. All the three OLs (OL1, OL5 and OL 10) reduced the particle size with time extension up to 60 min. OL1 reduced the particle size to 5.4 µm, while OL5 and OL10 reduced the particle size to 0.3 and 2.4 µm respectively with time extension up to 60 min. The minimal decrease in kaolin particle size by OL1 with time is due to its low charge density, which is also evident from Figure 6.9. On the other hand OL5 with high charge density enhanced the dispersion of kaolin particles by introducing more negative charges on kaolin as time progress. In case of OL 10, even though the size of kaolin particles reduced with time, the overall reduction in size is less than OL5. This is because, adsorption of high molecular weight OL10 with time results in entanglement of long

polymers chains in the suspension, and the possible bridge flocculation may counteracted the electrostatic repulsion between the particles [51].

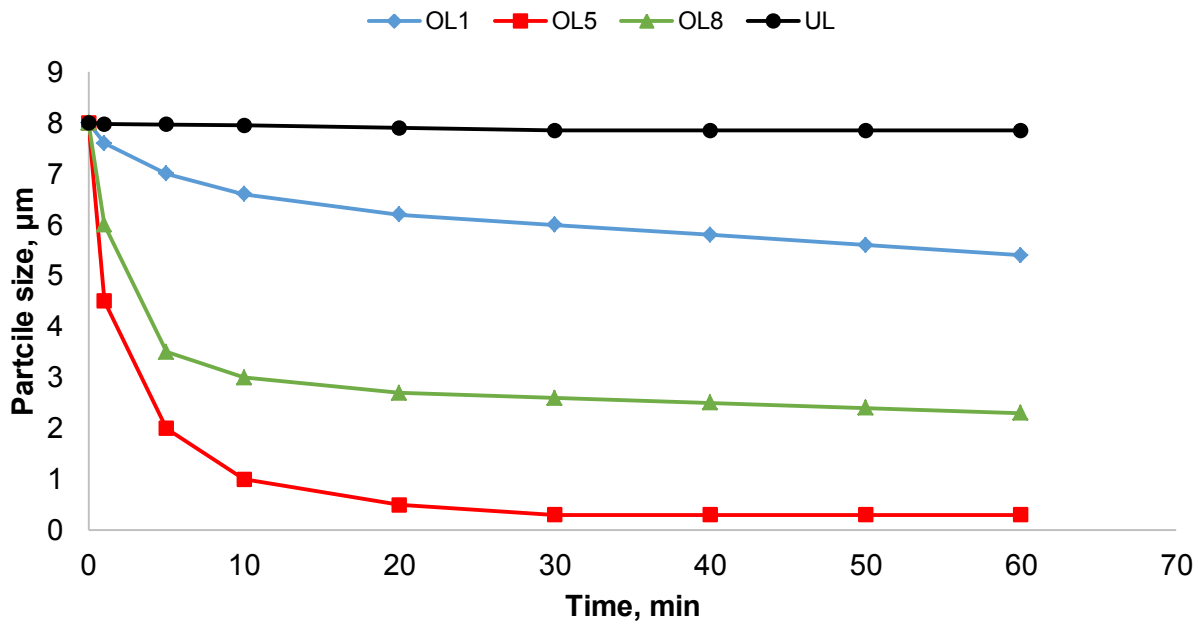


Figure 6-10: Effect of molecular weight and charge density of OLs on kaolin particle size as a function of time.

## 6.5 Conclusions

The adsorption of OLs on kaolin particles was influenced by charge density. OL6 having charge density of 3.6 meq/g and molecular weight of 11,000 g/mol showed the maximum adsorption of 0.81 mg/g on kaolin surface at 32 mg/g OL concentration. The amount of OL adsorbed affected the zeta potential and relative turbidity of kaolin suspensions. The zeta potential of kaolin particles is directly affected by the charge density of OLs, while molecular weight has no significant affect. Both charge density and molecular weight of OLs affected relative turbidity and size of kaolin particles under dynamic conditions. The maximum relative turbidity of 1.3 was obtained with OL8 having charge density (3.6 meq/g) and molecular weight (30,243 g/mol) at 16 mg/L dosage and pH 7. Dispersion studies under static conditions also proved that the stability of kaolin particles is affected by both charge density and molecular weight of OLs. Kinetic studies under static conditions confirms that the dispersion of kaolin particles with OLs improved with charge density, while molecular weight has negative effect. The results suggest

that polymer dosage, charge density and molecular weight of OLs had a great influence on stabilization of kaolin particles.

### 6.6 References


1. Sofra F, Boger DV. Environmental rheology for waste minimisation in the minerals industry. Chemical Engineering Journal, 2002, 319-330.
2. Penkavova V, Guerreiro M, Tihon J, Teixeira J. A. C. Deflocculation of kaolin suspensions – the effects of various electrolytes. Applied Rheology, 2015, 2524151-24160.
3. Yang D, Qiu X, Pang Y, Zhou M. Physiochemical properties of calcium lignosulfonate with different molecular weights as dispersant in aqueous suspension. Journal of dispersion Science and Technology. 2008, 29, 1296-1303.
4. Marco P, Llorens J. Adsorption of some linear copolymers onto kaolin particles in concentrated suspensions. Colloids and Surfaces A: Physicochemical and Engineering Aspects, 2005, 270-271, 291-295.
5. Triaphol N, Suntako R, Chanthornthip K. Roles of polymeric dispersant charge density on lead zirconate titanate aqueous processing. Ceramics International, 2010, 36, 2147-2153.
6. Zaman A, Tsuchiya R, Moudgil BM. Adsorption of low molecular weight polyacrylic acid on silica alumina and kaolin. Journal of Colloid Interface Science. 2002, 256, 73-78.
7. Brumbach M, Carty WM. Dispersant demand curves: effect of PAA on the viscosity of several clays. Ceramic Engineering and Science Proceedings. 2003, 24, 182
8. Papo A, Piani L, Ricceri R. Sodium tripolyphosphate and polyphosphate as dispersing agents for kaolin suspensions: rheological characterization. Colloids and Surfaces A. Physicochemical and Engineering Aspects, 2002, 201, 219-230.
9. Pawlik M. Polymeric dispersants for coal water slurries. Colloids and Surfaces A: Physicochemical and Engineering Aspects, 2006, 266, 82-90.
10. Qin Y, Yang D, Gu F, Li X, Xiaong W, Zhu JY. Biorefinery lignosulfonates as a dispersant for coal water slurry. Sustainable Chemical Processes, 2016, 4, 1-8.
11. Konduri MK, Kong F, Fatehi P. Production of carboxymethylated lignin and its application as a dispersant. European Polymer Journal. 2015, 70, 371-383.
12. Gan L, Zhou M, Yang D, Qiu X. Preparation and evaluation of carboxymethylated lignin as dispersant for aquous graphite suspension using Turbiscan lab analyzer. Journal of Dispersion Science and Technology, 2013, 34, 644-650.

13. Mekhamer WK. Al Andis N, EI Shabanat M. Kinetic study on the sedimentation behaviour of Na and Ca kaolinite suspension in the presence of polyethyleneimine. Journal of King Saudi University, 2009, 21, 125-132.
14. Lu JH, Wu L, Letey J. Effects of Soil and Water Properties on Anionic Polyacrylamide Sorption. Soil Science Society of American Journal, 2002, 66, 578–584.
15. Steven GV, Diane S, John G, Darell NL. Stability analysis of soil aggregates treated with anionic polyacrylamides of different molecular formulations. Soil Science, 2004, 169, 573-581.
16. Plank J, Hirsch C. Impact of zeta potential of early cement hydration phases on superplasticizer adsorption. Cement and. Concrete Research. 2007, 57, 537-542.
17. Sjoberg M, Bergstrom L, Larsson A, Sjostrom RE. The effect of polymer and rheology of kaolin dispersions. Colloids and Surfaces A. Physicochemical and Engineering Aspects, 1999, 159 197-208.
18. Deng Y, Dixon JB, White GN. Adsorption of Polyacrylamide on Smectite, Illite, and Kaolinite. Soil Science Society of American Journal, 2006, 70, 297-304.
19. Nasser, M. S.; James, A. E.; The effect of polyacrylamide charge density and molecular weight on the flocculation and sedimentation behaviour of kaolinite suspensions. Separation and Purification Technology, 2006, 52, 241-252.
20. Zhou Y, Gan Y, Wanless EJ, Jameson GJ, Franks GV. Interaction forces between silica surfaces in aqueous solutions of cationic polymeric flocculants: effect of polymer charge. Langmuir. 2008, 24, 10920-10928.
21. Chung YL, Ansari S, Estevez L, Hayrapetyan S, Gainnelis EP, Lai HM. Preparation and properties of biodegradable starch-clay nanocomposites. Carbohydrate Polymers. 2010, 79, 391-396.
22. Conceicao, S. I.; Velho, J. L.; Ferreira, J. M. F. Influence of carboxymethyl cellulose on rheological behaviour of precipitated calcium carbonate suspensions**.** The Ibero-American Journal of Rheology, 2004, 4, 29-38.
23. Ratinac KR, Standard OC, Bryant PJ. Lignosulfonate adsorption on and stabilization of lead zirconate titanate in aqueous suspension. Journal of Colloid Interface Science, 2004, 273, 442-454.

24. Kouisni L, Holt-Hindle P, Maki K, Paleologou M. The lignoforce system: a new process for the production of high-quality lignin from black liquor. Journal of Science and Technology for Forest products and processes, 2012, 2, 6-10.
25. He W, Fatehi P. Preparation of sulfomethylated softwood kraft lignin as a dispersant for cement admixture. RSC Advances, 2015, 5, 47031-47039.
26. Kong F, Parhiala K, Wang S, Fatehi P. Preparation of cationic softwood kraft lignin and its application in dye removal. European Polymer Journal. 2015, 67, 335-345.
27. Yu G, Li B, Wang H, Liu C, Mu X. Preparation of concrete superplasticizer by oxidation-sulfomethylation of sodium lignosulfonate. BioResources, 2013, 8, 1055-1063.
28. Li Z, Ge Y. Extraction of lignin from sugarcane bagasse and its modification into high performance dispersant for pesticide formulations. Journal of Brazilain Chemical Society**,** 2011, 22 (10) 1866-1871.
29. Kong F, Wang S, Price J, Konduri MKR, Fatehi P. Water soluble kraft lignin-acrylic acid copolymer: synthesis and characterization. Green Chemistry, 2015, 17, 4355-4366.
30. Bekhta P, Proszyk S, Krystofiak T, Lis B. Surface wettability of short-term thermo-mechanically densified wood veneers. European Journal of Wood and Wood Products*,* 2015, 73, 415-417.
31. Fengel D, Weneger G. Wood: Chemistry, Ultrastucture, Reactions. John Wiley & Sons, Inc: New York, 1983, pp. 304-310.
32. Zhang X, Liu W. Sodium titanium nanobelt as amicroparticle to induce clay flocculation with CPAM. BioResources, 2010, 5, 1895-1907.
33. Xiao X, Liu Z, Wiseman N. Synergetic effect of cationic polymer microparticles and anionic polymer on fine clay flocculation. Journal of Colloid Interface Science, 1999, 216, 409-417
34. Ovenden C, Xiao H. Flocculation behaviour and mechanisms of cationic inorganic microparticle/polymer systems. Colloids and Surfaces A: Physiochemical Engineering Aspects. 2002, 197, 225-234.
35. Mengual O, Menuier G, Cayre I, Puech K, Sanbre P. Characterization of instability of concentrated dispersions by a new optical analyzer: the Turbiscan MA 1000. Colloids and Surfaces A: Physiochemical Engineering Aspects, 1999, 152, 111-123.
36. He W, Zhang Y, Fatehi P. Sulfomethylated kraft lignin as a flocculant for cationic dye. Colloids and Surfaces A: Physiochemical Engineering Aspects, 2016, 503, 19-27.

37. Santos RB, Capanema EA, Balakshin MY, Chang HM, Jameel H. Effect of hardwood characteristics on kraft pulping process: Emphasis on lignin structure. Bioresources. 2011, 6, 3623-3637.
38. Loginov M, Larue O, Lebovka N, Vorobeiv E. Fludity of highly concentrated kaolin suspensions: Influence of particle concentration and presence of dispersant. Colloids and Surfaces A: Physiochemical Engineering Aspects, 2008, 325, 64-71.
39. Wisniewska M, Chibowski S, Urban T, Sternik D, Terpilowski K. Impact of anionic polyacrylamide on stability and surface properties of the $Al_2O_3$–polymer solution system at different temperatures. Colloid Polymer Science, 2016, 294, 1511-1517.
40. Atesok, G.; Somasundaram, P.; Morgan, L. J. Charge effects in the adsorption of polyacrylamide on sodium kaolinite and its flocculation. Powder Technology, 1998, 54, 77-83.
41. Boisvert JP, Persello J, Castaing JC, Cabane B. Dispersion of alumina coated TiO2 particles by adsorption of sodium polyacrylate. Colloids and Surfaces A: Physiochemical Engineering Aspects, 2001, 178, 187-198.
42. Jiang B, Zhou S, Ji H, Liao B, Pang H. Dispersion and rheological properties of ceramic suspensions using linear polyacrylate copolymers with carboxylic groups as superplasticizer. Colloids and Surfaces A: Physiochemical Engineering Aspects, 2012, 396, 310-316.
43. Yong-jie D, Feng G, Yong-jin L. Effect of the molecular weight of sodium polystyrene sulfonate on the properties of coal water slurry. Journal of Fuel Chemistry and Technology, 2006, 34, 3
44. Ersoy B, Evcin A, Uygunoglu G, Akdemir ZB, Brostow W, Wahrmund J.. Zeta potential-viscosity relationship in kaolinite slurry in the presence of dispersants. Arabian Journal of Science and Engineering, 2014, 39, 5451-5457.
45. Umaran MVC, Menachavez RL. Aqueous dispersion of red clay based ceramic powder with the addition of starch. Materials Research, 2013, 16, 375-384.
46. Ma X. Effect of a low-molecular-weight polyacrylic acid on the coagulation of kaolinite particles. International Journal of Mineral Processing, 2011, 99, 17-120.
47. Lentz RD, Sojka RE, Ross CW. Polymer charge and molecular weight effects on treated irrigation furrow processes. International Journal of Sediment Research, 2000, 15, 17-30.

48. Li Y, Zhang Y, Zheng J, Guo H, Yang C, Li Z, Lu M. Dispersion and rheological properties of concentrated kaolin suspensions with polycarboxylate copolymers bearing comb like side chains. Journal of European Ceramic Society, 2014, 34, 137-146.
49. Kirby GH, Harris DJ, Li Q, Lewis JA. Poly(acrylic acid)-poly(ethylene oxide) comb polymer effects on $BaTiO_3$ nano particle suspension stability. Journal of American Ceramic Society, 2004, 87 (2) 181-186.
50. Zhu Z, Li T, Lu J, Wang D, Yao C. Characterization of kaolin flocs formed by polyacrylamide as flocculation aids. International Journal of Mineral Processing, 2009, 91, 94-99.

# Chapter 7. Oxidized and sulfomethylated kraft lignin as a dispersant for coal water slurries

Mohan K. R. Konduri, Pedram Fatehi[a]

[a] Department of Chemical Engineering,
Lakehead University,
955 Oliver Road,
Thunder Bay, ON P7B 5E1, Canada

## 7.1 Abstract

In this study, oxidized and sulfomethylated lignin (OSL) with charge density of -4.4 meq/g was synthesized via treatment with nitric acid and sodium sulfite and applied as a dispersant for coal water slurry (CWS). The properties of OSL was systematically characterized using various techniques such as nuclear magnetic resonance spectroscopy (NMR) and gel permeation chromatography (GPC). The impact of the produced OSL and commercial lignosulfonate, lignosulfonic acid sodium salt (LSS), on coal with different particle sizes was fundamentally investigated. The results show that the size of particles greatly impacted the adsorption of OSL and LSS and thus their influences on the rheological and stability of the coal suspension. The maximum adsorption of OSL and LSS was found to be 0.96 mg/g and 0.68 mg/g on coal A with the minimum particle size of 22 μm. OSL improved the wettability of coal better than LSS, irrespective of particle size. The interfacial tension between coal and OSL and between coal and LSS reduced from 17 mN/m to 13 mN/m and 14 mN/m, when maximum of OSL and LSS of 0.96 and 0.68 mg/g was adsorbed on coal A. This maximum adsorption led to the maximum zeta potential drop from -30 mV to -47 mV for OSL and from -30 mV to -41 mV for LSS. The adsorption of OSL and LSS rendered the behavior of coal suspension more pseudo plastic. The viscosity of coal particles dropped from 1350 to 520 mPa.s when OSL (64 mg/L) was used and from 1365 to 670 mPa.s when LSS (64 mg/L) was used. The stability of coal particles was also increased as observed via reduction in destabilization index of coal particles from 4 to 0.2 for OSL (64 mg/L) and from 4 to 1.1 for LSS (64 mg/L). These results confirm that the produced OSL was a more effective dispersant than commercial lignosulfonate for coal water slurry.

Keywords: coal, lignosulfonate, sulphomethylated lignin, dispersants, biorefining

## 7.2 Introduction

Recently, the indiscriminate use of oil and its derived products have led to energy depletion [1, 2]. Numerous studies have reported alternative energy sources, such as biodiesel [3], hydrogen fuel [3], biofuel [4] and coal water slurry (CWS) for industrial use [5]. CWS seems to be a promising fuel due to its low production cost and ease of handling, and thus may be considered as an efficient alternative for replacing fossil fuels [6]. For CWS to be an effective fuel, it should have high coal content for heat demand and moderately low viscosity for storage and transportation [7, 8]. However, coal particles may not remain stable in slurry due to increased interactions between the coal particles, which would lead to a high apparent viscosity of CWS

(30-70 wt.%) that may exceed permissible range needed for its storage [9, 10]. The addition of chemicals, such as dispersants, can minimize the interaction of particles and improve the rheological behavior of the slurries, thus improving the performance of CWS as fuel.

Numerous chemical and synthetic polymeric dispersants have been studied for coal water slurries in the past [11, 12]. However, their non-biodegradable and toxic nature are their main barriers [13]. Recently, the products obtained via modification of kraft lignin found application as dispersants in many areas [14, 15]. In one study, sulfomethylated kraft lignin produced via treating alkali lignin with sodium sulfite and formaldehyde improved the dispersion efficiency of red dye by 98 % at a dosage of 0.6 wt.% [16]. Alternatively, anionic lignin-based product obtained via chemical modification of hardwood kraft lignin with sodium chloroacetate improved the dispersion efficiency of clay suspensions (20 g/L) by 50 % at the dosage of 0.2 wt.% [17]. In a study on the dispersion of dimethomorph pesticide granules in an aqueous medium, kraft lignin-polyethylene glycol copolymer at 2.5 wt.% dosage decreased the viscosity of suspension from 1000 to 100 mPa.s [18]. However, the application of lignin-based dispersants in coal water slurries have been rarely studied [19], which reported that dispersibility of CWS was improved up to 75 % by using lignosulfonate as a dispersant. However, kraft lignin based dispersants have not been used in CWS. The first objective of this work was to modify hardwood kraft lignin with nitric acid and sodium sulfite and study its application as a dispersant for CWS.

Recent findings [15, 20] showed that polymeric dispersants adsorb at coal/liquid interface via hydrophobic or hydrophilic interactions and affect the stability of coal particles. The main goal of adding dispersant is to minimize the particle-particle interaction either by increasing the electronegativity of the coal surface or steric repulsions or by increasing the wettability of coal particles [21]. Physicochemical factors such as dispersant dosage, surface tension of the dispersants at solid/liquid interface, functional groups associated with dispersants found to affect the interactions between the coal particles [22]. Hong and co-authors reported that polycarboxylic acid (0.5 wt.%) reduced the viscosity of coal suspensions from 1200 to 580 mPa.s via generating electrostatic repulsion between the coal particles [23]. In a study on the stabilization of CWS (50 wt.%) using polystyrene sulfonate (PSS) dispersant, the viscosity of CWS was reduced to 150 mPa.s with an increase in concentration of PSS from 1.0 to 1.8 wt.%, which was attributed to the adsorption of PSS on coal particles and thus to increase in wettability

of coal particles [24]. The second objective of this work was to study the influence of oxidized sulfomethylated lignin (OSL) on the viscosity and wettability of coal particles having different sizes and to determine the dispersibility of OSL for coal particles. As lignosulfonate was used for his purpose in the past [25, 19]. The results of this work were compared with those of commercially produced lignosulfonate as a dispersant in the CWS system.

The main novelty of this work is the investigation on the influence of oxidized sulfomethylated lignin (OSL) as a dispersant for coal particles with various sizes, and the mechanisms involved in dispersion of CWS. The OSL produced via oxidation and sulfomethylation of kraft lignin was characterized using different techniques such as $^{1}$H-NMR and gel permeation chromatography. The dispersion performance of OSL in CWS was investigated using contact angle, surface tension, rheology, stability and zeta potential studies and the results were compared with those of commercial lignosulfonate.

## 7.3 Materials & Methods

### 7.3.1 Materials:

Hardwood lignin used in the study was produced by the Lignoforce technology of FPInnovations located in Thunder Bay, ON [26]. Commercial lignosulfonic acid sodium salt (LSS), sodium sulfite (99 %), potassium nitrate (99.99 wt.%), potassium hydroxide, *Para*-hydroxybenzoic acid (PHBA) and dimethyl sulfoxide-d6 were all obtained from Sigma Aldrich Company and used as received. Bituminous coal was obtained from Fisher Scientific. Nitric acid was obtained from Sigma Aldrich company and diluted to 30 wt.% prior to use. Standard hydrochloric acid (HCl) solution (30-35 %) was obtained from Fluka analytical and used as received. Sulfuric acid (95-98 %) was obtained from Sigma Aldrich Company and diluted to 0.1 M prior to use. Cellulose acetate dialysis membrane (molecular weight cut off of 1,000 g/mol) was obtained from Spectrum Labs. Inc, USA. Polydiallyldimethylammonium chloride (PDADMAC) was obtained from Sigma Aldrich Company and diluted to 0.005 M prior to use. Potassium polyvinyl sulfate (PVSK) was obtained from Wako Pure Chemical Industries Ltd., Japan and diluted to 0.005 M prior to use.

### 7.3.2 Preparation of coal samples and CWS

Bituminous coal was ground using laboratory Micro mill, Bell Art Products (NJ, USA). The samples were then categorized into three fractions (coal A, coal B and coal C) via screening of crushed coal powder with sieve meshes (American standard testing sieves) of three different pore

openings (60, 200 and 400 mesh). The fractionated coal samples were then used to prepare coal water slurries (CWS) by mixing them in distilled water at 50 wt.% solid concentration for 24 h and 1000 rpm. The pH of the slurry was maintained at pH 7 in all the experiments.

### 7.3.3 Synthesis of oxidized and sulfomethylated kraft lignin

Oxidation and sulfomethylation of hardwood kraft lignin was performed as described previously [27]. In this experiment, 5 g of hardwood kraft lignin was mixed with 40 mL of nitric acid solution (25 wt.%) in 250 mL three neck flasks. The reaction was allowed to take place at desired temperature (100 °C) for 1 h with constant stirring at 200 rpm (i.e. optimized conditions based on the studies of He et al., 2015). After the reaction, the mixture was cool down under running tap water to room temperature and later, pH was adjusted to 7 with 0.1 M NaOH. To this reaction mixture, 1/1 molar ratio of lignin/formaldehyde and 0.6/1 molar ratio of sodium metabisulfite/lignin were maintained and sulfomethylation reaction was carried out at 100 °C for 2 h and 200 rpm. Upon completion of reaction, the mixture was cool down to room temperature and pH was adjusted to 7 using 0.1 M $H_2SO_4$. The reaction contents were dialysed for 2 days by changing water for every 12 h time interval. After the dialysis, the samples were dried at 105 °C and stored at room temperature until further use.

### 7.3.4 Charge density and sulfonated group analysis

The charge density of unmodified lignin (UL) and oxidized sulfomethylated lignin samples (OSL) was determined using a particle charge detector (Mutek, PCD 04, Germany). The samples were initially dried at 105 °C overnight in an oven. In this experiment, UL or OSL sample (0.2 g) was dissolved in 20 mL of deionized water and incubated in a water bath shaker (Classic C76, New Brunswick Scientific, Edison, NJ, USA) for 2 h at 30 °C and 150 rpm. After the incubation, the samples were centrifuged at 1000 rpm for 10 min and supernatants were collected for the charge density analysis. A 1 mL of supernatant was titrated against PDADMAC solution (0.005M) to measure the charge density of the samples.

The surface charge density analysis of coal particles was determined via a back titration method with a Mutek, PCD 04, particle charge detector (Germany). Approximately, 0.2 g of coal powder was suspended in 50 mL of PDADMAC (0.005M) solution and the suspension was incubated at 30 °C for 2 h at 150 rpm. After the incubation, the samples were filtered using Whatman#1 filter papers and the filtrates were titrated against PVSK (0.0055 M) solution. Similarly, the titration

analysis was conducted for control (i.e. PDADMAC solution) and the difference was employed to quantify the surface charge density of clay particles.

The sulfonated group content of UL, OSL and LSS samples was measured using an automatic potentiometer, Metrohm, 905 Titrado, Switzerland. In this experiment, a 1 g of dried sample was suspended in 100 mL of deionized water and pH was adjusted to 7.0 with 1M $H_2SO_4$. The solutions were then titrated against a cationic polymer, TEGO trant A 100, in order to determine the number of sulfonated groups. The sulfonated group content was calculated based on equation 7.1.

$$\text{Sulfonated group (SG)} = \frac{V \times C}{S} \qquad (7.1)$$

in which V is volume of titrant (TEGO trant) consumed in mL, C is the concentration of TEGO trant (mol/L) and S is the dried weight of lignin (g) samples used in this analysis.

### 7.3.5 Surface area analysis

The surface area of coal particles was determined using Quantachrome surface area analyzer, Nova2200e (USA). In this experiment, the samples were initially dried in an oven at 105 °C overnight and approximately 0.05 g of sample was pretreated for 4 h at 250 °C prior to analysis. The specific surface area of the samples was then analyzed according to Branuer-Emmett-Teller (BET) method via adsorption-desorption isotherms using nitrogen gas at -180 °C with in relative pressure range of 0.01 to 0.99 [28].

### 7.3.6 Particle size distribution analysis

In this study, 1 g of dried coal powder was added to 100 mL of deionized water and incubated in water bath shaker at 30 °C and 150 rpm. After the incubation, the samples were transferred to a MasterSizer 2000, Malvern, particle size analyzer (UK) equipped with a light scattering detector to measure the particle size distribution of the clay particles. All the measurements were carried out at room temperature. Three measurements were carried out for each sample and average values were reported.

### 7.3.7 Elemental Analysis

The elemental analysis of UL or OSL and coal samples was performed using an Elementar Vario EL Cube, Germany, elemental analyzer by combustion analysis method. The samples were first dried in a 105 °C oven overnight in order to remove any moisture. Approximately, 2 mg of sample was weighed in silver vessels and loaded in the integrated carousel of the elemental

analyzer. Then, the samples were automatically transferred into combustion tube and burnt at 1200 °C. Afterwards, the combustion gases were reduced and analyzed for carbon, hydrogen, nitrogen and oxygen content of the samples.

### 7.3.8 Molecular weight analysis

The molecular weight of UL and OSL samples were carried out using a gel permeation chromatograph (Malvern GPCmax VE2001 Module + Viscotek TDA305) equipped with refractive index and viscometer detectors. PolyAnalytic columns, PAA206 and PAA203, were used at the column temperature of 35 °C. Polyethylene oxide was used as standards. 0.1 mol/L $NaNO_3$ solution was used as eluent and flow rate set at 0.70 mL/min. The samples were oven dried at 105 °C before analysis and about 50 mg of UL or OSL were dissolved in 5 mL of 0.1 mol/L $NaNO_3$ solution and filtered with a nylon 0.2 μm filter (13 mm diameter). The filtered solutions were used for the molecular weight analysis.

### 7.3.9 $^{1}$H-NMR analysis

In this experiment, 35 mg of dried UL and OSL samples were weighed and dissolved in 2 mL of dimethyl sulfoxide-d6 for 2 h at 30 °C and 170 rpm. After incubation, the samples were characterized by NMR spectrophotometer, Varian Unity, INOVA 500 MHz, CA, USA [29]. The $^{1}$H-NMR spectra were recorded at 21 °C with 45° pulse flipping angle, 2 s relaxation delay time a 4.6 μs pulse width, a 2.05 s acquisition time for 16 scans.

### 7.3.10 Adsorption studies

The adsorption of UL or OSL samples onto coal particles was studied as a function of polymer dosage. In this experiment, UL or OSL concentrations ranging 2 -128 mg/L were controlled in 100 mL flasks containing 25 mL of coal suspension (50 wt.%) and the system was incubated at 25 °C for 0.5 h and 500 rpm. After the incubation, the mixture was filtered using Whatman#1 filter papers to separate coal particles from the suspensions. The concentration of UL or OSL in the filtrate was measured using UV-Vis spectrophotometer at a wavelength of 205 nm [30].

### 7.3.11 Zeta potential analysis

The zeta potential analysis of coal particles was performed using NanoBrook Zeta PALS (Brookhaven Instruments Corp, USA). In this study, 12.5 g of coal powder was added to 25 mL of deionized water (50 wt.%) and stirred at 500 rpm for 30 min at room temperature. After mixing, 1 mL of sample was used for the zeta potential analysis. Similarly, the zeta potential of coal particles in the presence of UL or OSL was measured at different polymer concentrations (2

-128 mg/L) under the same conditions as described above. The experiments were carried out three times and the mean values were reported in this study.

### 7.3.12 Rheological measurements

The rheological analysis of coal water slurries of varying particle sizes in the presence or absence of UL or OSL or LSS was carried out using a Rheometer, TA instruments (USA), equipped with peltier cylindrical cup and DIN concentric cylindrical rotor of 28.03 mm diameter and 41.96 mm of length. The gap between the rotor and cup was fixed at 5923 μm for all measurements. The shear rate range studied ranged from 0 to 200 $s^{-1}$ and the analysis was carried out for 2 min at 25 °C. In this experiment, OSL or UL of varying dosages (2-128 mg/L) were added to 25 mL of CWS (50 wt.%) having different particle sizes and mixed for 30 min at 500 rpm and room temperature. After mixing, approximately 20 mL of slurry was transferred into the cup and allowed to stand for 5 min prior to analysis. The viscosity measurements were taken at the shear rate of 100 $s^{-1}$. Similarly, the rheological behavior of CWS having altered particle sizes in the presence of LSS (2-128 mg/L) was also studied as described above. The pH of the experiments was controlled at 7. The shear stress and shear rate data obtained were fitted to Herschel Bulkely model (Eq 7.2) to investigate the rheological behaviour of CWS [8].

$$\tau = \tau_0 + k\gamma^n \qquad (7.2)$$

Where, $\tau$ is the shear stress in Pa, $\gamma$ is the shear rate in $s^{-1}$, $\tau_0$ is the yield stress in Pa, k is the consistency index in $Pa.S^n$ and n is the flow index.

Based on Herschel Bulkely model, the lower the yield stress ($\tau_0$) and consistency index (k) values, the higher the stability of CWS would be, which is ascribed to a decrease in aggregation of coal particles [23]. Flow index (n) values of CWS indicates the behaviour of fluids in that a decrease in (n) value corresponds to an increase in shear thinning behaviour of CWS, while increase in (n) value corresponds to increase in shear thickening behaviour of CWS [31].

### 7.3.13 Stability analysis

The stability of the CWS in the presence OSL or LSS was investigated using a Turbiscan Lab Expert, Formulaction, France. This analysis was conducted in the past to study the stability of emulsion and concentrated colloidal dispersions [32]. In one set of experiments, 20 ml of CWS (50 g/L) at pH 7 was transferred to cylindrical tubes of the instrument and then analyzed for

suspension stability by the instrument for 1 h. In another set of experiments, CWS (50 wt.%) in the presence of UL or OSL or LSS (2-64 mg/L) and pH 7 was prepared and changes in the suspension stability was analyzed for 1 h (single scans were collected every 2 sec) by the instrument at 30 ºC. This instrument uses laser lights at the wavelength of 880 nm to investigate the transmittance and backscattering efficiency of suspensions [33]. In this analysis, silicon oil is used as standard with fully transmittance behavior while teflon is used as standard for fully backscattering behavior [34]. The transmission and backscattering data collected by the instruments for the samples was analyzed by turbisoft 2.1 software and recorded as a percentage of transmittance signals in regard to that of the silicon oil.

The transmission and backscattering data was used for determining the destabilization index (DSI) of CWS according to Eq 7.3.

$$\mathrm{DSI} = \Sigma_i \frac{\Sigma_h |scan_i(h) - scan_{i-1}(h)|}{H} \qquad (7.3)$$

where $scan_i$ and $scan_{i-1}$ (h) are the transmission signals for two consecutive time intervals at a given height and H is the total height of sample

### 7.3.14 Surface and interface tension analysis.

The surface tension of OSL and LSS solutions was measured using a tensiometer (Attension sigma 700) equipped with platinum loop [35]. In this set of experiments, OSL was added at different concentrations of 2 and 128 mg/L to deionized water (50 mL) and mixed for 2 h at 150 rpm and 30 °C. After mixing, 20 mL of OSL solution was transferred to glass dish for surface tension analysis. The surface tension of OSL and LSS solutions was measured for 10 min and each measurement was replicated 10 times within the time frame. The platinum loop was cleaned with ethanol and deionized water between each test. All the measurements were carried out at 25 °C and pH 7.

An optical tensiometer instrument, Theta lite (Biolin Scientific, Finland) equipped with camera was used to determine the wettability of coal samples of varying particle sizes. All coal samples (coal A, coal B and coal C) were oven dried, and 0.5 g of each coal sample was mixed in 50 mL of deionized water (10 g/L) and mixed at 500 rpm for 2 h and 30 °C. After mixing, 2 mL of each coal sample was loaded onto microscopic glass slides and allowed to dry using a spin coater, WS-650 (Laurell Technologies Corp) under vacuum with 60 psi pressure at 250 rpm for 60 s.

The contact angle of water with coal samples coated on microscopic slides was measured by sessile drop method using optical tensiometer. Approximately, 5 µL of water droplet was placed on the coated slides and the contact angles between droplet and the coal samples coated on slides were determined using tensiometer, [36]. In another set of experiments, a droplet (5 µL) of OSL or LSS solution was loaded on the coal coated slides and the contact angle between the OSL or LSS droplet and coal coated slides was also measured as described above. Three replicates were performed for each experiment and average values were reported.

The surface tension of coal is analyzed using the tensiometer's OneAttension software via Zisman equation (eq 7.4) [37].

$$\text{Cos}\,\theta = 1 + \text{b}\,(\gamma_{\text{sv}} - \gamma_{\text{lv}}) \qquad (7.4)$$

where, $\gamma_{lv}$ and $\gamma_{sv}$ represents surface tension of liquid (OSL or LSS solution) and solid (coal) in mN/m, θ represents contact angle between liquid and solid in degrees (°).

The cosine of the contact angle θ is plotted against the surface tension of liquid ($\gamma_{lv}$) yielding a straight line with slope b.

The interfacial tension between coal and OSL or LSS droplet was determined by using Young equation (eq 7.5)

$$\gamma_{lv}\, cos\theta_Y = \gamma_{sv} - \gamma_{sl} \qquad (7.5)$$

where, $\gamma_{lv}$, $\gamma_{sv}$ and $\gamma_{sl}$ represent the tensions of liquid vapour, solid vapour and solid liquid, respectively, and $\theta_Y$ is the contact angle of solution droplets and coal coated glass slides.

## 7.4 Results & Discussion

### 7.4.1 Characterization of UL, OSL, LSS and coal samples

Table 7.1 lists the properties of coal samples and lignin samples. The charge density of UL was -0.2 meq/g, and after modification it became -4.4 meq/g (for OSL). This increase is attributed to the increased carboxyl and sulfonate contents of lignin via oxidation and sulphomethylation. The higher sulfur (3.26 wt.%) and oxygen (36.9 wt.%) contents of OSL than UL confirmed the grafting of carboxyl and sulfonate groups to UL in the treatment processes. The charge density of LSS was -1.8 meq/g with sulfonate group content of 1.6 mmol/g. OSL had a slightly higher molecular weight (21,000 g/mol) compared to UL (19,000 g/mol), which is ascribed to grafting

of carboxylate and sulfomethylate groups on UL. The polydispersity of OSL (1.28) was lower than that of UL (1.84), which is possibly due to cessation of kraft lignin macromolecule during nitric acid and sodium sulfite treatments [16]. Previously, He and Fatehi reported a rise in the molecular weight of softwood kraft lignin from 16,000 g/mol to 18,000 g/mol after treatment with nitric acid and sodium metabisulfite [27]. The molecular weight and polydispersity of LSS were found to be 9,000 g/mol and 2.88, respectively.

Table 7-1. Properties of UL, OSL and coal samples

| Sample | UL | OSL | LSS | Coal A | Coal B | Coal C |
|---|---|---|---|---|---|---|
| Surface charge density, meq/g | -0.2 | -4.4 | -1.8 | - | - | - |
| Carboxylate group, mmol/g | 0.04 | 2.7 | - | - | - | - |
| Sulfonate group, mmol/g | 0 | 1.6 | 1.6 | - | - | - |
| $M_w$, g/mol | 19,400 | 21,300 | 9,400 | - | - | - |
| $M_n$, g/mol | 10,500 | 16,500 | 3,200 | - | - | - |
| $M_w/M_n$ | 1.84 | 1.28 | 2.88 | - | - | - |
| BET surface area, $m^2/g$ | - | - | - | 7.22 | 4.64 | 2.10 |
| Particle size, μm | - | - | - | 22 | 47 | 125 |
| C, wt.% | 64.66 | 53.71 | - | 71.17 | 72.15 | 73.06 |
| H, wt.% | 5.82 | 4.71 | - | 5.14 | 4.85 | 5.35 |
| N, wt.% | 0.005 | 0.004 | - | 1.61 | 1.55 | 1.66 |
| S, wt.% | 1.05 | 3.26 | - | 0.41 | 0.57 | 0.52 |
| O, wt.% | 26.7 | 36.9 | - | 14.67 | 14.38 | 14.27 |
| Impurities, wt.% | 1.87 | 1.42 | - | 7.0 | 6.5 | 4.03 |
| Surface tension, mN/m | - | - | - | 39 | 28 | 12 |

The characteristics of coal A, B and C samples are also listed in Table 1. Coal A found to have a higher surface area (7.22 $m^2/g$) than other samples. The average particle size ($d_{50}$) of coal A, B and C samples were 22, 47 and 125 μm, respectively. All coal samples had a similar anionic (-3.2 μeq/g) and cationic surface charge density (+1.4 μeq/g). The anionic charge density of the samples is due to the presence of oxide complexes on coal surfaces, which act as weakly acidic groups in aqueous solutions [38]. The positive surface charge density of coal particles is possibly due to polyvalent metals in coals ($Al^{3+}$, $Si^{4+}$) [39]. The carbon content of the coal samples was found to be around 70 wt.% and the oxygen content of coal samples was similar (14 wt.%). The

nitrogen content of coal samples can be attributed to the presence of pyrrole and pyridine structures in coal samples, while thiols and sulphide structures possibly constituted to their sulfur content [40].The surface tension of coal ($\gamma_{sv}$) increased with reducing particle size, and coal A exhibited 39 mN/m, while coal B and coal C had 28 and 12 mN/m, respectively (Table 7.1). In the past, the surface free energy of titanium dioxide nanocrystals increased from 0.7 to 1.0 N/m with reduction in particle size to 14 nm, which was attributed to presence of more high energy sites (hydrophilic sites) on its surface [41]. Nikolokakis and coauthors reported that erythromycin powder with a high surface free energy (3 mN/m) exhibited greater amount of water adsorption (27 ° contact angle) compared to cephalexin (55 ° contact angle) having low surface free energy (0.07 mN/m) [42]. These results may suggest that solids with high surface tension adsorbs water more effectively.

### 7.4.2 $^{1}$H-NMR analysis

The $^{1}$H-NMR spectra of UL and OSL are shown in Figure 7.1. Peaks at 7.1, 6.9 and 6.7 ppm and between 8.6 and 9.0 ppm correspond to protons (a, b, c) of aromatic ring and protons (d) in phenolic OH groups in Figure 7.1a, respectively. The peaks between 5.4 and 5.1 ppm and between 4.5 and 4.2 ppm correspond to protons (e and f) attached to α and β carbons. Furthermore, the peak at 3.9 ppm designated to protons (i) of methoxyl groups, peaks between 3.5 and 3.8 are assigned to protons (g) of aliphatic OH groups and protons (h) attached to γ carbon atom [43, 44]. The peak at 3.4 corresponds to protons of water [45]. Compared to UL, the spectrum of OSL lignin (Figure 7.1b) showed a peak at 9.8 ppm corresponding to protons (x) of aldehyde groups generated via oxidation of lignin [46] and peak at 3.3 ppm corresponding to protons (z) of methyl groups grafted on the lignin via sulfomethylation [47]. The spectra confirmed the success of reactions and the groups introduced to UL after modification.

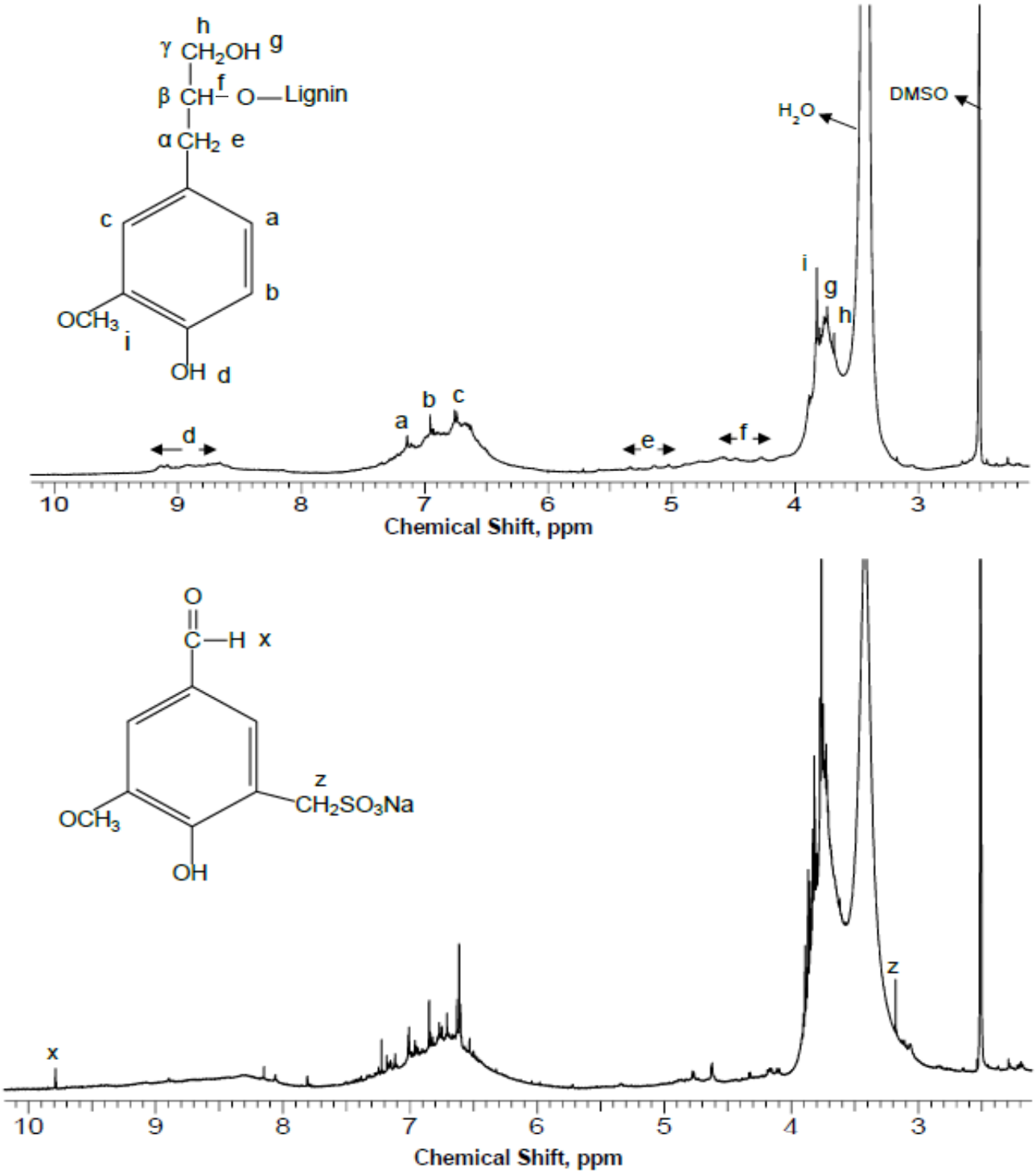


Figure 7-1: $^{1}$H-NMR spectra of a) unmodified lignin and b) oxidized sulfomethylated lignin

### 7.4.3 Adsorption studies

Figure 7.2 presents the adsorption of UL and OSL on the surface of coal samples. The adsorption of OSL on coal particles increased significantly with the addition of OSL in the suspension,

irrespective to the particle size. OSL exhibited the maximum adsorption of 0.96 mg/g on coal A. The higher adsorption of OSL on coal A is due to its higher surface area compared to other coal samples (Table 7.1). Similarly, lignosulfonate (LSS) had a similar trend with maximum adsorption of 0.68 mg/g on coal A particles compared to coal B (0.62 mg/g) and coal C (0.33 mg/g) particles (Figure 2b). In one study, increasing the concentration of sulfonated alkali lignin (SAL) polymer to 100 mg/L in CWS, the adsorption of SAL on coal particles increased to 1.5 mg/g [15]. However, OSL showed more adsorption than LSS on coal particles irrespective of particle size, which might be due to higher charge density of OSL than LSS (Table 7.1). On the other hand, UL exhibited a lower adsorption of 0.14 mg/g on coal samples. Zhang et al [6] described two possible interactions between polymers and coal suspension: hydrophobic/hydrophobic interactions developed between hydrophobic parts of coal particles and phenyl propane units of lignin (in this case OSL) and ionic interaction developed between carboxyl and sulfonate groups of OSL and positively charged sites of coal.

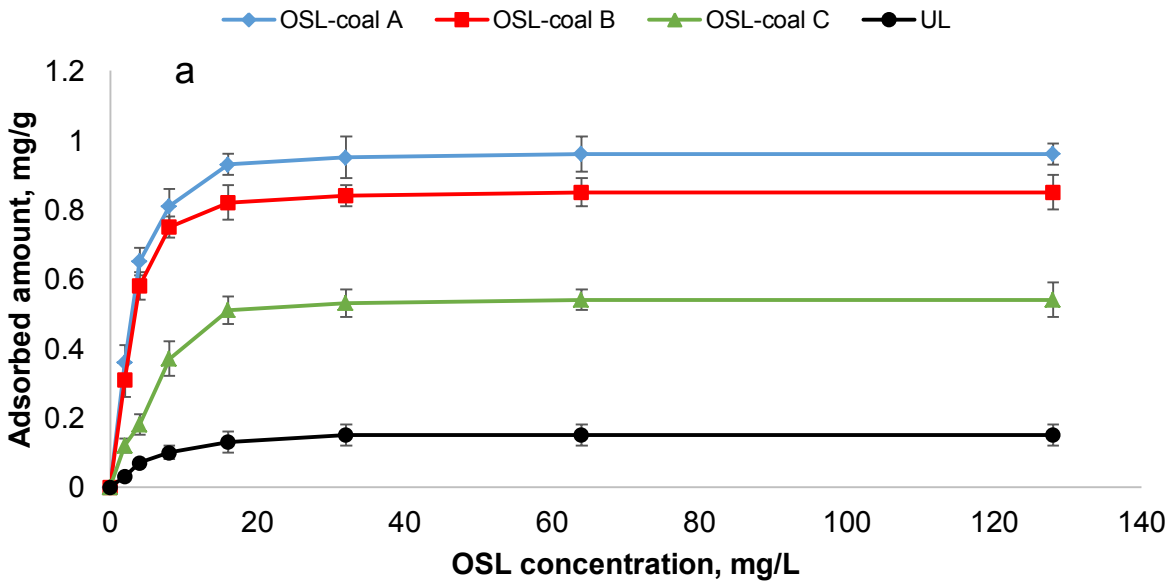

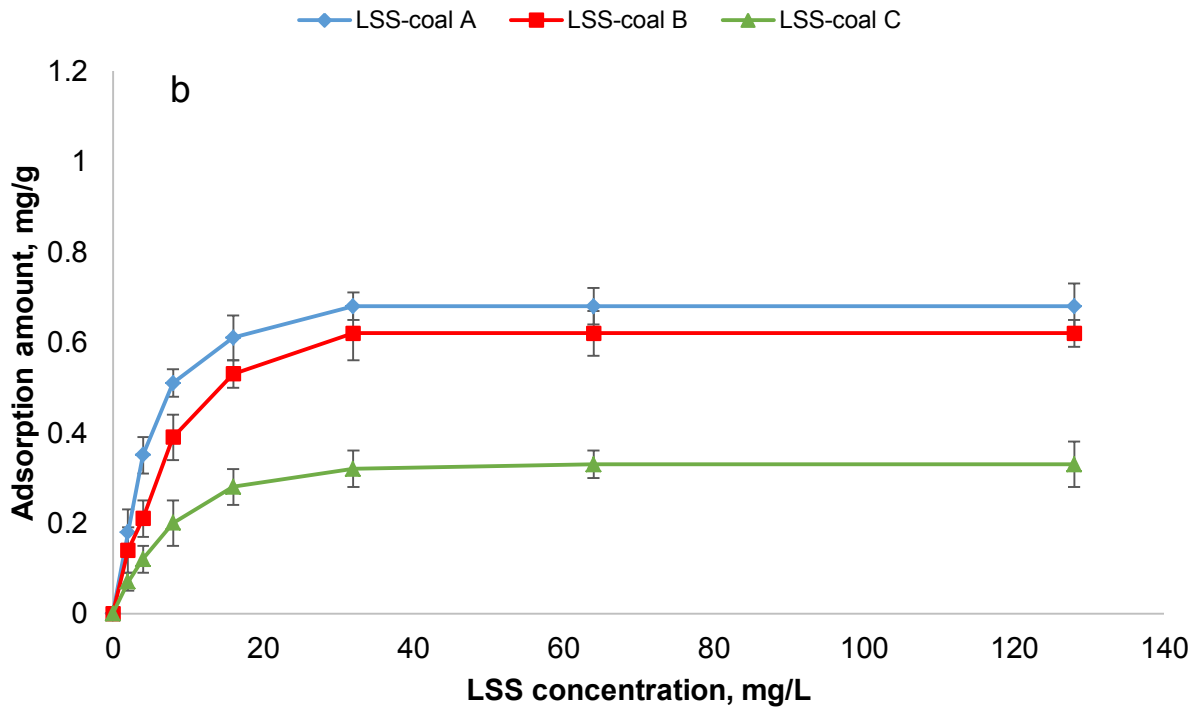


Figure 7-2: a) Adsorption of UL and OSL on coal particles having different particle sizes as a function of polymer dosage and b) adsorption of LSS on coal particles having different particle sizes as a function of dosage under the conditions of pH 7, 25 °C, 0.5 h and 50 wt.% coal concentration.

### 7.4.4 Surface tension and interfacial tension analysis

Figure 7.3 presents the effect of OSL and LSS on the surface tension of water and contact angle of water droplet on coal particles. The surface tension of water in the absence of OSL was found to be 72.8 mN/m [16]. When the concentration of OSL increased to 64 mg/L, the surface tension of water dropped to 63 mN/m (Figure 7.3a). Similarly, LSS reduced the surface tension to 65 mN/m at 64 mg/L concentration (Figure 7.3b). The functional groups (sulfonate and carboxylate) of OSL or LSS disrupted the interactions developed between the water molecules reducing the surface tension of water [8]. The higher reduction in surface tension of water with OSL than LSS is probably due to its higher charge density and molecular weight (Table 7.1).

The interfacial tension between coal and water droplet was reduced with the addition of OSL (Figure 7.3a). The interfacial tension ($\gamma_{SL}$) between coal A and water was reduced from 17 mN/m to 13.5 mN/m, and for coal B and coal C was reduced from 9.4 to 7.8 mN/m and 4.7 to 3.9 mN/m, respectively, at 64 mg/L OSL concentration. This behaviour indicates that the adhesion

of water droplet on coal surface improved by the addition of OSL and furthermore increased with reduction in coal particle size. This is in good agreement with reduction in contact angle ($\theta_Y$) of water, where coal A exhibiting maximum drop in contact angle from 73 to 66 °, and coal B and coal C exhibited drop in contact angle from 75 to 70 ° and from 84 to 81 °, respectively. The increase in adhesion of water droplet with reduction in a coal particle size is due to more adsorption of OSL on coal A than coal B and coal C (Figure 7.2) [48]. The limited change in the interfacial tension between coal and water droplet beyond 32 mg/L OSL concentration is attributed to its limited adsorption increase on coal particles (as shown in Figure 7.2a). The interfacial tension between water and coal A, coal B and coal C particles was reduced to 14.2, 8.1 and 4.0 mN/m, respectively, when LSS was used (Figure 7.3b). Furthermore, coal A exhibited maximum drop in contact angle (68 °) compared to coal B (72 °) and coal C (82 °). The better performance of OSL compared to LSS is due to its higher charge density (more functional group) and probably molecular weight. No significant change in surface tension and interfacial tension between water and coal samples was observed in the presence of UL. Previously, Hong and co-authors reported a contact angle change in the wettability of coal sample to 38° with adding polycarboxylic acid concentration from 0.16 to 0.9 g/L [23]

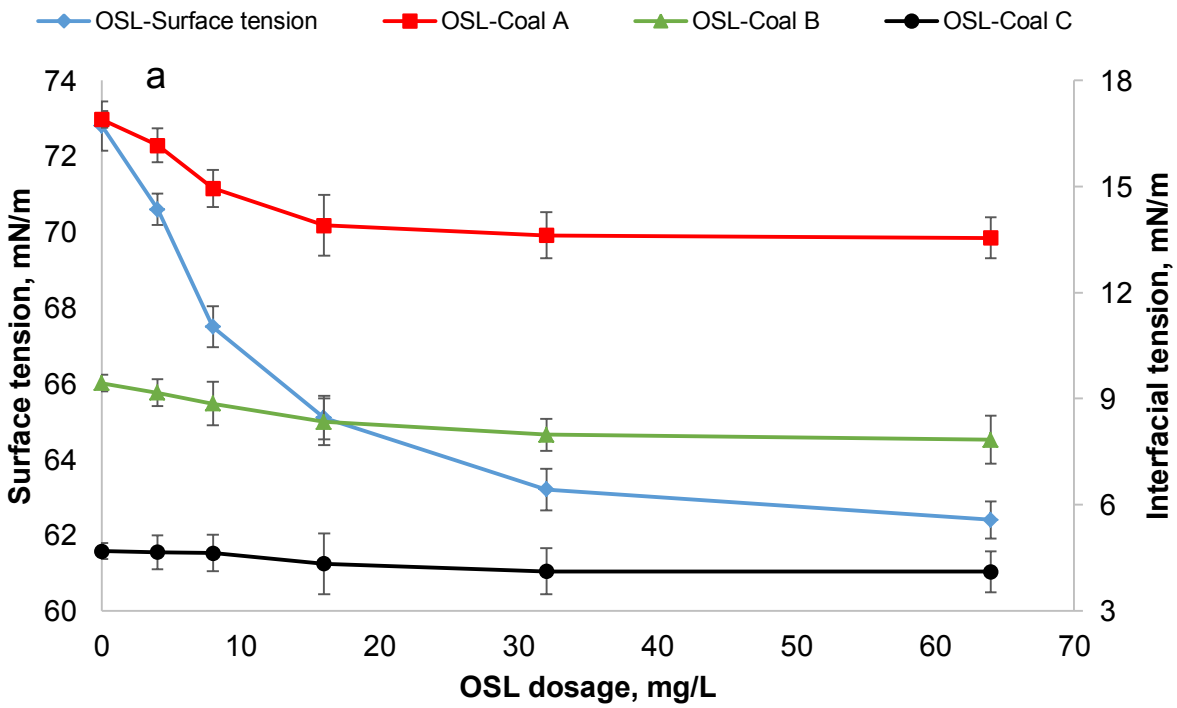

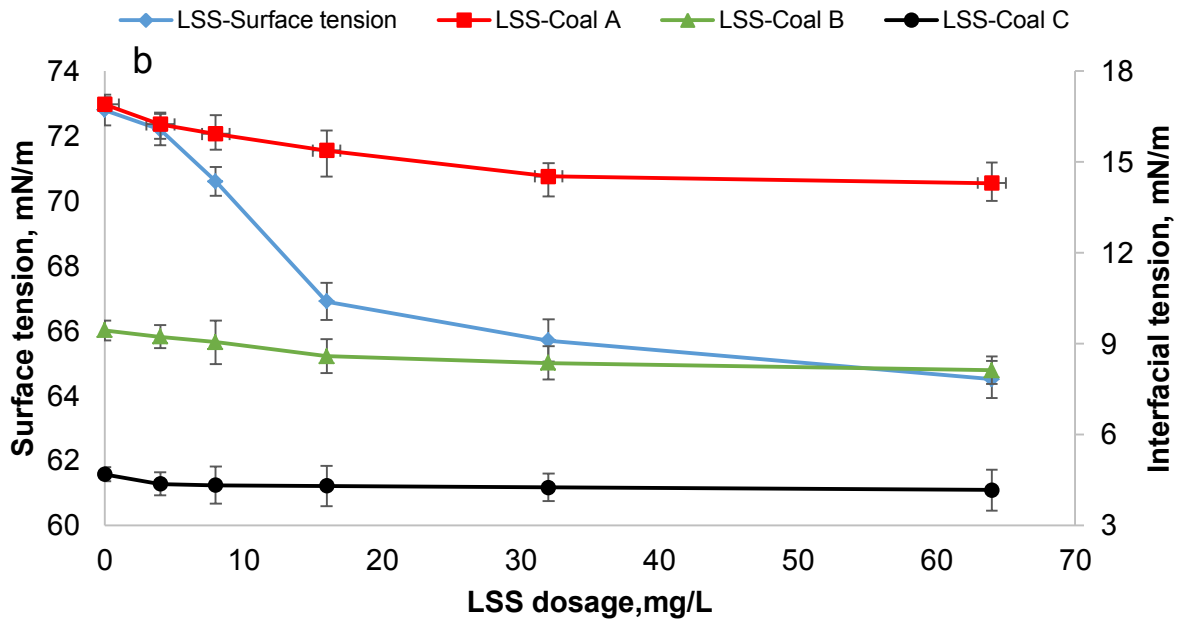


Figure 7-3: Effect of a) OSL concentration and b) LSS concentration on surface tension and interfacial tension of coal particles of varying particle size under the conditions of pH 7 and 25 °C.

### 7.4.5 Zeta potential analysis

Figure 7.4 presents the zeta potential of coal samples as a function of adsorbed amounts of UL, OSL or LSS at pH 7. In the absence of polymers, the zeta potential of clay particles was -32 mV, indicating coal suspension was negatively charged. As the coal samples contained oxygenic groups on their surface (Table 7.1), they would induce an anionic charge group on their surface at pH 7, and thus a negative zeta potential [15].

UL had no significant impact on the zeta potential of the coal particles. The zeta potential of the coal suspensions was reduced with the increase in the OSL adsorbed amount (Figure 7.4a). Coal A exhibited a maximum reduction in zeta potential (-48 mV), which is due to the maximum adsorption of OSL or LSS on coal A than other coal particles. As was suggested previously [49], adsorbed polymers (in this case OSL or LSS) on coal surface introduced negative charges on coal particles, which would cause a reduction in the zeta potential. Furthermore, OSL was generally more efficient than LSS in affecting the zeta potential of coal particles, regardless of their sizes. This behavior is due to the higher adsorption of OSL than LSS on coal particles. In one study, the zeta potential of coal particles found to decrease from -20 to -62 mV with an

increase in concentration of polycarboxylate acid (PC) to 0.8 g/L, which was attributed to negative charges introduced by the adsorption of PC [23].

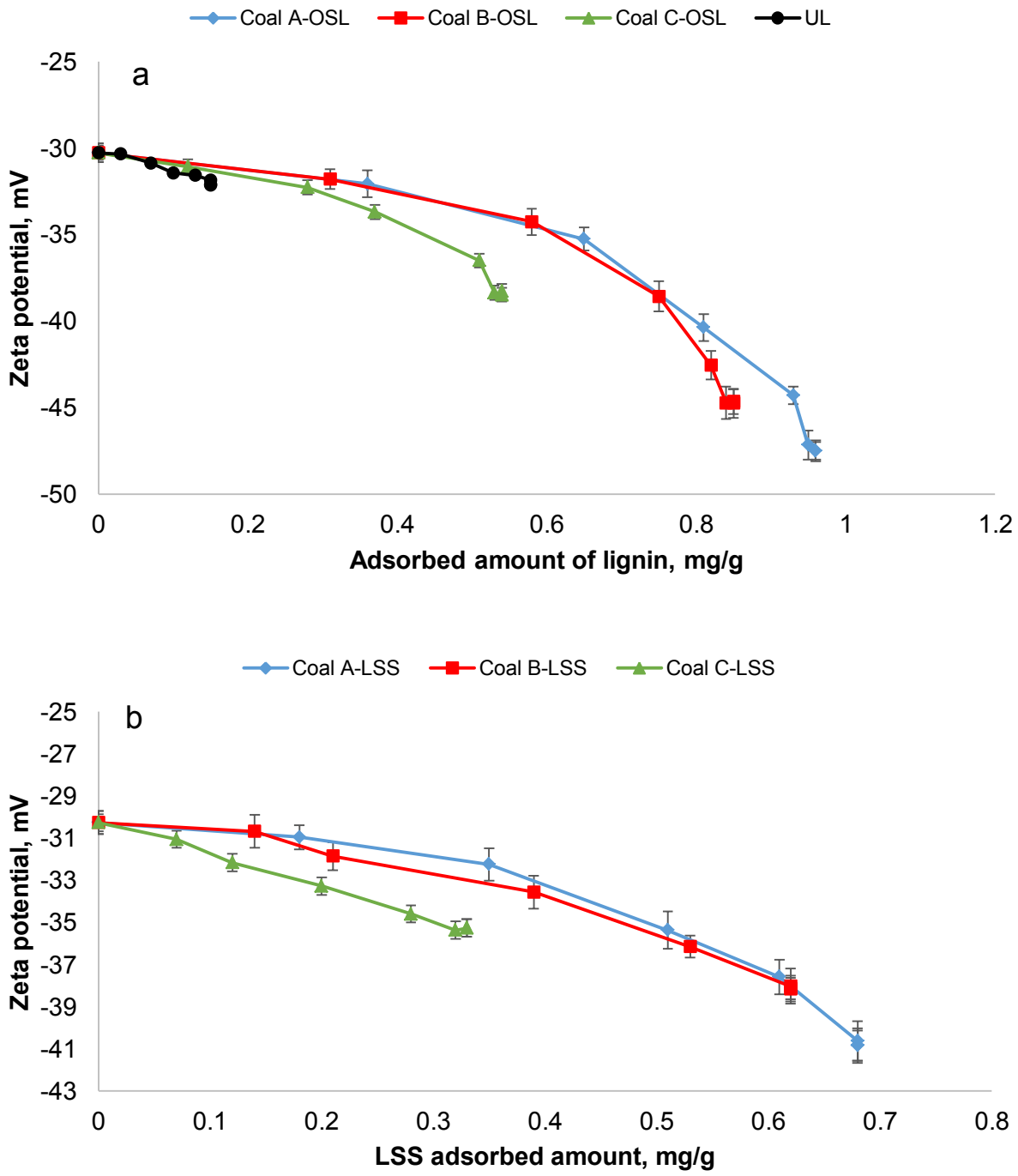


Figure 7-4: Effect of adsorbed amount of a) UL and OSL and b) LSS on the zeta potential of the coal particles having altered particle sizes studied under the conditions of pH 7, 50 wt.% coal concentration, 30 min and 25°C.

### 7.4.6 Viscosity studies

Figure 7.5 presents the effect of adsorbed amounts of OSL or LSS on the apparent viscosity of CWS. Coal A slurry exhibited a decrease in apparent viscosity to 500 mPa.s, while viscosity of coal B and coal C slurries was reduced further to 450 mPa.s and 280 mPa.s, respectively, with increase in OSL adsorption amount. The addition of OSL reduced the attraction forces between the coal particles by generating electrostatic repulsion forces via adsorbing on their surface (Figure 7.4). The more significant viscosity change is also attributed to the higher adsorption of OSL on coal A. Furthermore, viscosity of coal A, B and C suspensions were reduced to 680, 580 and 350 mPa.s when LSS was used, respectively (Figure 7.5b), which implies that OSL was more effective than LSS in reducing viscosity of coal suspensions. Previously, the addition of sodium polystyrene sulfonate (0.5 wt.%) reduced the viscosity of CWS (68 wt.%) from 7000 to 2500 mPa.s, which was attributed to the additional electrostatic repulsion forces developed between particles by the dispersant [24]. In another study, the addition of amphoteric polycarboxylate dispersant (0.3 wt.%) reduced the viscosity of CWS (63 wt.%) to 600 mPa.s, which was due to both electrostatic (generated by the charges introduced on coal particles by the dispersant) and steric repulsions from the associated polyether side chains in the dispersant structure [50].

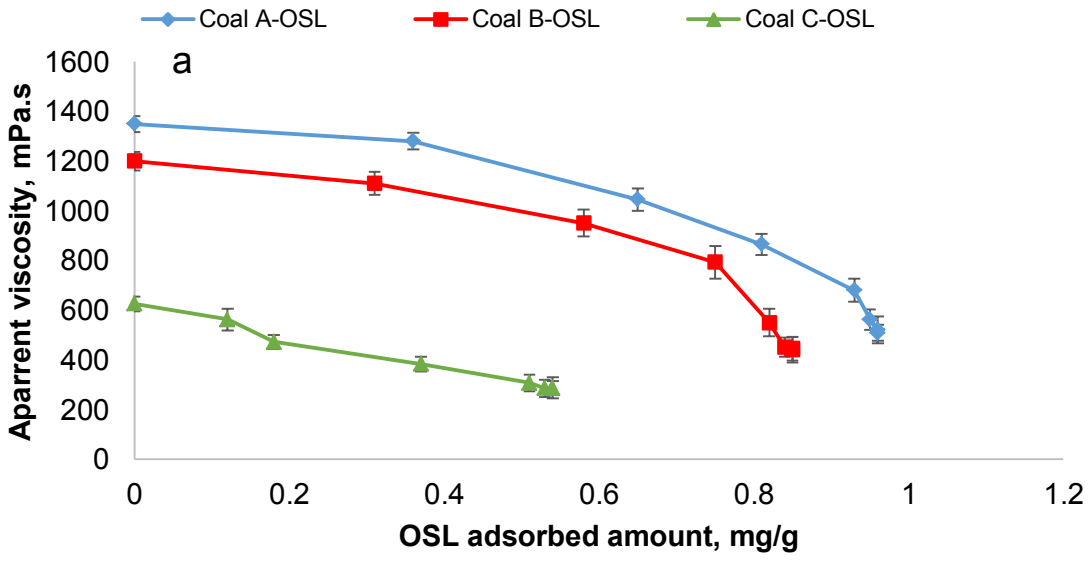

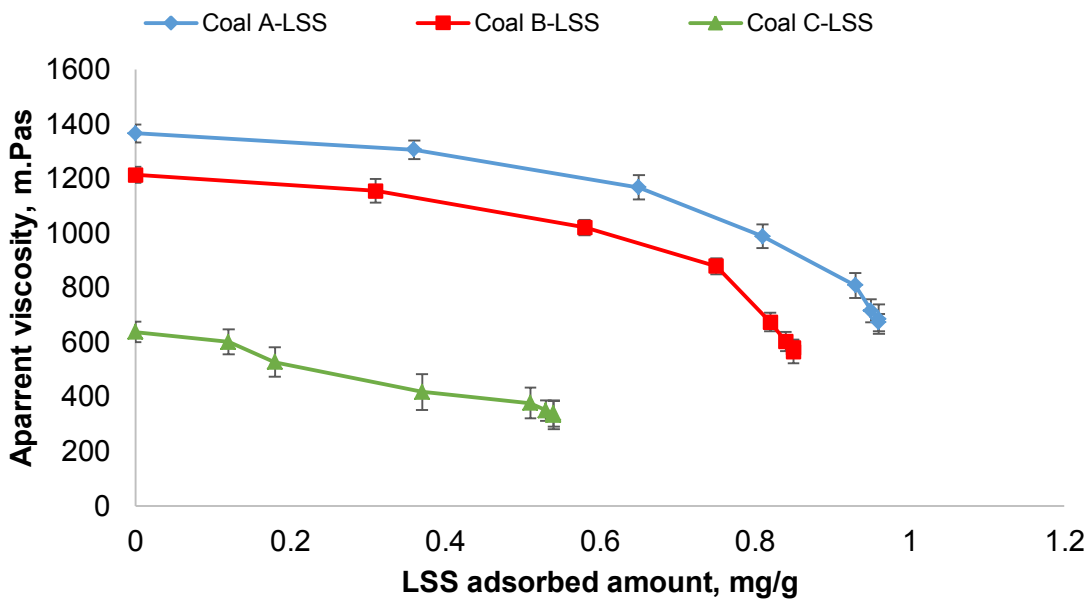


Figure 7-5: Influence of adsorbed amounts of a) OSL and b) LSS on the apparent viscosity of coal samples having different particle sizes under the conditions of pH 7, 25 °C, 100 $s^{-1}$ shear rate and 50 wt.% coal concentration.

### 7.4.7 Rheological studies

#### 7.4.7.1 Rheological behaviour of the CWS containing OSL

An ideal CWS has a high solid concentration, low viscosity, excellent stability and good flow pattern, which can be characterized by its rheological behaviour [51, 52]. Shear stress is plotted as a function of shear rate of CWS (50 wt.%) in the absence or presence of OSL at different concentrations in Figure 7.6. The CWS prepared at different OSL concentrations exhibited shear thinning behaviour. The intercept in shear stress indicates that the CWS has non-Newtonian and pseudoplastic behaviour in the absence of OSL as described elsewhere [20, 53]. By increasing the dosage of OSL, the intercept was reduced indicating that shear thinning behaviour of CWS was improved with OSL dosage. The data obtained in Figure 7.6 was fitted into Herschel-Bulkley model (Equation 7.2) and the parameters are listed in Table 7.2. The results exhibited good linear relationship for all the three coal samples as coefficient of correlation ($R^2$) was close to 1. The flow behaviour index (n) value for all the coal water slurries is less than 1 and decreased with adding more OSL in the CWS indicating improvement in the pseudoplastic behaviour of CWS [2]. The yield stress ($\tau_0$) and consistency coefficient (K) should be as low as possible for good stability and storage of CWS [1]. The change in the shear stress-rate

relationship was most significant for coal A when OSL was used. Among CWS, Coal C slurry at 32 mg/L OSL dosage had the lowest yield stress of 2.8 Pa and consistency coefficient of 0.63 Pa.S$^{n}$, which was in agreement with its lowest apparent viscosity (300 mPa.s) at a shear rate of 100 s$^{-1}$ as shown in Figure 7.5a. These results indicate that the OSL improved the psuedoplastic behaviour of highly concentrated CWS by reducing the yield stress.

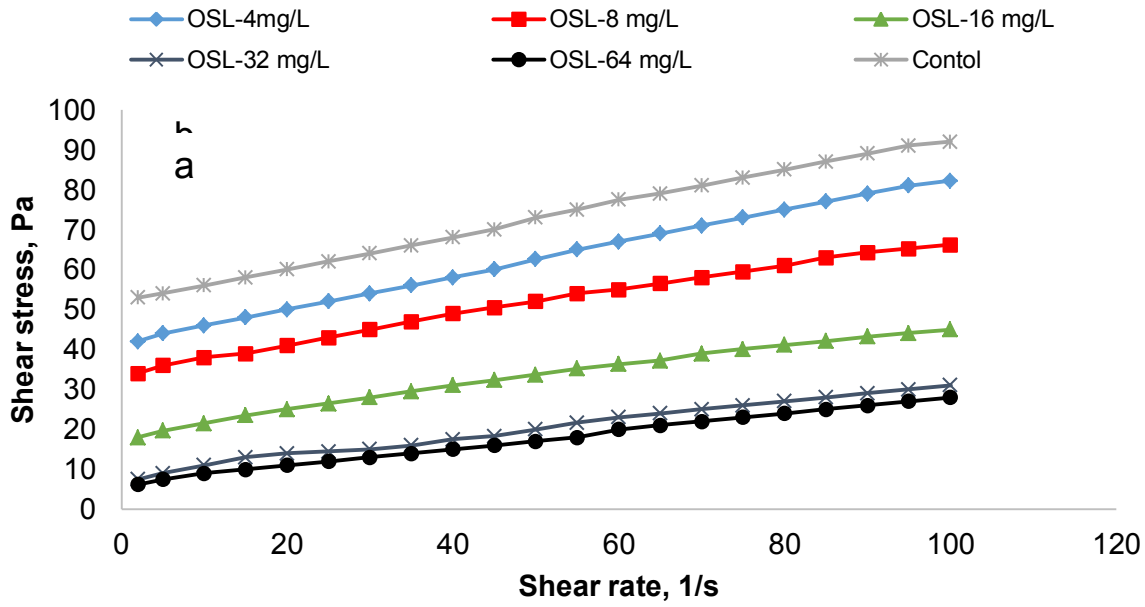


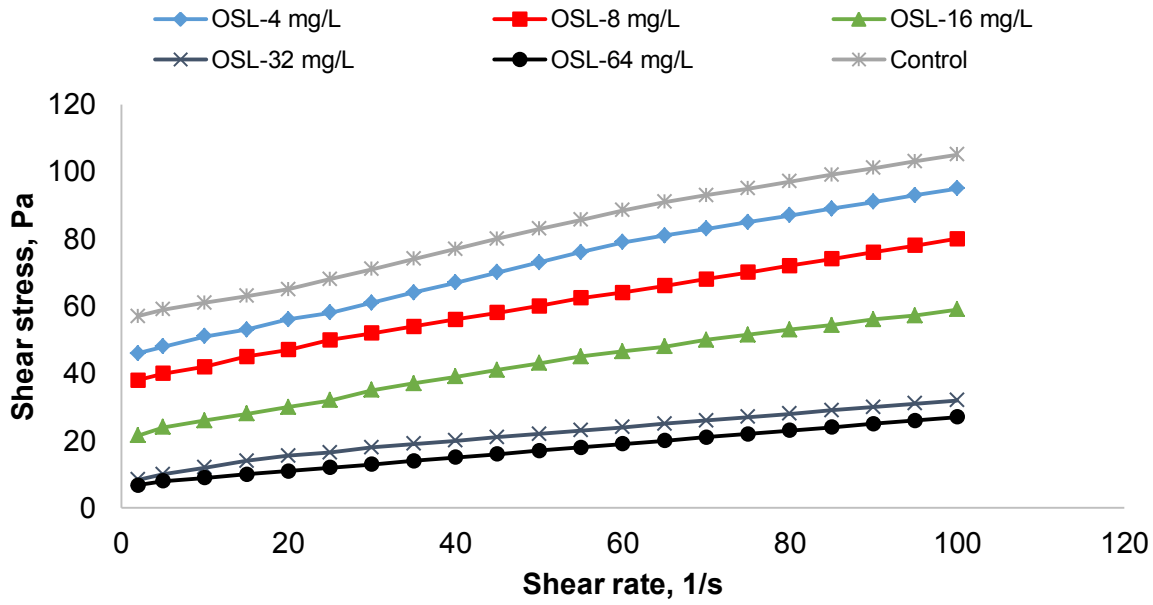

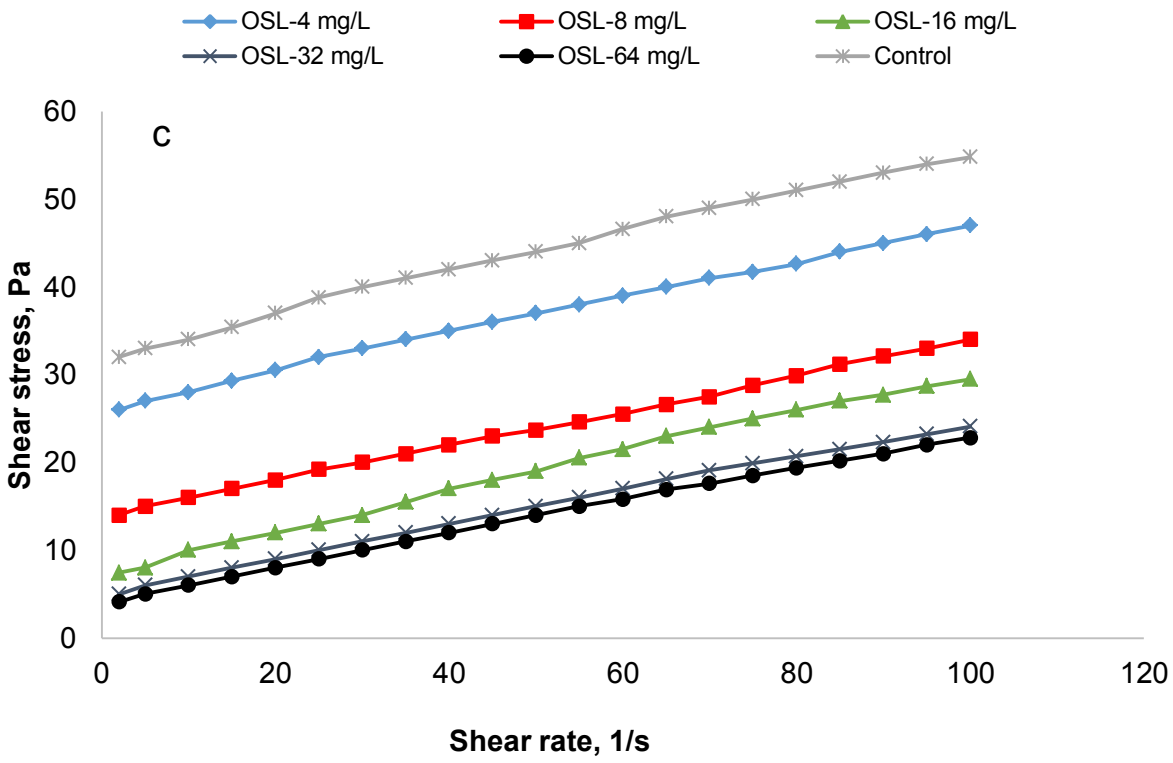


Figure 7-6: Shear stress as a function of shear rate for a) coal A, b) coal B and c) coal C slurries at different OSL concentrations which was conducted under the conditions of 50 wt.% coal concentration, pH 7 and 25 °C.

Table 7-2: Fitted Herschel-Bulkley parameter values of coal A, B and C slurries at different OSL dosages

| Sample | Coal A | | | | Coal B | | | | Coal C | | | |
|---|---|---|---|---|---|---|---|---|---|---|---|---|
| OSL dosage, mg/L | $\tau_0$, Pa | n | K, Pa.s$^n$ | $R^2$ | $\tau_0$, Pa | n | K, Pa.s$^n$ | $R^2$ | $\tau_0$, Pa | n | K, Pa.s$^n$ | $R^2$ |
| 0 | 54.3 | 0.88 | 0.92 | 0.975 | 50.4 | 0.90 | 0.91 | 0.976 | 28.8 | 0.96 | 0.67 | 0.998 |
| 4 | 45.2 | 0.85 | 0.91 | 0.991 | 41.5 | 0.88 | 0.89 | 0.989 | 25.3 | 0.96 | 0.66 | 0.998 |
| 8 | 36.5 | 0.81 | 0.87 | 0.986 | 33.1 | 0.84 | 0.84 | 0.998 | 12.6 | 0.94 | 0.65 | 0.995 |
| 16 | 20.2 | 0.71 | 0.82 | 0.991 | 16.7 | 0.75 | 0.79 | 0.995 | 5.4 | 0.93 | 0.64 | 0.987 |
| 32 | 7.0 | 0.63 | 0.78 | 0.995 | 5.4 | 0.69 | 0.74 | 0.997 | 2.9 | 0.93 | 0.63 | 0.989 |
| 64 | 6.9 | 0.63 | 0.77 | 0.988 | 5.4 | 0.69 | 0.73 | 0.992 | 2.8 | 0.93 | 0.63 | 0.992 |

#### 7.4.7.2 Rheological behaviour of the CWS containing LSS

Figure 7.7 presents relationship between shear rate and shear stress of CWS containing LSS. Similar to OSL, an increase in the dosage of LSS improved the shear thinning characteristics of CWS (Figure 7.7). LSS affected the shear stress-rate relationship more significantly for coal A than other coal samples. The data obtained in Figure 7.7 was also fitted into Herschel-Bulkley model (Equation 7.2) and the parameters are listed in Table 7.3. The results indicate that the flow behaviour index (n) value of all CWS containing LSS was less than 1 and decreased with dosage, representing improved pseudoplastic behaviour of CWS. All the statistical values obtained exhibited good linear relationship with correlation coefficient ($R^2$) value close to 1. A comparison between the results in Tables 7.2 and 7.3 show that a higher yield stress was obtained for samples containing LSS than OSL, which indicates that OSL was more effective in improving shear thinning characteristics of CWS. Furthermore, the higher consistency coefficient (K) values of CWS with LSS compared to OSL confirms the more efficient dispersion affinity of OSL than LSS.

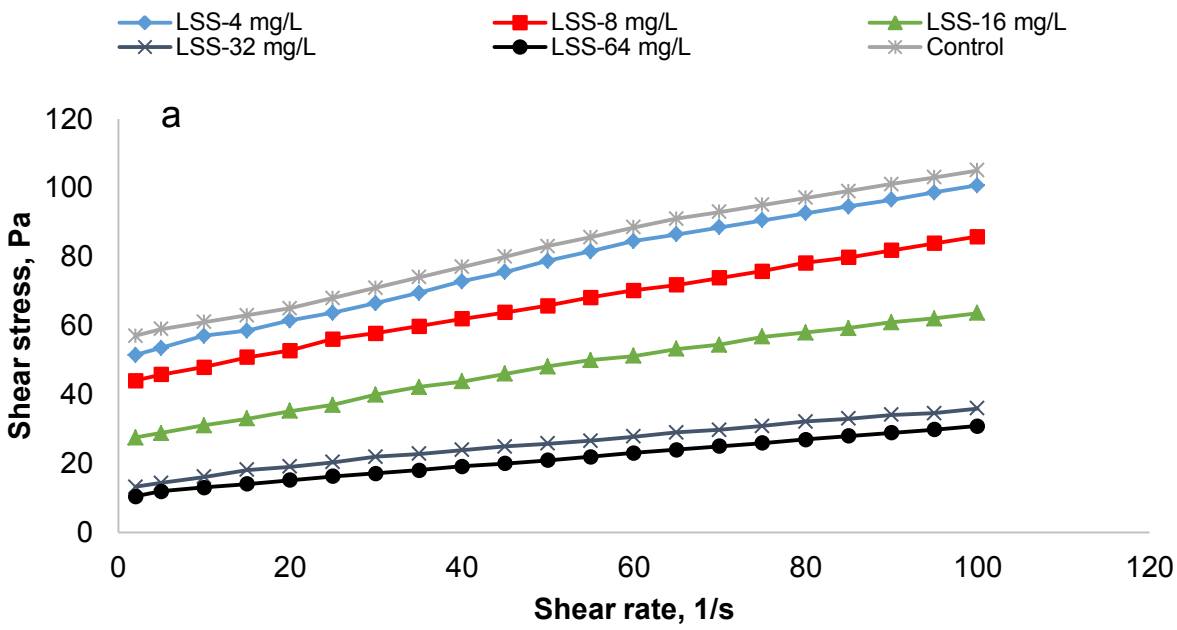
LSS-4 mg/L
LSS-8 mg/L
LSS-16 mg/L
LSS-32 mg/L
LSS-64 mg/L
Control
a
Shear stress, Pa
Shear rate, 1/s
0
20
40
60
80
100
120

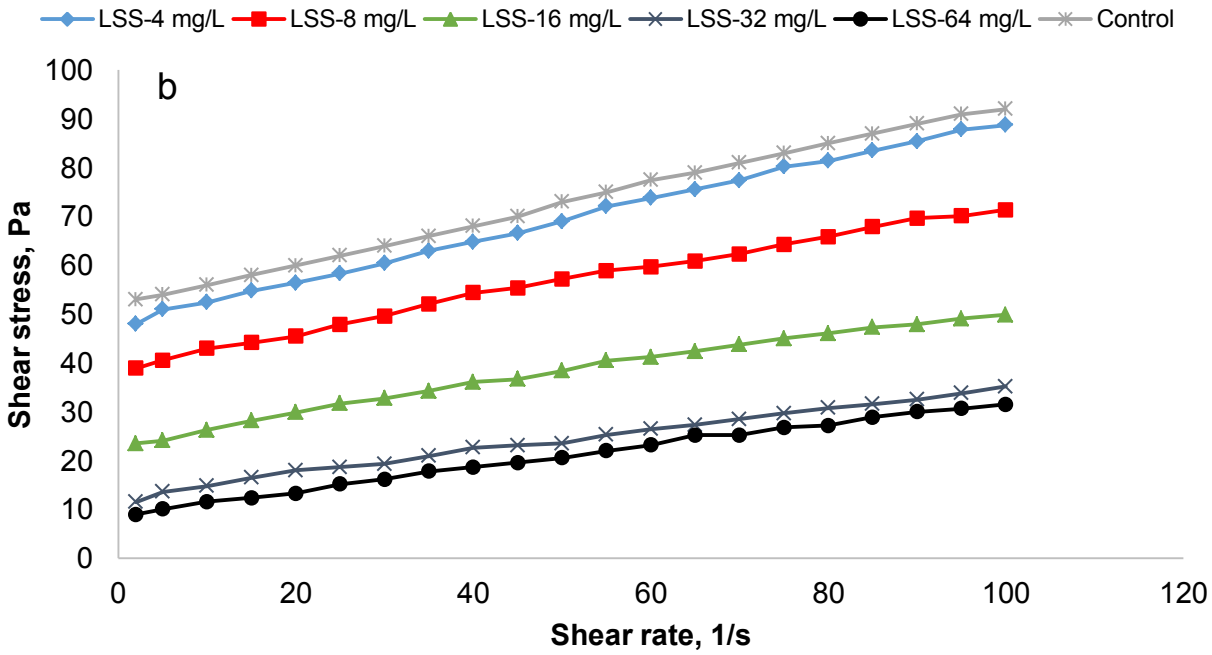
LSS-4 mg/L
LSS-8 mg/L
LSS-16 mg/L
LSS-32 mg/L
LSS-64 mg/L
Control
b
Shear stress, Pa
Shear rate, 1/s
0
10
20
30
40
50
60
70
80
90
100
120

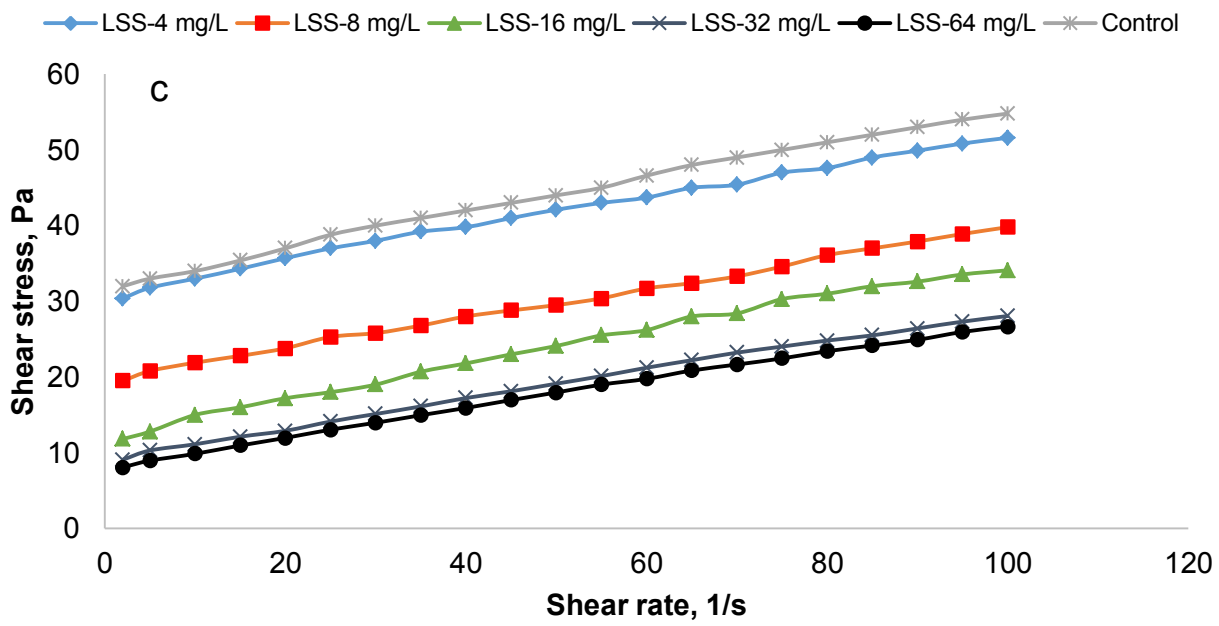


Figure 7-7: Shear stress as a function of shear rate for a) coal A, b) coal B and c) coal C slurries at different LSS concentrations, which was conducted under the conditions of 50 wt.% coal concentration, pH 7 and 25 °C.

Table 7-3: Fitted Herschel-Bulkley parameter values of coal A, B and C slurries at different LSS dosages.

| Sample | Coal A | | | | Coal B | | | | Coal C | | | |
|---|---|---|---|---|---|---|---|---|---|---|---|---|
| LSS dosage, mg/L | $\tau_0$, Pa | n | K, pa.S$^n$ | $R^2$ | $\tau_0$, Pa | n | K, pa.S$^n$ | $R^2$ | $\tau_0$, Pa | n | K, pa.S$^n$ | $R^2$ |
| 0 | 54.3 | 0.88 | 0.92 | 0.975 | 50.4 | 0.90 | 0.91 | 0.976 | 28.8 | 0.96 | 0.67 | 0.998 |
| 4 | 48.6 | 0.88 | 0.94 | 0.998 | 44.8 | 0.90 | 0.91 | 0.999 | 27.4 | 0.97 | 0.62 | 0.995 |
| 8 | 41.2 | 0.86 | 0.91 | 0.994 | 36.2 | 0.88 | 0.88 | 0.998 | 17.3 | 0.96 | 0.60 | 0.989 |
| 16 | 25.5 | 0.80 | 0.87 | 0.989 | 22.1 | 0.82 | 0.84 | 0.992 | 9.1 | 0.94 | 0.59 | 0.992 |
| 32 | 11.3 | 0.72 | 0.82 | 0.997 | 10.0 | 0.76 | 0.80 | 0.988 | 6.2 | 0.93 | 0.58 | 0.997 |
| 64 | 9.2 | 0.71 | 0.80 | 0.993 | 7.8 | 0.74 | 0.78 | 0.989 | 5.9 | 0.93 | 0.58 | 0.996 |

### 7.4.8 Stability studies

The influence of OSL and LSS on the stability of CWS was shown in Figure 7.8. The destabilization index of coal A, B and C suspensions in the absence of OSL and LSS were found to be 4, 4.4 and 9, respectively, which illustrates that coal A was more stable than other CWS. An increase in the adsorbed amount of OSL reduced the destabilization index of coal A, B and C suspensions to 0.2, 0.8 and 6.6, respectively (Figure 7.8a). These results confirm that the adsorption of OSL improved the stability of CWS irrespective to their particle size, but more promising results were obtained for coal A. This increase in stability of coal particles is due to electrostatic repulsion generated between the particles by the adsorbed OSL. LSS also exhibited similar behaviour, and coal A suspension exhibited the minimum destabilization index of 1.1 compared to other coal suspensions. Therefore, OSL was more effective in improving the stability of coal particles than LSS. Previously, Peng-wei and co-authors reported a decrease in the destabilization index of CWS from 0.85 to 0.6 with an increase in concentration of modified lignin dispersant in CWS to 1.4 wt.% [54].

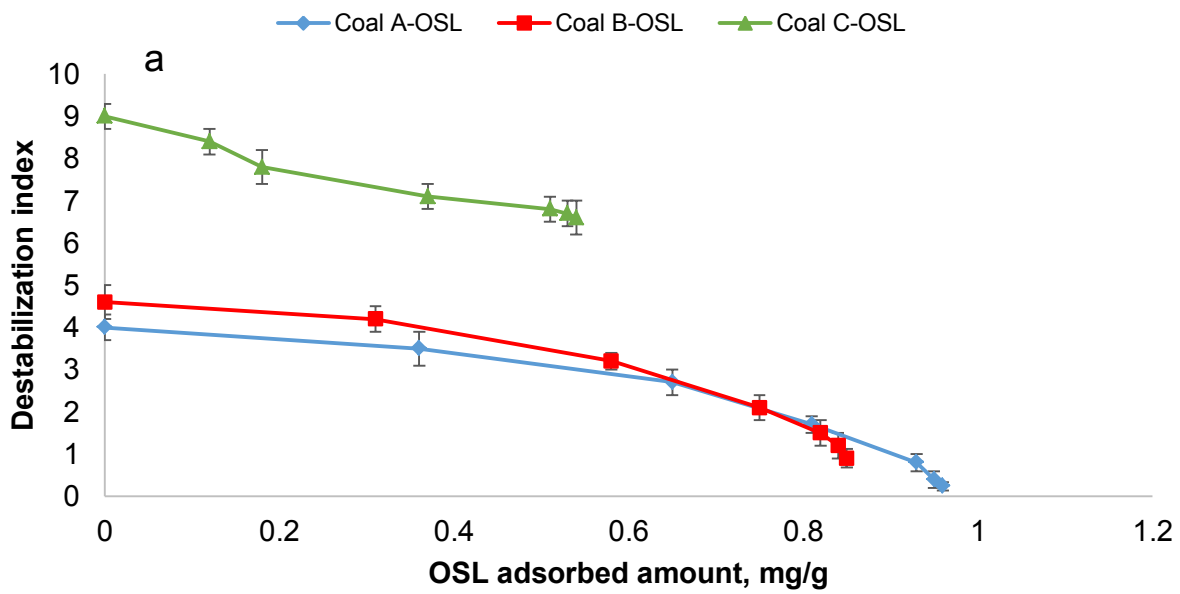

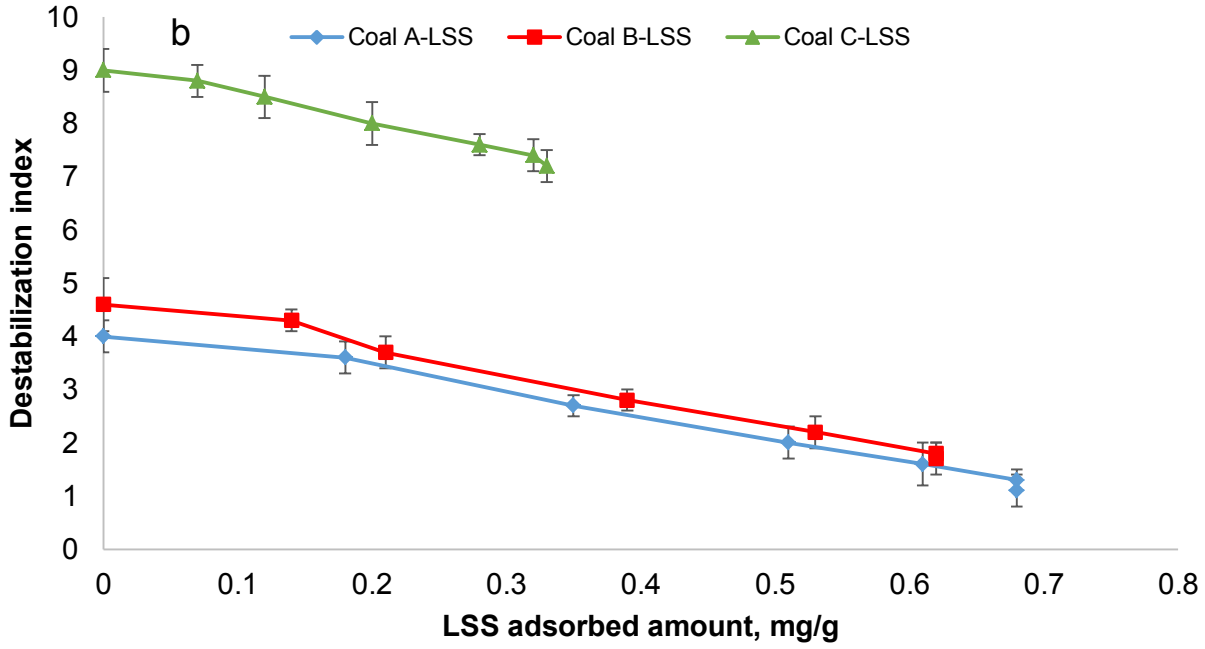


Figure 7-8: Effect of adsorbed amount of a) OSL and b) LSS on the destabilization index of coal samples having different particle sizes under the conditions of pH 7, 25 °C, 100 $s^{-1}$ shear rate and 50 wt.% coal concentration.

### 7.4.9 Mechanism of dispersion

Figure 7.9 presents a relationship between changes in the zeta potential and interfacial tension of coal particles and apparent viscosity of CWS. It is observable that smaller changes in the interfacial tension than in the zeta potential of coal particles were achieved for a similar change in the viscosity of the slurries, regardless of dispersant type. These results indicate that the adsorption of OSL affected both the surface energy and wettability of the particles as well as the repulsion between particles, and the adsorption affected the repulsion more significantly than the surface wettability. In other words, the interface energy and wettability of the particles changed as a result of OSL or LSS adsorption, implying that more interactions between particles and the medium (i.e. water) were developed, and the enhanced interaction of particles in water as well as more repulsion between particles (due to dispersant adsorption) dropped the viscosity of the slurries. The significant reduction in apparent viscosity was observed in regard to the changes in zeta potential of coal particles, irrespective of size. Coal A slurry with the maximum change of 56% in the zeta potential exhibited the maximum decrease in the apparent viscosity by 61 %. However, coal C slurry exhibited the minimum viscosity change compared to coal A and coal B slurries, indicating that particle size also influenced the viscosity change of CWS. A similar trend

was also observed in the presence of LSS, where apparent viscosity was reduced with changes in the zeta potential of CWS (Figure 7.9b). The maximum reduction in the apparent viscosity of coal A slurry by 50 % is accompanied by maximum change of 35% in the zeta potential.

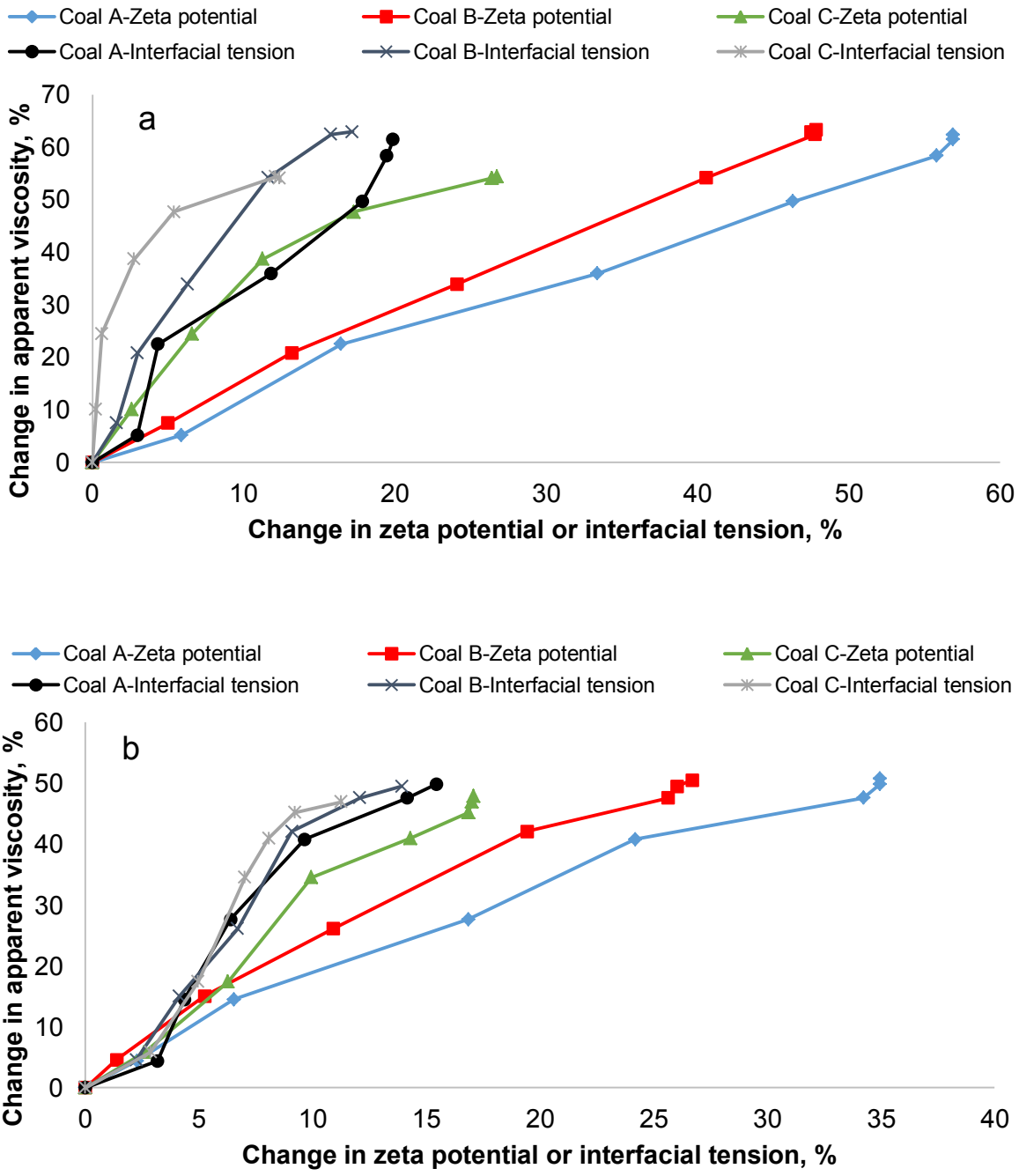


Figure 7-9: Change in apparent viscosity in relation with change in zeta potential and interfacial tension of coal particles in the presence of a) OSL and b) LSS conducted under the conditions of pH 7, 50 wt.% coal and 25 °C

## 7.5 Discussion

The size of coal particles greatly influenced the performance of OSL as a dispersant. A higher adsorption was obtained on coal A (Figure 7.2), and this adsorption reduced the interfacial tension between water and coal particles (Figure 7.3) and zeta potential of coal suspension (Figure 7.4). As the adsorption of OSL was the greatest on coal A, it introduced the maximum repulsion force to coal particles reducing their viscosity the most (Figure 7.5) and changing the behavior of the coal suspension to be more pseudo plastic (Figure 7.6) and stabilizing the suspension the most (Figure 7.8).

The results in Figures 7.2 to 7.8 also show that OSL was more effective than LSS in adsorbing on coal particles (Figure 7.2) and thus changing the hydrophilicity of coal particles (Figure 7.3) as well as the zeta potential of the suspension (Figure 7.4). These changes were more likely attributed to the higher charge density and molecular weight of OSL than LSS. These changes led to more pseudo plastic behavior (Figure 7.7), lower viscosity (Figure 7.5) and more stable suspension of CWS (Figure 7.8).

## 7.6 Conclusions

Oxidized sulfomethylated kraft lignin (OSL) was successfully produced and its characteristics were analyzed. Generally, more pronounced effects were observed for coal particles with a large surface area (coal A). The maximum adsorption of 0.9 mg/g and 0.68 mg/g of OSL and LSS was achieved on coal A. The interfacial tension between coal A and water was reduced from 17 mN/m to 13 mN/m or 14 mN/m via adsorbing OSL or LSS indicating an increase in the wettability of the particles. Surface tension and contact angle results suggested an increased wettability of coal particles with reduction in particle size and adsorption of OSL or LSS. The zeta potential of coal particles depends on the amount of OSL adsorbed on particle surface with coal A suspension exhibiting the minimum zeta potential of -48 mV. The viscosity of coal A dropped from 1350 to 520 mPa.s when OSL was adsorbed (0.96 mg/g) on coal particles under the conditions of 50 wt.% coal concentration, 25 °C, 100 1/s shear rate and pH 7. The stability of coal particles improved by adsorbing OSL with destabilization index lowered from 4 to 0.2. LSS dropped the zeta potential of coal A suspension from -30 to -41 mV and the viscosity of CWS from 1365 to 680 mPa.s under the conditions of 50 wt.% coal concentration, pH 7, 100 1/s shear rate and 25 °C reduced. The analysis revealed that the adsorption of the dispersant changed the

wettability and interaction of the particles with water and the dispersants, and the adsorbed dispersants on particles introduced repulsion that helped with the viscosity change (and behavior) and stability of the suspension, and these changes were more significant for OSL than LSS as it had a higher charge density and molecular weight.

## 7.7 References


1. Hong N, Zhang S, Yi C, Qiu X. Effect of polycarboxylic acid used a high performance dispersant on low rank coal water slurry. Journal of Dispersion Science and Technology, 2015, 3, 415-422.
2. Li R, Yong D, Lou H, Zhou M, Qiu X. Influence of sulfonated acetone-formaldehyde used as dispersant on low rank coal slurry. Energy Conservation and Management, 2012, 64, 139-144.
3. Manganaro J, Lawal A. Economics of Thermochemical Conversion of Crop Residue to Liquid Transportation Fuel. Energy Fuels. 2012, 26, 2442-2453.
4. Demirbas A. Bioethanol from Cellulosic Materials: A Renewable Motor Fuel from Biomass. Energy Sources. 2005, 27, 327-337.
5. Das D, Dash U, Nayak A, Misra PK. Surface Engineering of Low Rank Indian Coals by Starch-Based Additives for the Formulation of Concentrated Coal-Water Slurry. Energy and Fuels, 2010, 24, 1260-1268.
6. Zhang G, Li J, Zhu J, Wu Q, Xiong W. Synthesis and evaluations of three sulfonated polycondensate dispersants for coal-water slurries. Powder Technology, 2014, 24, 572-578.
7. Das D, Dash U, Meher J, Misra PK. Improving stability of concentrated coal-water slurry using mixture of a natural and synthetic surfactants. Fuel Processing and Technology, 2013, 113, 41-51.
8. Zhou M, Huang K, Yang D, Qiu X. Development and evaluation of polycarboxylic acid hyper-dispersant used to prepare high-concentrated coal–water slurry. Powder Technology. 2012, 229, 185-190.
9. Huang J, Xu J, Wang D, Li L, Guo X. Effects of amphiphilic copolymer dispersants on rheology and stability of coal water slurry. Industrial Engineering and Chemistry Research, 2013, 52, 8427-8435.

10. Phulkerd P, Thongchul N, Bunyakiat K, Petsom A. Coal water slurry using dispersant synthesized from cashew nut shell liquid (CNSL). Fuel Processing and Technology, 2014, 119, 256-262.
11. Dincer H, Boylu F, Serkeci AA, Atesok G. The effect of chemicals on the viscosity and stability of coal-water slurries. International Journal of Mineral Processing, 2003, 70, 41-51.
12. Tiwari KK, Basu SK, Bit KC, Banerjee S, Mishra KK. High concentration of coal-water slurry from Indian coals using newly developed additives. Fuel Processing and Technology. 2004, 85, 31-42.
13. Pawlik M. Polymeric dispersants for coal water slurries. Colloids and Surf., A: Physiochemical Engineering Aspects, 2005, 266, 82-92.
14. Syahbirin G, Darwis AA, Suryani A, Syafii W. Potential of Lignosulphonate of Eucalyptus Lignin from Pulp Plant as Dispersant in Gypsum Paste. Procedia Chemistry, 4 (2012) 343-351.
15. Qin Y, Yang D, Guo W, Qiu X. Investigation of grafted sulfonated alkali lignin polymer as dispersant in coal water slurry. Journal of Industrial Engineering Chemistry, 2015, 27, 192-200.
16. Wu H, Chen F, Feng Q, Yue X. Oxidation and sulfomethylation of alkali extracted lignin from corn stalk. Bioresources. 2012, 7, 2742-2751.
17. Konduri MKR, Kong F, Fatehi P, Production of carboxymethylated lignin and its application as a dispersant. European Polymer Journal, 2015, 70, 371-383.
18. Lin X, Zhou M, Wang S, Lou H, Yang D, Qiu X. Synthesis, Structure, and dispersion property of a novel lignin based polyoxyethylene ether from kraft lignin and poly(ethylene glycol). ACS Sustianable Chemistry and Engineering, 2014, 2, 1902-1909.
19. Qin Y, Yang D, Gu F, Li X, Xiong W, Zhu JY. Biorefinery lignosulfonates as a dispersant for coal water slurry. Sustainable Chemical Processes, 4, 2016, 1-8.
20. Das D, Panigrahi S, Mishra PK, Nayak A. Effect of organized assemblies, Part-4. Formulation of highly concentrated coal-water slurry using a natural surfactant. Energy Fuels, 2008, 22, 1865-1872.
21. Li P, Yang D, Lou H, Qiu X. Study on stability of coal water slurry using dispersant-stability analyzer. Journal of Fuel Chemistry and Technology, 2008, 36, 524-529.

22. Fang Z, Guang-hua Z, Jun-feng Z, Li-li S, Hai-long X. Preparation and performance study of starch coal-water mixture dispersants. Journal of China Coal Society, 2012, 37, 456-461.
23. Hong N, Zhang S, Yi C, Xueqing Q. Effect of Polycarboxylic Acid Used as High-Performance Dispersant on Low Rank Coal-Water Slurry. Journal of Dispersion Science and Technology, 37, 2015, 415-422.
24. Kakui T, Kamiya H. Effect of Sodium Aromatic Sulfonate Group in Anionic Polymer Dispersant on the Viscosity of Coal-Water Mixtures. Energy Fuels, 2004, 18, 652-658.
25. Yang D, Xueqing Q, Zhou M, Lou H. Properties of sodium lignosulfonate as dispersant of coal water slurry. Energy Conversion and management, 2007, 48, 2433-2438.
26. Kouisni L, Holt-Hindle P, Maki K, Paleologou M, The lignoforce sytem: A new process for the production of high quality lignin from black liquor. Journal of Science and Technology for Forest Products and Processes2012, 2, 6-10.
27. He W, Fatehi P. Preparation of sulfomethylated softwood kraft lignin as a dispersant for cement admixture. RSC Advances, 2015, 5, 47031-47039.
28. Wang S, Konduri MKR, Hou Q, Fatehi P. Cationic xylan-METAC copolymer as a flocculant for clay suspensions. RSC Advances, 2016, 6, 40258-40269.
29. Konduri MKR, Fatehi P. Production of Water-Soluble Hardwood Kraft Lignin via Sulfomethylation Using Formaldehyde and Sodium Sulfite. ACS Sustainable Chemistry and Engineering, 2015, 3, 1172-1182.
30. Zhu W, Westman G, Theilander H. Investigation and Characterization of Lignin Precipitation in the LignoBoost Process. Journal of Wood Chemistry and Technology, 2014, 34, 77-97.
31. Shin YJ, Shen YH. Preparation of coal slurry with 2 propanol, Journal of Hazardous Materials B, 2006, 137, 152-156.
32. Vie R, Azema N, Quantin JC, Touraud E, Fouletier M. Study of suspension settling: A approach to determine suspension classification and particle interactions. Colloids and Surfaces A: Physiochemical Engineering Aspects, 2007, 298, 192-200.
33. He W, Zhang Y, Fatehi P. Sulfomethylated kraft lignin as a flocculant for cationic dye. Colloids and Surfaces A: Physiochemical Engineering Aspects, 2016, 503, 19-27.
34. Mengual O, Menuier G, Cayre I, Puech K, Sanbre P. Characterization of instability of concentrated dispersions by a new optical analyzer: the Turbiscan MA 1000. Colloids and Surfaces A: Physiochemical Engineering Aspects, 1999, 152, 111-123.

35. Ouyang X, Ke L, Qiu X, Guo Y, Pang Y. Sulfonation of alkali lignin and its potential use in dispersant for cement. Journal of Dispersion Science and Technology, 2009, 30, 1-6.
36. Cao YJ, Li JS, Liu JT, Zhang HJ, Zhai X. Removal of unburned carbon from flyash using a cyclonic-static microbubble flotation column. Journal of South African Institute of Mining and Metallurgy, 112 (2012) 891-896.
37. Zhu R, Cui S, Wang X. Theoretical foundation of Zisman's empirical equation for wetting of liquids on solid surfaces. European Journal of Physics, 2010, 31, 251-256.
38. Chingombe P, Saha B, Wakeman RJ. Surface modification and characterization of a coal based activated carbon. Carbon, 2005, 43, 3132-3143.
39. Sabah E, Erkan ZE. Interaction mechanism of flocculants with coal waste slurry. Fuel, 2006, 85, 350-359.
40. Zhou G, Xu C, Cheng W, Zhang Q, Nie W. Effects of Oxygen Element and Oxygen containing Functional Groups on Surface Wettability of Coal Dust with Various Metamorphic Degrees Based on XPS Experiment. Journal of Analytical. Methods in Chemitsry, 2015, 10, 242-251.
41. Zhang, H, Chen, B, Banfield, J.F. The size dependence of the surface free energy of titania nanocrystals. Physical Chemistry Chemical Physics, 2009, 11, 2553-2558.
42. Nikolakais, I, Newton, J.M, Malamataris, S. Solid state 'adsorption' of fine antibiotic powders onto sorbitol: effects of particle size, state of sorbed water and surface free energy characteristics. European Journal of Pharamaceutical Sciences, 2002, 17, 229-238.
43. Li S, Lundquist K. A New Method for the Analysis of Phenolic Groups in Lignin's by $^{1}$H-NMR, Nordiac Pulp and Paper Research Journal, 1994, 3, 191-195.
44. Wen JL, Sun SL, X BL, Sun RC. Recent Advances in Characterization of Lignin Polymer by Solution-State Nuclear Magnetic Resonance (NMR) Methodology. Materials, 2013, 6, 359-391.
45. Fulmer GR, Miller AJM, Sherden AH, Gottleib HE, Nudelman A, Stolz BM, Berca JE, Goldberg KI. NMR chemical shifts of trace impurities: common laboratory solvents, organics, and gases in deuterated solvents relavent to organometallic chemist. Organometallics, 2010, 29, 2176-2179.
46. Zhang L, Gellerstedt G. NMR observation of a new lignin structure, a spiro-dienone. Chemical Communications, 2001, 24, 2744–2745.

47. Wu S, Argyropoulos DS. An improved method for isolating lignin in high yield and purity. Journal of Pulp and Paper Science, 2003, 29, 235–240.
48. Zhou G, Qiu H, Zhang Q, Xu M, Wang J, Wang G. Experimental investigation of coal dust wettability based on surface contact angle. Journal of Chemistry, 2016, 2016, 1-8.
49. Nasser MS, James AE. The effect of polyacrylamide charge density and molecularweight on the sedimentation behaviour of kaolinite suspensions. Separation and Purification Technology, 2006, 52, 241-252.
50. Zhu J, Zhang G, Miao Z, Shang T. Synthesis and performance of a comb like amphoteric polycarboxylate dispersant for coal–water slurry, Colloids and Surfaces A: Physiochemical Engineering Aspects, 2012, 412, 101-107.
51. Roh NS, Shin DH, Kim DC, Kim JD. Rheological behaviour of coal water mixtures. Fuel, 1995, 74, 1220-1225.
52. Mishra S.K, Kanungo SB. Factors affecting the preparation of highly concentrated coal-water slurry (HCCWS). Journal of Scientific and Industrial Research, 2000, 59, 765-790.
53. Tiwari KK, Basu SK, Bit KC, Banerjee S, Mishra KK. Highly concentrated coal water slurry from Indian coals using newly developed additives, Fuel Processing and Technology, 2003, 85, 31-42.
54. Peng-wei L, Dong-jie Y, Hong-ming L, Xue-king Q. Study on the stability of coal water slurry using dispersion-stability analyzer. Journal of Fuel Chemitsry and Technology, 2008, 36, 524−529.

# Chapter 8. CONCLUSIONS AND FUTURE DIRECTIONS

## 8.1 Summary of conclusions

The work presented in this dissertation focused on the preparation of anionic lignin or xylan polymers *viz*., CML, SML, CMX, OL and OSL and their dispersion performance in kaolin or coal suspensions. The adsorption behaviour of all the anionic lignin or xylans polymers prepared in this study on the surface of kaolin or coal samples was systematically investigated. The effects of the dosage of anionic lignin or xylan polymers and pH of suspension on the dispersion of kaolin or coal suspensions were studied fundamentally. The influence of charge density and molecular weight of anionic lignin polymers (OLs) on the adsorption behaviour and electro kinetic, turbidity and stability properties of kaolin dispersion were analyzed systematically. The application of OSL as a dispersant in coal water suspensions was investigated in details. The impact of OSL on the rheological behavior of CWS was studied under various conditions, and the influence of coal particle size on the dispersion of CWS in the presence of OSL was assessed.

In synthesizing carboxymethylated lignin, the results confirmed the success of the reaction, and revealed that the carboxymethylation was generally promoted the application of lignin as a dispersant. The addition of carboxylate groups to lignin was confirmed by FTIR, NMR, TGA and molecular weight analyses. CML with the maximum charge density and solubility was obtained under the conditions of 1.5 M NaOH concentration, 3 mol/mol of lignin/SCA ratio at 40 °C, 4 h and 16.7 g/L lignin concentration. The dispersion studies also indicated that CML could serve as an effective dispersant for a clay suspensions.

In synthesis of sulfomethylated lignin (SML), sodium sulfite and formaldehyde were used in grafting of sulfomethyl groups on the aromatic ring at the ortho position of lignin under alkali conditions. The reaction conditions were optimized using orthogonal array method and the results were signified using ANOVA. The SML with targeted charge density was produced under the conditions of 0.5 M of $NaOH_{(aq)}$, 0.9 mol/mol of sodium hydroxymethylsulfonate/lignin ratio, 100 °C, 3 h reaction time with a lignin concentration of 20 g/L. The produced SML was also soluble under aqueous conditions with maximum solubility of 40 g/L. The grafting of sulfomethyl groups on lignin was confirmed by FTIR, NMR and molecular weight analyses. The prepared SML also exhibited acceptable dispersion behaviour in cement admixtures.

In carboxymethylated xylan (CMX) preparation, the carboxymethyl groups were introduced in the beech wood xylan using sodium chloroacetate. The experimental and orthogonal modelling analysis was performed to optimize the conditions to produce CMX with targeted properties. The CMX with the maximum charge density (1.6 meq/g) and degree of substitution (DS) of 0.21 was achieved under the optimized conditions, 0.75 M NaOH, 1.0 mol/mol SCA/xylan (anhydroxylose unit) ratio, 2 h reaction time, temperature of 70 °C and 15 g/L xylan concentration. The structural, physical and chemical properties of CMX were analyzed using NMR, FTIR, TGA, DLS and molecular weight analyses. The dispersion analysis confirmed that CMX could be an effective dispersant for highly concentrated kaolin suspensions,.

The adsorption analysis confirmed that, electrostatic interactions play an important role in the adsorption of CMX on kaolin. By increasing CMX dosage and pH, the adsorption of CMX increased and the maximum adsorption of 2.48 mg/g was achieved at 15 mg/L CMX concentration and pH 6. Electrokinetic studies of kaolin suspensions revealed that the zeta potential of kaolin suspension varied with adsorbed amount of CMX. The dispersion properties of kaolin suspensions depended on the CMX dosage and pH, and also varied with adsorbed amount of CMX on kaolin under both dynamic and static conditions. The maximum relative turbidity of 1.25 was obtained at pH 6 at adsorbed amount of 25 mg/g CMX in the kaolin dispersions. The stability of kaolin particles increased with CMX dosage and pH . The addition of CMX was found to be more effective in stabilizing kaolin dispersions than a shear rate increase. Kinetic studies reveal that CMX adsorbs very quickly on the surface of kaolin.

The charge density (CD) and molecular weight (MW) of lignin significantly affected the performance of anionic lignin (OL) in the dispersion of kaolin suspensions. Anionic lignins (OLs) with varying charge densities and molecular weights were synthesised via oxidation of kraft lignin with nitric acid under different conditions. By adding 32 mg/L of OL having the charge density of 3.6 meq/g and molecular weight of 30,000 g/mol, the maximum relative turbidity of 1.31 for kaolin suspensions was achieved. The adsorption of OL on kaolin was greatly influenced by the charge density, whereas the MW of OL had an insignificant effect. The zeta potential of kaolin was also influenced by the charge density and MW had little impact, which confirmed that OLs adsorbed on kaolin via electrostatic interactions. Dispersion studies under both dynamic and static conditions indicated that the charge density and molecular weight of OLs had an influence on the dispersibility of kaolin suspensions. The change in the

dispersibility of kaolin suspensions with the charge density and MW of OLs could be attributed to the adsorbed configuration of OLs on kaolin surface. Kinetic studies also confirmed the effect of both charge density and molecular weight of OLs on kaolin dispersions.

The application of oxidised and sufomethylated lignin (OSL) in coal water suspensions (CWS) suggested that OSL could serve as an effective dispersant for CWS. The reduction in particle size of coal improved the adsorption of OSL on coal surface. Also an increase in the wettability of coal particles was observed with reduction in the presence of OSL. Adsorption of OSL on coal was increased with OSL concentration and the zeta potential of coal depended on the adsorbed amount of OSL on coal surface. The adsorption amount of OSL and size of coal particles were found to have great influences on the viscosity of CWS. The maximum viscosity drop (from 1350 to 520 mPa.s) was observed for CWS under the conditions of 50 wt.% coal concentration, 25 °C, 100 $s^{-1}$ shear rate, pH 7 and 0.96 mg/g of OSL adsorption. The pseudoplastic behaviour of CWS was improved by the addition of OSL irrespective of the particle size. The flow properties of CWS were enhanced effectively by the addition of OSL. The stability of coal particles was also improved by the adsorption of OSL, with destabilization index lowered from 4 to 0.2, which reduced the viscosity of CWS from 1365 to 680 mPa.s. A significant change in the apparent viscosity in relation to the changes in the zeta potential and interfacial tension of coal and water indicated that the OSL stabilized the coal particles via affecting the wettability of coal and improving the electrostatic repulsion between the coal particles.

## 8.2 Recommendation for future work

In this study, the application of anionic lignin or xylan polymers as a dispersant for kaolin dispersions was studied, which constricts the conclusions. As discussed in the dissertation, the anionic lignin or xylan significantly improved the dispersion of kaolin suspensions. However, type of clay differs for different processes, thus theresults may not be conclusive to all mineral processing industries. Therefore, a systematic study should be conducted on the application of anionic lignin or xylan polymers as dispersants for different mineral processes.

As investigated in the dissertation, synthetic suspensions were used as models. However, the industrially produced samples may have different properties and compositions. Therefore, the

analysis should be conducted on industrially produced clay suspension to generate more industrially attractive results.

The dispersion behaviour of anionic lignin and the mechansims involved in dispersion were investigated in clay suspesnions and CWS in this theiss. However, to confirm its dispersion performance, dispersion studies and detailed mechanisms involved in dispersion of clay particles should be studied in different colloidal systems for more comprehensive outcomes.

# PUBLICATIONS LIST

1. **Mohan K. R. Konduri**, Pedram Fatehi. Influence of pH and ionic strength on flocculation of clay suspensions with cationic xylan copolymer. Paper submitted to *Colloids and Surfaces A: Physiochemical Engineering Aspects*, 2017.
2. **Mohan K. R. Konduri**, Pedram Fatehi. Dispersion of kaolin particles with carboxymethylated xylan. *Applied Clay Science*, 137, **2017**, 183-191.
3. **Mohan K.R. Konduri**, Pedram Fatehi. Synthesis and characterization of carboxymethylated xylan and its application as a dispersant. *Carbohydrate Polymers*, 146, **2016**, 26-35.
4. **Mohan K. R. Konduri**, Pedram Fatehi. Production of water soluble kraft lignin via sulfomethylation using formaldehyde and sodium sulfite. *ACS: Sustainable Chemistry & Engineering*, 3, **2015**, 1172-1182.
5. **Mohan K. R. Konduri**, Fangong Kong, Pedram Fatehi. Production of water soluble kraft lignin via carboxymethylation using sodium chloroacetate. *European Polymer Journal*, 70, **2015**, 371-383.
6. Shoujuan Wang, **Mohan K. R. Konduri**, Qingxi Hou, Pedram Fatehi. Cationic xylan-METAC copolymer as flocculant for clay suspensions. *RSC Advances,* 6, **2016**, 40258-40269.
7. Fangong Kong, Shoujuan Wang, Jacquelyn T Price, **Mohan K. R. Konduri**, Pedram Fatehi. Water soluble kraft lignin-acrylic acid copolymer: synthesis and characterization. *Green Chemistry*, 17, **2015**, 4355-4366.
8. Jing Shen, Robin Singh, **Mohan Konduri**, Pedram Fatehi. Cationic hemicellulose as a product of dissolving pulp based biorefinery. *Industrial & Engineering Chemistry Research*, 54, **2015**, 1426-1432.